ERDC/CHL TR-22-16

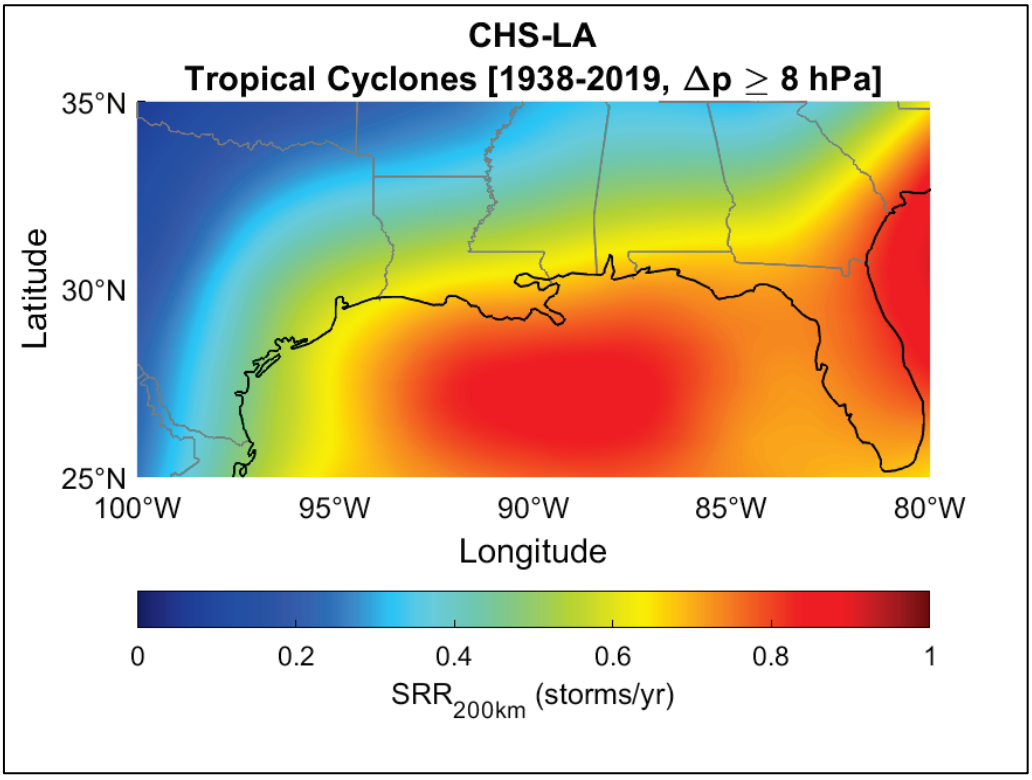
US Army Corps
of Engineers®
Engineer Research and
Development Center

ERDC
ENGINEER RESEARCH & DEVELOPMENT CENTER

Coastal Hazards System–Louisiana (CHS-LA)

Norberto C. Nadal-Caraballo, Madison C. Yawn,
Luke A. Aucoin, Meredith L. Carr, Alexandros A. Taflanidis,
Aikaterini P. Kyprioti, Jeffrey A. Melby, Efrain Ramos-Santiago,
Victor M. Gonzalez, Thomas C. Massey, Zach Cobell, and
Andrew T. Cox

August 2022



Approved for public release; distribution is unlimited.

Coastal and Hydraulics Laboratory

The US Army Engineer Research and Development Center (ERDC) solves the nation's toughest engineering and environmental challenges. ERDC develops innovative solutions in civil and military engineering, geospatial sciences, water resources, and environmental sciences for the Army, the Department of Defense, civilian agencies, and our nation's public good. Find out more at www.erdc.usace.army.mil.

To search for other technical reports published by ERDC, visit the ERDC online library at https://erdclibrary.on.worldcat.org/discovery.

ERDC/CHL TR-22-16
August 2022

Coastal Hazards System–Louisiana (CHS-LA)

Norberto C. Nadal-Caraballo, Madison C. Yawn, Luke A. Aucoin, Meredith L. Carr, Jeffrey A. Melby, Efrain Ramos-Santiago, Victor M. Gonzalez, and Thomas C. Massey

Coastal and Hydraulics Laboratory
US Army Engineer Research and Development Center
3909 Halls Ferry Road
Vicksburg, MS 39180-6199

Alexandros A. Taflanidis and Aikaterini A. Kyprioti

University of Notre Dame
Fitzpatrick Hall
Notre Dame, IN 46556

Zach Cobell

The Water Institute of the Gulf
1110 River Road S, Suite 200
Baton Rouge, LA 70802

Andrew T. Cox

Oceanweather, Inc.
5 River Road, Suite 1
Cos Cob, CT 06807

Final report

Approved for public release; distribution is unlimited.

Prepared for Coastal Protection and Restoration Authority
Baton Rouge, LA 70804-4027

Under Coastal Protection and Restoration Authority (CPRA) of Louisiana through
Cooperative Research and Development Agreement (CRADA) 65K08-B54G0B

Abstract

The US Army Engineer Research and Development Center (ERDC), Coastal and Hydraulics Laboratory (CHL) expanded the Coastal Hazards System (CHS) to quantify storm surge and wave hazards for coastal Louisiana. The Coastal Hazards System–Louisiana (CHS-LA) coastal study was sponsored by the Louisiana Coastal Protection and Restoration Authority (CPRA) and the New Orleans District (MVN), US Army Corps of Engineers (USACE), to support Louisiana's critical coastal infrastructure and to ensure the effectiveness of coastal storm risk management projects. The CHS-LA applied the CHS Probabilistic Coastal Hazard Analysis (PCHA) framework to quantify tropical cyclone (TC) responses, leveraging new atmospheric and hydrodynamic numerical model simulations of synthetic TCs developed explicitly for the Louisiana region. This report focuses on documenting the PCHA conducted for the CHS-LA, including details related to the characterization of storm climate, storm sampling, storm recurrence rate estimation, marginal distributions, correlation and dependence structure of TC atmospheric-forcing parameters, development of augmented storm suites, and assignment of discrete storm weights to the synthetic TCs. As part of CHS-LA, coastal hazards were estimated within the study area for annual exceedance frequencies (AEFs) over the range of 10 yr^{-1} to 1×10^{-4} yr^{-1}.

DISCLAIMER: The contents of this report are not to be used for advertising, publication, or promotional purposes. Citation of trade names does not constitute an official endorsement or approval of the use of such commercial products. All product names and trademarks cited are the property of their respective owners. The findings of this report are not to be construed as an official Department of the Army position unless so designated by other authorized documents.

DESTROY THIS REPORT WHEN NO LONGER NEEDED. DO NOT RETURN IT TO THE ORIGINATOR.

Contents

Abstract ii

Contents iii

Preface ix

1 Introduction 1
1.1 Background 1
1.2 Objective 2
1.3 Approach 3

2 Coastal Hazards System (CHS) 6
2.1 Joint probability method (JPM) 7
2.2 Joint probability method with optimal sampling (JPM-OS) 8
2.3 The CHS Probabilistic Coastal Hazard Analysis (PCHA) 11
2.4 An integrated coastal hazards platform 16
2.4.1 CHS-LA available data 20
2.4.2 StormSim suite of tools 21

3 Characterization of Storm Climatology 23
3.1 Data sources 23
3.2 Period of record for the PCHA 24
3.3 Coastal reference locations (CRLs) 28
3.4 Selection of historical tropical cyclones (TCs) 31
3.5 Geospatial storm recurrence rate (SRR) 33
3.6 Distance adjustment of historical TCs 41

4 Joint Probability Analysis of Coastal Storm Hazards 44
4.1 Marginal distribution of TC parameters 44
4.1.1 Central pressure deficit (Δp) 45
4.1.2 Radius of maximum winds (R_{max}) 49
4.1.3 Forward translation speed (V_t) 51
4.1.4 Track heading direction (θ) 53
4.2 Joint probability analysis using the Meta-Gaussian Copula (MGC) 55
4.3 Discretization of marginal distributions 60
4.4 Augmented synthetic TC suite (ATCS) and discrete storm weights (DSWs) 60

5 Development of Synthetic TC Suite 64
5.1 TC master tracks 64
5.2 Along-track variation of TC parameters 69
5.2.1 Determination of pre-landfall filling 71
5.2.2 Determination of landfall filling 73
5.2.3 Scale pressure radius 73

5.3 Summary of tropical wind and pressure fields 73
5.4 Planetary boundary layer (PBL) model 76
5.5 Validation storm set development 78

6 Quantification of Coastal Storm Hazards 82
6.1 Hydrodynamic modeling considerations 82
6.1.1 Dry-node correction (DNC) 83
6.1.2 Metamodel training 87
6.2 Geospatial bias correction and uncertainty quantification 88
6.2.1 Aleatory and epistemic uncertainties 90
6.2.2 Sources of modeling error 91
6.2.2.1 Storm surge modeling error 92
6.2.2.2 Nearshore wave modeling error 92
6.2.2.3 Atmospheric modeling error 92
6.2.3 Absolute and relative forms of bias and uncertainty 93
6.2.4 Geospatial bias estimation and correction 95
6.2.5 Estimation of geospatial uncertainty 98
6.3 Astronomical tides 99
6.4 Quantification of the still water level (SWL) hazards 100
6.5 Quantification of wave hazards 103
6.5.1 Significant wave height 103
6.5.2 Peak wave period 107
6.6 Joint probability method-Monte Carlo (JPM-MC) approach for quantifying coastal compound hazards 109
6.6.1 Probabilistic Q scenario 110
6.6.2 Coastal compound hazard curves 113

7 Conclusions 116

References 117

Appendix A: Historical TC Selection (CRL 128) 125

Appendix B: Synthetic Tropical Cyclone Suite 143

Appendix C: Geospatial Bias and Uncertainty 164
C.1 Bias and uncertainty of ADCIRC simulations 165
C.2 Bias and uncertainty of PBL simulations 167

Appendix D: Astronomical Tide Uncertainty 169

Symbols 173

Abbreviations 174

Report Documentation Page (SF 298) 179

Figures and Tables

Figures

Figure 2-1. Diagram of the CHS PCHA framework (Nadal-Caraballo et al. 2020). 15
Figure 2-2. Components within the Coastal Hazards System (CHS). 16
Figure 2-3. Screen capture of the CHS website. 18
Figure 2-4. Screen capture of the CHS webtool. 19
Figure 2-5. Screen capture of save points within the CHS webtool. 19
Figure 2-6. Geospatial distribution of save points within the CHS-LA study area. 21
Figure 3-1. Reconstruction of Δp for a 1938 historical TC using metamodeling techniques. 26
Figure 3-2. Reconstruction of Δp for Hurricane Sandy using metamodeling techniques. 26
Figure 3-3. Reconstruction of R_{max} for a 1938 historical TC using metamodeling techniques. 27
Figure 3-4. Reconstruction of R_{max} for Hurricane Sandy using metamodeling techniques. 27
Figure 3-5. The idealized coastline of CRLs developed for the PCHA. 30
Figure 3-6. CRLs (*blue*) used in the PCHA for the CHS-LA study area. 30
Figure 3-7. Optimal sampling locations of selected historical TCs within 600 km of CRL 128. 32
Figure 3-8. UKF, GKF, and EKF weights as a function of distance from CRL. 34
Figure 3-9. Geospatial SRR for all TCs within the CHS-LA study area. 36
Figure 3-10. Geospatial SRR for HI TCs within the CHS-LA study area. 37
Figure 3-11. SRR for MI TCs within the CHS-LA study area. 37
Figure 3-12. SRR for LI TCs within the CHS-LA study area. 38
Figure 4-1. DTWD for sampled Δp ranging from 8 to less than 28 hPa at CRL 128. 46
Figure 4-2. DTWD for all sampled Δp of 28 to 148 hPa at CRL 128. 46
Figure 4-3. Marginal distribution (DTWD) of Δp for HI TCs at CRL 128. 47
Figure 4-4. Marginal distribution (DTWD) of Δp for MI TCs at CRL 128. 48
Figure 4-5. Marginal distribution (DTWD) of Δp for LI TCs at CRL 128. 48
Figure 4-6. Marginal distribution (lognormal) of R_{max} for HI TCs at CRL 128. 49
Figure 4-7. Marginal distribution (lognormal) of R_{max} for MI TCs at CRL 128. 50
Figure 4-8. Marginal distribution (lognormal) of R_{max} for LI TCs at CRL 128. 50
Figure 4-9. Marginal distribution (normal) of V_t for HI TCs at CRL 128. 52
Figure 4-10. Marginal distribution (normal) of V_t for MI TCs at CRL 128. 52
Figure 4-11. Marginal distribution (lognormal) of V_t for LI TCs at CRL 128. 53
Figure 4-12. Marginal distribution (DSRR) of θ for HI TCs at CRL 128. 54
Figure 4-13. Marginal distribution (DSRR) of θ for MI TCs at CRL 128. 54
Figure 4-14. Marginal distribution (DSRR) of θ for LI TCs at CRL 128. 55
Figure 4-15. TC parameter correlation tree with 1.1 dependence. 56
Figure 4-16. Correlation matrix for all TCs. 58
Figure 4-17. Correlation matrix for HI TCs. 58
Figure 4-18. Correlation matrix for MI TCs. 59

Figure 4-19. Correlation matrix for LI TCs. 59
Figure 4-20. Diagram of the DSW workflow within the PCHA. 63
Figure 5-1. All master track paths (blue) with landfall/closest approach location (red). Master tracks developed for the SACS and CTXS (gray) shown for reference. 65
Figure 5-2. JPM heading −80° track paths. 65
Figure 5-3. JPM heading −60° track paths. 66
Figure 5-4. JPM heading −40° track paths. 66
Figure 5-5. JPM heading −20° track paths. 67
Figure 5-6. JPM heading 0° track paths. 67
Figure 5-7. JPM heading 20° track paths. 68
Figure 5-8. JPM heading 40° track paths. 68
Figure 5-9. JPM heading 60° track paths. 69
Figure 5-10. Tracks 1938–2019 in northern Gulf of Mexico with landfall location (red), track location pre-landfall (blue), and track location post-landfall (green). 72
Figure 5-11. Linear fit to ratio of pressure deficit at 250 km and landfall as a function of pressure deficit at 250 km. Ratio of > 1 indicates storms weakening as they approach landfall, ratio < 1 are storms strengthening towards landfall. Relationship applied in Texas Coast/SACS study shown in green. 73
Figure 5-12. Summary of JPM track path and derived parameters for the 645 storm set. 74
Figure 5-13. Summary of CHS-LA TC 1 (JPM0001) model input. 75
Figure 5-14. Summary of CHS-LA TC 1 (JPM0001) model graphical output of minimum pressure (mb, *left*) and maximum winds (knots, 30 minute average, *right*). 75
Figure 5-15. Summary of winds and pressures during 2018280N18273 (Michael 2018) for L1. 80
Figure 5-16. Summary of winds and pressures during 2018280N18273 (Michael 2018) for L2. 80
Figure 5-17. Summary of winds and pressures during 2018280N18273 (Michael 2018) for L3. 81
Figure 6-1. Idealized across-shore sketch illustrating the dry-node correction. 84
Figure 6-2. PCHA workflow incorporating the two-fold DNC and metamodeling of storm responses. 86
Figure 6-3. Nodes selected within bounds of the study area. LPV and WBV are shown for geospatial reference. 87
Figure 6-4. Illustration of bias and uncertainty in model prediction. 89
Figure 6-5. Comparison of methods for characterizing uncertainty. 94
Figure 6-6. Example SWL hazard curve near NOAA gauge 8761305 at Shell Beach. 102
Figure 6-7. Example SWL hazard curve near NOAA gauge 8761724 at Grand Isle. 102
Figure 6-8. Example SWL hazard curve near NOAA gauge 8761927 at New Canal Station. 103
Figure 6-9. Example H_{m0} hazard curve near NOAA gauge 8761305 at Shell Beach. 105
Figure 6-10. Example H_{m0} hazard curve near NOAA gauge 8761724 at Grand Isle. 106
Figure 6-11. Example H_{m0} hazard curve near NOAA gauge 8761927 at New Canal Station. 106
Figure 6-12. Example T_p hazard curve near NOAA gauge 8761305 at Shell Beach. 108

Figure 6-13. Example T_p hazard curve near NOAA gauge 8761724 at Grand Isle. 108
Figure 6-14. Example T_p hazard curve near NOAA gauge 8761927 at New Canal Station. 109
Figure 6-15. Mississippi River Q (top) and TC intensity (bottom) for May–November. 111
Figure 6-16. Relationship between discrete TC intensity bins and month of the year. 111
Figure 6-17. Exceedance probability (EP) of Mississippi River Q by month. 112
Figure 6-18. Graphical representation of parameter dependencies, including Q and m, on the storm response τ. 113
Figure 6-19. Geospatial distribution of example nodes along the Mississippi River. 114
Figure 6-20. SWL hazard curve including Q_p at node 1345110. 114
Figure 6-21. SWL hazard curve including Q_p at node 1338475. 115
Figure 6-22. SWL hazard curve including Q_p at node 1334141. 115
Figure C-1. Distribution of validation data points within the CHS-LA study area. 164
Figure C-2. Absolute form of ADCIRC bias for the CHS-LA study area. 165
Figure C-3. Relative form of ADCIRC bias for the CHS-LA study area. 165
Figure C-4. Absolute form of ADCIRC uncertainty for the CHS-LA study area. 166
Figure C-5. Relative form of ADCIRC uncertainty for the CHS-LA study area. 166
Figure C-6. Absolute form of PBL bias for the CHS-LA study area. 167
Figure C-7. Relative form of PBL bias for the CHS-LA study area. 167
Figure C-8. Absolute form of PBL uncertainty for the CHS-LA study area. 168
Figure C-9. Relative form of PBL uncertainty for the CHS-LA study area. 168

Tables

Table 3-1. Period of record considered for each TC parameter. 28
Table 3-2. SRR results for all intensity bins and CRLs in the CHS-LA study area. 38
Table 4-1. Marginal distribution parameters of Δp at CRL 128. 47
Table 4-2. Atmospheric-forcing parameters of the ITCS in the CHS-LA study. Error! Bookmark not defined.
Table 4-3. Marginal distribution parameters of R_{max} at CRL 128. 49
Table 4-4. Marginal distribution parameters of V_t at CRL 128. 51
Table 4-5. Atmospheric-forcing parameters from the ATCS. 61
Table 5-1. Length of JPM storms as a function of translation speed. 70
Table 5-2. CHS-LA validation storms. 78
Table 6-1. Riverine discharge (Q) scenarios simulated for the CHS-LA. 83
Table 6-2. GPM cross-validation statistics. 88
Table 6-3. Average values of absolute and relative bias estimated in CHS-LA. 97
Table 6-4. Average values of absolute and relative uncertainty estimated in CHS-LA. 99
Table A-1. Historical TCs. coordinates, distance from CRL 128, and Δp. 125
Table A-2. Historical TCs with unadjusted atmospheric parameters at CRL 128. 131

Table A-3. Historical TCs with distance-adjusted atmospheric parameters at CRL 128..... 137
Table B-1. Master tracks defined for the CHS-LA ITCS..... 143
Table B-2. Atmospheric-forcing parameters of the CHS-LA ITCS..... 146
Table D-1. Tidal uncertainty computed at NOAA gauges surrounding the CHS-LA study area..... 169

Preface

The study summarized in this report was performed to estimate storm surge and wave hazards for Louisiana's coastal areas. The study was funded by the Louisiana Coastal Protection and Restoration Authority of Louisiana through Cooperative Research and Development Agreement 65K08-B54G0B, and the New Orleans District, US Army Corps of Engineers. This study was conducted at the US Army Engineer Research and Development Center (ERDC), Coastal and Hydraulics Laboratory (CHL), Vicksburg, MS, from January 2020 to September 2021.

This work was performed by the Harbors, Entrances, and Structures Branch of the Navigation Division at CHL, the Coastal Processes Branch of the Flood and Storm Protection Division at CHL, the University of Notre Dame, and Oceanweather, Inc.

At the time of publication of this report, Mr. Chad R. Bounds was chief, Harbors, Entrances, and Structures Branch; Ms. Ashley E. Frey, chief, Navigation Division; Mr. Victor M. Gonzalez, chief, Coastal Processes Branch; Dr. Cary A. Talbot, chief, Flood and Coastal Division. Dr. Ty V. Wamsley was director, CHL, and Mr. Keith W. Flowers was deputy director, CHL.

The commander of ERDC was COL Christian Patterson, and the director was Dr. David W. Pittman.

1 Introduction

1.1 Background

In the aftermath of Hurricanes Katrina and Rita in 2005, the US Army Corps of Engineers (USACE) was authorized by Congress to conduct the Louisiana Coastal Protection and Restoration (LACPR) study (USACE 2009c), which followed the recommendations of the Interagency Performance Evaluation Task Force (IPET) (IPET 2009). Results from the LACPR study, based on a variant of the joint probability method (JPM), were implemented in the design and construction of the Greater New Orleans Hurricane and Storm Damage Risk Reduction System (HSDRRS). The HSDRRS was constructed at the cost of $14.6 B and encompassed more than 350 mi[1,2] of levees and floodwalls, 73 pump stations, and multiple canal-closure structures. The USACE and the Federal Emergency Management Agency (FEMA) also carried out two concurrent Flood Insurance Studies (FIS) for the Southeastern and Southwestern Parishes of Louisiana (USACE 2009a, 2009b). These FIS leveraged the joint probability analysis of storm surge conducted in the LACPR study to revise coastal flood insurance rate maps for the state of Louisiana.

The Louisiana Coastal Protection and Restoration Authority (CPRA) has various coastal programs that authorize the assessment of storm surge and coastal risk for Louisiana's coastlines, including performing risk-assessment evaluation required for the HSDRRS recertification. In 2021, under the Lowermost Mississippi River Management Program, CPRA sponsored the current study, leading to the expansion of the Coastal Hazards System (CHS) (https://chs.erdc.dren.mil) to the state of Louisiana. The Coastal Hazards System–Louisiana (CHS-LA) coastal study was conducted by the US Army Engineer Research and Development Center (ERDC), Coastal and Hydraulics Laboratory (CHL), and the University of Notre Dame, in collaboration with the USACE New Orleans District. The work described in this technical report follows the CHS Probabilistic Coastal

[1] For a full list of the spelled-out forms of the units of measure used in this document, please refer to *US Government Publishing Office Style Manual*, 31st ed. (Washington, DC: US Government Publishing Office 2016), 248-52, https://www.govinfo.gov/content/pkg/GPO-STYLEMANUAL-2016/pdf/GPO-STYLEMANUAL-2016.pdf.

[2] For a full list of the unit conversions used in this document, please refer to *US Government Publishing Office Style Manual*, 31st ed. (Washington, DC: US Government Publishing Office 2016), 345-7, https://www.govinfo.gov/content/pkg/GPO-STYLEMANUAL-2016/pdf/GPO-STYLEMANUAL-2016.pdf.

Hazard Analysis (PCHA) framework (Nadal-Caraballo et al. 2020). The application of PCHA encompassed state-of-the-art models, methods, and technically defensible data for accurate and robust quantification of coastal compound hazards in support of Louisiana's coastal flood risk management and HSDRRS recertification efforts.

1.2 Objective

The CHS-LA study sought to quantify hurricane-induced coastal hazards for the state of Louisiana. This study provides necessary engineering knowledge and data to support storm surge and compound (storm surge + riverine discharge) flood risk assessments required as part of the HSDRRS recertification process, including evaluating potential levee lifts and floodwall modifications. This study takes advantage of the CHS PCHA framework previously implemented in other recent USACE regional coastal studies, such as the CHS South Atlantic Coastal Study[1,2,3] (SACS), leading to the consistency of methodology applied and results obtained for US hurricane-expose coastlines. The PCHA is a statistical and probabilistic framework that builds on previous joint probability analysis methodologies. It incorporates several statistical and machine-learning advancements for more robust and accurate quantification of coastal storm hazards and uncertainty.

The joint probabilistic analysis of coastal storm hazards requires the evaluation of historical tropical cyclone (TC) data, including the characterization of regional storm climatology and the development of a joint probability model of TC atmospheric-forcing parameters. Standard TC parameters used to describe tropical cyclones (e.g., tropical storms and hurricanes) are track reference location, track direction, central pressure deficit (intensity), radius of maximum winds (size), and forward translation speed. The magnitude and extent of storm surge, for example, are primarily a function of storm intensity and size and the along-shore

[1] Nadal-Caraballo, N. C., M. C. Yawn, M. J. Torres, V. M. Gonzalez, E. Ramos-Santiago, T. C. Massey, A. A. Taflanidis, and A. T. Cox. In preparation. *Coastal Hazards System: Puerto Rico and the US Virgin Islands*. ERDC/CHL Technical Report. Vicksburg, MS: US Army Engineer Research and Development Center.

[2] Yawn, M. C., N. C. Nadal-Caraballo, M. L. Carr, E. Ramos-Santiago, V. M. Gonzalez, M. J. Torres, T. C. Massey, A. A. Taflanidis, and A. T. Cox. In Preparation. *Coastal Hazards System: South Atlantic*. ERDC/CHL Technical Report. Vicksburg, MS: US Army Engineer Research and Development Center.

[3] Yawn, M. C., N. C. Nadal-Caraballo, M. L. Carr, E. Ramos-Santiago, V. M. Gonzalez, M. J. Torres, T. C. Massey, A. A. Taflanidis, and A. T. Cox. In preparation. *Coastal Hazards System: Gulf of Mexico*. ERDC/CHL Technical Report. Vicksburg, MS: US Army Engineer Research and Development Center.

location relative to the eye of the storm, as discussed in Toro et al. (2010b). The PCHA framework was extended as part of CHS-LA study to characterize the hurricane storm surge and Mississippi River compound flooding problem in the vicinity of the HSDRRS.

Results from this study include the estimation of annual exceedance frequencies (AEFs) of still water level (SWL) and wave climate parameters: significant wave height (H_{mo}) and peak wave period (T_p). The AEF represents the number of times per year that a given event is expected to be equaled or exceeded and taking the inverse of the AEF, where $ARI = 1/AEF$, returns the average recurrence interval (ARI). The ARI represents the average time of occurrence between two events of interest and is often referred to as the *return period*. The magnitude of hazards can also be quantified in terms of annual exceedance probability (AEP), which represents the annual probability of an event occurring within a given year. Equations (1-1) and (1-2) convey the methods for converting between AEP and AEF:

$$AEP = \frac{e^{AEF}-1}{e^{AEF}} \tag{1-1}$$

$$AEF = -\log(1 - AEP) \tag{1-2}$$

The primary results quantified as part of this study are hazard curves depicting the magnitude of a given hazard (y-axis) as a function of AEF (x-axis). In general, the magnitude of a given hazard and the corresponding AEF are inversely correlated, meaning the magnitude of the hazard increases with decreasing AEF values.

1.3 Approach

Accurate estimation of hurricane-induced hazards is particularly challenging. The occurrence of these events is sparse, both in time and space, and is not well represented in historical observation records. The CHS PCHA framework employs an enhanced JPM-based methodology to quantify TC hazards. Rather than relying on extreme value analysis of hydrodynamic observations (e.g., storm surge and waves) that extrapolate beyond the historical record, the PCHA requires developing a sufficient number of synthetic TCs to efficiently cover a wide range of hurricane atmospheric and hydrodynamic characteristics. Spanning the atmospheric-forcing parameter and probability spaces is necessary to

quantify coastal storm hazards accurately over the study area. Building on the results and lessons learned from the North Atlantic Coast Comprehensive Study (NACCS) (Nadal-Caraballo et al. 2015) and the Coastal Texas Restoration and Feasibility Study[1] (CTXS), the PCHA addresses the limitations of previous JPM studies by integrating (1) regional storm climatology characterization, (2) marginal distributions of TC atmospheric-forcing parameters, (3) synthetic storm development, (4) dependence modeling of storm forcing parameters, (5) a joint probability model of atmospheric forcing and hydrodynamic responses, (6) high-resolution numerical simulations, (7) machine learning storm-response predictions, and (8) estimation of geospatial bias and uncertainty.

Quantifying storm hazards for coastal Louisiana required expanding the geographical coverage of the CHS and extending the PCHA framework by introducing new cutting-edge methods to specifically address compound coastal-riverine flooding in the vicinity of the HSDRRS. In the CHA-LA study, sampling of the multivariate TC parameter space yielded an initial TC suite (ITCS) of 645 unique storms covering a wide range of probabilities, from frequent (10 yr^{-1}) to rare (10^{-4} yr^{-1}) coastal events. This ITCS constituted the input to the high-resolution atmospheric and numerical hydrodynamic models used to simulate the coastal storm responses. An augmented TC suite (ATCS) consisting of 748,200 storms was subsequently developed through hyper-discretization of the TC parameter space. The hydrodynamic responses of the ATCS were estimated through the application of Gaussian process metamodeling (GPM), a machine learning technique developed in collaboration with the University of Notre Dame.

CHS-LA considered two different approaches for estimating the AEF of coastal compound hazards resulting from the interaction between storm surge and the discharge (Q) from the Mississippi River:

1. Deterministic Q scenario (Q_d): Probabilistic-deterministic analysis considering a single representative Q value across all TC hydrodynamic simulations.

[1] Nadal-Caraballo, N. C., A. B. Lewis, V. M. Gonzalez, T. C. Massey, and A. T. Cox. 2019. *Coastal Texas Protection and Restoration Feasibility Study, Probabilistic Modeling of Coastal Storm Hazards*. Report submitted to USACE-SWG. Vicksburg, MS: US Army Engineer Research and Development Center.

2. Probabilistic Q scenario (Q_p): Fully probabilistic analysis accounting for the stochastic coincidence between TC hazards and specific Q values as a function of month of occurrence.

The Q_p scenario required the extension of the CHS PCHA framework through a hybrid joint probability method-Monte Carlo (JPM-MC) approach. Hazard curves describing the magnitude of SWL (storm surge + astronomical tide), H_{mo}, and T_p as a function of AEF were developed at over 1.2 M point locations across coastal Louisiana and the vicinity of the HSDRRS.

The following sections describe the PCHA framework and its implementation within this study in detail. Section 2 provides context to the probability analysis of TC responses using the JPM, and Section 2.3 describes advancements of the PCHA over the standard JPM approach. The storm climatology of coastal Louisiana and the storm recurrence analysis is discussed in Section 3. The joint probability analysis of TC parameters through the development of marginal probability distributions and correlation coefficients and the storm suite applied in this study are described in Section 4. In Section 5, the detailed development of the synthetic storm suite for application in the meteorological numerical model is discussed. Section 6 provides details on the GPM development, computation of hazards, including the estimation of geospatial bias and uncertainty, methods used for waves, and the integration of TC responses. This section also documents an analysis of the impact of multiple riverine Q scenarios on the SWL. Finally, Section 7 summarizes the analysis performed herein for coastal Louisiana.

2 Coastal Hazards System (CHS)

The CHS (https://chs.erdc.dren.mil) is a national-scale, multi-agency initiative to quantify coastal storm hazards along US coastlines and other strategic locations critical to national security. Coastal hazards from hurricanes and extratropical storms can include storm surge, waves, wind, rainfall, compound coastal-inland flooding, seiche, and extreme tides. Climate change and sea level rise (SLR), which are expected to significantly exacerbate coastal flooding in the upcoming decades, are also part of the CHS scope. These coastal storm hazards can threaten the lives of millions of people living in coastal regions and devastate coastal communities and infrastructure, resulting in profound adverse social, economic, and environmental impacts. The foundation of the CHS is its PCHA framework.

The PCHA is a comprehensive statistical and probabilistic framework for quantifying coastal storm hazards. The framework encompasses the characterization of regional storm climatology, joint probability analysis of storm forcing and response, high-resolution numerical atmospheric and hydrodynamic modeling, machine learning, and estimation of associated uncertainties. The end goal of the PCHA is to develop a joint probability model linking storm forcing and responses. S*torm forcing* refers to the characteristics of a storm, including atmospheric pressure and wind fields. S*torm response* not only describes a hydrodynamic reaction to storm forcing, such as surge, waves, and currents, but could also include specific atmospheric variables such as maximum wind speed or rainfall. Results from the joint probability analysis are conveyed through hazard curves, which express the magnitude of a given hazard as a function of its AEF. The CHS also features a database hosting dozens of terabytes of coastal data, a web tool for easy access to results, and a website with corresponding documentation and metadata.

In the CHS PCHA framework, past tropical storms and hurricanes are parameterized according to their track (storm path), track heading direction, central pressure deficit, radius of maximum winds, and forward translation speed. Marginal (or conditional) distribution functions are fitted to these TC atmospheric parameters. These parameters' marginal distributions and dependencies form a multivariate probability distribution. Multiple parameter combinations are extracted to efficiently cover the plausible range of the storm parameter and probability spaces. Each of these parameter combinations constitutes a synthetic TC. Discrete

storm weights (DSW) are computed for the resulting synthetic TC suite by discretizing the multivariate probability distribution, which along with the magnitudes of the predicted storm responses, represents the joint probability model. Finally, the DSW are integrated over the range of storm responses to develop the hazard curves (i.e., response magnitude as a function of AEF).

The CHS database includes PCHA results currently encompassing more than 4,300 synthetic TCs, hundreds of extratropical cyclones (XC) (for regions of the coast that experience XC), and multiple future SLR scenarios, totaling more than 15,000 unique high-resolution numerical hydrodynamic simulations resolving nonlinear interactions between storm surge, wind waves, astronomical tide, and sea-level rise. The CHS ensures accurate, robust, and consistent quantification of coastal hazards along all Atlantic, Gulf of Mexico, and Great Lakes coastlines of the United States, thus facilitating nationwide coastal storm risk management and resilience strategies. CHS data also support individual feasibility studies, economic analyses, evaluation of nature-based features, stochastic engineering design, and risk assessments. The CHS PCHA framework's primary goal is to address the limitations of the JPM and derived optimal sampling (OS) approaches, which are discussed in the following sections.

2.1 Joint probability method (JPM)

The joint probability analysis of storm surge and waves from TCs, in most cases, suffers from a lack of historical observations resulting in small sample sizes. Moreover, some of the characteristics of the TCs that impact a particular area may make it necessary to consider them as belonging to different subpopulations, further reducing the already small sample sizes. The JPM addresses these limitations by characterizing the atmospheric forcing of storms instead of their responses. In broad terms, TCs are defined by several forcing parameters and corresponding probability distribution functions (PDFs), which are discretized to generate the wind and pressure fields required to simulate storm surge and waves. Typical TC parameters include track reference location, track heading direction, central pressure deficit, radius of maximum winds, and forward translation speed.

The JPM has become a standard joint probabilistic model for estimating coastal storm hazards in hurricane-prone areas. Gonzalez et al. (2019)

summarized the development and evolution of the JPM, and a brief synopsis is provided here. Early characterization and probabilistic analyses of individual hurricane parameters were performed by Myers (1954). The precursor of the JPM was pioneered in the late 1960s (Russell 1968a, 1968b) using a full Monte Carlo simulation to estimate probabilities of wind, storm surge, and wave loads on offshore structures. In the 1970s, National Oceanic and Atmospheric Administration (NOAA) further developed and adapted the JPM for hurricane climatology and probabilistic storm surge studies in the US Atlantic and Gulf of Mexico coastal areas (e.g., Myers 1970, 1975; Ho 1974; Ho and Myers 1975). The total annual frequency of a given water level was determined by adding the frequencies of landfalling TCs, bypassing TCs, and XCs. By the late 1980s, FEMA had adopted the JPM (FEMA 1988) as presented in the National Weather Service report NWS-38 (Ho et al. 1987).

Although the JPM approach has been implemented since the 1970s, recent advancements in sampling techniques and the development of the JPM with optimal sampling (JPM-OS) made it possible to reduce the necessary number of synthetic storms, more efficiently characterizing the parameter and probability spaces. Different implementations of the JPM emerged from several studies conducted after 2005 following the devastation caused by Hurricane Katrina. These approaches and their application are discussed in the following sections.

2.2 Joint probability method with optimal sampling (JPM-OS)

The destruction caused by Hurricane Katrina in 2005 led to the proliferation of storm surge hazard studies that brought further improvements to the JPM. Of particular importance was the work done by the IPET (2009), in which JPM-OS approaches were developed for the statistical analysis of extreme water levels to evaluate the performance of the Southeast Louisiana hurricane surge protection system. The IPET provided the basic framework for storm surge modeling approaches used in later works. This effort, led by a team of USACE, FEMA, NOAA, private sector, and academic researchers, was documented in the IPET report. These JPM-OS developments aimed to reduce the number of storms required for populating the parameter space without sacrificing resolution and accuracy relative to the probability space.

JPM variants labeled as *OS* include the JPM by Bayesian Quadrature (JPM-OS-BQ) and the JPM with augmented sampling using a Response Surface (JPM-OS-RS). In practice, the optimal sampling, and thus the reduction in the number of storms, is accomplished by either (1) expert selection of TC parameter combinations (e.g., JPM-OS-RS) or (2) trial-and-error sampling of a storm subset that closely matches target hazard curves produced by a much larger storm set simulated using a low-fidelity hydrodynamic model or a high-fidelity model with a coarse grid (e.g., JPM-OS-BQ). Applying these techniques in practice, the number of sampled storms generally decreases from tens of thousands of storms (denoted as the reference set) to a few hundred.

The JPM-OS-RS approach (Resio et al. 2007), as described in Toro et al. (2010a), requires careful selection of TC parameter combinations based on expert judgment. This selection should yield a moderate number of synthetic TC simulations used to construct a storm surge response surface. The TC parameter space is filled in by interpolating intermediate surge values from the response surface using a finer discretization primarily considering the Δp-R_{max} bivariate space. The surge response is assumed to have a small, linear variation along the θ-V_t space in this scheme. Storm surge values interpolated from the response surface have been shown to introduce uncertainty with a root-mean-square deviation on the order of 0.70 m (CPRA 2013). The JPM-OS-RS approach was applied to regional studies such as LACPR (USACE 2009c), the Mississippi Coastal Improvements Project (USACE 2009d), and the FIS for Coastal Counties in Texas (USACE 2011).

As stated in the Operating Guidance No. 8-12 document (FEMA 2012), FEMA's guidelines focused on the JPM-OS-BQ (Toro 2008) approach "since it is more readily automated than the [JPM-OS-RS], which requires a greater degree of expert judgment in the selection of storms." This acknowledgment made JPM-OS-BQ the de facto JPM approach of FEMA's National Flood Insurance Program (NFIP) Risk Mapping, Assessment, and Planning program. Beginning with the Mississippi Coastal Analysis Project (MCAP) (FEMA 2008), most FEMA studies to date have relied on this approach.

Reliance on choices made based on judgment is not unique to the JPM-OS-RS. The JPM-OS-BQ approach requires the development and simulation of a JPM storm set consisting of thousands or tens of

thousands of TCs to construct a *reference set* of storms and corresponding target hazard curves before conducting the storm sampling. The primary shortcoming of the JPM-OS-BQ approach is that, due to computational constraints, in practice, it must rely on either (1) low-fidelity hydrodynamic models that do not incorporate all physical processes or (2) models with coarse-resolution grids to efficiently simulate the storms that constitute the reference set.

Moreover, the JPM-OS-BQ employs a double-exponential covariance function (Toro et al. 2010a) as a pseudo dependence structure with correlation distances as inputs that dictate the discretization of the TC marginal distributions. As discussed by Niedoroda et al. (2010) and Toro et al. (2010a, 2010b), the Bayesian quadrature (BQ) correlation distances must be specified based on expert judgment. The JPM-OS-BQ sampling scheme consists of a trial-and-error process where various combinations of these correlation distances yield different storm sets. Each set's storm surge hazard curves are compared to the target hazard curves from the reference set at select locations within the study area. The end goal is to select the storm set that produces storm surge hazard curves with the smallest difference from the reference set. However, the reliability of the target hazard curves is unknown, particularly outside open water domains, and they potentially incorporate significant bias from the low-fidelity or coarse-grid simulations of the storm in the reference set. Another limitation of what is referred to as the OS approach is the lack of an actual joint probability model or consideration of joint probability distribution. In practice, TC parameters have been assumed to be independent, or pairs of TC parameters have been linked through simplified linear relationships.

In summary, the JPM-OS approaches initially adopted by federal agencies (e.g., BQ and response surface [RS]) include some limitations that have not been adequately documented and corrected. This report discusses how the CHS PCHA framework developed by USACE overcomes some of the previous JPM limitations, including lack of a dependence structure correlating the TC atmospheric-forcing parameters, optimal sampling scheme, dry-node correction of hydrodynamic results, and correction of geospatial bias and estimation of uncertainty.

2.3 The CHS Probabilistic Coastal Hazard Analysis (PCHA)

As part of the CHS, the USACE initially developed a version of the JPM with a hybrid optimal sampling approach for the NACCS (Cialone et al. 2015; Nadal-Caraballo et al. 2015) and the CTXS[1] (Melby et al. 2021). This hybrid JPM approach evolved into the PCHA framework by incorporating significant advancements that will be discussed later in this section. In addition to CHS-LA, the PCHA framework has been implemented in the three phases of the CHS-SACS: (1) Puerto Rico and US Virgin Islands[2], (2) North Carolina to Southeast Florida[3], and (3) Southwest Florida to Mississippi[4]. Although the application of the JPM can vary significantly by study, the different approaches typically follow a general methodology, depending on the dominant processes and respective solution strategies. The JPM methodology generally includes the following steps:

- characterization of historical storm climatology
- computation of historical storm recurrence rate (SRR)
- development of PDFs of historical TC atmospheric parameters
- discretization of PDFs of TC parameters
- development of synthetic TC suite
- atmospheric and hydrodynamic modeling of synthetic TC suite
- quantification of uncertainties (e.g., numerical model skill)
- integration of DSWs and responses to compute hazard curves (i.e., magnitude of response versus AEF).

The AEF of coastal hazards such as storm surge or waves at any given site is a function of three main components: the SRR, the joint probability of characteristic TC parameters, and the storm responses. Recent CHS studies, including CHS-LA, employ the form of the JPM integral without error term, since uncertainty is conveyed through non-exceedance

[1] Nadal-Caraballo, N. C., A. B. Lewis, V. M. Gonzalez, T. C. Massey, and A. T. Cox. 2019. *Coastal Texas Protection and Restoration Feasibility Study, Probabilistic Modeling of Coastal Storm Hazards*. Report submitted to USACE-SWG. Vicksburg, MS: US Army Engineer Research and Development Center.

[2] Nadal-Caraballo, N. C., M. C. Yawn, M. J. Torres, V. M. Gonzalez, E. Ramos-Santiago, T. C. Massey, A. A. Taflanidis, and A. T. Cox. In preparation. *Coastal Hazards System: Puerto Rico and the US Virgin Islands*. ERDC/CHL Technical Report. Vicksburg, MS: US Army Engineer Research and Development Center.

[3] Yawn, M. C., N. C. Nadal-Caraballo, M. L. Carr, E. Ramos-Santiago, V. M. Gonzalez, M. J. Torres, T. C. Massey, A. A. Taflanidis, and A. T. Cox. In preparation. *Coastal Hazards System: South Atlantic*. ERDC/CHL Technical Report. Vicksburg, MS: US Army Engineer Research and Development Center.

[4] Yawn, M. C., N. C. Nadal-Caraballo, M. L. Carr, E. Ramos-Santiago, V. M. Gonzalez, M. J. Torres, T. C. Massey, A. A. Taflanidis, and A. T. Cox. In preparation. *Coastal Hazards System: Gulf of Mexico*. ERDC/CHL Technical Report. Vicksburg, MS: US Army Engineer Research and Development Center.

confidence limits (CLs), as further discussed in Section 6.4. The AEF is computed from the JPM integral:

$$\lambda_{\tau_{max}>\tau} = \lambda \int P[\tau_{max}(\hat{x}) > \tau|\hat{x}]\, f_{\hat{x}}(\hat{x}) d\hat{x} \quad (2\text{-}1a)$$

$$\approx \sum_i^n \hat{\lambda}_i\, P[\tau_{max}(\hat{x}_i) > \tau|\hat{x}_i] \quad (2\text{-}1b)$$

where $\lambda_{\tau_{max}>\tau}$ = AEF of storm response τ due to the atmospheric-forcing vector $\hat{x} = f(x_o, \theta, \Delta p, R_{max}, V_t)$; λ = SRR (storms/year/km); and n = number of TCs. The expression $P[\tau_{max}(\hat{x}) > \tau|\hat{x}]$ represents the conditional probability that response $\tau_{max}(\hat{x})$ is greater than τ given $\hat{x}$. In the discrete form of the JPM integral (Equation 2-1b, $\hat{\lambda}_i$ is defined as the discrete storm weight of the i-th synthetic TC, where $\hat{\lambda}_i = \lambda p_i$, and p_i is the product of its discrete joint probability (i.e., normalized probability densities) and the spacing between synthetic storm tracks (in kilometers) defined in the JPM. The discrete storm weight, expressed in units of storms/year, is defined as the product of the SRR, storm probability densities, and track spacing. For this study, a track spacing of 60 km was applied for developing the synthetic TC suite.

The JPM integral with the error term, which is presented in Nadal-Caraballo et al. (2019), takes the following form:

$$\lambda_{\tau_{max}>\tau} = \lambda \int P[\tau_{max}(\hat{x}) + \varepsilon > \tau|\hat{x}, \varepsilon]\, f_{\hat{x}}(\hat{x}) f_{\varepsilon}(\varepsilon) d\hat{x} d\varepsilon \quad (2\text{-}2a)$$

$$\approx \sum_i^n \hat{\lambda}_i\, P[\tau_{max}(\hat{x}_i) + \varepsilon > \tau|\hat{x}_i, \varepsilon] \quad (2\text{-}2b)$$

where ε = the unbiased uncertainty of the storm responses; and the expression $P[\tau_{max}(\hat{x}) + \varepsilon > \tau|\hat{x}, \varepsilon]$ represents the conditional probability that $\tau_{max}(\hat{x}) + \varepsilon$ produces a response greater than τ given $\hat{x}$ and ε.

The TC atmospheric-forcing parameters commonly used in the JPM for the characterization of TCs and included in the forcing vector $\hat{x}$ are the following:

- track reference location (x_o)
- track heading direction (θ)
- central pressure deficit (Δp)
- radius of maximum winds (R_{max})
- forward translation speed (V_t).

The parameter x_o is characterized through the computation of SRR (Section 3.5). Subsequently, either a marginal or a conditional PDF is fitted to each of the remaining atmospheric-forcing parameters (i.e., θ, Δp, R_{max}, and V_t). This is done to adequately capture the likelihood of occurrence of each of these parameters according to historical hurricane records. The PCHA implements a hybrid approach for discretizing these PDFs. This hybrid sampling approach employs a structured discretization of the θ and Δp distributions to ensure (1) optimal coverage of the probability and parameter spaces, and (2) complete geospatial coverage of the study region. Discretization of R_{max} and V_t is performed by BQ method. Synthetic TCs are thus developed as likely combinations of the atmospheric-forcing parameters, as sampled from their respective PDFs. The parameters of the synthetic TCs are used as inputs to the planetary boundary layer (PBL) model to estimate the time histories of the wind and pressure fields that drive high-fidelity numerical hydrodynamic storm surge and wave models.

In conjunction with the common JPM steps previously listed in this section, the recent PCHA advancements included in this study are summarized as follows:

- characterization of storm climate and TC hazards at over 1,000 coastal reference locations (CRLs) along US hurricane-exposed coastlines
- use of GPM, a machine learning method, to fill in gaps in the HURricane DATa 2nd generation (HURDAT2) database (Landsea and Franklin 2013) and incorporate long-term estimates of R_{max}
- use of GPM for the development of an ATCS to achieve hyper-resolution of the TC forcing parameter space
- computation of an accurate joint probability model of TC forcing parameters through the use of meta-Gaussian copula (MGC) as the dependence structure, explicitly accounting for the correlation between TC parameters
- performance of dry-node correction (DNC) to fill in missing storm surge values
- correction of geospatial bias and estimation of uncertainty.

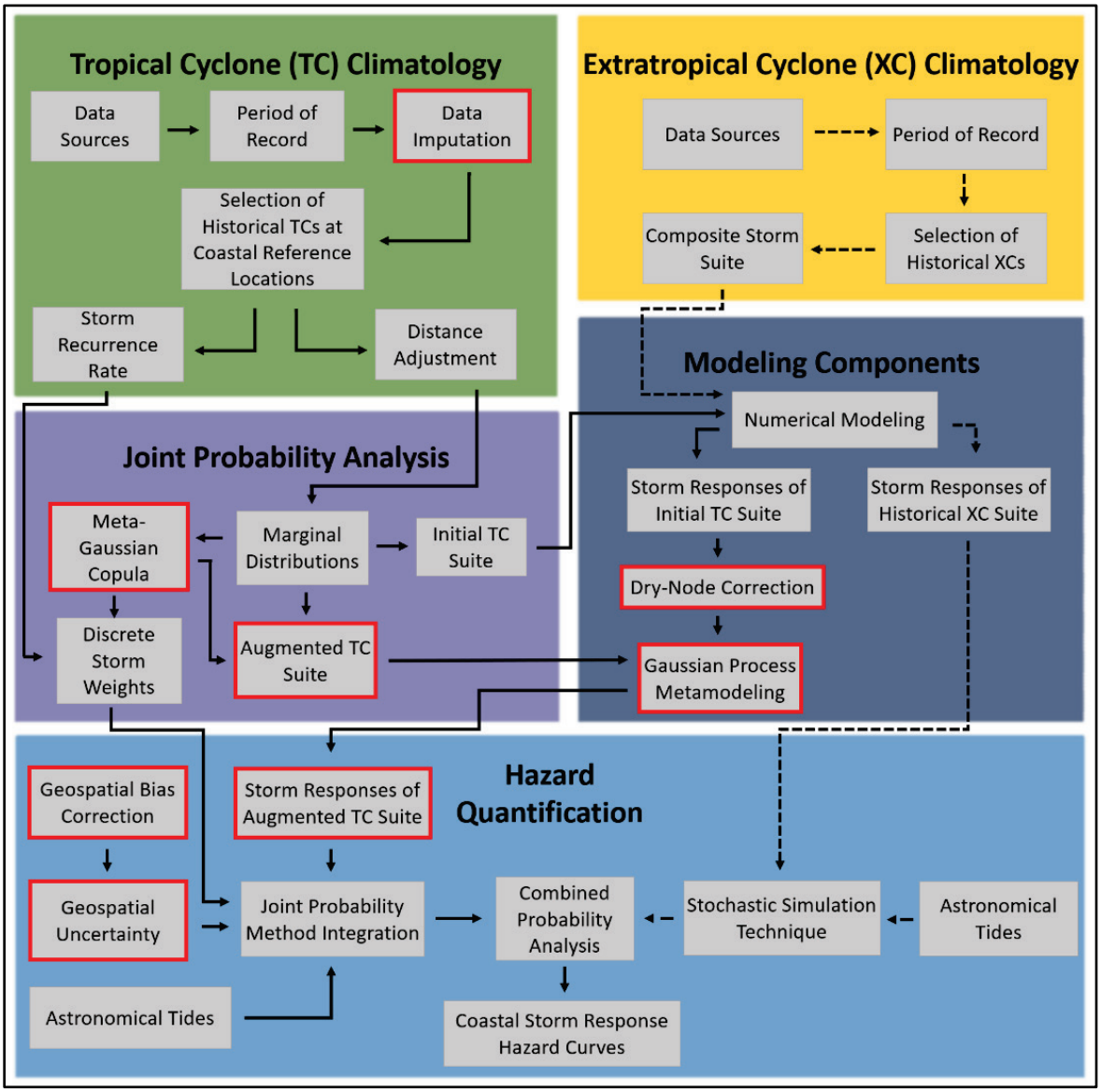
The interconnections of the main components of the CHS PCHA framework are illustrated in Figure 2-1. The PCHA-related advancements are represented in the diagram below as red-bordered boxes. In the

diagram, processes related to TCs are shown by solid arrows whereas dashed arrows illustrate XC processes.

The implementation of metamodeling technologies, such as the GPM (Jia et al. 2016; Zhang et al. 2018), is fundamental to the PCHA framework. A metamodel is first trained and applied within the PCHA to perform data imputation, which is a process to estimate missing TC parameter values and fill gaps in the HURDAT2 historical record. The primary function of the GPM, however, is the development of an ATCS consisting of tens of thousands to millions of synthetic TCs that retain the high-fidelity nature of the numerical simulation of the ITCS. The ATCS' finer discretization of the TC atmospheric-forcing parameter space made possible by GPM is coupled with the use of the MGC, which incorporates the dependencies between the TC parameters for a more accurate representation of the historical hurricane climatology. The metamodeling capabilities are then applied to predict storm responses (i.e., storm surge, waves) produced by the ATCS for the development of hazard curves. The GPM component of the PCHA framework supersedes the OS-RS approach previously developed by USACE, given the GPM's capability to explicitly use all storm forcing parameters as inputs and the higher accuracy of its predictions.

The PCHA introduced the DNC method to fill in missing storm surge information at dry nodes. DNC is performed either through the use of a geospatial GPM approach for sparse hydrodynamic data (e.g., at save points) or through the application of weighted *k*-nearest neighbor (*k*NN) regression in cases where hydrodynamic results are available at high geospatial resolution (e.g., ADCIRC nodes), such as in the CHS-LA study. The PCHA also applies a Gaussian kernel function (GKF) to assess geospatial model errors across all nodes to include uncertainty within the hazard curves.

Figure 2-1. Diagram of the CHS PCHA framework (Nadal-Caraballo et al. 2020).



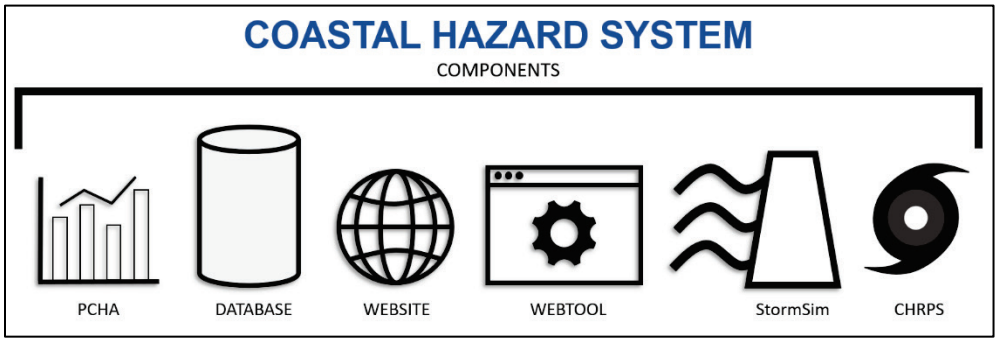
The PCHA introduced the DNC method to fill in missing storm surge information at dry nodes. DNC is performed either through the use of a geospatial GPM approach for sparse hydrodynamic data (e.g., at save points) or through the application of weighted *k*-nearest neighbor (*k*NN) regression in cases where hydrodynamic results are available at high geospatial resolution (e.g., ADCIRC nodes), such as in the CHS-LA study. The PCHA also applies a Gaussian kernel function (GKF) to assess geospatial model errors across all nodes to include uncertainty within the hazard curves.

The application of the PCHA components (Figure 2-1) to the CHS-LA study area is detailed in Sections 3 through 6. The *Tropical Cyclone (TC) Climatology* (green box) analysis is documented in Section 3, which details the storm recurrence analysis and distance adjustment of TC parameters from historical storms before developing the PDFs. The *Joint Probability Analysis* of the TC parameters (purple box), including the application of the MGC and the development of the ATCS, is discussed in Section 4. In Section 5, a detailed description of developing the meteorological *Modeling Components* (navy box) for input into the hydrodynamic models is provided (navy box). Section 6 (navy and light blue boxes) documents the postprocessing of the hydrodynamic modeling results and metamodeling development (navy box) and the *Hazard Quantification* (light blue box) including the application of the ATCS storm responses for developing hazard curves.

2.4 An integrated coastal hazards platform

The CHS is a national-scale effort for quantifying coastal hazards for US coastlines based on high-fidelity modeling and a cutting-edge statistical framework. Along with this framework, the CHS encompasses multiple components (Figure 2-2) including a webtool for accessing coastal hazards information, a website with documentation and metadata, the StormSim suite of tools for engineering applications, and the Coastal Hazards Rapid Prediction System (CHRPS) for real-time probabilistic and deterministic predictions of coastal storm hazards.

Figure 2-2. Components within the Coastal Hazards System (CHS).



The CHS stores and distributes high-fidelity coastal storm data from USACE and FEMA comprehensive regional studies. Modeling results and probabilistic coastal hazards data derived from the TC and XC simulations are converted into consistent and efficient, standard formats and stored in

a centralized system that is relatively easily maintained due to an innovative database architecture. The user-friendly web interface includes a multiaccess environment where the user can query data through a map interface or through a text-based navigation window or a combination of the two. The CHS website, shown in Figure 2-3, can be accessed at https://chs.erdc.dren.mil.

The CHS-LA numerical modeling and statistical analysis effort generated a large amount of data including probabilistic analysis and modeling results for the coastal region of Louisiana. These data and data products will serve the coastal engineering and coastal management communities for many years. Managing and providing access to this vast quantity of information is made possible via the CHS website and webtool. The data stored include comprehensive, high-fidelity, storm-response computer modeling results including synthetic storms, storm surge, SWL, wind, currents, and waves. Extremal statistics and uncertainties are also stored, and the data are easily accessed, mined, plotted, and downloaded through a user-friendly web interface (Figure 2-4 and Figure 2-5).

Figure 2-3. Screen capture of the CHS website.



Figure 2-4. Screen capture of the CHS webtool.

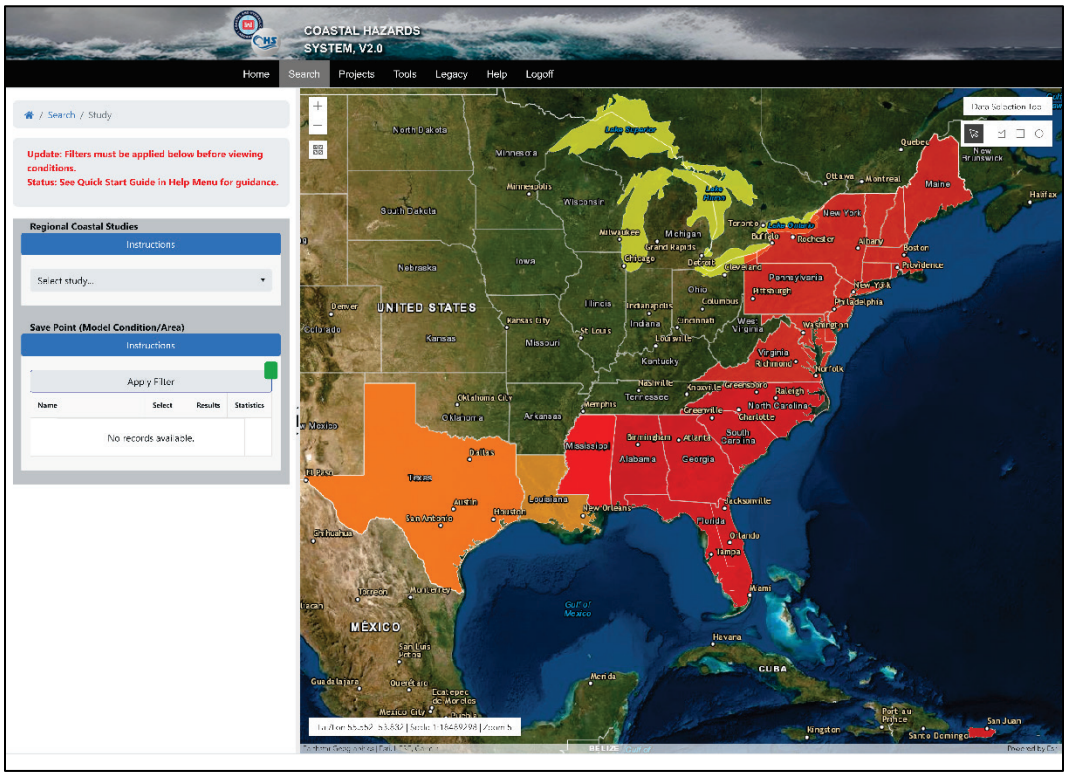
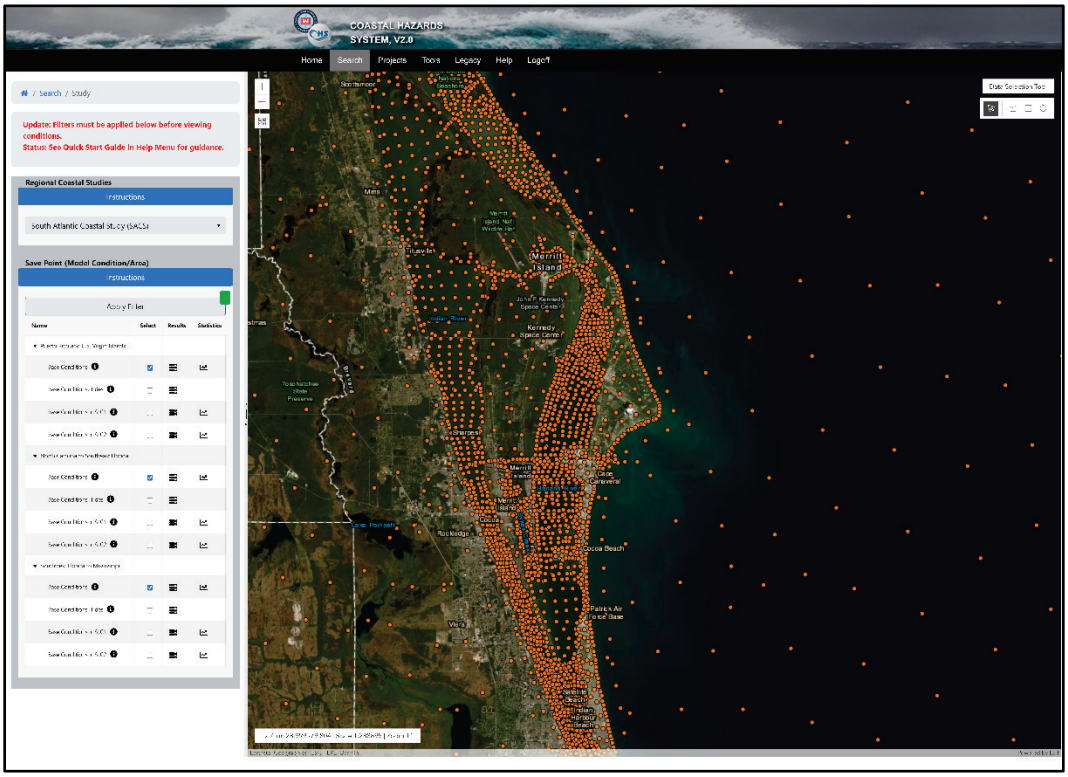


Figure 2-5. Screen capture of save points within the CHS webtool.



2.4.1 CHS-LA available data

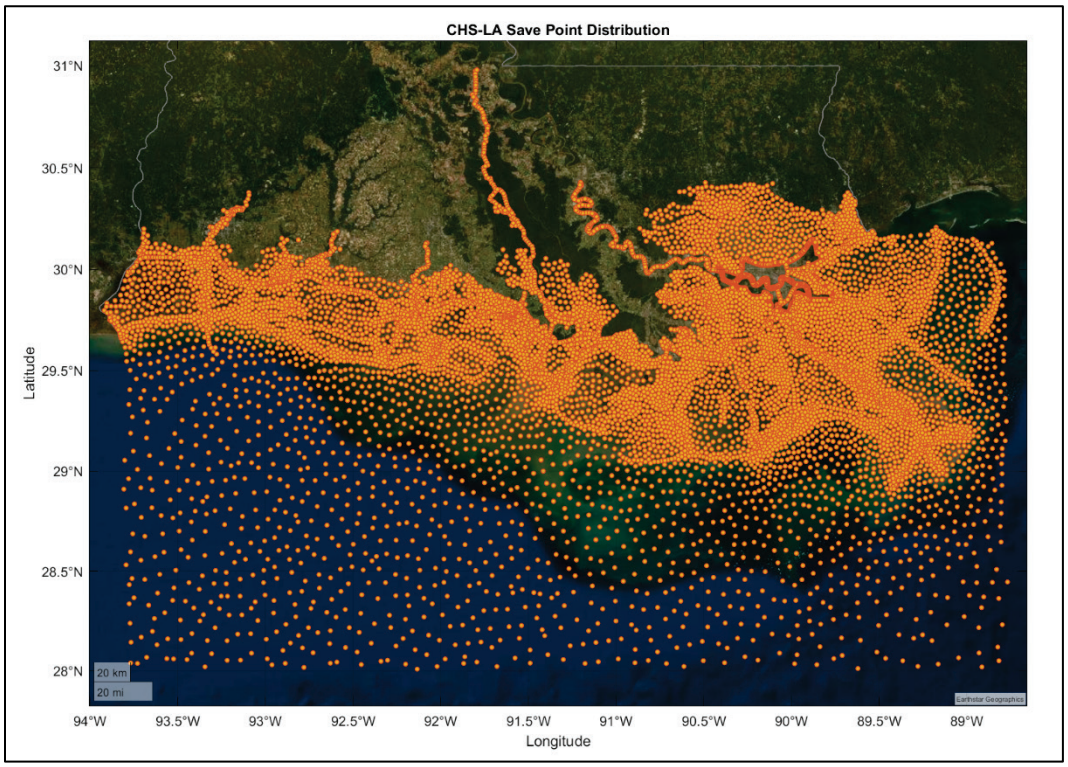
As discussed herein, the CHS data are comprehensive and span the practical probability space of the study regions. Following the completion of the hydrodynamic modeling and probabilistic analysis, the final data are stored and accessed by regional study within the CHS webtool. The types of data to be distributed for CHS-LA include the following:

- ADCIRC model output
- Simulating WAves Nearshore (SWAN) model output
- storm tracks and parameters
- discrete storm weights
- storm recurrence rates
- storm response statistics
- hazard curves
- uncertainty data.

Both time-varying and maxima data as well as statistics results are stored by save point location within CHS. For this study, the hydrodynamic responses and hazard curves were computed at more than 1.2 million node locations within the CHS-LA study area. To reduce the computational burden of hosting the nodal data in CHS, a set of 21,209 nodes was optimally selected to represent save point locations for storing and sharing the study results. These locations were selected using *k*-means clustering (MathWorks 2022) in MATLAB to establish an optimal set of locations distributed throughout the study area, while maintaining a high-resolution of save points near the HSDRRS. The distribution of the save point locations is illustrated in Figure 2-6. Responses for all storms for a specific save point are stored in a unique file. The CHS native file formats are self-describing compressed HDF5; however, the capability for online conversion to comma-separated values format exists within the CHS website.

Uncertainties, computed using the methods discussed in this report, are stored in files containing this data at the save points. Documentation for the system, data, and file formats is contained in easily accessible documents within the CHS Library.

Figure 2-6. Geospatial distribution of save points within the CHS-LA study area.



2.4.2 StormSim suite of tools

StormSim is a suite of tools that addresses a wide range of federal needs including applications within coastal research, emergency management, coastal planning, and coastal engineering. The StormSim tool suite is a collection of scripts related to hazard computations, engineering responses, stochastic simulations, and metamodeling, making them applicable to various research and engineering areas of interest. These tools were developed with the intent of accurately simplifying and automating the complex processes within the PCHA framework. The StormSim tools include

- StormSim-Storm Selection: storm selection methods for developing small-scale storm suites
- StormSim-JPM: quantification of tropical cyclone induced hazards through application of the JPM
- StormSim-SST: quantification of extratropical cyclone induced hazards using the extreme value analysis based Stochastic Simulation Technique (SST)

- StormSim-MCS/CSR: Monte Carlo simulations (MCS) for coastal structure life-cycle response analyses and coastal structure reliability (CSR)
- StormSim-PROS: response-based assessment of coastal structure threshold responses (e.g., Peaks, Runup, Overtopping, and Stone sizing [PROS]) using peak storm parameters.

The tools readily apply regional study data available through the CHS such as the AEFs of coastal storm hazards and peak storm responses from the hydrodynamic simulation results. The development of the StormSim software system is an ongoing effort that has been funded through USACE Flood and Coastal Systems Research and Development program.

3 Characterization of Storm Climatology

Louisiana's coastlines are frequently subjected to coastal flooding due to hurricanes or TCs. As previously discussed, the characterization of historical TCs for statistical analysis of coastal storm hazards is based on the primary TC parameters accounted for in the JPM: x_o, θ, Δp, R_{max}, and V_t. In this report, the definition of track and landfall conforms to that used within the HURDAT2 database. The TC track is defined as the center of the eye, which is defined as the location of minimum central pressure within HURDAT2. Landfall occurs when the track crosses the coastline, where the coastline is defined as the interface between mean-sea-level (MSL) and land. An idealized coastline defined by CRLs was constructed from NOAA's National Geophysical Data Center data.

The following section describes the climatological data sources used in this study, period of record considered, selection of historical TCs, and the computation of geospatial SRR.

3.1 Data sources

The screening of TCs refers to the identification of historical TCs for the computation of SRR, marginal probability distributions of TC parameters, and correlation of TC parameters. For TC screening, the primary data source was HURDAT2. HURDAT2 is a product of the NOAA's National Hurricane Center (NHC) Re-Analysis Project. It consists of the reanalysis of all historical TCs recorded in the North Atlantic basin (i.e., North Atlantic Ocean, Gulf of Mexico, and the Caribbean Sea) from 1851 to 2019 ([https://www.aoml.noaa.gov/hrd/hurdat/hurdat2.html]). Data for the 2020 hurricane season were collected from the Automated Tropical Cyclone Forecast (ATCF) System's Tropical Cyclone Database (https://www.nrlmry.navy.mil).

A significant limitation of HURDAT2 is the lack of R_{max} observations. The PCHA framework incorporates R_{max} from the extended best track (EBTRK) database (http://rammb.cira.colostate.edu) (Demuth et al. 2006). This database was created to supplement HURDAT2 best track data with storm structure information, including R_{max}. The EBTRK data set applied in this study covers the 1988 to 2018 time period. Table 3-1 lists the sources used in this study for the primary TC parameters.

3.2 Period of record for the PCHA

The period of record to be considered in the PCHA was assessed before selecting historical TCs. The SRR and the marginal distributions of TC parameters are sensitive to the historical record length. The 1940s decade marked the dawn of modern aircraft reconnaissance missions to measure hurricane parameters, resulting in much more reliable estimates of both storm characteristics, including frequency and intensity.

Before 1944, the primary data sources were land stations and ship reports, and it was typical for storm to go undetected (Jarvinen et al. 1984). After 1944 and due to World War II, aerial reconnaissance led to increased data collection incidence and measurement accuracy, including storm position, track, wind speed, and pressure. Satellite imagery was introduced during the 1964 hurricane season (Neumann et al. 1985) and was considered one of the significant advances in TC tracking (Jarvinen et al. 1984).

The undersampling of TCs before the 1940s has been well documented. Mann et al. (2007) estimated an undercount in the preaircraft reconnaissance era (1870–1943) ranging from 0.5 to 2.0 TC/yr, with a mean of 1.2 TC/yr. Landsea et al. (2010) argued that the increase in reported TCs during the 1940s and until approximately 1960 had been interpreted as a result of climate change. This increase, however, is likely the result of improved observing and recording of short-lived TCs with the advent of aircraft reconnaissance and satellite imagery.

Worley et al. (2005) identified fewer recorded moderate- to long-track TCs during the 1910s and 1940s due to reduced ship observations during World War I and World War II, respectively. Vecchi and Knutson (2011), after adjusting HURDAT data for unrecorded TCs, concluded that the mid-twentieth century was a high-activity period that extended from the 1940s to the 1960s.

A review of technical literature indicates that although the 1940s decade saw improvements in the observation and recording of TCs, there was still a significant undercount of events during this period. In recent flood hazard studies where the JPM-OS methodology was used, the period of record that was considered in the analysis started in the early 1940s (FEMA 2008, 2012; Resio et al. 2007). The NACCS performed by the USACE for the Virginia to Maine coastline used a period of record from

1938 to the present corresponding to a few years before the dawn of Hurricane Hunter aircraft reconnaissance missions to capture The Great New England Hurricane of 1938. Therefore, due to concerns of TC undercount before the 1940s and climatic nonstationarity, the PCHA framework avoids these issues by using the period of record from 1938 to 2020 for the computation of geospatial SRR (Section 3.5) and directional SRR (DSRR) (Section 4.1.4).

Because of issues with data collection, data gaps are present within the HURDAT2 database. GPM techniques are also used in a data imputation process to estimate missing values and fill in the database gaps to overcome this limitation of missing values. The data imputation within the PCHA framework is completed with two main goals: (1) to fill in central pressure gaps in the HURDAT2 database and (2) to fill in R_{max} gaps in the EBTRK database. The metamodel trained to predict Δp is trained on the following input vector: $\hat{x}_{\Delta p} = f(lat, lon, W_{max}, V_t, \theta)$; where W_{max} = maximum sustained wind speed. Similarly, the metamodel trained to predict R_{max} considered the previous input vector, with the addition of Δp: $\hat{x} = f(lat, lon, W_{max}, \Delta p, Vt, \theta)$.

Examples of the reconstructed values for Δp and R_{max} are shown in Figures 3-1 through 3-4. These figures illustrate the performance of the GPM in filling in missing values of Δp and R_{max} during historical TCs. In each figure, the blue line and associated points indicate the values filled in by the GPM estimates as compared to the observed historical data points (red points).

Figure 3-1. Reconstruction of Δp for a 1938 historical TC using metamodeling techniques.

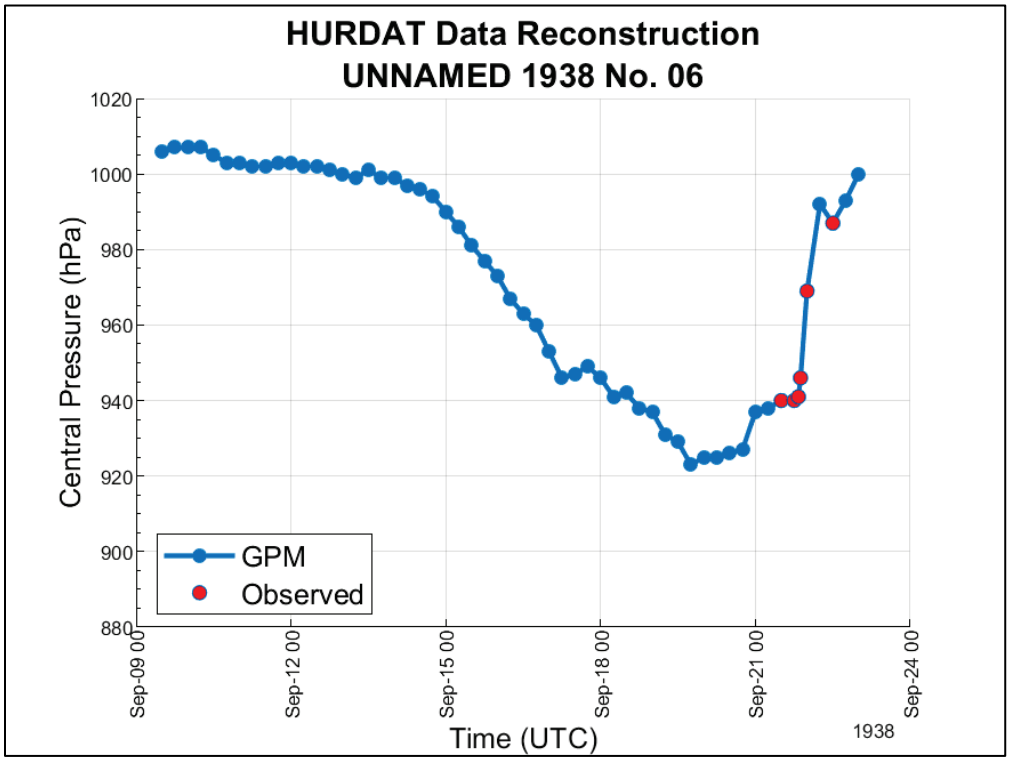


Figure 3-2. Reconstruction of Δp for Hurricane Sandy using metamodeling techniques.

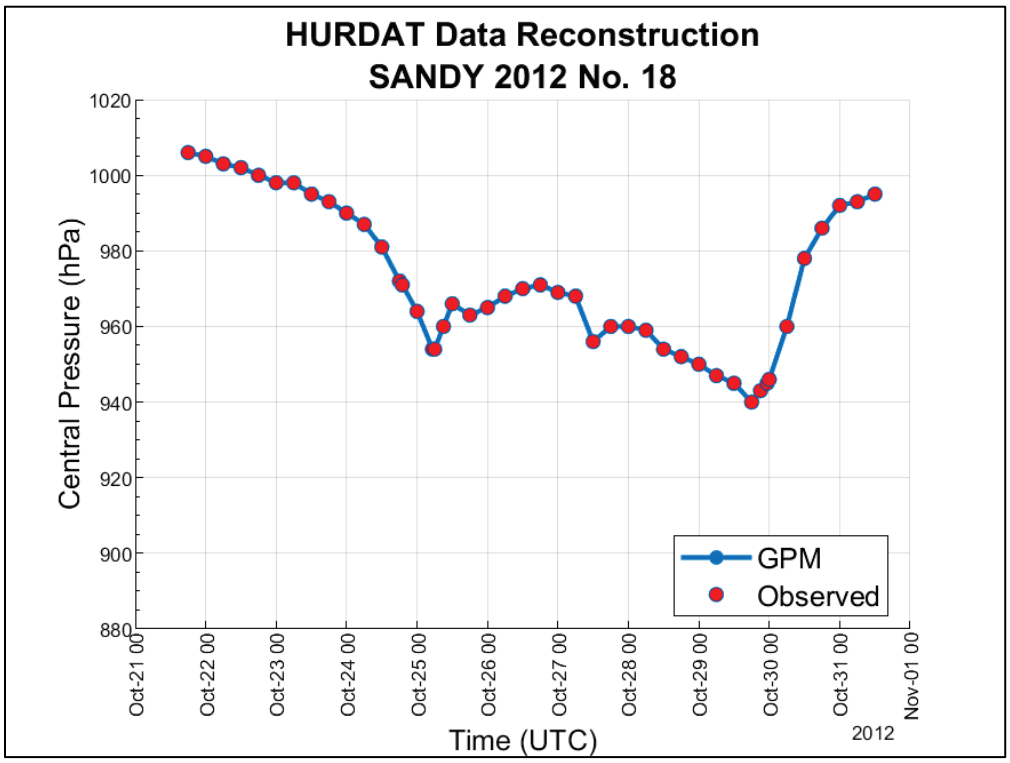


Figure 3-3. Reconstruction of R_{max} for a 1938 historical TC using metamodeling techniques.

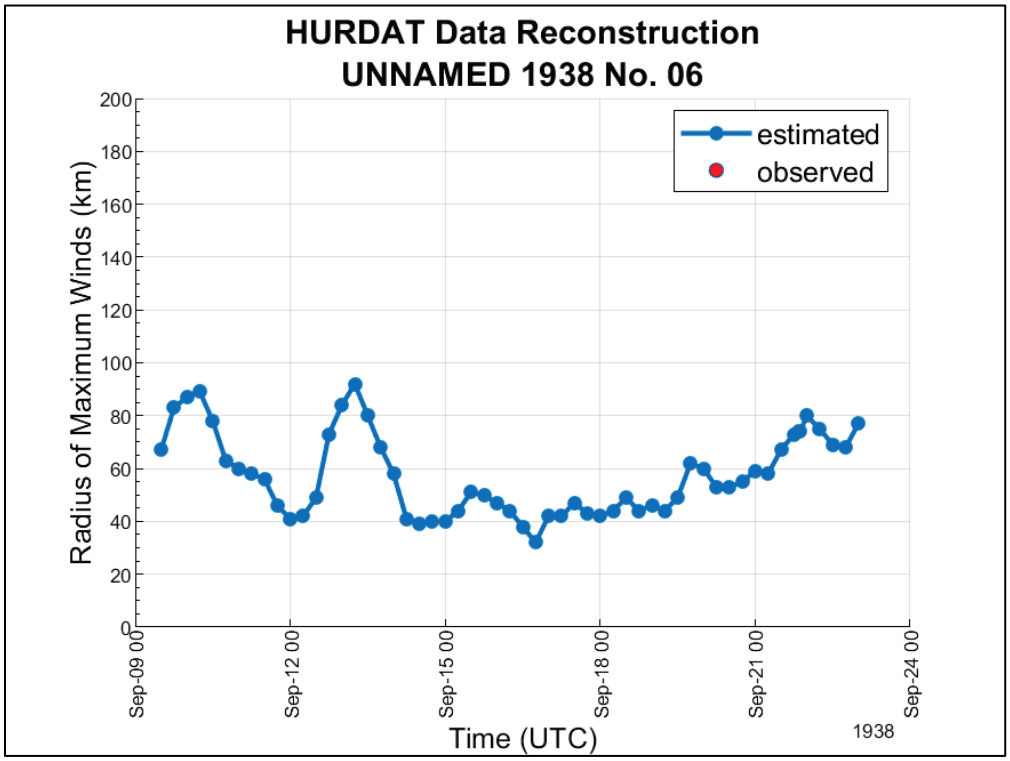
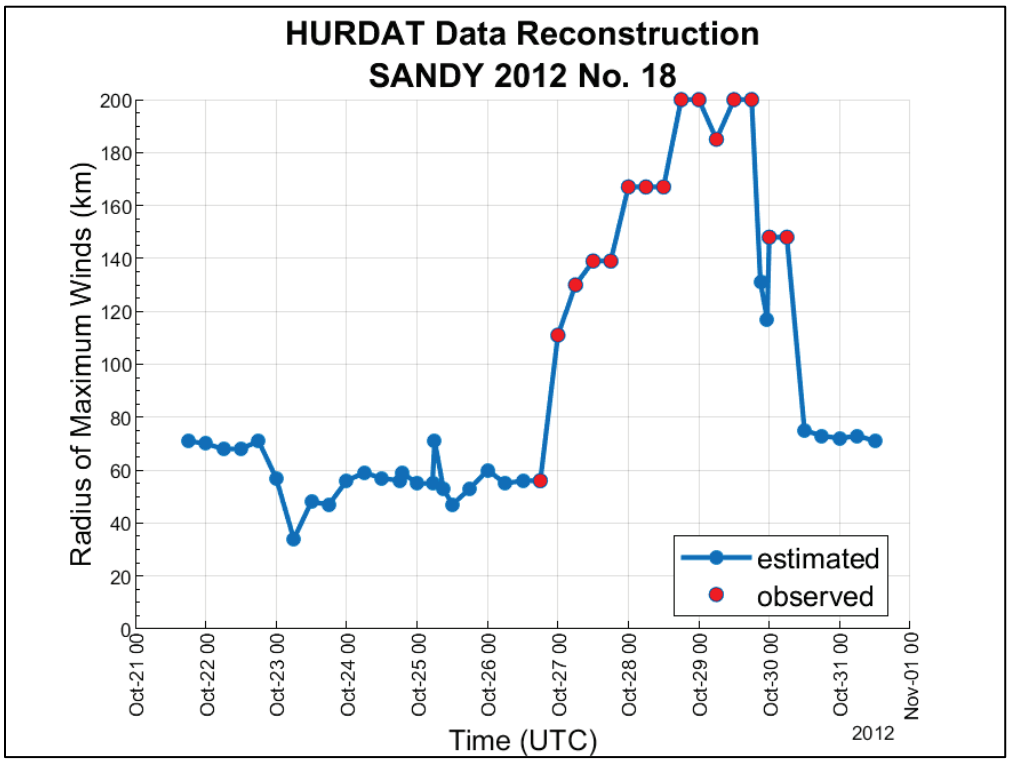


Figure 3-4. Reconstruction of R_{max} for Hurricane Sandy using metamodeling techniques.



After performing data imputation using GPM, gaps in Δp were filled for the entire HURDAT2 period of record from 1851 to 2019, including the ATCF TC data for 2020. Similarly, GPM was used to fill in gaps in the EBTRK data record to extend R_{max} values to the 1851–2020 period of record. However, due to concerns of nonstationarity and undercounting of TC occurrences, only TC data from the 1938–2020 period was considered to develop marginal distributions for the following TC parameters: Δp, V_t, θ, and R_{max}. Table 3-1 provides the period of record considered for each TC parameter.

Table 3-1. Period of record considered for each TC parameter.

Tropical Cyclone Parameter	Source and Availability	Period of Record Applied in PCHA
Track reference location	HURDAT2 (1851–2019) ATCF (2020)	1938–2020
Track heading direction	Estimated from HURDAT2 (1851–2019) ATCF (2020)	1938–2020
Central pressure deficit	HURDAT2 (1851–2019) ATCF (2020)	1938–2020
Forward translation speed	Estimated from HURDAT2 (1851–2019) ATCF (2020)	1938–2020
Radius of maximum winds	EBTRK (1988–2018)	1938–2020

3.3 Coastal reference locations (CRLs)

The quantifying coastal hazards for the CHS is completed on a national scale for the coverage of all hurricane-prone coastlines of the United States This requires the consistent characterization of storm climate to be conducted at a high geospatial resolution.

The PCHA characterizes the storm climate at points along an idealized coastline defined by a series CRLs. The average spacing between adjacent CRLs is 10 km. Additional CRLs are also positioned in offshore locations to characterize bypassing TCs in regions like the North Atlantic Coast, Puerto Rico, and the US Virgin Islands. These point locations mark where (1) the

SRR, (2) each TC parameter probability distribution, and (3) computation of the joint probability through the MGC are defined to characterize the storm climate at that given location. The network of over 1,000 CRLs allows for the computation of the DSWs at a high geospatial resolution.

For the contiguous United States (CONUS), 663 CRLs (IDs 1–663) have been established along an idealized coastline starting south of the Mexico-Texas boundary (23.5°N) and ending in northern Nova Scotia (45.0°N). The idealized coastline was constructed using data obtained from NOAA's National Centers for Environmental Information (https://www.ngdc.noaa.gov/mgg/shorelines). It can also be accessed directly through the Global Self-consistent, Hierarchical, High-resolution Geography Database (GSHHG) website (http://www.soest.hawaii.edu/pwessel/gshhg).

For offshore locations established for bypassing storms, 117 CRLs (identifiers (IDs) 664–780) were placed around the North Atlantic Coast from Virginia to Maine, and 65 CRLs were set off the southern tip of Florida (IDs 961–1025). For the Caribbean, 180 CRLs (IDs 781–960) were placed near Puerto Rico and the US Virgin Islands, for a total of 1,025 CRLs along the coastline and offshore. For this study area, only 108 CRLs (57–164) were used in the PCHA as they bounded the region covered by the synthetic TC tracks. Additional CRLs might be placed in the future to improve the geospatial resolution of the PCHA at particular locations. Figure 3-5 illustrates the current network of 1,025 CRLs (*red circles*), and Figure 3-6 shows the CRLs implemented in the PCHA for this study. In the following sections, examples of the PCHA framework will be illustrated at CRL 128 due to its location on the coastline and proximity to New Orleans. The location of CRL 128 relative to the study area is shown by the red point in Figure 3-6.

Figure 3-5. The idealized coastline of CRLs developed for the PCHA.

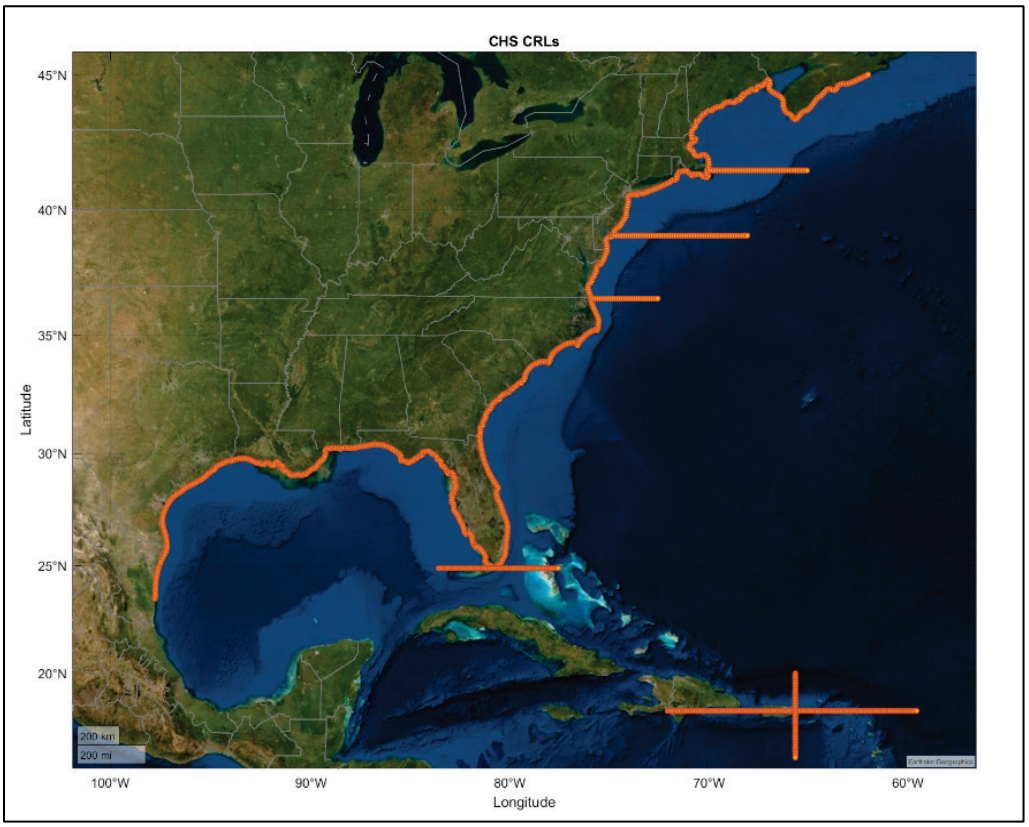
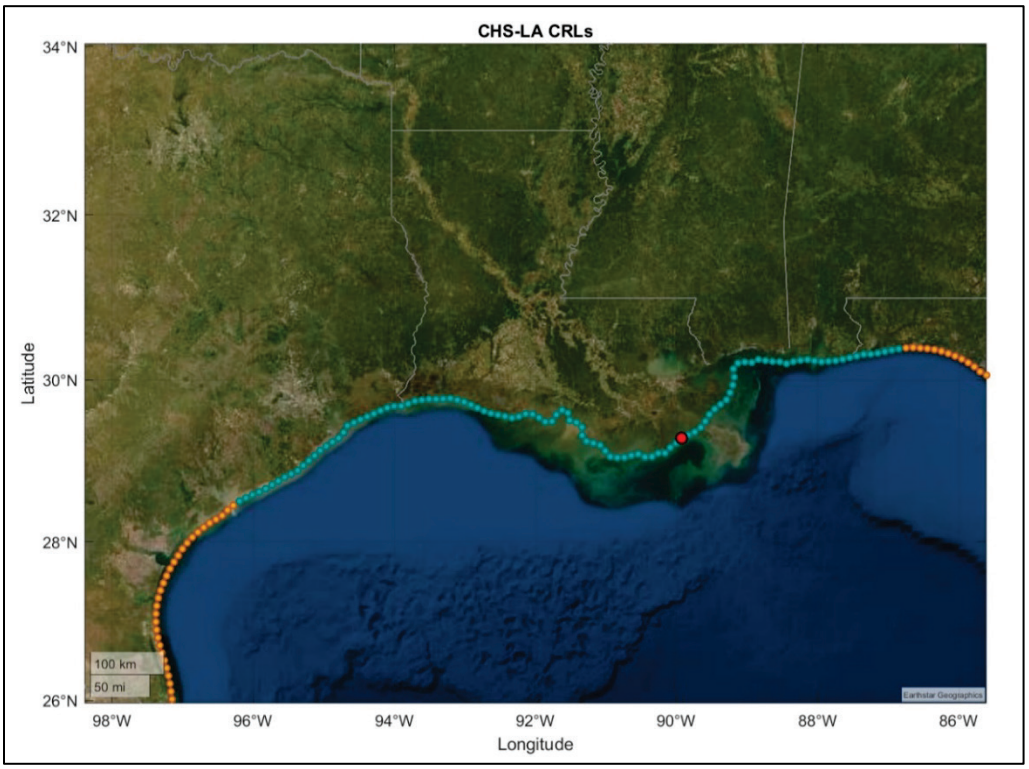


Figure 3-6. CRLs (*blue*) used in the PCHA for the CHS-LA study area.



3.4 Selection of historical tropical cyclones (TCs)

The probabilistic characterization of storm climatology for the CHS-LA study area requires sampling a set of storms from the historical record (i.e., HURDAT2, ATCF, EBTRK). The PCHA is then performed with this set of TCs as its basis, including the computation of SRR and the development of marginal distributions of individual TC parameters. The sampling of historical TCs for the SRR and the fitting of marginal distributions was limited to the 1938–2020 period.

In the PCHA framework, TCs are sampled on a per CRL basis. TCs with $\Delta p \geq 8$ hPa within 600 km of a CRL are selected and assigned to that specific CRL. Note that Δp is computed as the difference between a far-field atmospheric pressure of 1,013 hPa and the TC minimum central pressure (c_p) (FEMA 2008). The sampling process is repeated for each of the CRLs. For CHS-LA, the tracks of the 645 synthetic storms lie between CRLs 57–164. Therefore, these CRLs were used to select historical TCs and characterize the climatology within the CHS-LA region.

For the selected TCs, an assessment of track data points is performed to identify the closest point of highest intensity to each CRL using Equation 3-1. All track points within a 600 km radius of each CRL are evaluated for each TC to select the most influential track location considering both TC intensity and distance from the CRL. The intensity index function (Nadal-Caraballo et al. 2015) is applied to determine the optimal sampling location along each track:

$$I_{\Delta p_i} = w(d_i)\Delta p_i \tag{3-1}$$

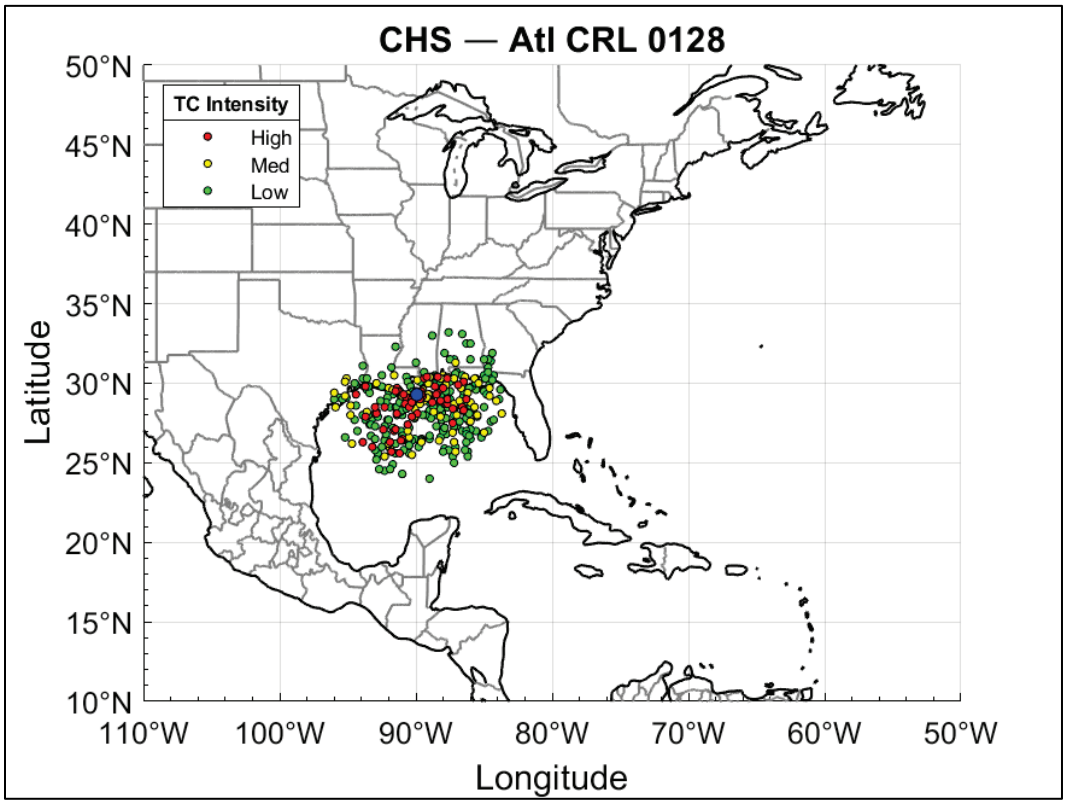
where $I_{\Delta p_i}$ = TC intensity index for a given TC, computed at all track points within 600 km of a particular CRL; Δp_i = central pressure deficit at individual track points; $w(d_i)$ = distance-adjusted Gaussian weights from the GKF method developed by Chouinard and Liu (1997); d_i = distance from the location of interest (CRL) to a track point (kilometer).

The distance-adjusted Gaussian weights were calculated considering the distance between TC track points and each CRL as follows:

$$w(d_i) = \frac{1}{\sqrt{2\pi}h_d} exp\left[-\frac{1}{2}\left(\frac{d_i}{h_d}\right)^2\right] \tag{3-2}$$

where h_d = optimal kernel size (kilometer). The optimal kernel size applied in the study was 200 km, consistent with the value selected from numerical experiments described in Nadal-Caraballo et al. (2019). In the PCHA, each CRL within the boundaries of the study area has its own set of sampled storms. For each CRL, the most influential track location is identified in the probabilistic analysis as the point along each TC track with the largest $I_{\Delta p_i}$. This approach results in a storm sampling approach consistent with the GKF method and balances the distance from the historical TC track to CRL with the TC intensity. It also avoids bias that could have been introduced if sampling was limited to the track point with the shortest geospatial distance to the CRL. Considering CRL and TC track pairs, the track point with the shortest distance to the CRL will generally be selected unless one of the following closest track points (with similar distance) has significantly higher intensity, in which case the latter will be chosen. The R_{max}, V_t, and θ were identified from this optimal sampling location for the marginal distribution development. Figure 3-7 shows the sampling location for TCs selected for CRL 128. Further discussion on using a kernel size of 200 km and sampling storms within 600 km of each CRL is provided in Section 3.5.

Figure 3-7. Optimal sampling locations of selected historical TCs within 600 km of CRL 128.



After the historical TCs are selected, they are partitioned into three bins, according to their intensity:

- Low intensity (LI); $8 \le \Delta p < 28$ hPa
- Medium intensity (MI); $28 \le \Delta p < 48$ hPa
- High intensity (HI); $\Delta p \ge 48$ hPa.

Partitioning TCs into low, medium, and high-intensity bins is primarily done to account for potential differences in the correlation of pairs of atmospheric-forcing parameters between intense and weak cyclones. The PCHA seeks to represent the categories defined by the Saffir-Simpson Hurricane Wind Scale (SSHWS) (NHC 2022) using these three bins. Regarding the wind speed categories established by the SSHWS, the LI bin captures TCs of tropical storm intensity whereas the MI bin contains Category 1 and 2 hurricanes. Category 3 through 5 hurricanes are captured by the HI bin. Note that historical TCs represent more variability in intensity than the defined bins.

3.5 Geospatial storm recurrence rate (SRR)

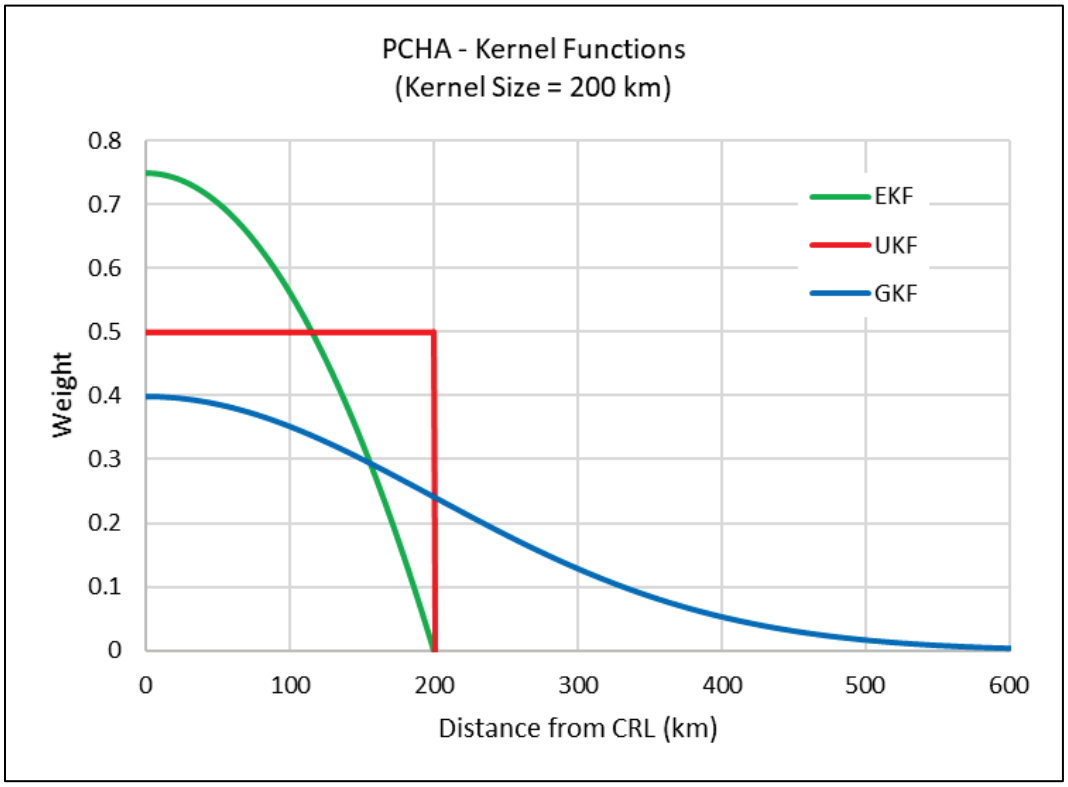
Efficient TC sampling from the historical record and statistical computation of SRR can be achieved through several different approaches. In recent studies, some of the techniques used to compute the geospatial variation of SRR have included area-crossing, line-crossing, GKF, and other combined methods. Area-crossing and line-crossing are examples of capture zone methods. In the area-crossing approach, only storms passing through a particular area are counted in the computation of the SRR. The line-crossing approach usually consists of an idealized coastline or a reference line representing a segment of the coastline. Only storms making landfall along the chosen segment of the coastline are captured and counted towards the computation of the SRR. The SRR is the single most significant parameter in the JPM and PCHA framework as it describes the expected annual recurrence of storms at the CRLs.

Capture zones can also be defined in other ways, such as a rectangular or circular window or any other finite geospatial region. In past studies, the standard was to apply any capture zone method to count the storms and assign uniform weights to all captured storms. The main limitation of the capture zone approach is that, while all storms within the chosen capture zone are given uniform weights, storms outside this zone are given a

weight of zero. The problem lies in establishing a capture zone sufficiently large to minimize uncertainty associated with reduced sample sizes but small enough to reduce uncertainty related to geospatial variability and population heterogeneity.

Nadal-Caraballo et al. (2019) conducted an extensive evaluation of different methods for the computation of SRR, including GKF, uniform kernel function (UKF), and the Epanechnikov kernel function (EKF). The curves of distance-adjusted weights for the UKF, GKF, and EKF with a kernel size of 200 km are shown in Figure 3-8. The curves are shown relative to the weight of a TC track point located at the CRL (distance = 0 km). All three kernel functions decrease with distance from the CRL, as expected. The weights of both UKF and EKF fall to zero when the distance reaches the kernel size of 200 km. On the other hand, the GKF weight decreases following the well-known bell shape, decreasing almost to zero at a distance of 600 km and extending indefinitely.

Figure 3-8. UKF, GKF, and EKF weights as a function of distance from CRL.



The study by Nadal-Caraballo et al. (2019) also found that the line-crossing approach can lead to underestimating the hazard due to its exclusion of bypassing events. The area-crossing method was treated as a particular case of the kernel approach through the application of the UKF. A significant advantage of the GKF is that it can consider a more substantial number of storms than the capture zone approach and the EKF. For the same ranges of optimal capture zone radii and Gaussian kernel sizes, the GKF SRR estimates exhibited a reduced coefficient of variation compared to UKF estimates. The GKF was deemed to be the best method to be used for conducting the SRR computational experiments.

As discussed above, the GKF method, developed by Chouinard and Liu (1997), can overcome the main limitations of capture zone approaches. The standard application of the GKF consists of establishing a grid of nodes where estimates of the SRR are sought. All storms within this gridded space can be counted at any given node, but the weight assigned to each storm decreases with increasing distance from storm to node. The GKF SRR equation, with $w(d_i)$ = Gaussian distance-adjusted weights given by Equation (3-2), has the form

$$\lambda = \frac{1}{T}\sum_i^n w(d_i) \tag{3-3}$$

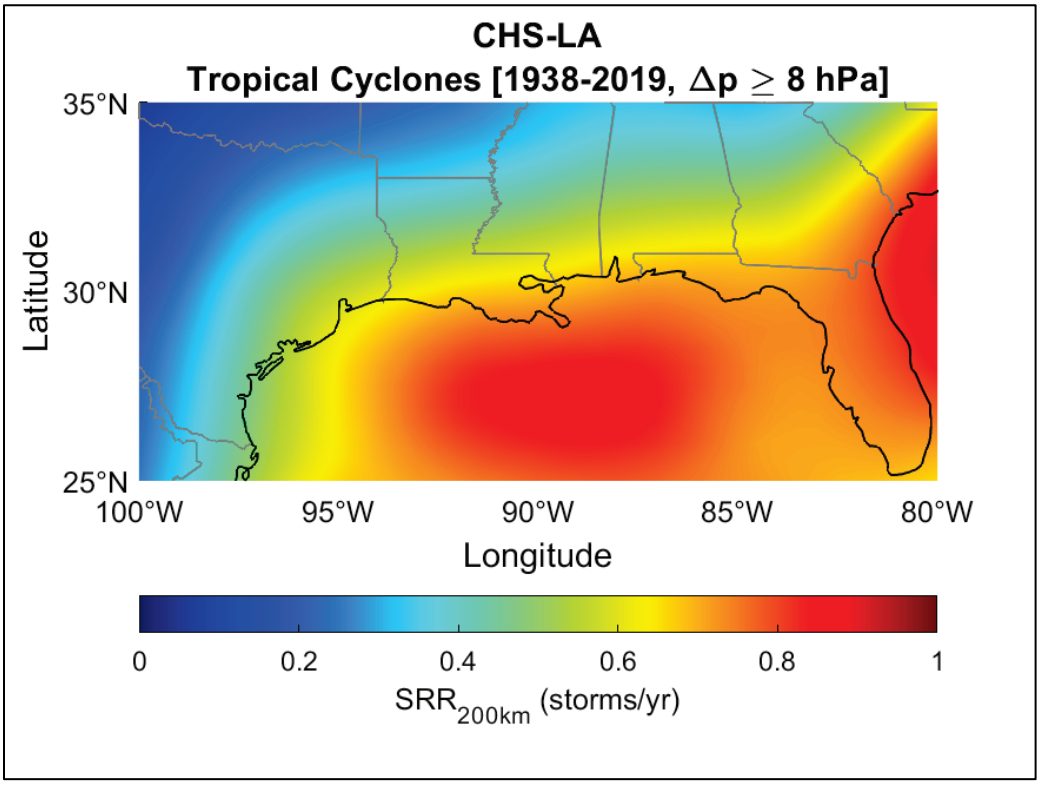
where λ = SRR in storms/yr/km; T = record length in (yr); d_i = distance from location of interest (e.g., CRL) to a track point (km). Using the GKF weights minimizes sample size uncertainty by taking full advantage of all available storm data while significantly reducing the uncertainty associated with geospatial variability and potentially heterogeneous populations.

The PCHA conducted for CHS-LA adopted an optimal kernel size of 200 km, similar to previous studies such as the CTXS[1] and the CHS-

[1] Nadal-Caraballo, N. C., A. B. Lewis, V. M. Gonzalez, T. C. Massey, and A. T. Cox. 2019. *Coastal Texas Protection and Restoration Feasibility Study, Probabilistic Modeling of Coastal Storm Hazards*. Report submitted to USACE-SWG. Vicksburg, MS: US Army Engineer Research and Development Center.

SACS[1,2,3]. Since the kernel size is representative of a standard deviation, TCs were sampled at a distance of 3 standard deviations, or 3*h_d. In previous studies such as NACCS, a distance of 800 km was chosen for sampling landfalling storms. However, further evaluations have shown that no measurable differences in SRR are observed between 600 km and 800 km sampling radius. This study will subsequently use a sampling distance of 600 km to calculate SRR for each CRL. Table 3-2 summarizes the SRR results for all CRLs considered for CHS-LA. Additionally, Figures 3-9 through 3-12 illustrate the geospatial variance in SRR across the study area for each intensity bin. Note the scale applied to Figures 3-9 through 3-12 varies with the change in TC intensity.

Figure 3-9. Geospatial SRR for all TCs within the CHS-LA study area.



[1] Nadal-Caraballo, N. C., M. C. Yawn, M. J. Torres, V. M. Gonzalez, E. Ramos-Santiago, T. C. Massey, A. A. Taflanidis, and A. T. Cox. In preparation. *Coastal Hazards System: Puerto Rico and the US Virgin Islands.* ERDC/CHL Technical Report. Vicksburg, MS: US Army Engineer Research and Development Center.

[2] Yawn, M. C., N. C. Nadal-Caraballo, M. L. Carr, E. Ramos-Santiago, V. M. Gonzalez, M. J. Torres, T. C. Massey, A. A. Taflanidis, and A. T. Cox. In preparation. *Coastal Hazards System: South Atlantic*. ERDC/CHL Technical Report. Vicksburg, MS: US Army Engineer Research and Development Center.

[3] Yawn, M. C., N. C. Nadal-Caraballo, M. L. Carr, E. Ramos-Santiago, V. M. Gonzalez, M. J. Torres, T. C. Massey, A. A. Taflanidis, and A. T. Cox. In preparation. *Coastal Hazards System: Gulf of Mexico*. ERDC/CHL Technical Report. Vicksburg, MS: US Army Engineer Research and Development Center.

Figure 3-10. Geospatial SRR for HI TCs within the CHS-LA study area.

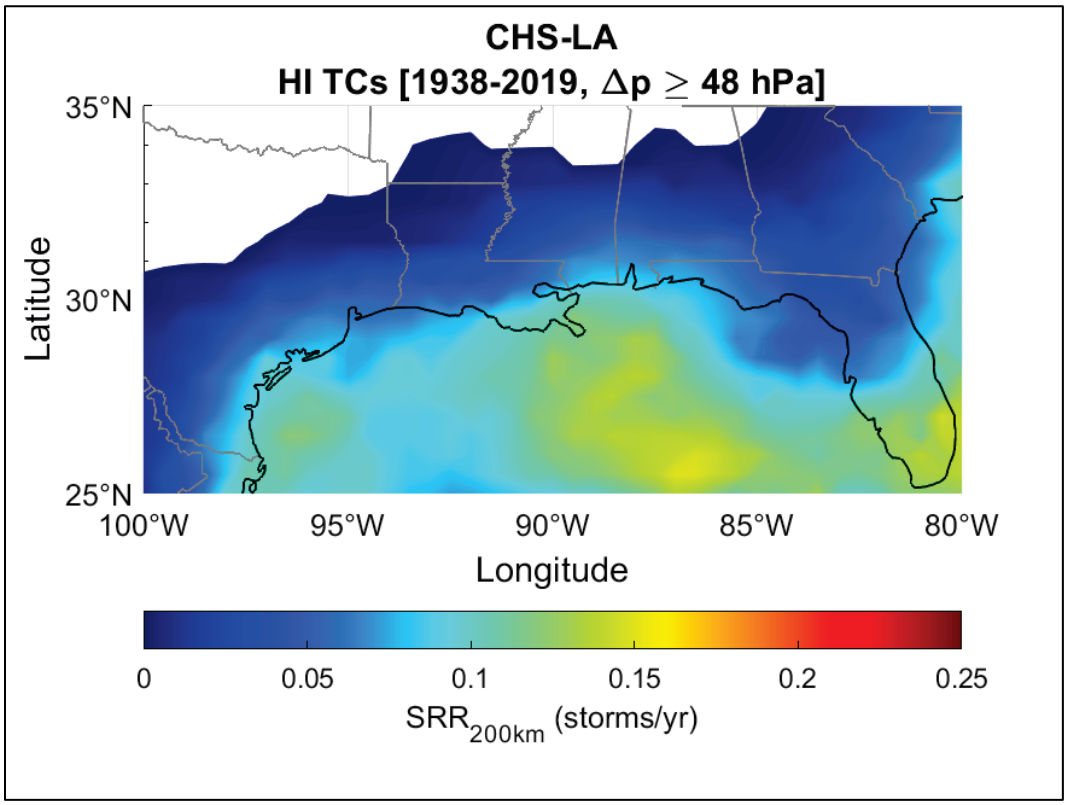


Figure 3-11. SRR for MI TCs within the CHS-LA study area.

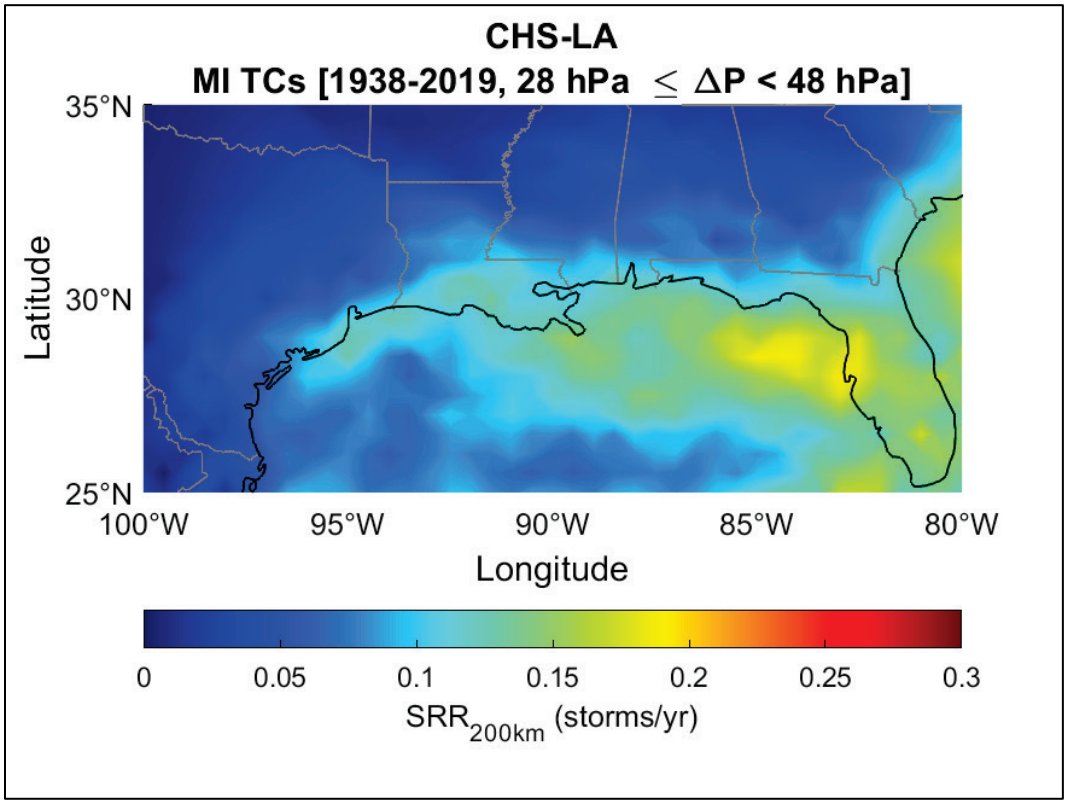


Figure 3-12. SRR for LI TCs within the CHS-LA study area.

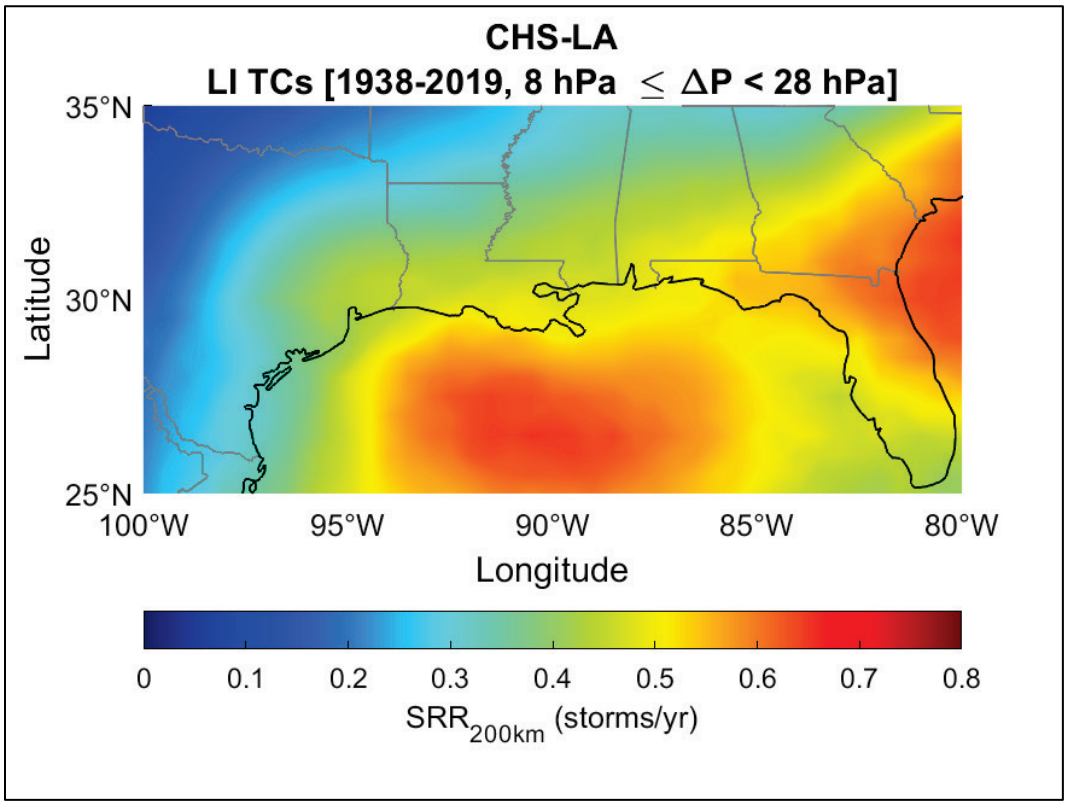


Table 3-2. SRR results for all intensity bins and CRLs in the CHS-LA study area.

CRL	SRR (storms/yr/km)			
	LI	MI	HI	Total
57	8.40E-04	2.49E-04	2.97E-04	1.39E-03
58	8.51E-04	2.47E-04	3.07E-04	1.40E-03
59	8.61E-04	2.76E-04	2.84E-04	1.42E-03
60	8.72E-04	2.82E-04	2.86E-04	1.44E-03
61	8.83E-04	2.87E-04	2.88E-04	1.46E-03
62	8.93E-04	2.92E-04	2.89E-04	1.47E-03
63	8.99E-04	3.00E-04	2.91E-04	1.49E-03
64	9.07E-04	3.20E-04	2.77E-04	1.50E-03
65	9.16E-04	3.26E-04	2.77E-04	1.52E-03
66	9.24E-04	3.31E-04	2.78E-04	1.53E-03
67	9.28E-04	3.35E-04	2.78E-04	1.54E-03
68	9.32E-04	3.39E-04	2.78E-04	1.55E-03
69	9.36E-04	3.42E-04	2.77E-04	1.56E-03
70	9.38E-04	3.45E-04	2.77E-04	1.56E-03
71	9.33E-04	3.56E-04	2.77E-04	1.57E-03

Table 3-2. (cont.) SRR results for all intensity bins and CRLs in the CHS-LA study area.

CRL	SRR (storms/yr/km)			
	LI	MI	HI	Total
72	9.37E-04	3.59E-04	2.77E-04	1.57E-03
73	9.40E-04	3.61E-04	2.77E-04	1.58E-03
74	9.38E-04	3.66E-04	2.74E-04	1.58E-03
75	9.32E-04	3.66E-04	2.73E-04	1.57E-03
76	9.35E-04	3.68E-04	2.74E-04	1.58E-03
77	9.39E-04	3.70E-04	2.76E-04	1.58E-03
78	9.43E-04	3.72E-04	2.77E-04	1.59E-03
79	9.41E-04	3.80E-04	2.78E-04	1.60E-03
80	9.66E-04	3.82E-04	2.56E-04	1.60E-03
81	9.69E-04	3.84E-04	2.56E-04	1.61E-03
82	9.74E-04	3.86E-04	2.57E-04	1.62E-03
83	9.82E-04	3.90E-04	2.58E-04	1.63E-03
84	9.85E-04	3.76E-04	2.74E-04	1.64E-03
85	1.02E-03	3.46E-04	2.74E-04	1.64E-03
86	1.03E-03	3.26E-04	2.98E-04	1.65E-03
87	1.03E-03	3.28E-04	2.98E-04	1.66E-03
88	1.03E-03	3.31E-04	3.07E-04	1.67E-03
89	1.05E-03	3.21E-04	3.07E-04	1.68E-03
90	1.06E-03	3.22E-04	3.08E-04	1.69E-03
91	1.07E-03	3.24E-04	3.09E-04	1.70E-03
92	1.10E-03	3.07E-04	3.09E-04	1.72E-03
93	1.11E-03	3.15E-04	3.04E-04	1.73E-03
94	1.13E-03	3.18E-04	3.04E-04	1.75E-03
95	1.14E-03	3.20E-04	3.03E-04	1.76E-03
96	1.17E-03	3.03E-04	3.03E-04	1.78E-03
97	1.19E-03	3.01E-04	3.03E-04	1.79E-03
98	1.21E-03	2.85E-04	3.04E-04	1.80E-03
99	1.20E-03	3.07E-04	3.05E-04	1.81E-03
100	1.20E-03	3.11E-04	3.05E-04	1.82E-03
101	1.20E-03	3.12E-04	3.05E-04	1.82E-03
102	1.21E-03	3.14E-04	3.05E-04	1.82E-03
103	1.19E-03	3.17E-04	3.27E-04	1.84E-03
104	1.21E-03	3.21E-04	3.28E-04	1.85E-03
105	1.21E-03	3.24E-04	3.28E-04	1.86E-03
106	1.19E-03	3.24E-04	3.27E-04	1.84E-03

Table 3-2. (cont.) SRR results for all intensity bins and CRLs in the CHS-LA study area.

CRL	SRR (storms/yr/km)			
	LI	MI	HI	Total
107	1.18E-03	3.27E-04	3.27E-04	1.84E-03
108	1.19E-03	3.30E-04	3.27E-04	1.85E-03
109	1.21E-03	3.33E-04	3.29E-04	1.87E-03
110	1.21E-03	3.37E-04	3.29E-04	1.88E-03
111	1.22E-03	3.41E-04	3.30E-04	1.89E-03
112	1.24E-03	3.43E-04	3.31E-04	1.92E-03
113	1.24E-03	3.65E-04	3.32E-04	1.93E-03
114	1.24E-03	3.69E-04	3.32E-04	1.94E-03
115	1.25E-03	3.76E-04	3.20E-04	1.95E-03
116	1.26E-03	3.80E-04	3.21E-04	1.96E-03
117	1.27E-03	4.04E-04	3.00E-04	1.98E-03
118	1.27E-03	4.07E-04	3.00E-04	1.98E-03
119	1.27E-03	4.10E-04	3.00E-04	1.98E-03
120	1.26E-03	4.12E-04	3.00E-04	1.98E-03
121	1.26E-03	4.14E-04	3.00E-04	1.98E-03
122	1.27E-03	4.17E-04	3.01E-04	1.98E-03
123	1.26E-03	4.20E-04	3.01E-04	1.99E-03
124	1.26E-03	4.27E-04	2.96E-04	1.98E-03
125	1.28E-03	4.09E-04	2.97E-04	1.98E-03
126	1.26E-03	3.76E-04	3.31E-04	1.97E-03
127	1.25E-03	3.76E-04	3.31E-04	1.96E-03
128	1.24E-03	3.77E-04	3.30E-04	1.95E-03
129	1.23E-03	3.79E-04	3.30E-04	1.94E-03
130	1.22E-03	3.80E-04	3.31E-04	1.93E-03
131	1.21E-03	3.81E-04	3.31E-04	1.92E-03
132	1.17E-03	4.05E-04	3.30E-04	1.91E-03
133	1.16E-03	4.05E-04	3.28E-04	1.89E-03
134	1.17E-03	3.82E-04	3.27E-04	1.88E-03
135	1.16E-03	3.83E-04	3.25E-04	1.87E-03
136	1.15E-03	3.83E-04	3.24E-04	1.86E-03
137	1.13E-03	3.86E-04	3.21E-04	1.84E-03
138	1.12E-03	3.91E-04	3.11E-04	1.82E-03
139	1.11E-03	3.89E-04	3.08E-04	1.81E-03
140	1.09E-03	3.87E-04	3.05E-04	1.78E-03
141	1.08E-03	4.09E-04	2.80E-04	1.77E-03

Table 3-2. (cont.) SRR results for all intensity bins and CRLs in the CHS-LA study area.

CRL	SRR (storms/yr/km)			
	LI	MI	HI	Total
142	1.08E-03	4.10E-04	2.79E-04	1.77E-03
143	1.08E-03	4.11E-04	2.78E-04	1.77E-03
144	1.08E-03	4.09E-04	2.76E-04	1.77E-03
145	1.09E-03	4.12E-04	2.76E-04	1.77E-03
146	1.09E-03	4.17E-04	2.75E-04	1.78E-03
147	1.09E-03	4.18E-04	2.74E-04	1.78E-03
148	1.10E-03	4.22E-04	2.73E-04	1.79E-03
149	1.10E-03	4.40E-04	2.54E-04	1.79E-03
150	1.10E-03	4.46E-04	2.52E-04	1.80E-03
151	1.10E-03	4.47E-04	2.48E-04	1.80E-03
152	1.10E-03	4.57E-04	2.47E-04	1.80E-03
153	1.11E-03	4.59E-04	2.45E-04	1.81E-03
154	1.11E-03	4.61E-04	2.44E-04	1.81E-03
155	1.13E-03	4.33E-04	2.48E-04	1.81E-03
156	1.14E-03	4.21E-04	2.46E-04	1.81E-03
157	1.14E-03	4.21E-04	2.44E-04	1.81E-03
158	1.14E-03	4.18E-04	2.42E-04	1.80E-03
159	1.14E-03	4.15E-04	2.41E-04	1.80E-03
160	1.14E-03	4.00E-04	2.54E-04	1.80E-03
161	1.14E-03	4.00E-04	2.51E-04	1.79E-03
162	1.14E-03	3.99E-04	2.48E-04	1.79E-03
163	1.14E-03	3.99E-04	2.45E-04	1.78E-03
164	1.14E-03	4.00E-04	2.42E-04	1.78E-03

3.6 Distance adjustment of historical TCs

JPM-OS studies in the Gulf of Mexico have often sampled TCs hundreds of kilometers away from a CRL simply because its track crossed an idealized coastline. For example, in previous studies, TCs making landfall near the Florida Keys have been sampled for CRLs as far away as Alabama or Mississippi. The geospatial and temporal occurrence of TCs is a natural stochastic process. Therefore, it is difficult to justify that a TC making landfall 500 km away from a Louisiana CRL is more relevant to the climatology of Louisiana's coastlines than a TC bypassing the CRL just 250 km out.

For this reason, the PCHA framework has adopted a normalization and distance adjustment process for the sampled historical TCs. As discussed in previous sections, all TCs within 600 km from each CRL are sampled and assigned to that particular CRL. Continuing with the example above, and analogous to the computation of SRR, a bypassing TC just offshore of a CRL in Louisiana should carry more weight relative to that CRL than a TC making landfall in Florida. Therefore, the concept of computing geospatial SRR through the application of GKF and distance weights is extended to the selected TCs. The GKF generates distance weights required to normalize the TC parameters. The goal is to transform the TC parameters so the sampled population reflects distance-weighted mean and standard deviation.

Z-score normalization is a common technique used by machine learning practitioners to adjust population parameters even if the populations are not normally distributed. The first step in the normalization of a TC parameter (x_i) (e.g., one set of values per TC taken at the optimal sampling location relative to CRL) is the computation of the mean (μ) and standard deviation (σ) of the parameter for the i-th sampled TC:

$$\mu = \frac{\sum_{i=1}^{N} x_i}{N} \tag{3-4}$$

$$\sigma = \sqrt{\frac{\sum_{i=1}^{N} (x_i - \mu)^2}{N-1}} \tag{3-5}$$

The normalized TC parameters (z_i) are determined through the basic z-score formula:

$$z_i = \frac{x_i - \mu}{\sigma} \tag{3-6}$$

The next step is the computation of the distance-weighted mean (μ_{DW}) and standard deviation (σ_{DW}) for each TC parameter:

$$\mu_{DW} = \frac{\sum_{i=1}^{N} w(d_i) x_i}{\sum_{i=1}^{N} w(d_i)} \tag{3-7}$$

$$\sigma_{DW} = \sqrt{\frac{\sum_{i=1}^{N} w(d_i)(x_i - \mu_{DW})^2}{\left(\frac{N'-1}{N'}\right)\sum_{i=1}^{N} w(d_i)}} \tag{3-8}$$

where $w(d_i)$ = distance weights computed using the GKF (Equation 3-2); x_i = individual parameter values of sampled TCs (e.g., one set of parameter values per TC taken at the optimal sampling location relative to a CRL); and N = number of sampled TCs, and $\acute{N}$= the number of sampled TCs with nonzero weights. Finally, the adjusted TC parameters (x'_i) are obtained from the following equation:

$$x'_i = z_i \sigma_{DW} + \mu_{DW} \tag{3-9}$$

The historical TCs sampled from the HURDAT2 data set within 600 km of CRL 128 (1938–2020 period), and their distance-adjusted atmospheric parameters are listed in Table A-3 of Appendix A.

4 Joint Probability Analysis of Coastal Storm Hazards

Most joint probability analyses of coastal storm hazards in hurricane-prone regions, including the PCHA, require the development of synthetic TC suites to cover the TC parameter and probability spaces adequately. Given that the PCHA framework builds on the JPM approach, it employs the same primary TC atmospheric-forcing parameters: track reference location (x_0), track heading direction (θ), central pressure deficit (Δp), radius of maximum winds (R_{max}), and forward translation speed (V_t). These TC parameters are required as inputs to the PBL model used to generate wind and pressure fields for each storm. The work described here consists of fitting TC parameter probability distributions and correlation analysis. The selection of a parametric or nonparametric probability distribution to characterize the likelihood of a given TC parameter is ultimately based on expert judgment. There is no single best solution.

Sections 4.1 and 4.2 describe the development of marginal probability distributions and correlation coefficients used in the joint probability model needed for estimating AEFs. The ITCS and ATCS developed for this study, and the computation of DSWs are documented in Sections 4.3 and 4.4.

4.1 Marginal distribution of TC parameters

The development of probability distributions was required to characterize the storm climatology for the construction of the CHS-LA synthetic storm suite. These distributions were developed from the HURDAT2 1938–2019 data record and appended with 2020 ATCF data, which were used to assess the historical maxima and variances of the individual TC atmospheric-forcing parameters. This section discusses the PCHA steps to develop marginal distributions at the 108 CRLs specific to the CHS-LA and provides examples plots and marginal distributions at CRL 128.

As discussed in Section 3.4, for each TC track, the forcing parameters were selected at an optimal location balancing intensity and distance from a given CRL. Marginal probability distributions were then fit to the distance-adjusted TC parameters. The historical TCs sampled from the HURDAT2 database within 600 km from CRL 128 (1938–2020 period), and their distance-adjusted atmospheric parameters are listed in

Appendix A. Sections 4.1.1 through 4.1.4 discuss the distribution fitted to each parameter.

4.1.1 Central pressure deficit (Δp)

The c_p is a measurement of TC intensity and is inversely proportional to intensity. However, for convenience and to facilitate statistical analyses, hurricane intensity is usually expressed in terms of Δp. It is common practice to use these parameters interchangeably. In most JPM studies, the Δp has been computed from an assumed far-field atmospheric pressure of 1,013 hPa, known as the standard atmospheric pressure.

Past JPM studies have typically chosen either the Weibull or the Gumbel distribution to fit Δp, resulting in very similar storm surge hazard curves (USACE 2009d, 2011). The probabilistic model of Δp is represented in the PCHA by the Weibull distribution:

$$F[\Delta p > x] = 1 - \ exp\left[-\left(\frac{x}{U}\right)^k\right] \tag{4-1}$$

where U = scale parameter; and k = shape parameter. The Weibull best fit is shown in Figures 4-1 and 4-2. Since the PCHA employs three TC intensity bins (i.e., LI, MI, and HI), a doubly truncated Weibull distribution (DTWD) is used to characterize the data from these bins. Figure 4-1 illustrates the Weibull best fit for Δp values ranging from $8 \leq x < 28$ hPa. In Figure 4-2, the Weibull is fit to Δp values truncated at 28 and 148 hPa.

Figure 4-1. DTWD for sampled Δp ranging from 8 to less than 28 hPa at CRL 128.

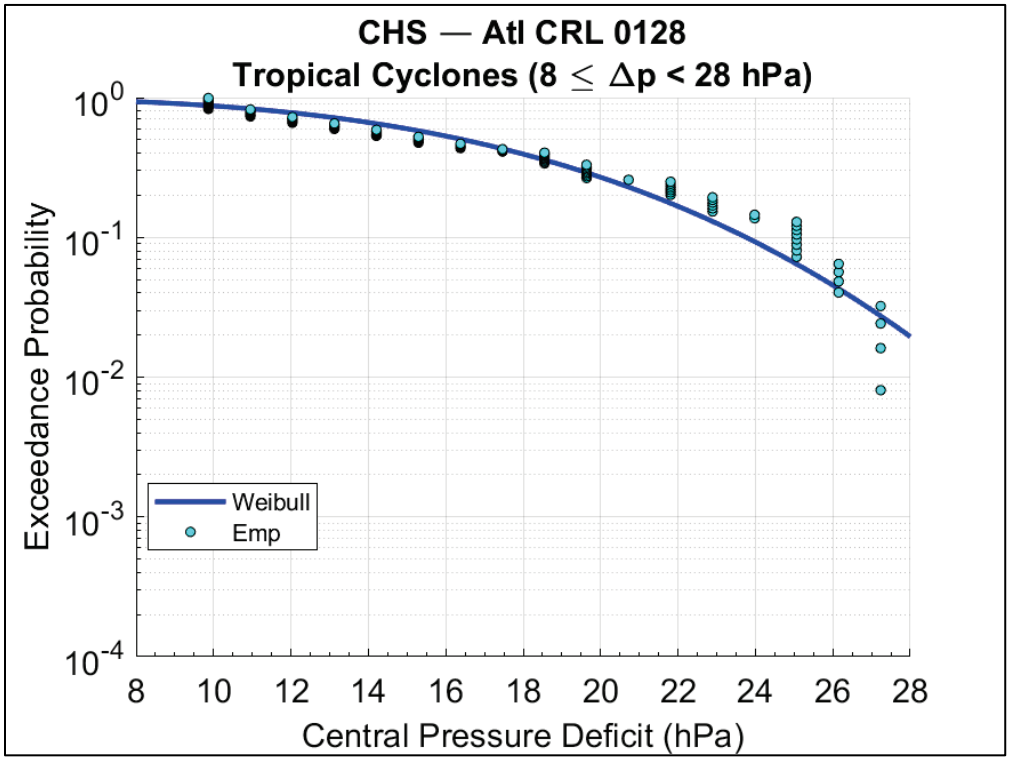
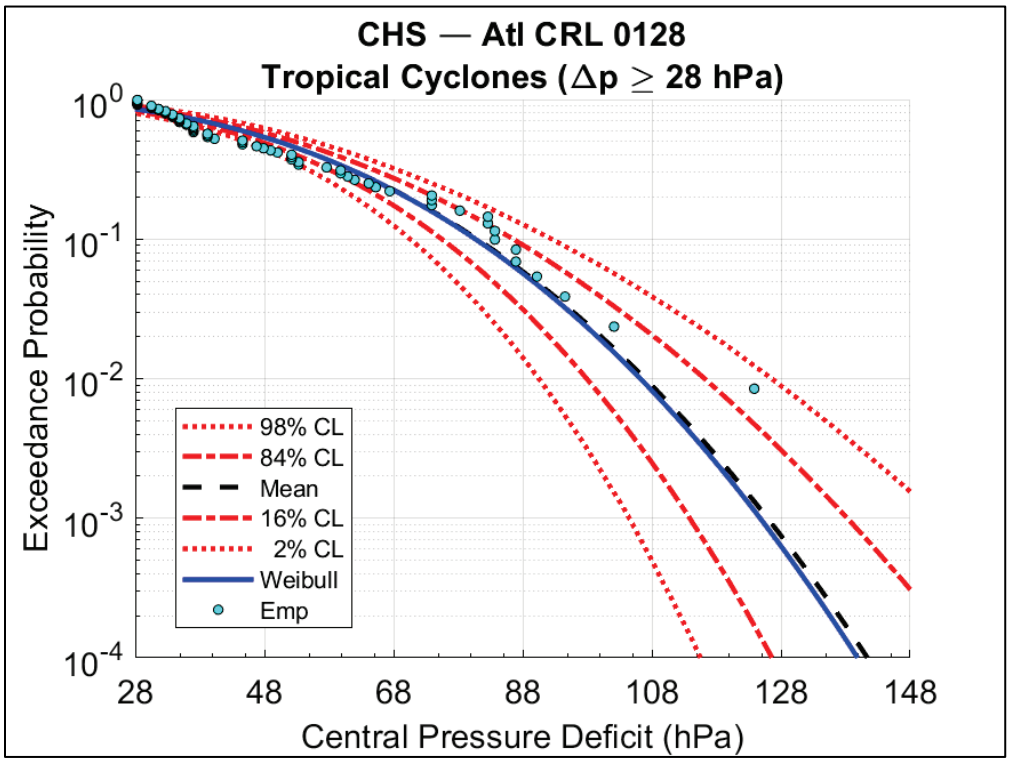


Figure 4-2. DTWD for all sampled Δp of 28 to 148 hPa at CRL 128.



The scale and shape parameters and truncation limits of the Δp for CRL 128 are listed in Table 4-1. The Weibull distribution fits corresponding to each intensity group are shown in Figures 4-3, 4-4, and 4-5.

Table 4-1. Marginal distribution parameters of Δp at CRL 128.

TC Intensity	U	k	Δp_1	Δp_2
High (DTWD)	57.9	2.52	48	148
Medium (DTWD)	57.9	2.52	28	48
Low (DTWD)	18.4	3.26	8	28

Figure 4-3. Marginal distribution (DTWD) of Δp for HI TCs at CRL 128.

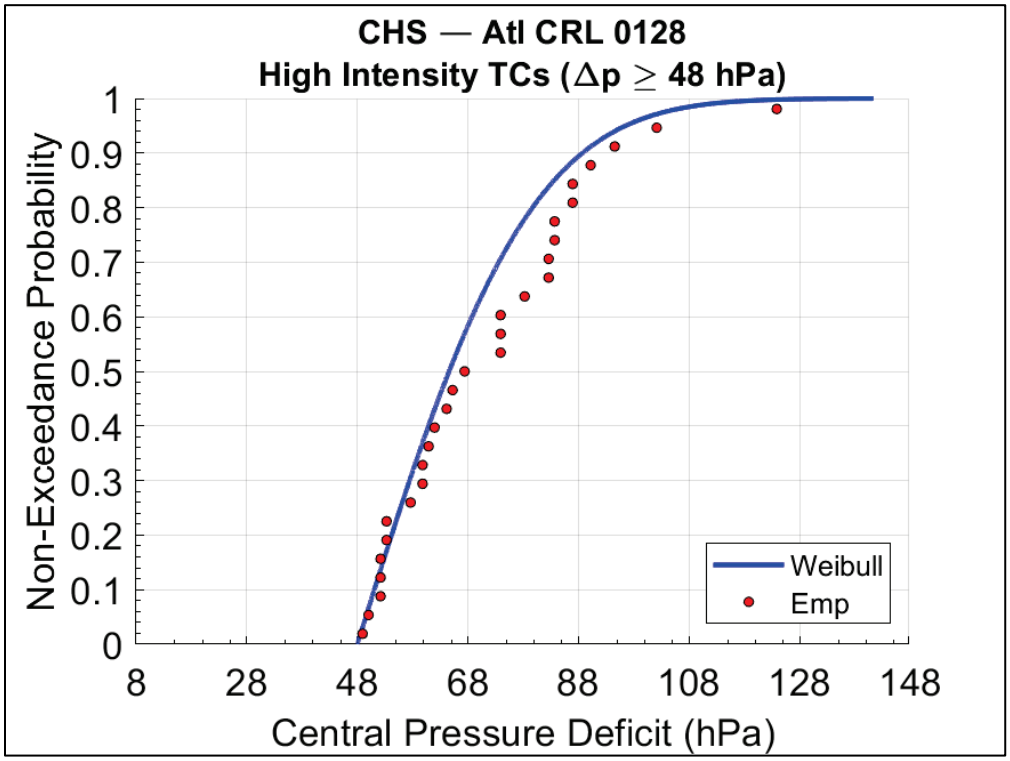


Figure 4-4. Marginal distribution (DTWD) of Δp for MI TCs at CRL 128.

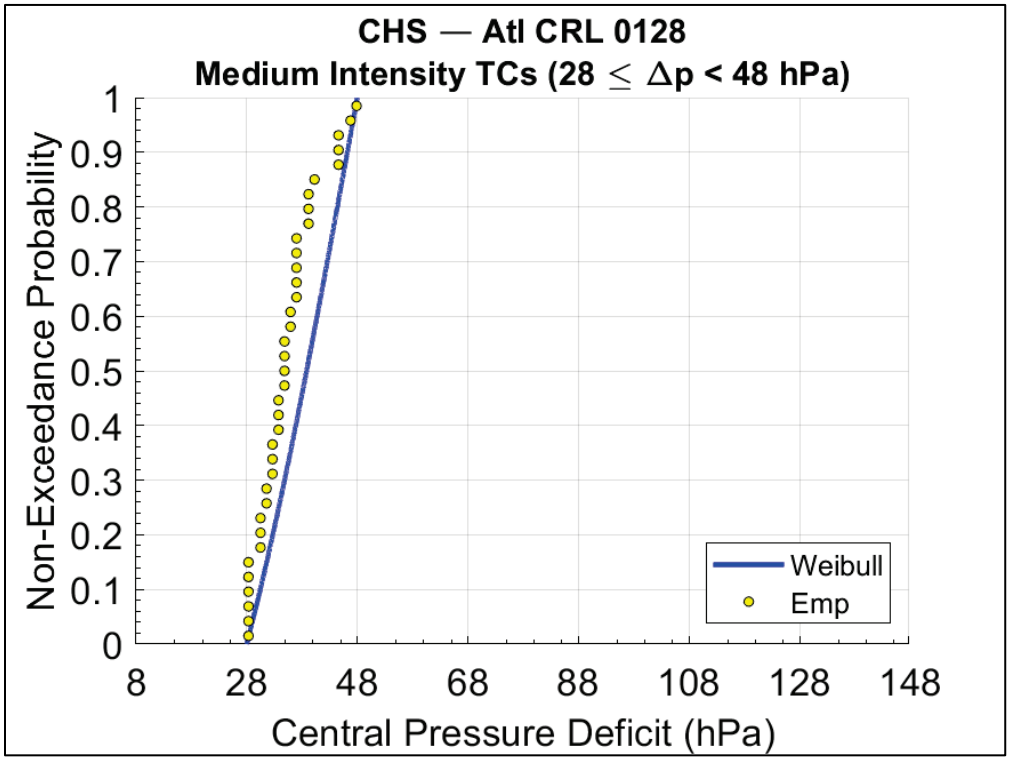
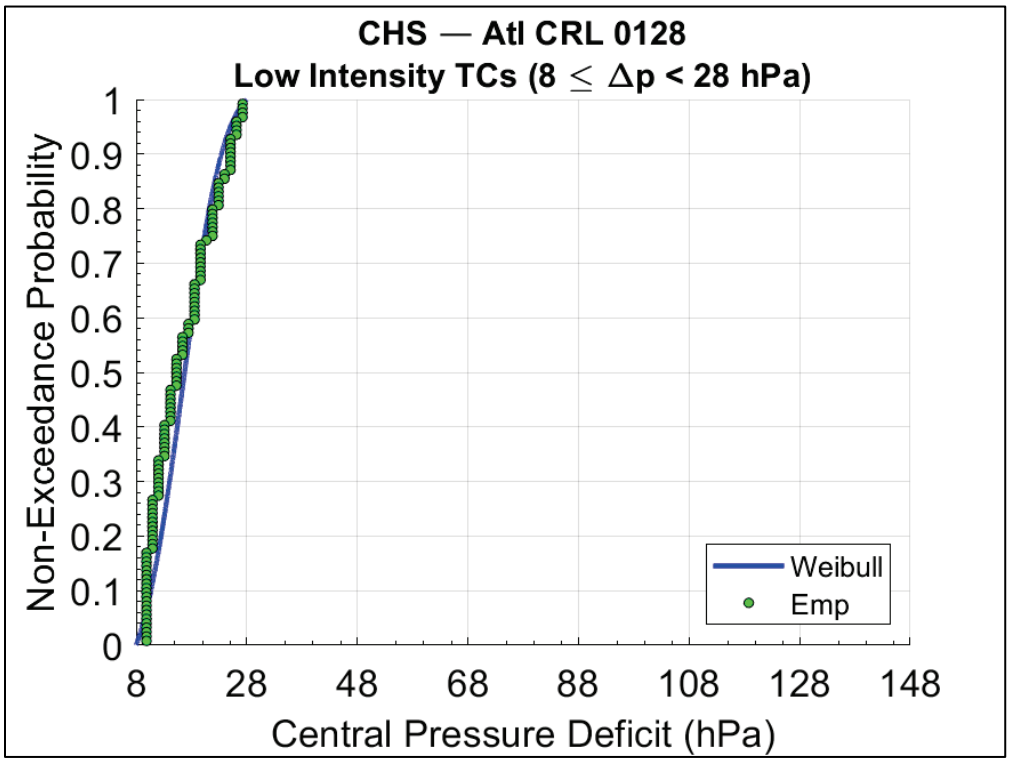


Figure 4-5. Marginal distribution (DTWD) of Δp for LI TCs at CRL 128.



4.1.2 Radius of maximum winds (R_{max})

In this study, the parameter R_{max} is represented by the lognormal distribution, which has the form

$$f(x) = \frac{1}{x\sigma\sqrt{2\pi}} exp\left[-\frac{1}{2}\left(\frac{ln(x)-\mu}{\sigma}\right)^2\right] \quad (4\text{-}2)$$

where μ = mean of $ln(x)$; σ= standard deviation of $ln(x)$. The main difference between the normal and lognormal distribution is that in the latter, $ln(x)$ is the normally distributed variable rather than x itself. The R_{max} lognormal distribution parameters corresponding to CRL 128 are listed in Table 4-3. Figures 4-6, 4-7, and 4-8 show the marginal distribution fitted to R_{max} for each intensity bin.

Table 4-2. Marginal distribution parameters of R_{max} at CRL 128.

TC Intensity	$\mu_{ln(x)}$	$\sigma_{ln(x)}$
High	4.01	0.29
Medium	3.96	0.31
Low	4.18	0.32

Figure 4-6. Marginal distribution (lognormal) of R_{max} for HI TCs at CRL 128.

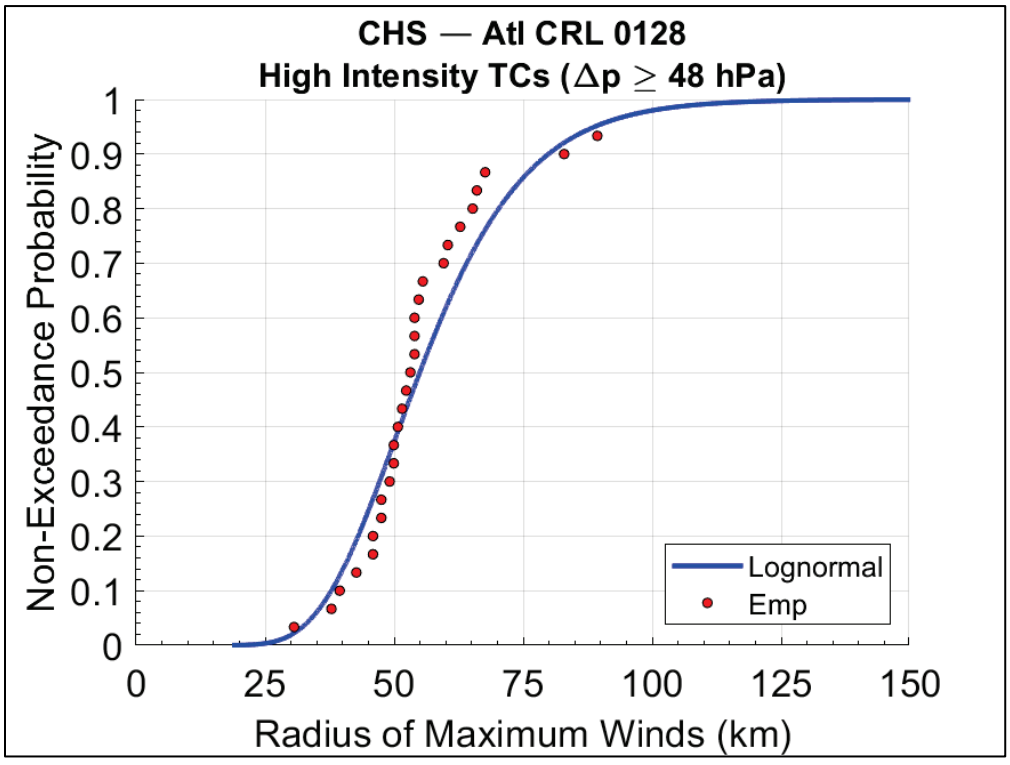


Figure 4-7. Marginal distribution (lognormal) of R_{max} for MI TCs at CRL 128.

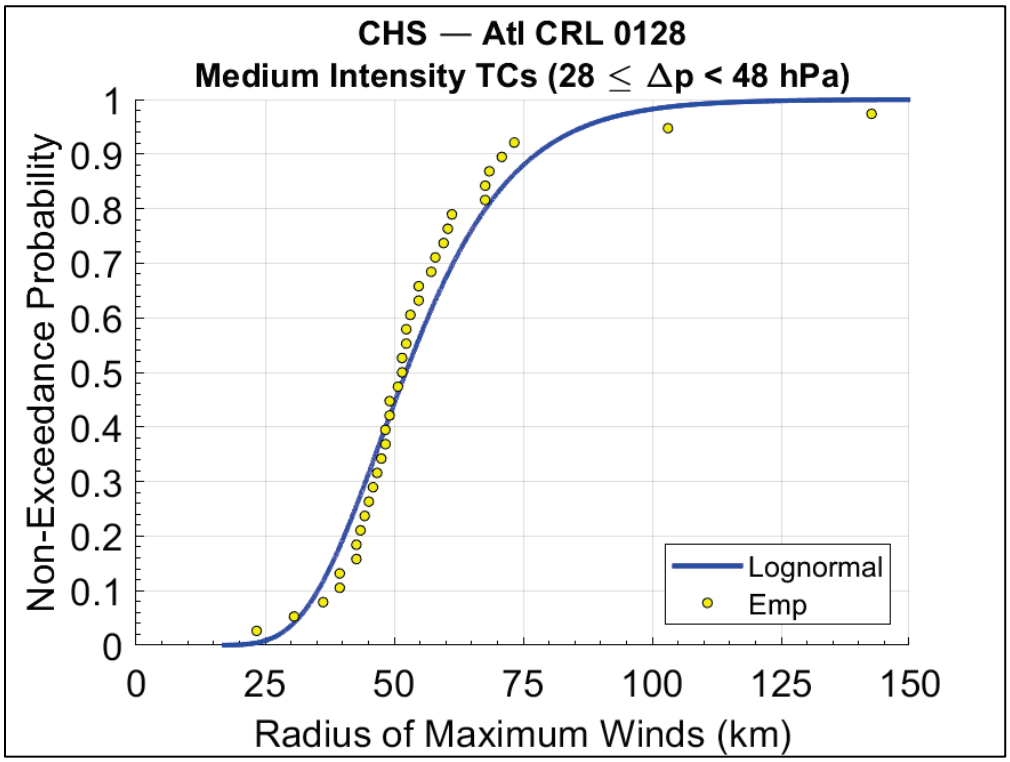
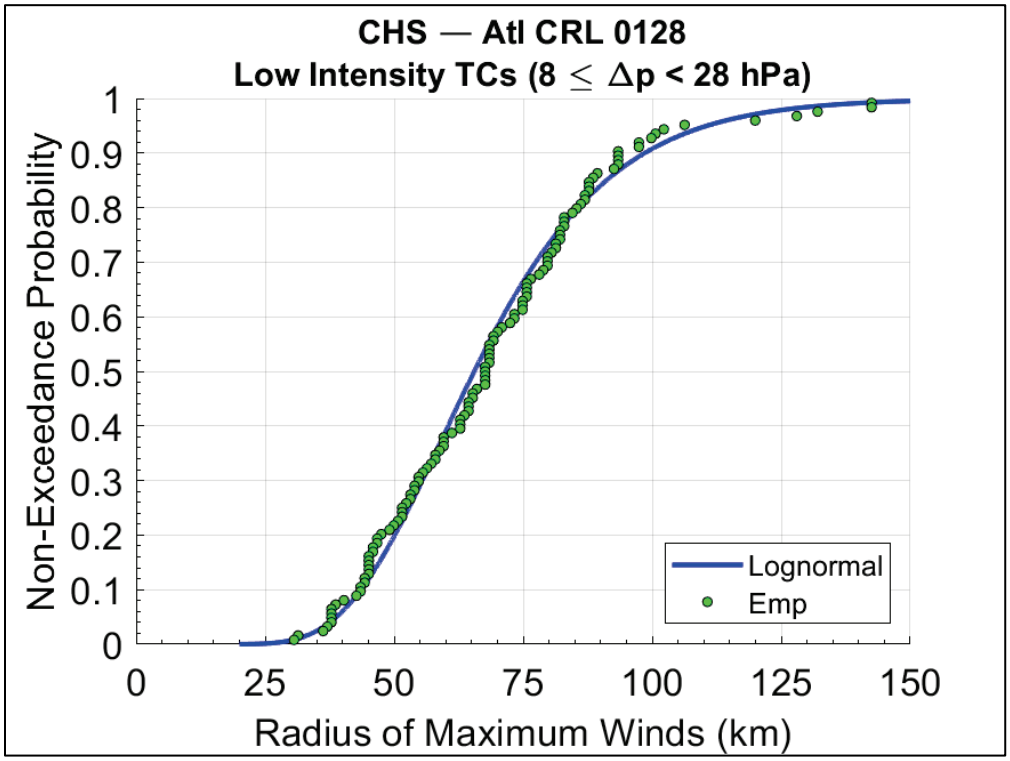


Figure 4-8. Marginal distribution (lognormal) of R_{max} for LI TCs at CRL 128.



4.1.3 Forward translation speed (V_t)

The V_t data requires two different parametric distributions. The lognormal distribution, discussed in the previous section (Equation 4-2), is used to fit LI TCs in an effort to capture the variability which exists within the empirical data for this intensity bin. The V_t of MI and HI TCs exhibits less variability and is represented by the normal distribution with the form

$$f(x) = \frac{1}{\sigma\sqrt{2\pi}} exp\left[-\frac{1}{2}\left(\frac{x-\mu}{\sigma}\right)^2\right] \quad (4\text{-}3)$$

where μ = mean of random variable x; σ= standard deviation of x.

The marginal distributions of V_t for HI, MI, and LI TCs corresponding to CRL 128 are listed in Table 4-4. Figures 4-9, 4-10, and 4-11 show the marginal distribution fitted to V_t at CRL 128 or each intensity bin.

Table 4-3. Marginal distribution parameters of V_t at CRL 128.

TC Intensity (Normal)	μ	σ
High	23.4	10.18
Medium	21.3	7.86
TC Intensity (Lognormal)	$\mu_{ln(x)}$	$\sigma_{ln(x)}$
Low	2.79	0.58

Figure 4-9. Marginal distribution (normal) of V_t for HI TCs at CRL 128.

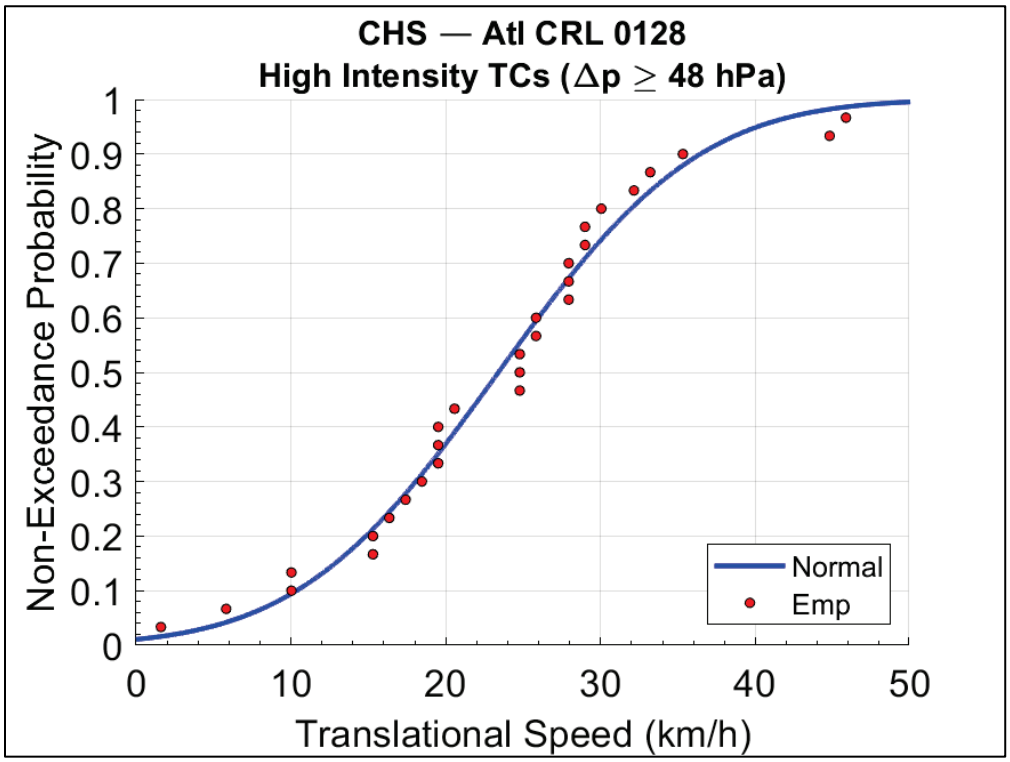


Figure 4-10. Marginal distribution (normal) of V_t for MI TCs at CRL 128.

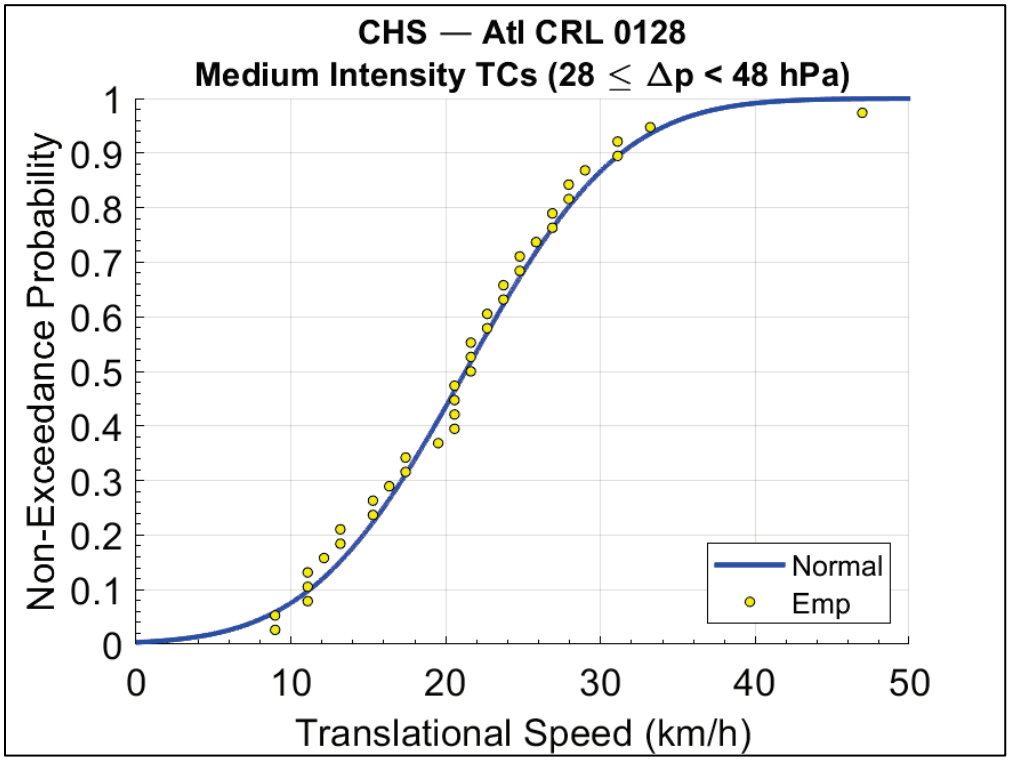
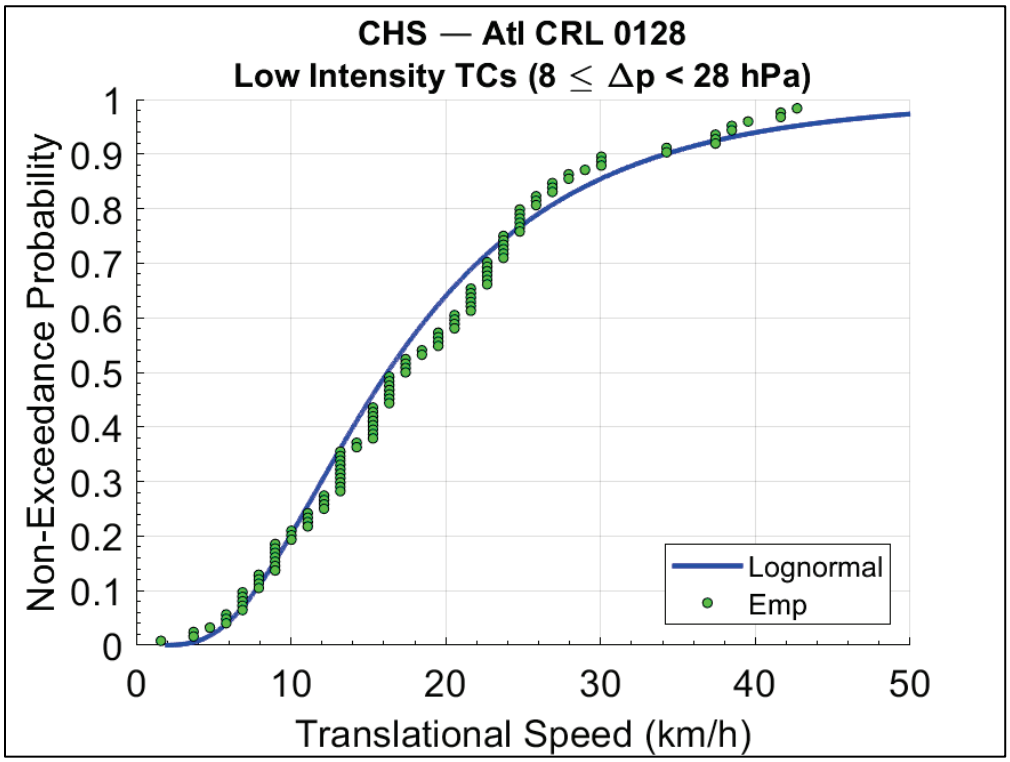


Figure 4-11. Marginal distribution (lognormal) of V_t for LI TCs at CRL 128.



4.1.4 Track heading direction (θ)

In the PCHA, the θ marginal distribution is taken as the directional SRR (DSRR) estimated from the GKF model (Chouinard and Liu 1997). The DSRR is given by

$$\lambda_\theta = \frac{1}{T}\sum_i^n w(d_i)\, w(\theta_i - \theta) \tag{4-4}$$

$$w(\theta_i - \theta) = \frac{1}{\sqrt{2\pi}h_\theta}\exp\left(-\frac{1}{2}\left(\frac{\theta_i-\theta}{h_d}\right)^2\right) \tag{4-5}$$

where λ_θ = the DSRR in storms/yr/km; T = record length in (yr); d_i = distance from location of interest to a storm data point (km); h_d = optimal kernel size (km); $w(\theta_i)$ = radial distance weights from the track heading direction GKF (deg^{-1}); θ_i = track heading direction (deg); h_θ = optimal directional kernel size (e.g., 30 deg); and $w(d_i)$ = distance weights computed using the GKF (Equation 3-2). Figures 4-12, 4-13, and 4-14 show the marginal distribution of θ derived from the DSSR for HI, MI, and LI TCs, respectively.

Figure 4-12. Marginal distribution (DSRR) of θ for HI TCs at CRL 128.

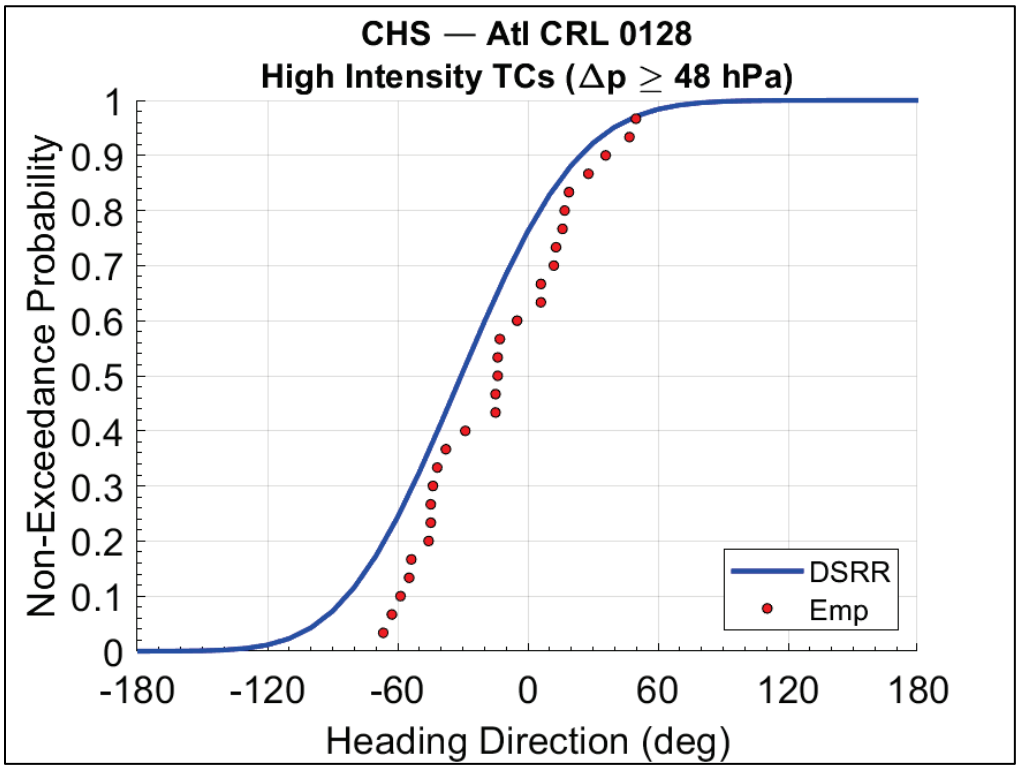


Figure 4-13. Marginal distribution (DSRR) of θ for MI TCs at CRL 128.

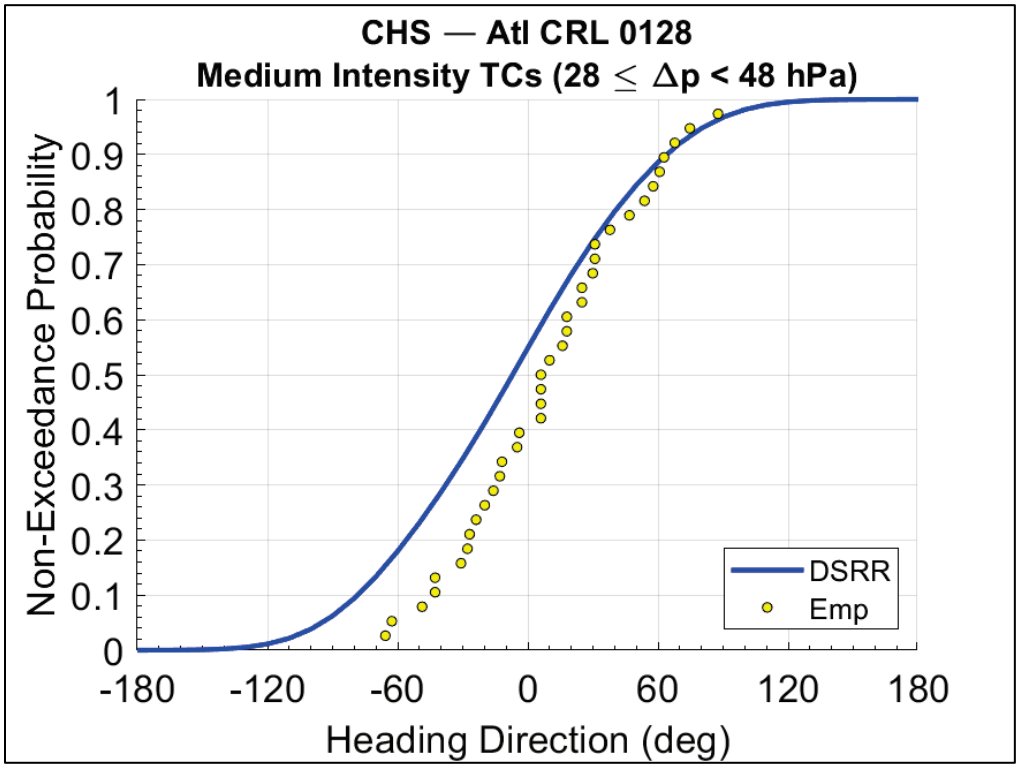
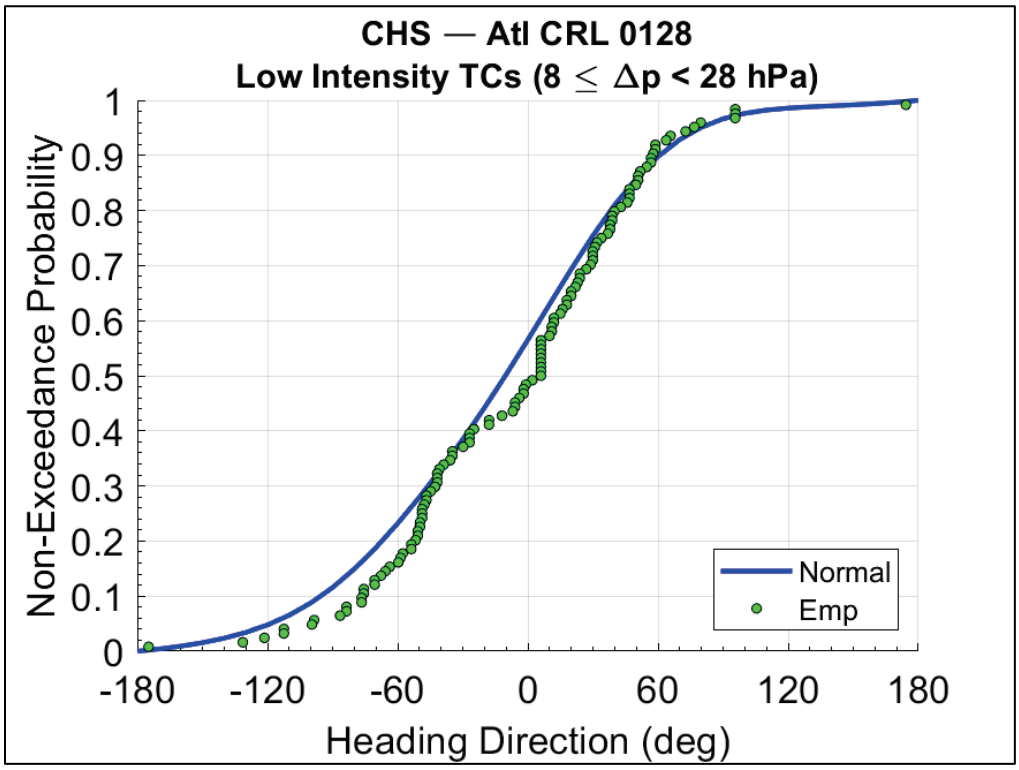


Figure 4-14. Marginal distribution (DSRR) of θ for LI TCs at CRL 128.



4.2 Joint probability analysis using the Meta-Gaussian Copula (MGC)

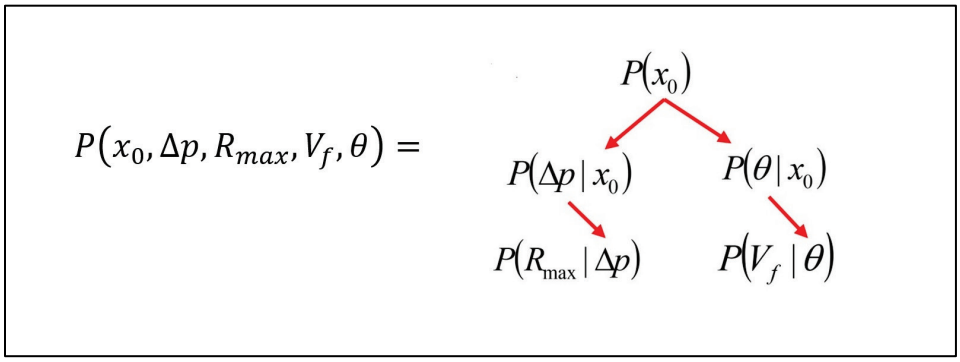
The main limitation in JPM studies as applied to date is the lack of an actual joint probability model. Typical joint probability approaches often involve unrealistic assumptions that either (1) all random variables are independent of one another or (2) that variables follow a joint normal distribution. TC parameters have some level of correlation between them (FEMA 2012). The correlation of TC parameters with location is implicitly considered since the analysis is centered on a CRL; therefore, the SRR and the TC parameters used for fitting the probability distributions correspond to that location. The dependence between Δp and R_{max} is often considered in JPM studies, particularly if the latter is computed using a statistical model such as Vickery and Wadhera (2008), which explicitly uses Δp as input.

The JPM-OS-BQ, for example, uses a double-exponential covariance function (Toro et al. 2010b) as a pseudo dependence structure. Instead of computing the correlation between pairs of JPM atmospheric-forcing parameters, this approach relies on expert judgment to set correlation distances that dictate the discretization of marginal distributions of JPM parameters. Previous studies have either assumed independence between

the parameters (Equation 2-1) or used a correlation tree with 1:1 dependence, as seen in the diagram in Figure 4-15. The latter approach was described by Resio et al. (2007):

$$P(x_0, \Delta p, R_{max}, V_f, \theta) = P(x_0) \cdot P(\Delta p) \cdot P(R_{max}) \cdot P(V_f) \cdot P(\theta) \quad (4\text{-}6)$$

Figure 4-15. TC parameter correlation tree with 1.1 dependence.



Other approaches have proposed using conditional distributions linking pairs of random variables, but in practice, variables are often interconnected through simplified linear relationships.

The PCHA framework uses copula theory to overcome the limitations mentioned above. A copula is a dependence function that links a set of marginal distributions to form a unique joint probability distribution. According to the seminal Sklar's (1959) theorem, any joint (multivariate) distribution, H, can be deconstructed into marginal distributions, $F_{1,\ldots,n}$, and a copula, C, as follows:

$$H(x_1, \ldots, x_n) = C(F_1(x_1), \ldots, F_n(x_n)) \quad (4\text{-}7)$$

where n is the number of dimensions of the cumulative distribution function (CDF).

A copula must be expressed in terms of uniform marginal distributions (u_n) defined on the interval [0, 1]. The general formulation is

$$C(u_1, \ldots, u_n) = H(F_1^{-1}(x_1), \ldots, F_n^{-1}(x_n)) \quad (4\text{-}8)$$

where $F^{-1}( )$ is the inverse of the marginal distribution.

Zhang and Singh (2019) recommend using meta-elliptical copulas since this family frequently outperforms other multivariate copulas in capturing the full range of dependence while also excelling due to simplicity of construction and ease of parameter estimation, particularly in the case of the MGC.

The MGC consists of a multivariate CDF that links a set of marginal probability distributions with a multivariate Gaussian copula as the dependence structure. The CDF of the Gaussian copula is expressed as

$$C_R^{Gauss}(u) = \Phi_R\left(\Phi^{-1}(u_1), \ldots, \Phi^{-1}(u_n)\right) \tag{4-9}$$

where $\Phi^{-1}(\,)$ is the inverse of the standard Gaussian distribution and Φ_R is the multivariate distribution of n Gaussian distributions with correlation matrix R, given by

$$R = \begin{pmatrix} 1 & \rho_{1,2} & \cdots & \rho_{1,n} \\ \rho_{2,1} & 1 & \cdots & \rho_{2,n} \\ \vdots & \vdots & \ddots & \vdots \\ \rho_{n,1} & \rho_{n,2} & \cdots & 1 \end{pmatrix} \tag{4-10}$$

The dependence between pairs of random variables is given by correlation coefficients (ρ). In the case of JPM, ρ must be computed for all pairs of TC forcing parameters. The correlation is accounted for in the PCHA by first computing the rank correlation between the TC atmospheric-forcing parameters using Kendall's Tau (Kendall 1970). By computing the rank correlation, the correlation between TC parameters is preserved following the nonlinear transformations required for the MGC. The rank correlation is then transformed to Pearson's rho (Fang et al. 1990, 2002), a linear correlation, using the following form for application in the MGC approach:

$$\rho = \sin\left(\frac{\tau\pi}{2}\right) \tag{4-11}$$

Below are the correlation matrices (R) constructed for HI, MI, and LI TCs from Equation 4-10. For each intensity bin, Figures 4-16 through 4-19 illustrate the correlation between the JPM parameters computed as both the rank correlation and Pearson's correlation. In each correlation matrix, the reported correlations correspond first to the rank correlation and second to the Pearson's correlation shown in parentheses.

Figure 4-16. Correlation matrix for all TCs.

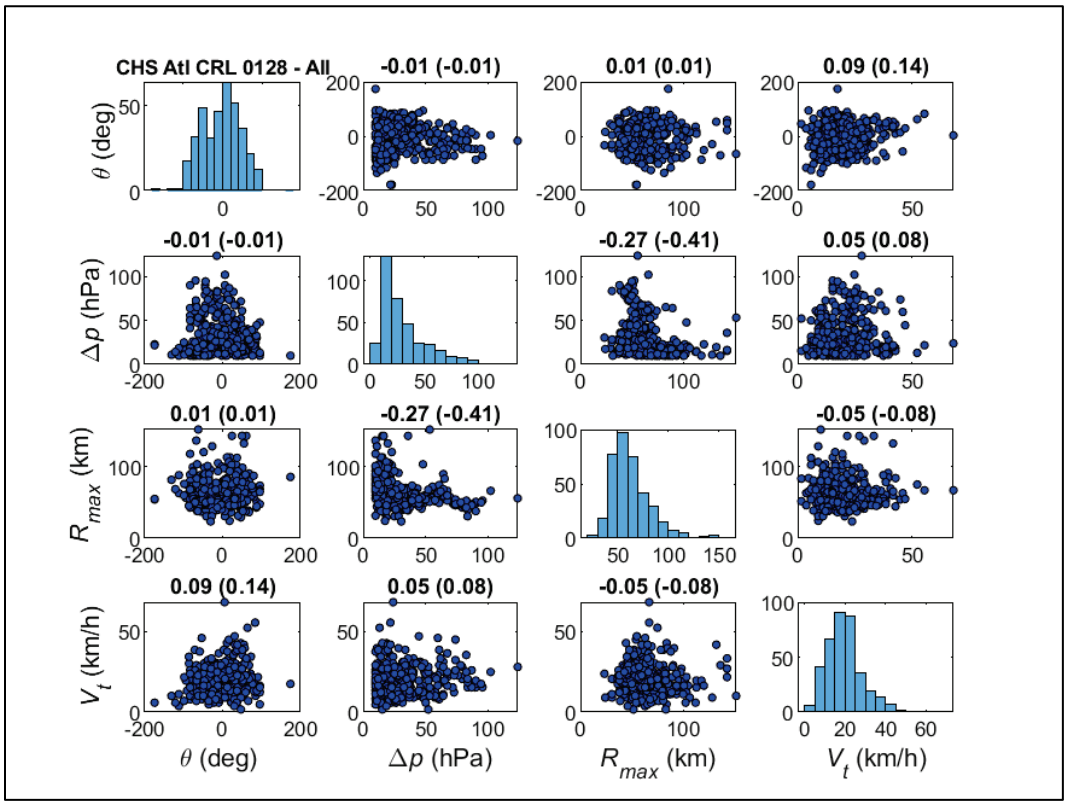


Figure 4-17. Correlation matrix for HI TCs.

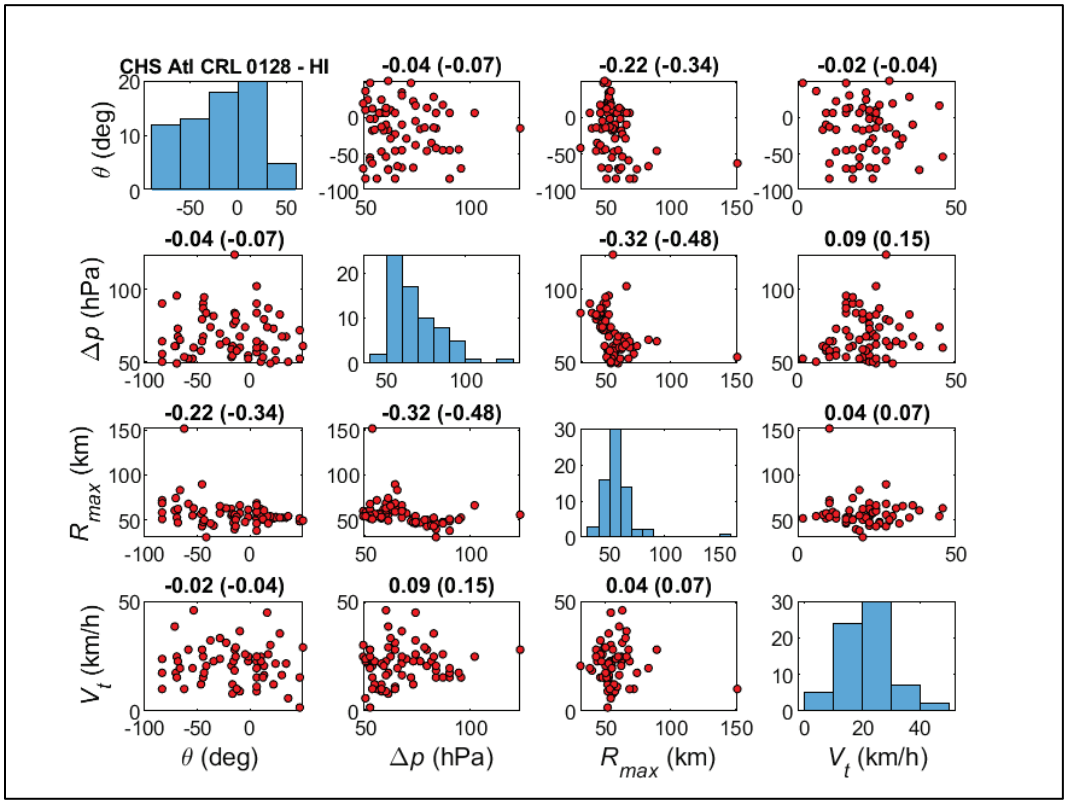


Figure 4-18. Correlation matrix for MI TCs.

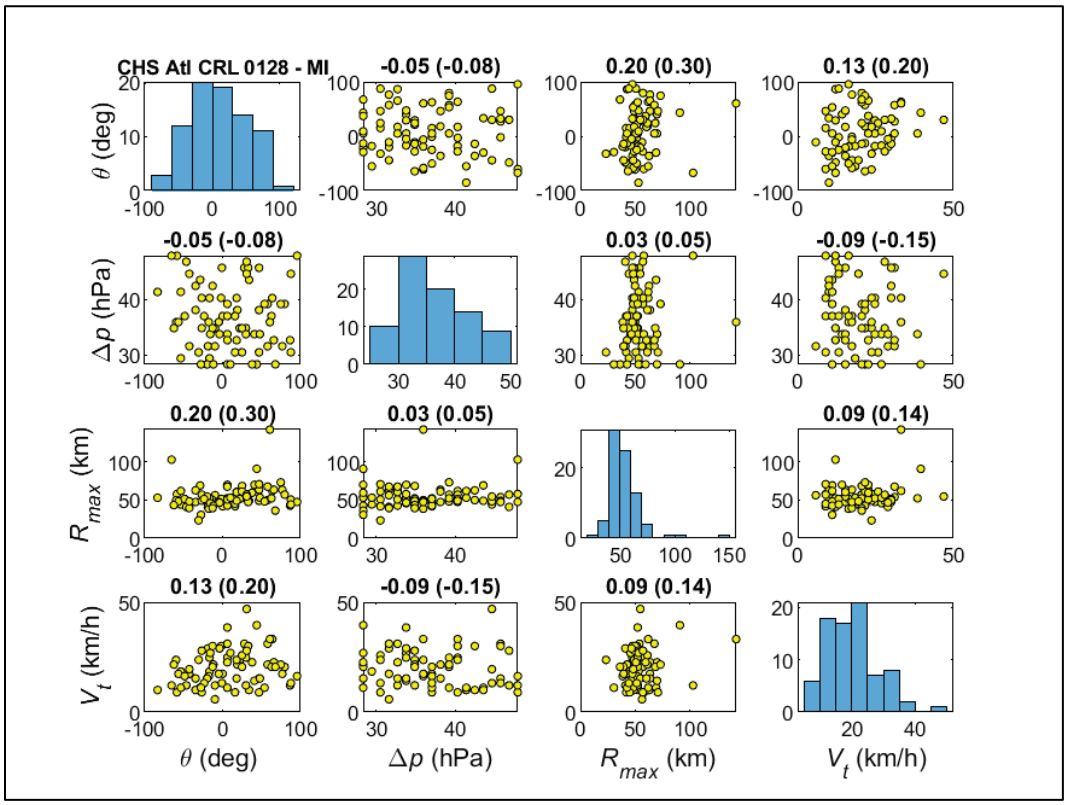
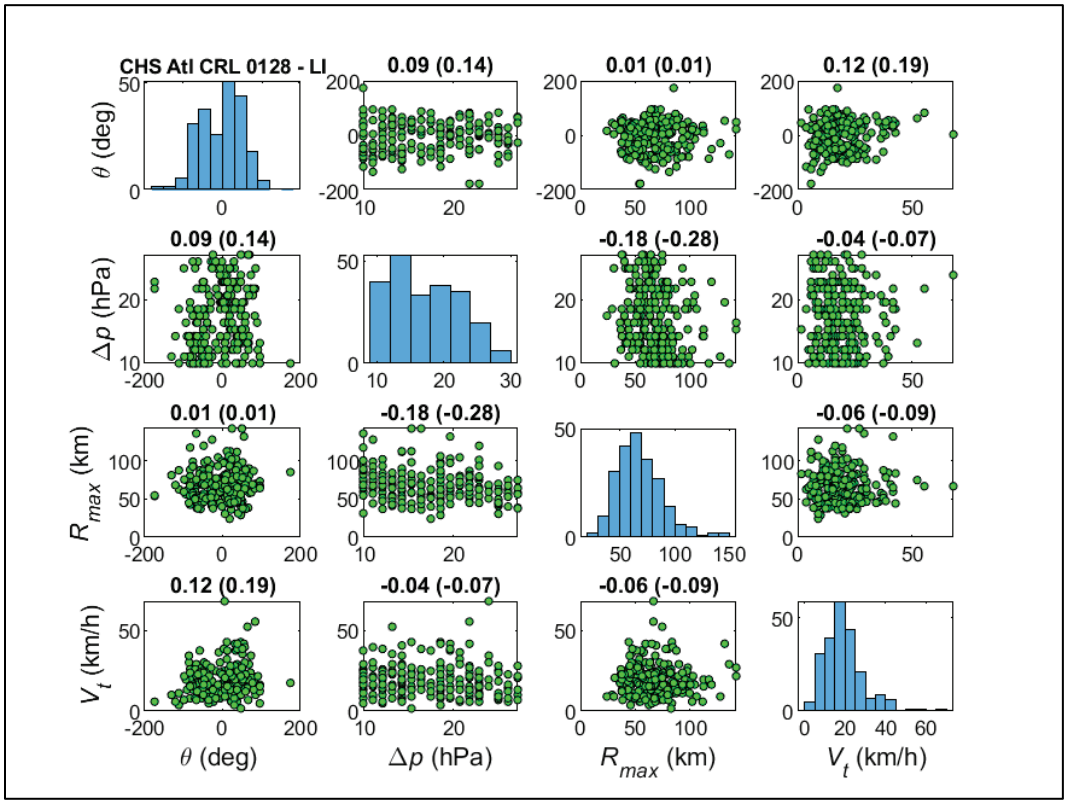


Figure 4-19. Correlation matrix for LI TCs.



4.3 Discretization of marginal distributions

A hybrid optimal sampling method was employed to discretize the marginal distributions of TC parameters. It is termed *hybrid* because it combines uniform discretization procedures evolved from those used in the LACPR study (USACE 2009c) with the BQ optimization approach developed for FEMA (2012). To ensure optimal coverage of the TC probability and parameter spaces and ensure adequate geospatial coverage of the study area, a structured discretization approach was used for the Δp and θ marginal distributions. The discretization of the R_{max} and V_t marginal distributions was performed using the BQ approach. The range of values resulting from the discretization of marginal distributions is provided in Table 4-2. Combining storm tracks and TC parameter permutations resulted in an ITCS of 645 synthetic storms. The along-track variation of these parameters for implementation in the PBL model is discussed in Section 5.

Table 4-4. Atmospheric-forcing parameters of the ITCS in the CHS-LA study.

TC parameter	Range
θ	−80°, −60°, −40°, −20°, 0°, +20°, +40°, +60° (clockwise from North)
Δp	8, 18, 28, 38, 48, 58, 68, 78, 88, 98, 108, 118, 128, 138, 148 hPa
R_{max}	8 to 141 km (from BQ sampling)
V_t	8 to 50 km/h (from BQ sampling)

4.4 Augmented synthetic TC suite (ATCS) and discrete storm weights (DSWs)

The PCHA methodology includes the development of an ATCS to fully cover the parameter and probability spaces for the study area. This requires the simulation of hundreds of TCs (up to several thousand in regional studies) from the ITCS to ensure high-resolution, high-fidelity hydrodynamic results. After the ITCS is defined, the ATCS is developed using the discretized marginal distributions to create a higher density of synthetic TCs. GPM is then introduced to predict the responses of an augmented suite of tens of thousands to millions of TCs that retain the

high-fidelity nature of the initial suite. As described by Jia et al. (2016) and Zhang et al. (2018), the GPM establishes the relationship between the input atmospheric-forcing vector $\hat{x} = f(x_o, \theta, \Delta p, R_{max}, V_t)$ and output TC responses (e.g., storm surge, wave parameters). However, to avoid an excessive computational cost, the size of the ATCS needs to be balanced with the number of points where the JPM integral is solved.

For the CHA-LA study, the first step in defining the ATCS was to discretize the distributions of the TC atmospheric-forcing parameters at a much higher resolution than the ITCS. The discretization of the TC parameter spaced used in the definition of the ATCS is shown in Table 4-5. Multiplying the number of discrete values for Δp (29), R_{max} (30), and V_t (10) resulted in 8,700 TCs per master track. These 8,700 TCs are replicated across all 86 master tracks covering the CHS-LA study area, resulting in an ATCS of 748,200 synthetic TCs. Using the high-fidelity hydrodynamic modeling results produced by simulating the ITCS, GPMs were trained to predict storm responses produced by the ATCS.

Table 4-5. Atmospheric-forcing parameters from the ATCS.

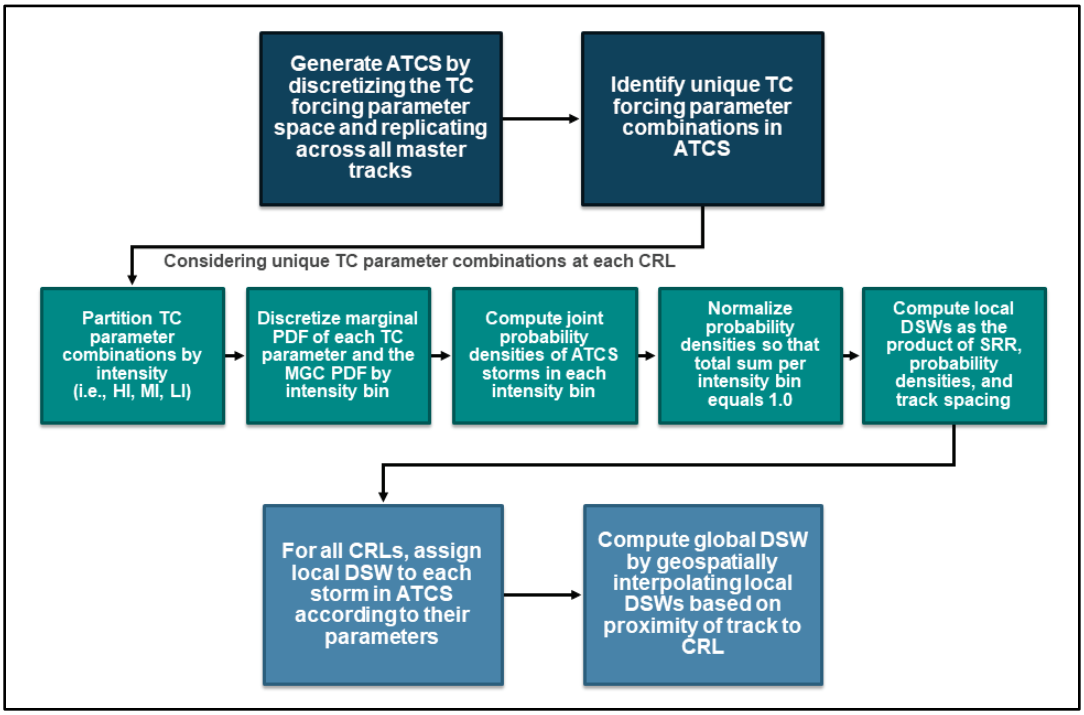
TC parameter	Range	Discretization	Number of Discrete Values
Δp	8 to 148 hPa	5 hPa	29
R_{max}	10 to 155 km	5 km	30
V_t	5 to 50 km/h	5 km/h	10
Master tracks	θ = −80°, −60°, −40°, −20°, 0°, +20°, +40°, +60° (clockwise from North)		86
Total number of TCs			748,200

Following the development of the ATCS, the DSWs were computed for each storm as defined by Equation 2-1b and 2-2b, where $\hat{\lambda}_i$ is a product of the SRR, the joint probability densities of the TC parameters, and the track spacing. In this formulation, the SRR is the most important factor for quantifying hazards, because it represents the average number of storms that a specific location is likely to experience in any given 1-year period. Each TC in the synthetic suite constitutes a partition of this SRR and is represented by its DSW. Increasing the number of storms in the synthetic TC suite (e.g., upgrading from ITCS to ATCS) also increases the resolution

of both the probability and physical parameter spaces while decreasing the DSW of each TC. The computation of DSWs relies on historical TC datasets established at each CRL to assign a realistic relative likelihood to each synthetic storm. As shown by the diagram in Figure 4-20, the workflow for computing DSWs begins by generating the ATCS and identifying the unique combinations of TC forcing parameters that exist within the augmented suite. This is necessary as some TC parameter combinations are identical and are replicated across different master tracks to constitute different synthetic storms.

The steps illustrated by the green-bordered boxes are repeated across all CRLs within the study area to compute DSWs for all storms in the ATCS. These steps take advantage of the copula-based joint probability model and TC intensity stratification for the computation of joint probability densities. The probability densities are determined by discretizing the joint distribution with multivariate copula given by Equation (4-9) but in PDF form. These probability densities are then normalized to produce a total probability density sum equal to 1.0 for all unique TC parameter combinations at a given CRL. The local DSWs are computed for the different TC parameter combinations, as previously described, and assigned back to the storms in the ATCS based on each storm's specific parameter combination and intensity bin. The result is a local DSW value for each storm in the ATCS specific to each CRL considered in the storm climatology analysis (Section 3.3). The final step in computing the final set of global DSWs for the ATCS is geospatially interpolating the local DSW for each storm based on the proximity of its track to the CRLs. As a result, the global DSWs computed for the ATCS account for the joint probability of the TC parameters with respect to geographical location and intensity stratification, which is important for accurate quantification of coastal hazards.

Figure 4-20. Diagram of the DSW workflow within the PCHA.



5 Development of Synthetic TC Suite

This section describes the generation of the synthetic TC track paths and the along-track variation of TC parameters needed as input into the PBL model. The ITCS' wind and pressure fields generated by the PBL model were implemented as forcing in the hydrodynamic models. Section 5.1 presents the generation of the synthetic TC tracks. Section 5.2 describes how TC parameters were used and how the storm parameters were modified for pre-landfall and post-landfall changes. Section 5.3 summarizes the tropical wind and pressure forcing inputs. Section 5.4 discusses the application of the PBL model.

5.1 TC master tracks

For CHS-LA, eight landfalling track heading directions of −80°, −60°, −40°, −20°, 0° (north), 20°, 40°, and 60° (clockwise from north) were applied in the PCHA based on analysis of characteristic track angles determined from historic TCs in the HURDAT2 database. Generation of the landfall locations lay linear tracks with a starting location of 30.4°N, 87.0°W with parallel track spacing of 60 km. All tracks apply a constant heading, as defined by the JPM track headings, from 250 km before and post-landfall or bypassing reference point. A smoothed bearing path is used before the 250 km offshore reference location to result in track paths, or master tracks, consistent with climatology. Track paths for all 86 master tracks (blue tracks) are depicted in Figure 5-1, with master tracks by heading direction in Figures 5-2 through 5-9.

Figure 5-1. All master track paths (blue) with landfall/closest approach location (red). Master tracks developed for the SACS and CTXS (gray) shown for reference.

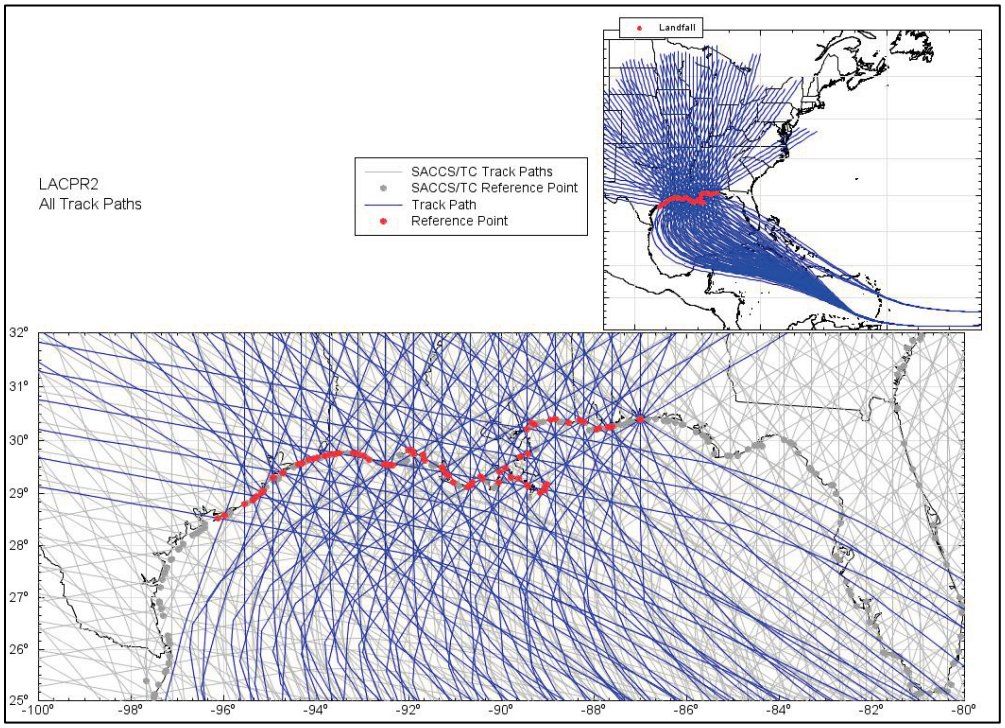


Figure 5-2. JPM heading −80° track paths.

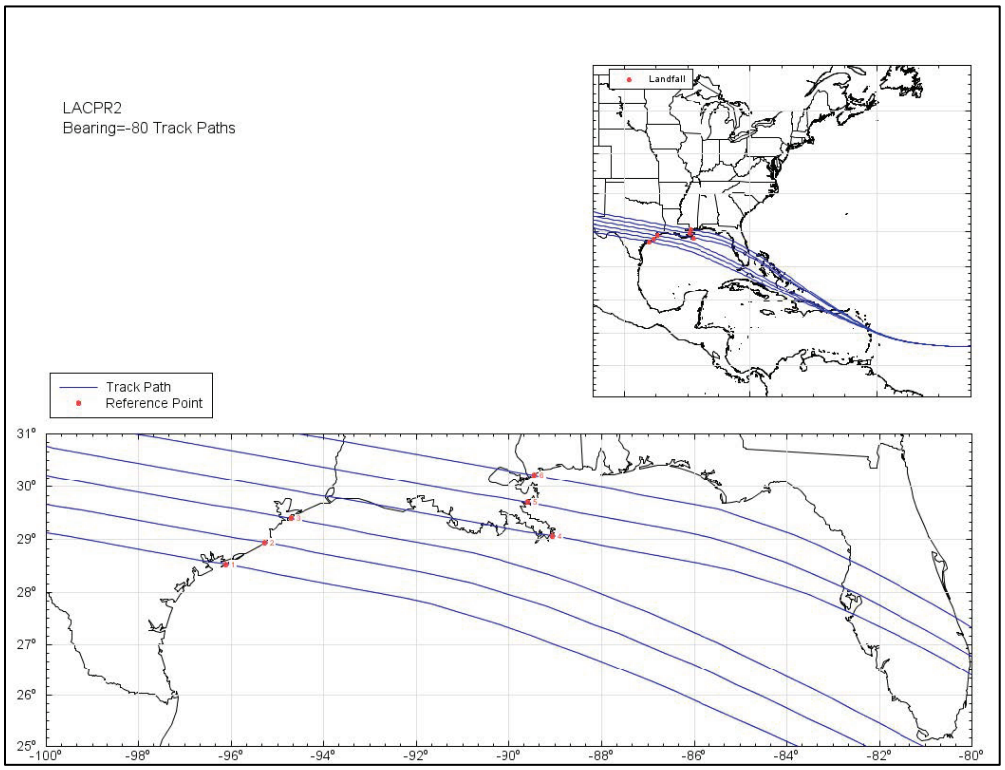


Figure 5-3. JPM heading −60° track paths.

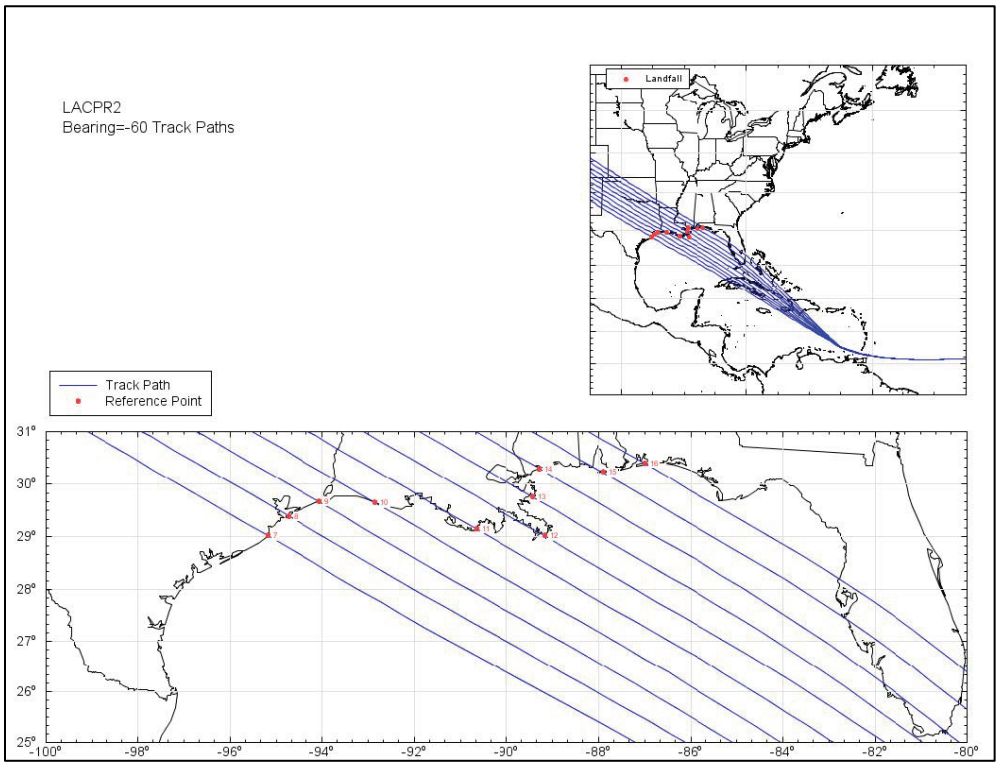


Figure 5-4. JPM heading −40° track paths.

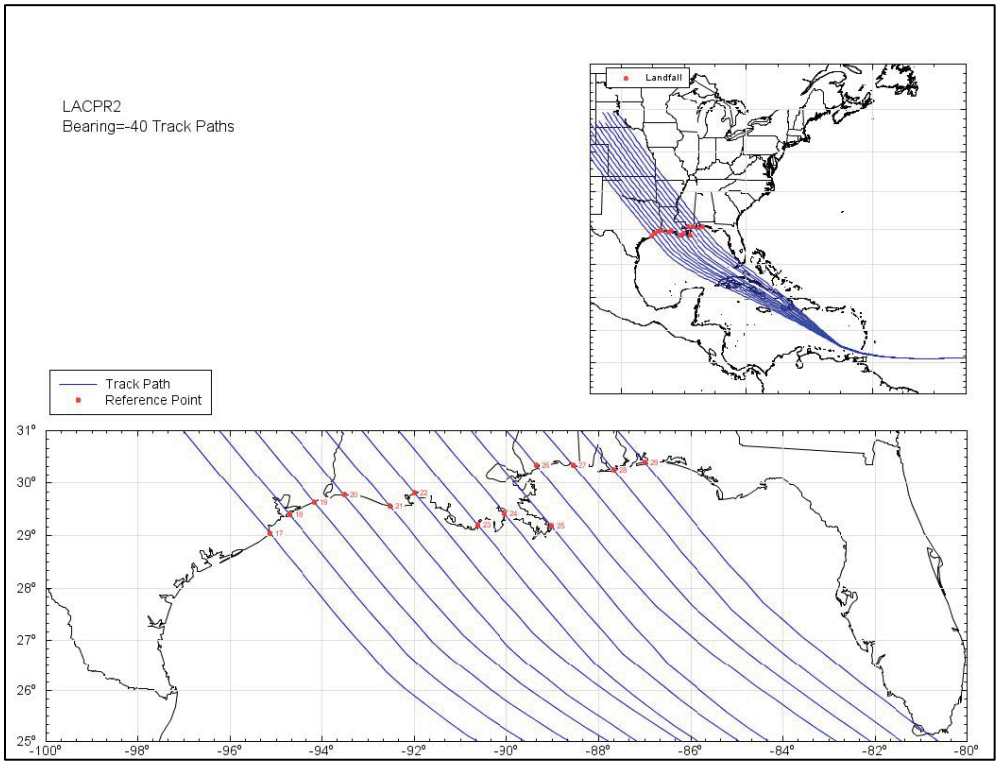


Figure 5-5. JPM heading −20° track paths.

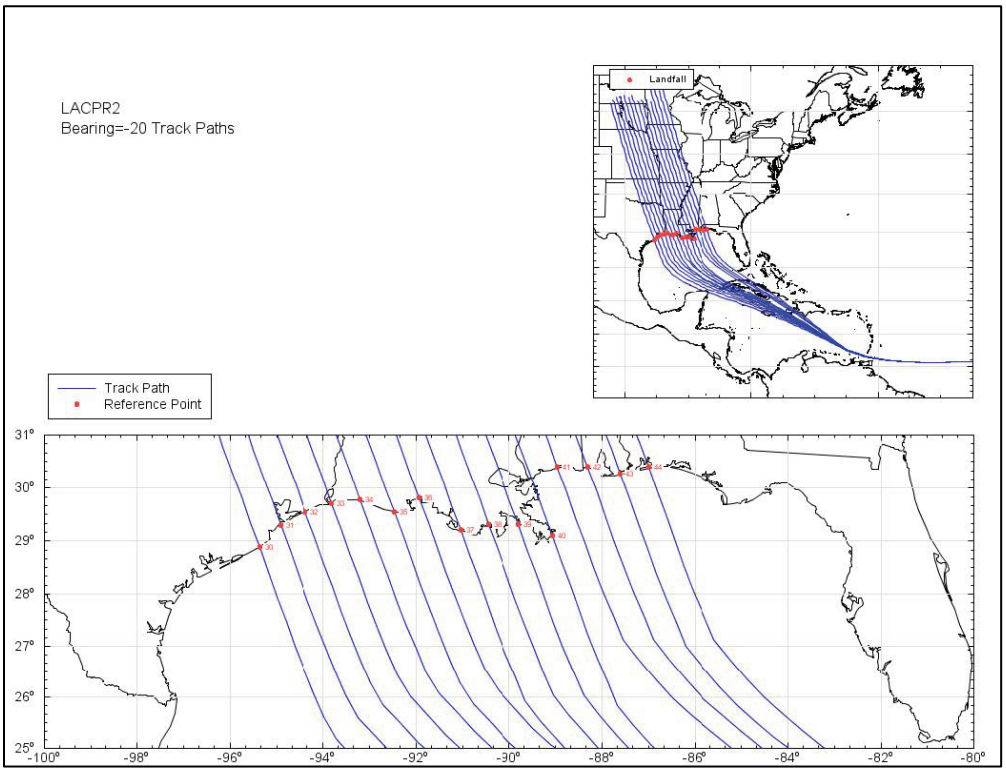


Figure 5-6. JPM heading 0° track paths.

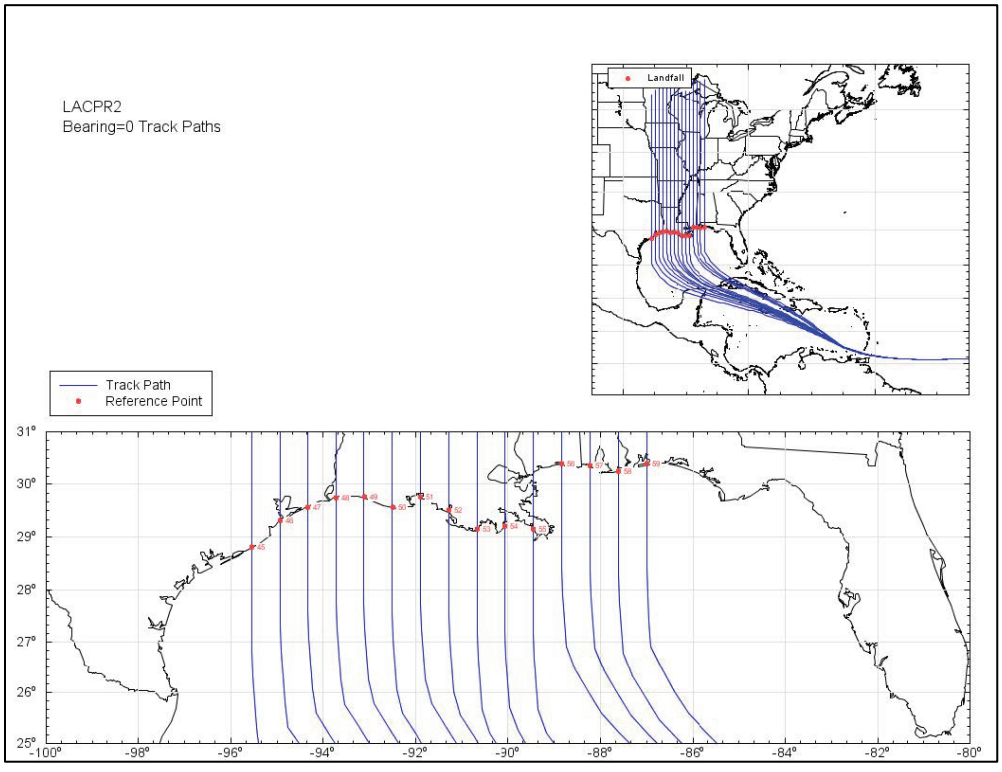


Figure 5-7. JPM heading 20° track paths.

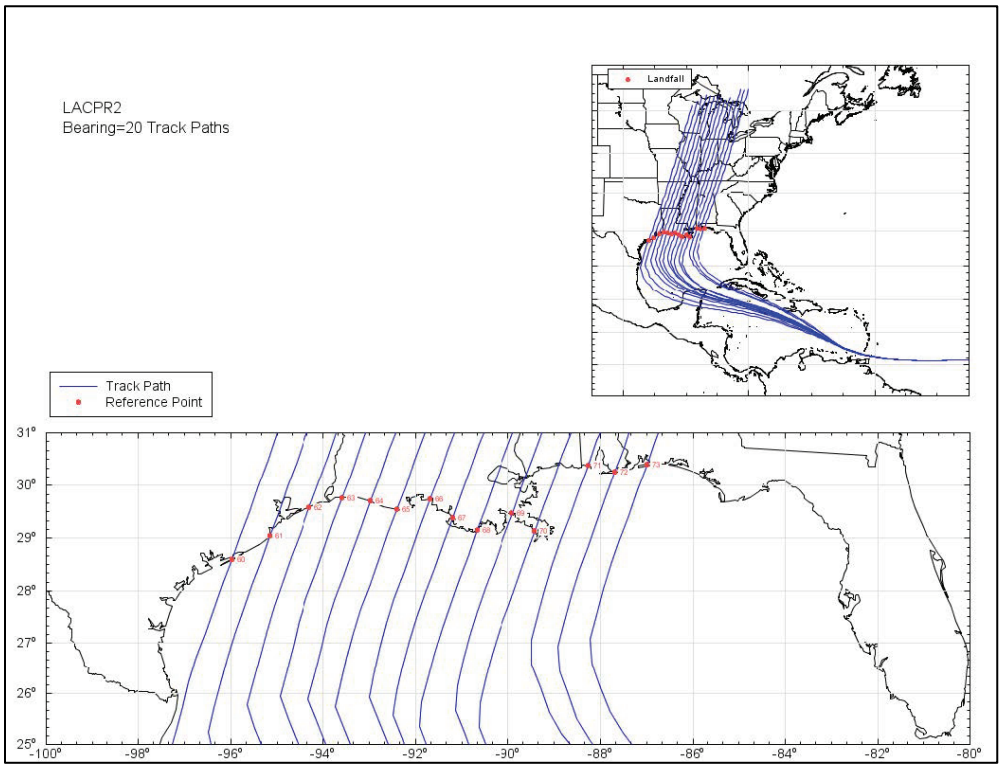


Figure 5-8. JPM heading 40° track paths.

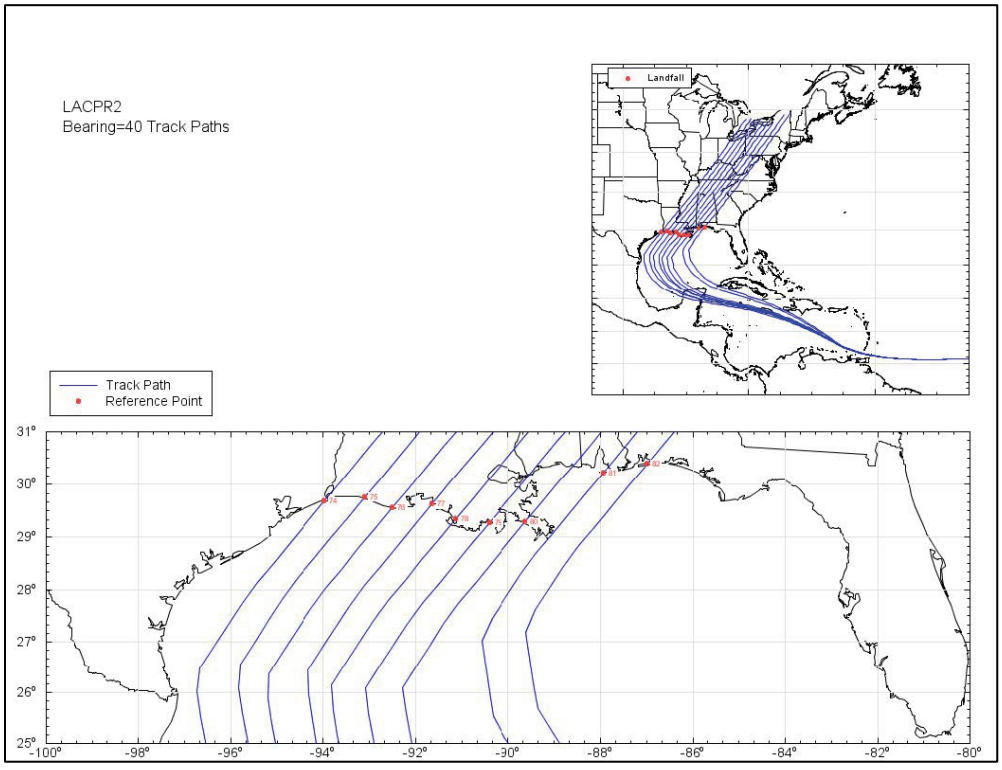
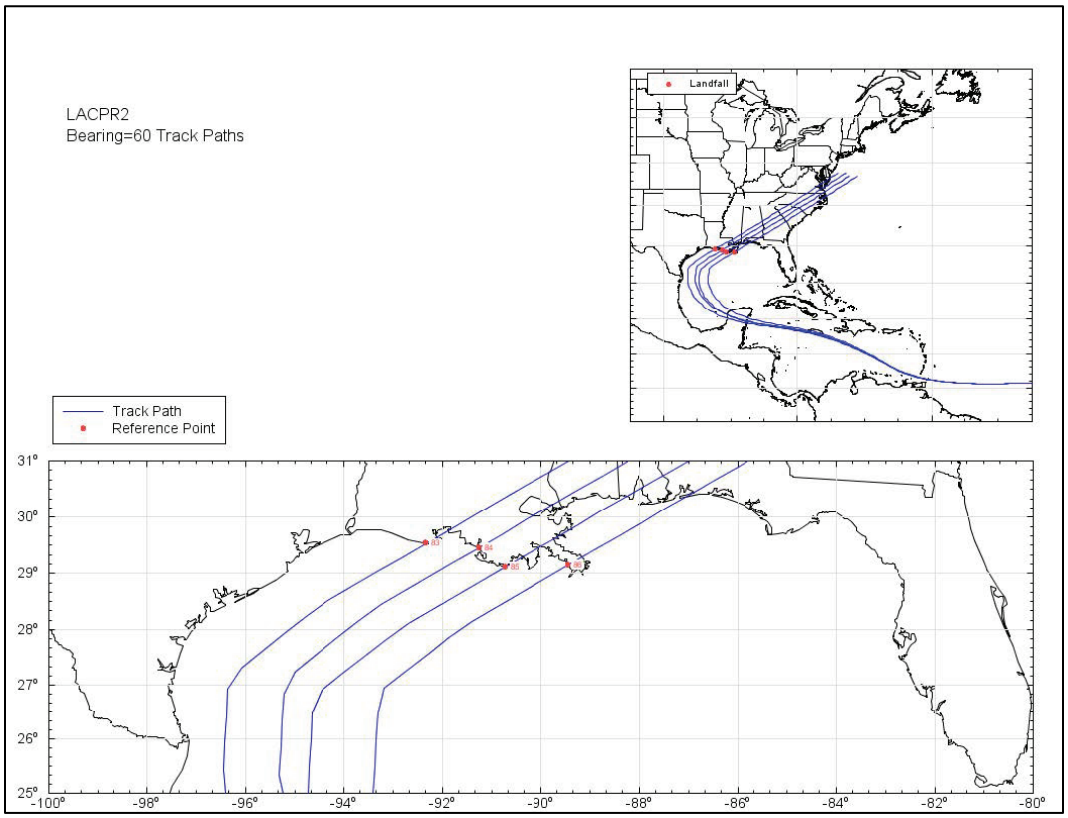


Figure 5-9. JPM heading 60° track paths.



5.2 Along-track variation of TC parameters

Varying the storm position (x_o) and track heading direction (θ) resulted in a total of 86 master tracks (Appendix B). To complete the synthetic storm set, different combinations of the remaining parameters, Δp, R_{max}, V_t, must be assigned to each of the master tracks. In Section 4.3, it was discussed that structured discretization was used for Δp and θ. Discretization of the marginal distributions through BQ optimization was used for the remaining parameters R_{max} and V_t. This process resulted in 645 synthetic TCs for the coastal Louisiana region with the number of storms per track varying between 7 and 8 TCs. The final synthetic TC suite is listed in Appendix B: CHS-LA Synthetic Tropical Cyclone Master Tracks.

The storm parameters Δp, R_{max}, and V_t are valid at the offshore reference point (ORP), 250 km from the point of landfall, or at a reference bypass location. All track sets include a single landfall location and apply the post-landfall filling model described in Vickery (2005), which used relationships for Gulf of Mexico (GOM) storms. Forward translation speed helped inform storm time lengths, as shown in Table 5-1.

Table 5-1. Length of JPM storms as a function of translation speed.

Forward Translation Speed (knots)	Hours Prior to ORP (spin up)	Hours Post ORP (spin down)	Model Time-Step (minute)
$V_t < 5.0$	144	60	15
$V_t \leq 7.5$	132	54	15
$V_t \leq 10.0$	120	48	5
$V_t \leq 12.5$	108	42	5
$V_t \leq 15.0$	96	36	5
$V_t \leq 17.5$	84	30	5
$V_t \leq 20$	72	24	5

All storms applied a far-field pressure of 1,013 hPa to be consistent with the value used to determine pressure deficit in the JPM development. The Holland *B* parameter, which controls the peakedness of the wind profile, was based on Equation 5-1. For this study, the Holland *B* parameter was estimated based on the statistical model with the following form:

$$B = 1.7642 - 1.2098\sqrt{A} \tag{5-1}$$

$$\sigma_B = 0.226$$

$$A = \frac{R_{max} \cdot f_c}{\sqrt{2R_d T_s \cdot \ln\left(1 + \frac{\Delta p}{c_{p \cdot e}}\right)}} \tag{5-2}$$

where

R_d = gas constant for dry air (287 N m $k^{-1\,kg\,1}$)
c_p = central pressure (mb or hPa)
T_s = sea surface temperature (˚C)
Δp = central pressure difference (mb or hPa)
f_c = 0.00001454 sin θ, where θ is the latitude
R_{max} = radius of maximum winds (m).

A mean sea surface temperature of 26.3C° was applied in Equation 22, based on the annual mean of National Center for Environmental

Prediction/National Center for Atmospheric Research reanalysis of sea surface temperature data. To avoid unrealistic *B* values for weak storms, central pressure was capped to a maximum of 980 mb when applied in Vickery and Wadhera (2008) Equation 22 to match the development of the referenced statistical model. Intense storms with c_p <=930 mb and R_{max} >= 40 km at the JPM reference point applied a mean *B* of 1.01 with σ_B = 0.082. A randomly generated standard deviation of +/-1 was generated for each storm and applied in the *B* calculations per storm basis.

Sections 5.2.1 through 5.2.3 describe the work done to develop synthetic TC time series by varying the JPM parameter sets along each TC master track. The along-track variations in TC parameters were based on climatological analysis of historical storms in the northern GOM.

5.2.1 Determination of pre-landfall filling

Historical storm reference landfalls in the study area from the 1938–2019 period were used to determine any pre-landfall modifications to be applied from the reference points 250 km offshore to the landfall/bypassing reference location for each synthetic TC (Figure 5-10). This period of record was applied, since this pre-landfall filling analysis for the storm suite development was performed near the beginning of the study. Storm locations and central pressures were obtained from the IBTracs (International Best Track Archive for Climate Stewardship) (Knapp et al. 2010; 2018) archive based on HURDAT2. Given the landfall time/location specified from the IBTracs archive, over-water estimates of central pressure up to the greater of 500 km or 48 hr before the closest approach was extracted from the IBTracs archive. When the ratio of pressure deficit offshore to the landfall pressure deficit [$\Delta p/\Delta p$ (Ref)] is expressed as a function of distance (Figure 5-6), the storm data show both storms weakening [$\Delta p/\Delta p$ (Ref) > 1] and strengthening [$\Delta p/\Delta p$ (Ref) < 1] as a function of distance to the closest approach point. On average, there appears to be very little change in storm intensity before the closest approach. When the data are stratified by Atlantic, and GOM landfall (Figure 5-6 middle and bottom panels), a more remarkable change is found for GOM landfalling storms.

To explore the effect of storm strength on prefilling, a series of linear fits were made on a per storm basis to determine the pressure deficit at 250 km before the closest approach. A fit of all the GOM storms shown in

Figure 5-6 showed little difference from the relationship applied in the CTXS and SACS studies and was retained for the CHS-LA set. The relationship of the pressure deficit ratio $\Delta p(250\text{ km})/\Delta p(Ref)$ is expressed as a function of 250 km pressure deficit: all (top), Atlantic (middle), and GOM (bottom) landfall storms. Atlantic storms show little to no change from the 250 km reference point offshore to landfall. GOM storms show a strong relationship with regard to the intensity of weaker storms ($\Delta p <$ ~50 mb) gaining strength to the coastline and stronger storms ($\Delta p >\sim 50$ mb) weakening from 250 km offshore to the coastline.

The following relationship was applied in the JPM:

$$\Delta p(Landfall) = \Delta p(250\ km)/[0.8091 + 0.00341 \times \Delta p(250\ km)] \quad (5\text{-}3)$$

where $\Delta p(250\ km)$ is the pressure deficit at 250 km before landfall in millibars. Pressures are modified linearly from 250 km offshore to the computed landfall intensity. Since both Holland B and R_{max} functions from Vickery and Wadhera (2008) depend on Δp, these parameters were also recomputed during the pre-landfall filling process in the JPM.

Figure 5-10. Tracks 1938–2019 in northern Gulf of Mexico with landfall location (red), track location pre-landfall (blue), and track location post-landfall (green).

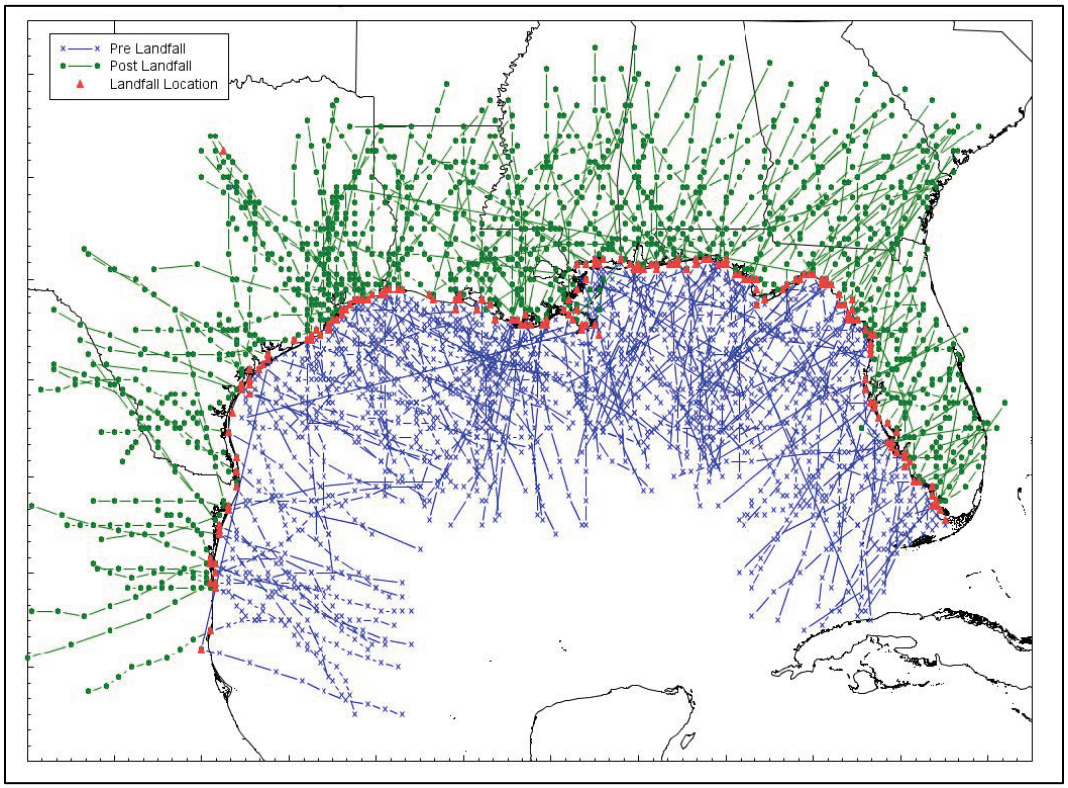
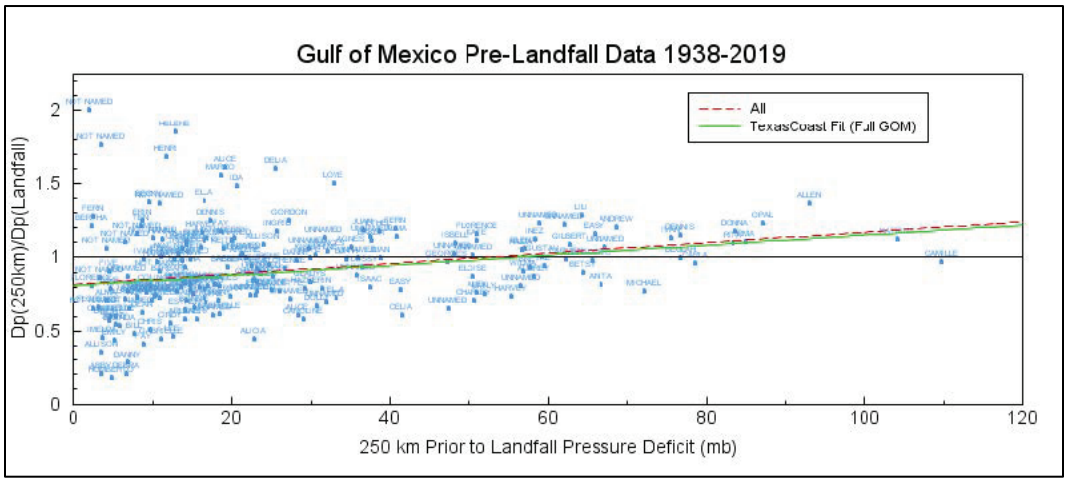


Figure 5-11. Linear fit to ratio of pressure deficit at 250 km and landfall as a function of pressure deficit at 250 km. Ratio of > 1 indicates storms weakening as they approach landfall, ratio < 1 are storms strengthening towards landfall. Relationship applied in Texas Coast/SACS study shown in green.



5.2.2 Determination of landfall filling

All track sets that include a landfall location apply the post-landfall filling model described in Vickery (2005). The Holland B and R_{max} parameters were also recomputed during the post-landfall filling based on the functions from Vickery and Wadhera (2008).

5.2.3 Scale pressure radius

In both the JPM development and in the pre-landfall/post region filling application, the R_{max} was used as a parameter to describe each storm. In the PBL, the R_{max} is not an input value but rather the end result of running the model with the prescribed inputs. The storm's radius is primarily controlled by the scale pressure radius (R_p) and thus requires a function to convert R_{max} to R_p. Equation 5-4 was developed by Oceanweather, Inc., (OWI) as part of the MORPHOS project and was based on a series of actual historical storms of various radii, forward speeds, and latitudes and has been applied in the CTXS and the SACS studies.

$$Rp(Nmi) = -1.1964089822 + 1.0833507089 * R_{max}(Nmi) + 0.00697299296 * R_{max}(Nmi)^2 \quad (5\text{-}4)$$

5.3 Summary of tropical wind and pressure fields

Following the determination of along-track variations in TC parameters, the 645 storm suite described in Section 4 was run through the PBL

model. Wind and pressure fields were developed on two working grids. The large scale Western North Atlantic Domain is a latitude-longitude grid covering the domain 5°–47°N, 99°–55°W at a 0.2-degree resolution. The more refined grid, referred to as the LandDomain grid, is a 0.02° latitude-longitude grid centered at the landfall location and extends ±1.5°.

The time-step for all output is 15 or 5 min depending on forward speed (Table 5-1). Output files are in WIN/PRE format, a standard preprocessor input to ADCIRC. Winds are a 30 min average wind at 10 m height about MSL, representing marine exposure. Pressures are at MSL in millibars.

Figure 5-12 depicts an overall summary of the track paths and model inputs in scale pressure radius, Holland *B*, and forward speed versus storm intensity for the entire 645 storm set. Figures like those shown in Figures 5-13 and 5-14 depict both the storm inputs and determination of along-track TC parameter variations, for an example TC.

Figure 5-12. Summary of JPM track path and derived parameters for the 645 storm set.

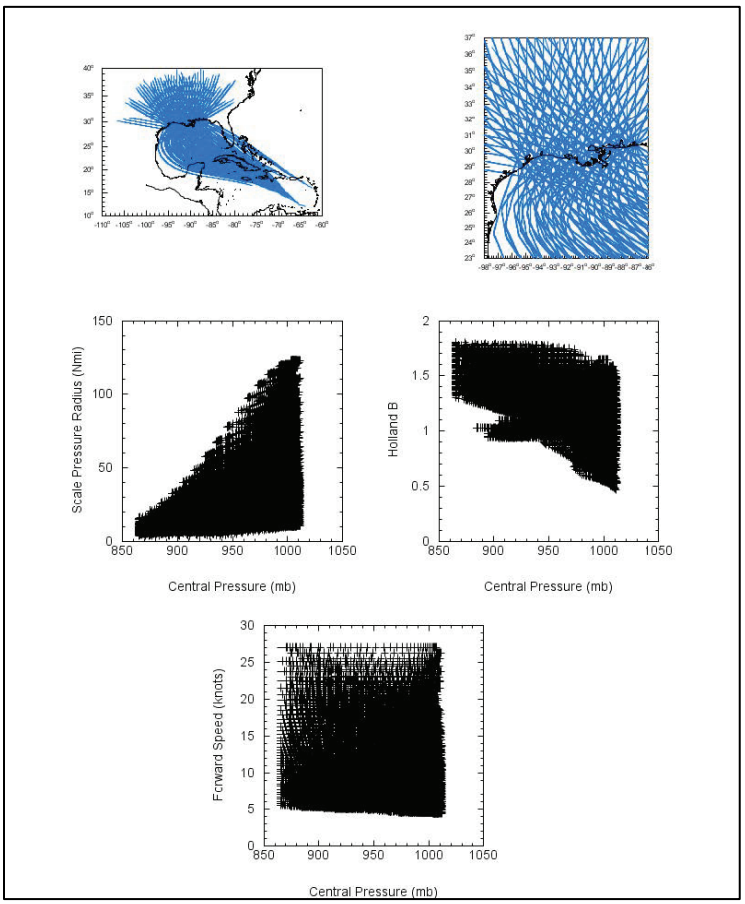


Figure 5-13. Summary of CHS-LA TC 1 (JPM0001) model input.

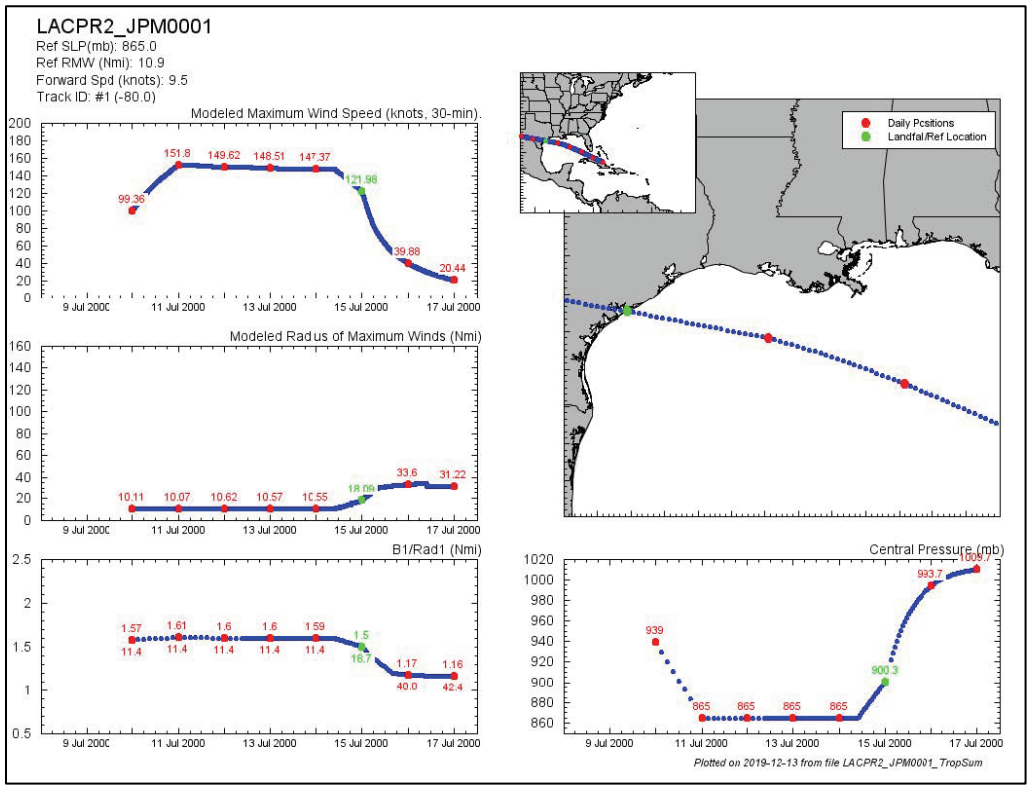
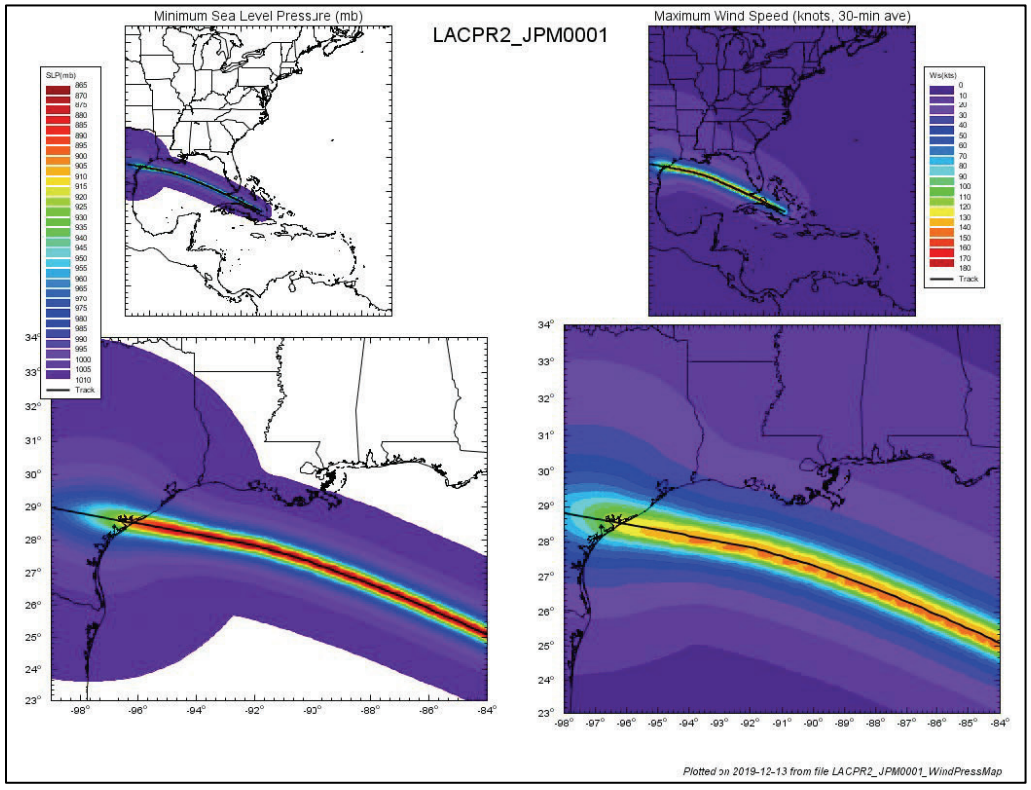


Figure 5-14. Summary of CHS-LA TC 1 (JPM0001) model graphical output of minimum pressure (mb, *left*) and maximum winds (knots, 30 minute average, *right*).



5.4 Planetary boundary layer (PBL) model

The OWI Tropical Model (i.e., PBL model) was first developed into a practical tool in the Ocean Data Gathering Program (ODGP) (Cardone et al. 1976). This model provides a fairly complete description of the time-space evolution of the surface winds in the boundary layer of a tropical cyclone from the simple model parameters available in historical storms. The model applies a theoretical description of the horizontal airflow in the boundary layer of a moving vortex. That model solves, by numerical integration, the vertically averaged equations of motion that govern a boundary layer subjected to horizontal and vertical shear stresses. The equations are resolved in a Cartesian coordinate system whose origin translates at constant V_t, with the storm center of the pressure field associated with the cyclone. A series of quasi-steady-state solutions represent variations in storm intensity and motion. The original theoretical formulation of the model is given by Chow (1971). A similar model was described more recently in the open literature by Shapiro (1983).

The present version of the model results from three major upgrades: The first upgrade involved mainly replacing the empirical scaling law by a similarity boundary layer formulation to link the surface drag, surface wind, and the model vertically averaged velocity components (Cardone et al. 1992). The second upgrade (Cardone et al. 1994) added geospatial resolution and generalized the pressure field specification. A complete description of the theoretical development of the model as upgraded is given by Thompson and Cardone (1996). Last and most recently, modifications to the model PBL physics allowed for the introduction of a saturation roughness formulation (a capped drag coefficient) consistent with that found by Powell (2007) for the Modeling of Relevant Physics of Sedimentation (MORPHOS) project (MORPHOS 2009).

The model pressure field is the sum of an axially symmetric part and a large-scale pressure field of constant gradient. The symmetric part is described in terms of an exponential pressure profile, which has the following parameters:

$$P(r) = P_o + \sum_i^n dp_i e^{-\left(\frac{R_{p_i}}{r}\right)^{B_i}} \tag{5-5}$$

where P_o = minimum central pressure; dp_i = total pressure deficit; R_{p_i} = scale radius of exponential pressure profile; B_i = profile peakedness

parameter (Holland B); and r = radius. Holland B is an additional scaling parameter whose significance was discussed by Holland (1980). This analytical form is also used to explicitly model the storm pressure field for use in the hydrodynamic model. The model may be prescribed with a single profile (1 combination of Δp, B, and R_p) for storm systems with simple wind profiles. More complex wind profiles such as those which display wind maxima at two radii or those with a shelf structure to the wind profile are described with a double profile. Cox and Cardone (2007) describe the methodology applied in analyzing historical tropical cyclones, while Cardone and Cox (2009) discuss the affect of complex wind profiles on the ocean response.

As presently formulated, the wind model is free of arbitrary calibration constants, which might link the model to a particular storm type or region. For example, differences in latitude are appropriately handled in the primitive equation formulation through the Coriolis parameter. The variations in structure between tropical storm types manifest themselves basically in the characteristics of the pressure field of the vortex itself and the surrounding region. Therefore, the interaction of a tropical cyclone and its environment can be accounted for by a proper specification of the input parameters. The assignable parameters of the PBL formulation, namely PBL depth and stability and of the sea surface roughness formulation, are taken from studies performed in the GOM.

The PBL model was validated initially against winds measured in several ODGP storms. It has since been applied to nearly every recent hurricane to affect the United States offshore area, to all major storms to affect the South China Sea since 1945, and to storms affecting many other foreign basins, including the Northwest Shelf of Australia, Tasman Sea of New Zealand, Bay of Bengal, Arabian Sea and the Caribbean Sea. Many wind comparisons have been published (e.g., Ross and Cardone 1978; Cardone and Ross 1979; Forristall et al. 1977; 1978; 1980; Cardone et al. 1992; Cardone and Grant 1994). More recent publications on the application of the PBL model in driving the ADCIRC and coupled ADCIRC/SWAN modeling system can be found in Hope et al. (2013) (Hurricane Ike 2008), Dietrich et al. (2011) (Hurricane Gustav 2008), Bacopoulos et al. (2011) (Hurricane Jeanne 2004), and Bunya et al. (2010) (Hurricanes Katrina and Rita 2005). Application in Hurricane Harvey (2017) is presented in Cox et al. (2017).

5.5 Validation storm set development

Wind and pressure inputs were developed for three tropical cyclones (Table 5-2) using *best-effort* analysis, which combines the OWI Tropical PBL model and Interactive Objective Kinematic Analysis (IOKA) system to produce research quality forcing. Winds and pressures were developed on three working grids covering the grid domains:

- L1 (WNAT): iLat=211, iLong=221, DX=0.2000, DY=0.2000, SWLat=5.000000, SWLon=−99.000
- L2(GOM): iLat=163, iLong=226, DX=0.0800, DY=0.0800, SWLat=18.00000, SWLon=-98.0000
- L3 (LandFall−- Moves location): iLat=151, iLong=151, DX=0.0200, DY=0.0200.

Storm analysis performed typically applies the double exponential pressure profile fit in the OWI Tropical PBL model. Tropical inputs, also referred to as "Trop" files, using the single exponential option (single Holland *B*/Scale Pressure Radius) were developed from the original analysis, attempting to best mimic the maximum wind and more complex wind profile from the initial examination.

Single exponential storms developed were then translated on idealized track(s) as defined in the storm set. Storm winds/pressures were generated on the same working grids.

Table 5-2. CHS-LA validation storms.

IBTrACS Name	Start Date (YYYYMMDDHH format)	End Date (YYYYMMDDHH format)	System Name	Landfall Ref Date (YYYYMM format)	Landfall Ref Date (DDHHMM format)	Landfall Latitude	Landfall Longitude	JPM Track
1900239N15318	1900083000	1900091000	Not Named	190009	090200	29.10	−95.10	TC_JPM0257
2018280N18273	2018100418	2018101112	Michael	201810	101730	30.01	−85.54	SACS_JPM1192
2019192N29274	2019070900	2019071418	Barry	201907	131500	29.60	−92.20	LACPR2_JPM0153

Analysis of each storm begins with a reanalysis of the track and intensity of each storm. Then, individual fits of the radial pressure profile are applied to determine PBL model inputs such as Holland *B* and scale pressure radius. When appropriate, a *double exponential* pressure profile fit is used, requiring two Holland *B* and two radii. This more advanced profile describes better storms that depict multiple wind maxima or a

shelf-like structure to the wind profile outside the R_{max}. More information on the model-fitting methodology and its impact on the ocean response can be found in Cox and Cardone (2007) and Cardone and Cox (2009).

Once model inputs are determined and the PBL model run, the resultant winds are compared to available in situ, aircraft, and satellite observations. As needed, fields are modified using the Interactive Objective Kinematic Analysis system (Cox et al. 1995). The kinematic analysis using the IOKA system includes blending the PBL winds within a synoptic wind field and incorporating external storm reanalysis performed using the HWind system when deemed appropriate.

Three sets of output were developed for the historical storm set. Tropical files, the input set to the PBL model, were created for each storm as analyzed. An additional set of *single exponential* fits were also developed for each storm. The single fits only apply a single Holland *B*/Rad1 combination and represent a more simplified fit of the radial wind profile. Finally, wind and pressure files on the working grids were developed using the IOKA system.

Figures 5-15 through 5-17 depict the tropical inputs applied in the analysis along with the envelope of maximum winds/minimum sea level pressure for Hurricane Michael. Some storms depict wind maxima from other active tropical systems in the basin. Michael and Barry applied the reanalysis wind fields and sea level pressures from the ERA5 hindcast (https://www.ecmwf.int/en/forecasts/data sets/reanalysis-data sets/era5) to fill out the basin. In contrast, the 1900 Galveston storm used wind fields only from the NCEP twentieth-century reanalysis project.

Figure 5-15. Summary of winds and pressures during 2018280N18273 (Michael 2018) for L1.

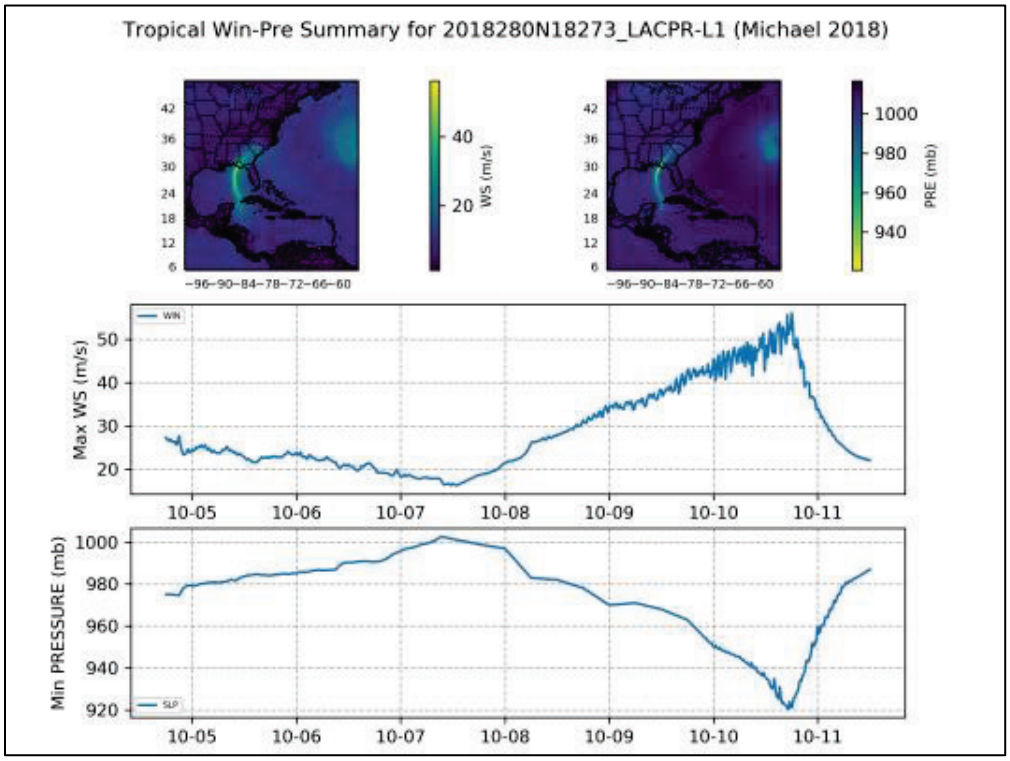


Figure 5-16. Summary of winds and pressures during 2018280N18273 (Michael 2018) for L2.

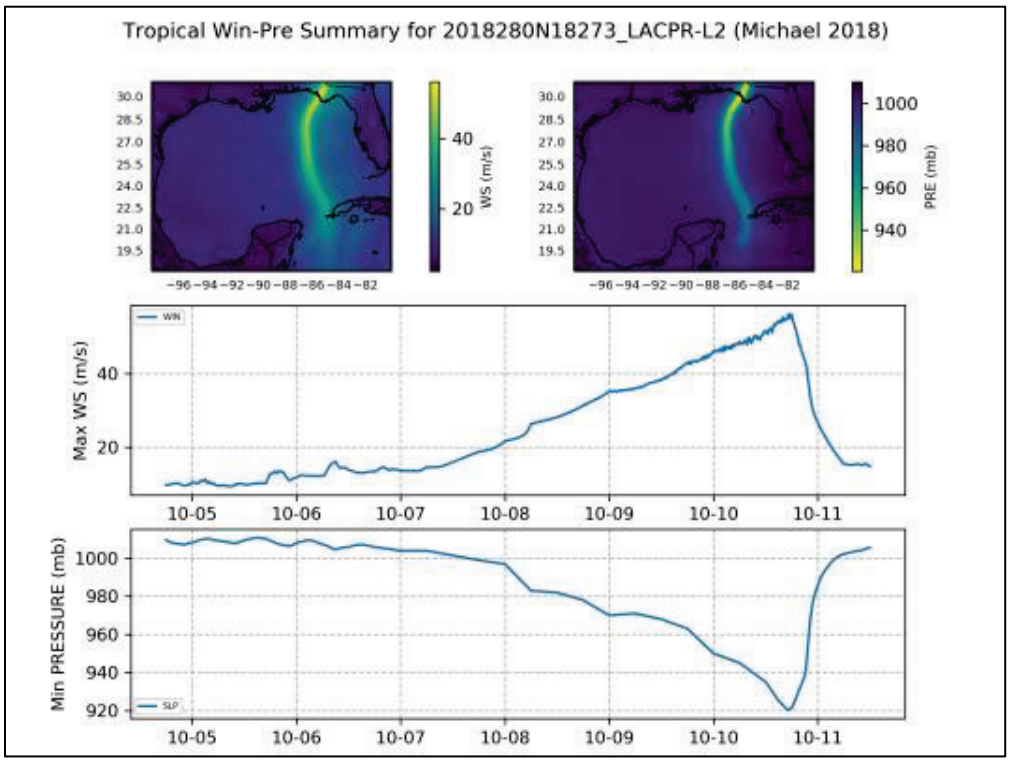
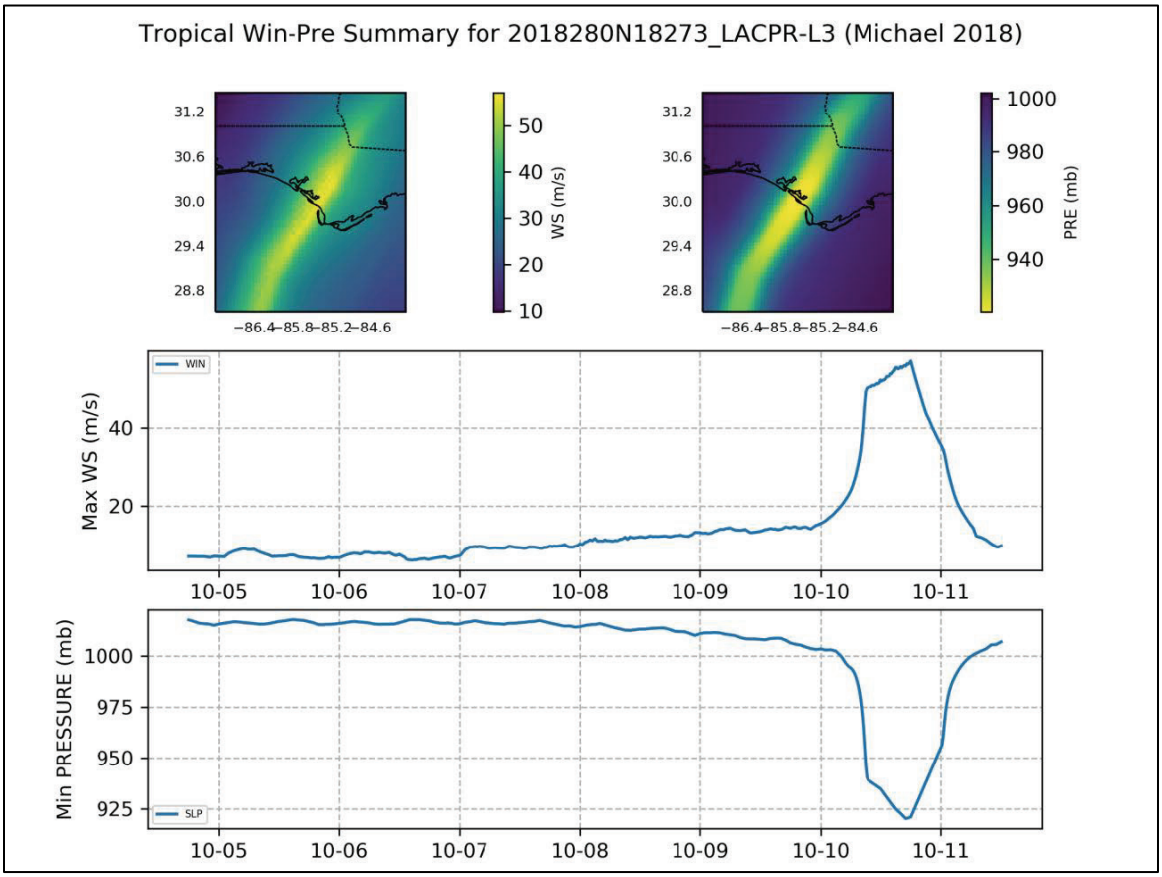


Figure 5-17. Summary of winds and pressures during 2018280N18273 (Michael 2018) for L3.



6 Quantification of Coastal Storm Hazards

The following subsections describe the application of the CHS PCHA framework for quantifying coastal storm hazards and developing hazard curves of SWL, H_{mo}, and T_p for 1.2 M point locations within the CHS-LA study area. Details related to the hydrodynamic modeling, DNC, and training of the GPMs are provided in Section 6.1. Section 6.2 describes the correction of bias and uncertainty estimation for the JPM integration of TC responses. The incorporation of astronomical tides is described in Section 6.3. The analysis of the TC responses considering a single deterministic riverine Q value (Q_d) is discussed in Sections 6.4 and 6.5. The extension of the PCHA framework to quantify coastal compound hazards accounting for multiple probabilistic Q values (Q_p) is presented in Section 6.6.

6.1 Hydrodynamic modeling considerations

The ADCIRC and SWAN numerical models were used in the CHS-LA study to simulate the hydrodynamic responses of the ITCS. The simulations of the ITCS were conducted considering an initial water level of 1.19 ft relative to NAVD88 2009.65 and 2020 as the base year (Cobell and Roberts 2021). Wave effects were included in the ADCIRC simulations; however, astronomical tides were excluded from the simulations, given the relatively small tidal range within the study area.

CHS-LA evaluated the effect of Q on storm response AEFs through the application of storm simulations run under Q_d and Q_p scenarios. The 645 storms within the ITCS were simulated in ADCIRC, including a constant Mississippi River discharge of 11,326.74 m^3/s and Atchafalaya River discharge of 4,854.36 m^3/s. A 100-TC subset from the ITCS was selected for hydrodynamic simulations run under five other Q values. The storm simulations listed in Table 6-1 comprise a 1,145 set of synthetic TCs, which were applied in the present study. The Q scenarios defined in Table 6-1 are daily Q values derived from the 1976–2019 historical record, beginning in May and continuing through the Atlantic hurricane season, that is, June to November. The period of record was chosen due to the anthropomorphic nonstationarity in the daily Q values before 1976. The Q values selected for each scenario in Table 6-1 are based on the 70% and 30% split in discharge directed through the Mississippi and Atchafalaya Rivers, respectively, at the USGS gauge 07295100 at Tarbert Landing. The maximum regulated Q

allowed for the Mississippi River through the HSDRRS is 35,396 m^3/s, as represented by Scenario 6 in the table below.

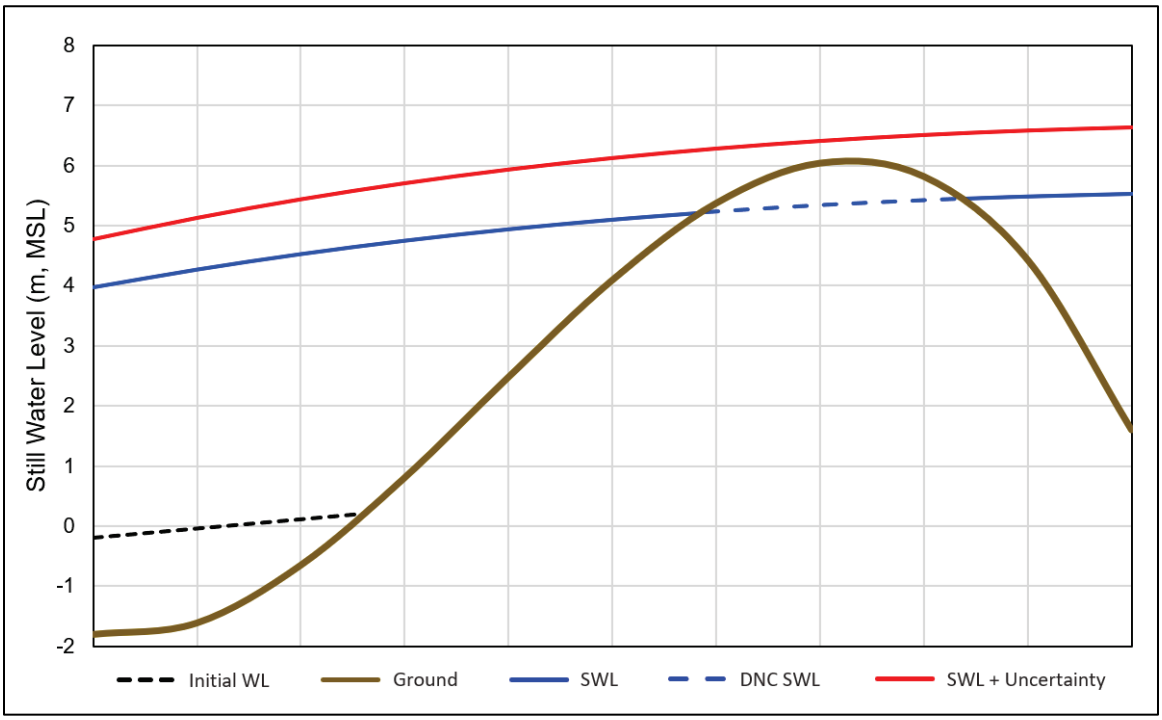
Table 6-1. Riverine discharge (Q) scenarios simulated for the CHS-LA.

Q Scenario	Number of Storms	Mississippi River Q (m^3/s)	Atchafalaya River Q (m^3/s)
1	645	11,326.74	4,854.36
2	100	0	0
3	100	3,152	1,351
4	100	7,329	3,104
5	100	23,361	10,016
6	100	35,396	15,176

6.1.1 Dry-node correction (DNC)

When considering storm surge results for any given study area, some locations are not inundated (remain dry) for some TCs. The occurrence of these dry computational locations (nodes), if left uncorrected, can adversely affect the reliability of the GPM and the accuracy of hazard estimates due to both the reduced number of support points for training a metamodel and the loss of discrete TC weight associated with TCs that do not inundate a given node. In CHS studies that incorporate hydrodynamic results at the nodes (i.e., very high geospatial resolution), such as CHS-LA, the PCHA framework performs DNC by applying a weighted kNN regression. This regression interpolates the water level beneath the dry ground, thus providing an accurate estimate of the storm surge at each dry node in each storm simulation. The weighted kNN regression completes the SWL surface over the project domain on a per-storm basis to fill in missing information at the dry nodes. In this scheme, the forcing vector $\hat{x}$ is replaced with geospatial information from nodes, including latitude, longitude, and ground elevation. Figure 6-1 shows an idealized cross-section to demonstrate the implementation of the DNC.

Figure 6-1. Idealized across-shore sketch illustrating the dry-node correction.



The dashed-black and solid-brown curves represent the initial water level and ground elevation, respectively. The SWL surface (solid blue curve) is interrupted by a section of high ground elevation (e.g., coastal bluff, dune, or barrier island). In typical JPM applications, nodes within this high ground area are inundated by only the most extreme TCs, leaving an incomplete representation of the SWL, which could result in a significant underestimation of the storm surge hazard at these locations. For these uncorrected locations, the DNC completes the SWL surface over the entire domain and across the high ground sections (dashed blue curve) to provide an accurate estimate along the whole blue line. Extending the SWL surface, even below ground, allows for proper integration of JPM uncertainty (per Equation 2-1; 2-2). As a result, the SWL + uncertainty surface (red curve) may exceed the elevation of the high ground section.

The DNC procedure was used only to correct nodes inside the bounding box defined by [26°N, 32°N, 96.5°W, 85.5°W]. Before performing the DNC, any node that remained dry across all 645 storm simulations was removed from the hydrodynamic modeling results. The DNC applied the *k*NN regression to interpolate missing values for any node which remained dry within at least one storm simulation. When identifying the *k*NN for each dry node, the hydraulic connectivity of the ADCIRC mesh was

considered to identify disconnected domains in the mesh. The identification of disconnected domains helped prevent the DNC from interpolating unrealistically high storm surge behind protected areas, such as the levee structures surrounding the West Bank & Vicinity (WBV) and the Lake Pontchartrain & Vicinity (LPV). The interpolated surge, or pseudo-surge, the calculation was performed in three steps:

1. Identify the number of wet nodes from the set of the *k* nearest neighbors.
2. Assign weights to the wet nodes according to their inverse distances to the dry node.
3. Compute the pseudo-surge using the weighted average of the storm surges of the wet nodes.

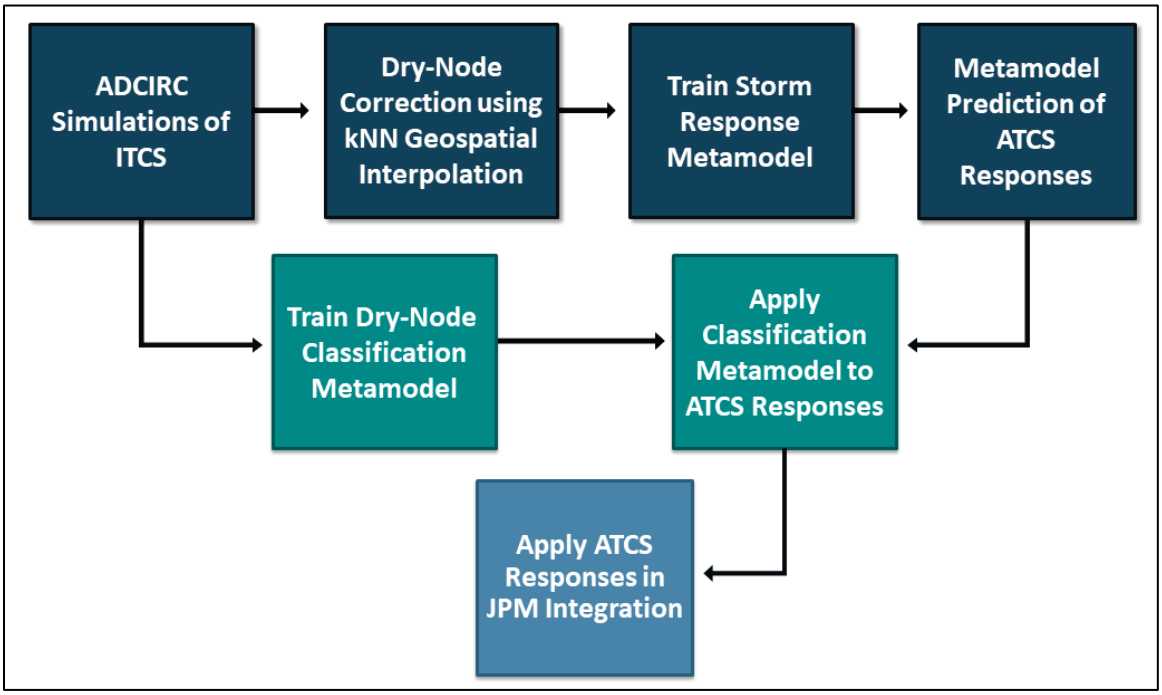
In this process, there are often problematic nodes in areas of complex geomorphology where the pseudo-surge is higher than the node ground elevation. The remedy for these problematic nodes is combining the pseudo-surge predictions with a classification metamodel (Kyprioti et al. 2021). The pseudo-surge values are kept in the training database for developing the surge metamodel; in doing so, the gaps of missing information in the training database are eliminated, which improves the accuracy of the metamodel applied in predicting surge values from the augmented suite. If any node was misclassified as wet within the ATC suite predicted storm responses, the classification metamodel is then applied to set the node conditions as dry.

The DNC is a two-fold process meaning that both the *k*NN geospatial interpolation and the classification metamodel are applied separately. Note that since the DNC applies both *k*NN regression and a classification model, the process for correcting dry nodes involves both the ITCS simulations and the ATCS predicted responses. The *k*NN regression is initially applied to the hydrodynamic simulations of the ITCS. The classification metamodel is then trained, and responses are predicted for the ATCS. The classification metamodel predicts binary outputs that determine whether a storm wets a node or remains dry. After the storm responses have been predicted for the augmented suite, the classification metamodel is applied to correct any nodes that were misclassified as wet.

This two-fold process is particularly important for areas of complex geomorphology, given that the *k*NN interpolation may predict the pseudo-surge to be higher than the elevation of a given dry node. Therefore, the

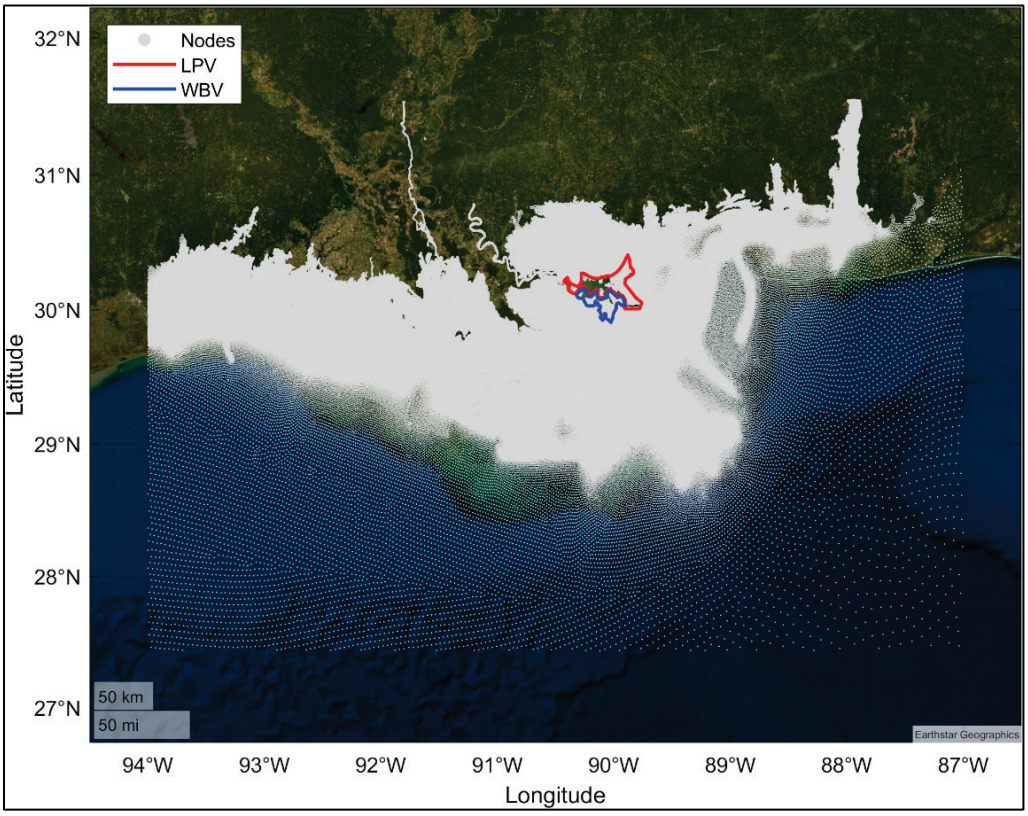
predicted values from the ATCS are kept unless the classification metamodel predicts that node as dry, in which case the node conditions will then be set to dry. As an example, Figure 6-2 illustrates the workflow applied to include the two-fold DNC process and metamodeling of the storm responses discussed in Section 6.1.2 within the PCHA for CHS-LA.

Figure 6-2. PCHA workflow incorporating the two-fold DNC and metamodeling of storm responses.



After the DNC, the node count was further reduced by removing nodes outside the boundary defined as [28°N, 31°N, 94°W, 87°W]. In total, more than 1.23 M nodes were identified within this bounded area at which the AEFs of TC responses were computed. Figure 6-3 shows the geospatial distribution of nodes considered for the CHS-LA. This figure also illustrates the location of the levee structures surrounding the WBV and the LPV. The following subsections describe the methods applied to train metamodels to predict surge and H_{mo}.

Figure 6-3. Nodes selected within bounds of the study area. LPV and WBV are shown for geospatial reference.



6.1.2 Metamodel training

The CHS-LA ITCS was defined by a five-parameter set: $x = [x_o, \theta, \Delta p, v_t, R_{max}]$. For the GPM training, the number of input parameters increased to six to consider both the latitude and longitude of the landfall locations, thus: $x = [Latitude, Longitude, \theta, \Delta p, v_t, R_{max}]$. To extend the PCHA framework to quantify coastal compound hazards in the vicinity of the HSDRRS, the 1,145-storm ITCS with six unique values for the Mississippi River Q required explicitly including Q as an input parameter for the GPM, increasing the number of inputs to seven, such that: $x = [Latitude, Longitude, \theta, \Delta p, v_t, R_{max}, Q]$. To fully cover the TC parameter and probability spaces and improve the accuracy of the storm hazard estimates, an ATCS consisting of 748,200 events was created through the discretization of the TC parameter range, as discussed in Section 4.4. Three metamodels were trained to predict the following respective responses for the ATCS: (1) storm surge at 1.1 M nodes for the 645 ITCS with Q_d; (2) H_{mo} at 1.1 M nodes for the 645 ITCS with Q_d; and (3) storm surge at 1.1 M nodes for the 1,145 ITCS with variable Q_p.

The metamodel estimates the hydrodynamic responses with a kriging prediction equation (Zhang et al. 2018). Before the kriging development, the storm surge values in the 645- and 1,145-storm sets were normalized to facilitate decreasing the dimensionality of the synthetic TC parameters by Δp. The main requirements of the equation for the metamodel are basis vectors, $f(x)$, and a correlation structure $R(x^i, x^j|s)$, where s is a set of hyperparameters (Zhang et al. 2018). For this study, linear basis functions were chosen for $f(x)$, and the predictive cross-validation method was used to optimize s. The raw predictions generated by the kriging model were transformed to the original, high-dimensional response space with the Principal Component Analysis transformation. The resulting average validation statistics show good accuracy for the GPM predictions for CHS-LA. Below, Table 6-3 presents several of the cross-validation statistics for the respective metamodels, including $\overline{cc}$, the correlation coefficient; $\overline{R^2}$, the coefficient of determination; and $\overline{\sqrt{se}}$, the square root of the squared error. The bar over the statistics indicates the statistics are averaged over all storms.

Table 6-2. GPM cross-validation statistics.

Variable	Storms	Number of nodes	$\overline{cc}$	$\overline{R^2}$	$\overline{\sqrt{se}}$ (m)
Surge	1145	1,239,389	98.45%	96.98%	0.1153
Surge	645	1,239,389	93.16%	88.04%	0.1587
H_{m0}	645	1,238,592	91.14%	85.00%	0.0718

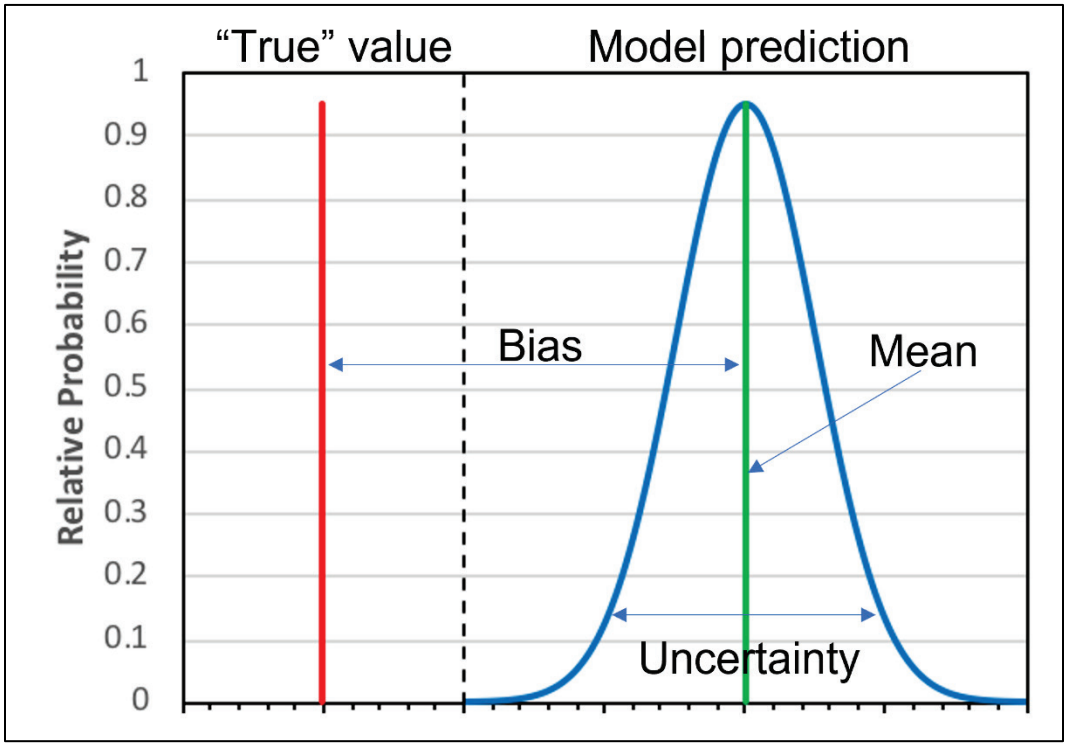
After the metamodels were trained, the surge and H_{mo} responses were calculated for the ATCS. Nodes inundated by fewer than 32 of the original 645 storms, that is, 5% of the initial simulations, were removed from further analysis. The final results retained 1,098,858 nodes for SWL hazard curves and 1,098,096 nodes for H_{mo}.

6.2 Geospatial bias correction and uncertainty quantification

A natural consequence of the inherent simplification associated with the modeling of complex natural systems is that model outputs will differ to some degree from the actual values of the evaluated phenomena. Quantification of the difference or error is necessary to calibrate model parameters, validate the results, and characterize the model performance. Errors in hydrodynamic modeling may originate from the idealization of

wind fields, discretized approximation of the bathymetry and topography, shallow water approximations of the governing hydrodynamic equations, simplified wave model equations, or assumptions related to boundary conditions. As shown in Figure 6-4, the two main error components are systematic error (bias) and spread (uncertainty), which relate to model accuracy and precision. In the JPM approach, it has been typically assumed that the error is unbiased and the uncertainty has been addressed by using an error term within the JPM integral. Bias correction is required before the JPM integration if found in the assessment of model error. Generally, errors in SWL and H_{mo} are evaluated by comparing the validation storm simulation results to observations. For SWL, the comparison is primarily made with water level gauge measurements and high-water marks (HWM). While gauge measurements are typically reliable, HWMs often include wave effects that limit their usefulness for SWLs as well as some degree of human interpretation of the HWM. As a result, HWM data are carefully screened to remove HWMs that could include significant wave effects. The validation storms considered in the CHS-LA study area were Hurricanes Gustav (2008), Ike (2008), Isaac (2012), Katrina (2005), and Rita (2005). This distribution of the validation data points for these storms as applied for the estimation of bias and uncertainty for this study is illustrated in Appendix C.

Figure 6-4. Illustration of bias and uncertainty in model prediction.



6.2.1 Aleatory and epistemic uncertainties

As discussed by Gonzalez et al. (2019), uncertainties associated with coastal storm hazards are generally classified as either aleatory or epistemic. *Aleatory* uncertainty, also called aleatory variability, describes the stochastic (i.e., random) nature of hazard events and processes. *Epistemic* uncertainty refers to the scientific uncertainty associated with the modeling of natural processes and arises due to a lack of data, information, or knowledge about the physical world. This form of uncertainty is often called subjective or reducible uncertainty since it can theoretically be reduced through further research and additional data collection efforts. In practice, this possibility of reduction is also present for aleatory uncertainty and is not exclusive to epistemic uncertainty (Vrouwenvelder 2003). Estimates of stochastic processes that are characterized as aleatory uncertainty cannot be significantly reduced in the short-term, but they can be improved. Therefore, differentiating between aleatory and epistemic uncertainties can be challenging, depending on the nature of the model (USNRC 1997; IPET 2009). Furthermore, Brun et al. (2011) contend that aleatory and epistemic uncertainties are not mutually exclusive. Der Kiureghian and Ditlevsen (2009) state that the characterization of uncertainty as either epistemic or aleatory is a pragmatic choice that depends on the application; uncertainty can be defined as epistemic in one model and as aleatory in another. The distinction between epistemic and aleatory uncertainty should serve the practical purpose of acknowledging the sources of uncertainty that could be reduced at present without demanding major scientific or engineering advances.

In coastal storm hazard applications, aleatory uncertainty arises due to the prevalence of geospatial and temporal variability in atmospheric, hydrodynamic, and other natural physical processes that cannot be exactly replicated by current models. Aleatory coastal storm events are characterized by their likelihood of occurrence and by probability distribution functions describing their intensity, size, forward translation speed, and track heading direction in the case of tropical cyclones. As discussed by Bensi and Kanney (2015), accounting for aleatory uncertainty results in a hazard curve. In contrast, the standard for quantifying and propagating epistemic uncertainty in general probabilistic hazard analysis is the use of logic trees to consider alternative data, methods, and models necessary to perform the analysis (USNRC 1997; Bommer and Scherbaum

2008; IPET 2009; Kammerer and Ake 2012; Kammerer 2013; Gonzalez et al. 2019). Bensi and Kanney (2015) describe various examples of epistemic uncertainty specific to coastal storm hazards analysis, including (1) the selection of probability distribution functions for characterizing aleatory uncertainty associated with storm parameters, (2) the selection of storm sampling technique, (3), the appropriateness of atmospheric and hydrodynamic simulation model applications, and (4) the choice of parameters used in these models. Epistemic uncertainty reflects the lack of understanding of the validity of models and corresponding numerical parameters employed in the quantification of these hazards. The logic tree approach yields a family of hazard curves. Each individual curve represents a unique set (i.e., branch) of alternative data, methods, and models, and the range of uncertainty is conveyed through fractile hazard curves.

The use of logic trees is one alternative for quantifying epistemic uncertainty associated with coastal hazards. However, the implementation of logic trees has fallen outside the scope of JPM-based studies to date due to computational burdens and complexity. In logic tree hazard analysis, differences between the observed and modeled outcomes of coastal storm events are attributed to aleatory uncertainty. Specific sources of model error accounted for in the PCHA framework include (1) hydrodynamic modeling errors potentially arising from unresolved physical processes, inadequate resolution, and bathymetry/topography inaccuracy and (2) atmospheric modeling errors due to idealized wind and pressure fields and wind variations not captured by the PBL model. In practice, even after proper model verification and validation, estimates of hydrodynamic and atmospheric model errors can be improved, but they cannot be significantly reduced in the near term due to the prevalent spatiotemporal randomness of natural processes. Therefore, these model errors are characterized as aleatory uncertainty following the logic tree paradigm.

6.2.2 Sources of modeling error

The sources of bias and uncertainty errors accounted for in this study include hydrodynamic modeling errors and atmospheric modeling errors. Quantifying coastal storm hazards requires correcting bias and estimating uncertainty across all point locations where hazard curves are developed. Storm surge, wave, and atmospheric modeling errors are discussed below.

6.2.2.1 *Storm surge modeling error*

Hydrodynamic modeling errors have been estimated as part of several recent FEMA studies. For example, in the MCAP study (FEMA 2008), the hydrodynamic modeling or calibration error was computed from the differences between simulated and measured storm surge elevations, or HWMs. However, the uncertainty associated with this error was estimated based on the difference between the standard deviations of the calibration and measurement errors. The measurement error was calculated as a standard deviation representing the variability in HWMs from the actual maximum water level. The hydrodynamic modeling uncertainty resulting from the MCAP analysis of these errors was 0.23 m. The hydrodynamic modeling uncertainty calculated in the Coastal Texas FIS (USACE 2011) for the GOM region was estimated to be in the range of 0.53–0.76 m. For NACCS, the hydrodynamic modeling uncertainty was computed based on the differences between ADCIRC results and HWMs and was estimated to be 0.48 m. For CHS-LA, ADCIRC modeling results were compared with HWM data for the simulations of validation Hurricanes Gustav, Ike, Isaac, Katrina, and Rita (Cobell and Roberts 2021). As a result of this effort, relative and absolute forms of bias and uncertainty were computed for the 1.2 M nodes considered for storm surge.

6.2.2.2 *Nearshore wave modeling error*

For the estimation of uncertainty associated with the skill of the wave model, a global H_{mo} uncertainty was estimated as an average across all the nodes due to the sparse availability of buoy measurements for the validation storms. The H_{mo} global uncertainty was assessed by comparing model simulations of validation Hurricanes Gustav, Ike, Isaac, Katrina, and Rita to measurements recorded at buoys within the study.

6.2.2.3 *Atmospheric modeling error*

Errors in atmospheric modeling were estimated from the variability in water levels when comparing levels simulated using PBL winds to those simulated using handcrafted best-winds. The wind and pressure fields derived from best winds employ techniques that combine inputs from various meteorological sources. In previous studies such as the MCAP, the Coastal Texas FIS, and the NACCS (FEMA 2008; USACE 2011; and Nadal-Caraballo et al. 2015), a range of uncertainty of 0.30–0.75 m was

determined from the validation efforts. In particular, the MCAP study, which was completed in parallel with LACPR (USACE 2009c), documented a standard deviation of 0.36 m.

6.2.3 Absolute and relative forms of bias and uncertainty

As shown in this section, uncertainty can be characterized as an absolute quantity (e.g., 0.60 m) or a relative quantity (e.g., 20%). Exclusively accounting for absolute uncertainty is problematic when applied to small surges. For example, a surge and uncertainty of equal magnitudes would superimpose 0.60 m of uncertainty on a 0.60 m surge. Conversely, accounting for relative uncertainty alone could yield unrealistic uncertainty values for extreme surge elevations. The quantified relative uncertainty can be considerable if based on relatively small surge values. The dynamics of applying either an absolute or relative uncertainty are illustrated in Figure 6-5. The horizontal green line represents an example of absolute uncertainty of 0.6 m. Relative uncertainties of 20% and 40% are shown as the solid red and blue lines, respectively.

The PCHA framework overcomes these limitations by quantifying and combining both the absolute and the relative forms of uncertainty. Combining both forms of uncertainty is performed based on statistical data assimilation methods. Quantification of SWL hazard, for example, requires estimating the components of uncertainty introduced by ADCIRC and the PBL model. Absolute and relative uncertainties are first estimated separately for each of these numerical models. The total absolute model uncertainty is then computed by aggregating the absolute uncertainties of the ADCIRC and PBL models. Likewise, aggregating the relative uncertainties for both models results in the total absolute model uncertainty. Finally, to combine the absolute and relative forms of the total model uncertainty, Equation 6-1 corresponding to the scalar case of the data assimilation error statistics described in Gao et al. (2012) is applied across the nodes:

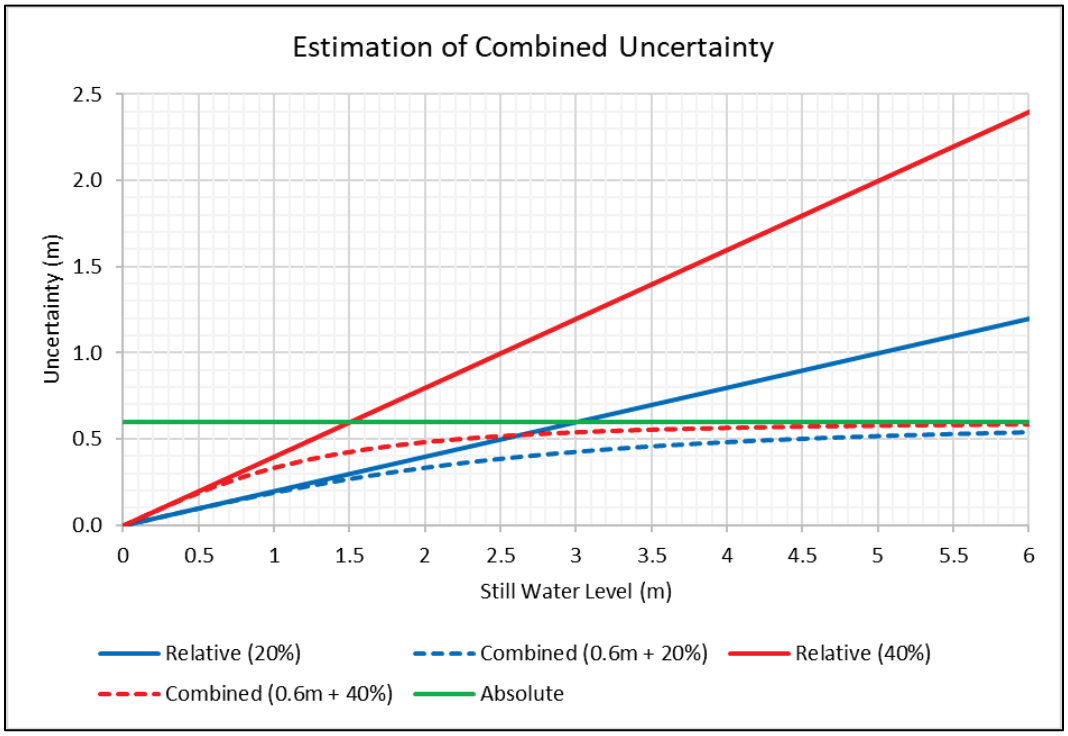
$$\frac{1}{{\sigma_c}^2} = \frac{1}{{\sigma_{a_{Total}}}^2} + \frac{1}{(\sigma_{r_{Total}} \cdot \tau)^2} \tag{6-1a}$$

$$\text{or: } \sigma_c = \frac{1}{\sqrt{\frac{1}{{\sigma_{a_{Total}}}^2} + \frac{1}{(\sigma_{r_{Total}} \cdot \tau)^2}}} \tag{6-1b}$$

where σ_c = total combined uncertainty (m); $\sigma_{a_{Total}}$ = total absolute model uncertainty (m); $\sigma_{r_{Total}}$ = total relative model uncertainty (m/m); and τ = storm response (m) (e.g., SWL, H_{mo}).

Using Equation 6-1b, $\sigma_{a_{Total}}$ and $\sigma_{r_{Total}}$ are combined in a manner that prevents the overestimation of uncertainty and limits the over prediction of both low- and high-magnitude SWL values. The effects of this application are shown in the example combined uncertainty curves shown in Figure 6-5. These examples of combined uncertainty curves apply an absolute uncertainty of 0.6 m to relative uncertainties of 20% and 40%. As seen in the red and blue dashed lines, the combined uncertainty increases as a function of the SWL, but the rate of growth follows an asymptotic behavior and diminishes on approaching the absolute uncertainty.

Figure 6-5. Comparison of methods for characterizing uncertainty.



Numerical model bias is also estimated in absolute and relative forms. The total absolute and relative model biases are calculated individually and subsequently aggregated. The total combined model bias (μ_c) is determined at each computational node using Equation 6-2 as follows:

$$\mu_c = \frac{\mu_{a_{Total}}}{\left\|\mu_{a_{Total}}\right\|} \frac{1}{\sqrt{\frac{1}{\mu_{a_{Total}}{}^2} + \frac{1}{\left(\mu_{r_{Total}} \cdot \tau\right)^2}}} \tag{6-2}$$

where μ_c = total combined bias (m); $\mu_{a_{Total}}$= total absolute model bias (m); $\mu_{r_{Total}}$ = total relative model bias (m/m). Note that differently from Equation (6-1b), a nondimensional factor $\frac{\mu_{a_{Total}}}{\left\|\mu_{a_{Total}}\right\|}$ is incorporated into Equation (6-2) to retain the sign of the bias, which is necessary for the bias correction before estimating uncertainty. The following sections discuss the estimation and correction of geospatial model biases and the quantification of uncertainties. The estimation of the total model bias and uncertainties is documented in Sections 6.2.4 and 6.2.5, respectively.

6.2.4 Geospatial bias estimation and correction

In hydrodynamic numerical model simulations, there is bias if the output tends to either overpredict or underpredict the magnitude of observed responses. The bias associated with the ADCIRC and PBL models was assessed by comparing historical measurement data with simulation results of the validation Hurricanes Gustav, Ike, Isaac, Katrina, and Rita. Because of the geospatial and temporal spareness of the wave buoy measurements, bias associated with the SWAN simulations was not evaluated as part of this study. Relying on the sparse observational data available for the validation storms to perform bias correction could in turn introduce bias in the simulations; therefore, bias was not corrected for the SWAN simulations. In the case of SWL, the bias is estimated as the mean difference between simulated and observed water levels at the location of a water level gauge or HWM. The bias generally has length units, but nondimensional bias can also be quantified. In cases where the bias is negligible, the hydrodynamic predictions are considered unbiased. This dimensional bias is referred to as the weighted absolute form of the bias (μ_a) and is defined at each node as follows:

$$\mu_a = \frac{\sum_{i=1}^{N} w_i (\varepsilon_a)_i}{\sum_{i=1}^{N} w_i} = \frac{\sum_{i=1}^{N} w_i (\tau_{sim} - \tau_{obs})_i}{\sum_{i=1}^{N} w_i} \tag{6-3}$$

where $(\varepsilon_a)_i$= absolute model error (m); $(\tau_{sim} - \tau_{obs})_i$ = simulated storm response (m) minus observed response (m); w_i = weight assigned to each error value i based on the GKF Equation (3-2) with d_i computed as the distance from validation data point i to each node; and N = is the number

validation data points (i.e., simulation-observation pairs considered in model validation). A positive bias indicates over-prediction of the observations by the numerical model, whereas a negative bias represents underprediction of the observations.

Bias that varies as a function of hydrodynamic response magnitude is considered to be a weighted relative bias (μ_r). This form of bias is estimated by normalizing each simulated-observed difference by the simulated value:

$$\mu_r = \frac{\sum_{i=1}^{N} w_i(\varepsilon_r/\tau_{sim})_i}{\sum_{i=1}^{N} w_i} = \frac{\sum_{i=1}^{N} w_i[(\tau_{sim}-\tau_{obs})/\tau_{sim}]_i}{\sum_{i=1}^{N} w_i} \quad (6\text{-}4)$$

where ε_r = relative model error (m/m). In the PCHA framework, both the geospatial bias and uncertainty are estimated by applying a Gaussian kernel surface (GKS). The GKS method takes advantage of the available validation information to characterize local variability of numerical model biases within the study area. Evidence-based correction of these biases, even when considering a small subset of storms, is crucial to avoid underestimation of coastal hazards and risk. The data assimilation approach used to perform bias correction minimizes the potential for overcorrection in relation to the development of the storm response hazard curves.

This method results in two-dimensional (2D) surfaces of the relative and absolute forms of bias and uncertainty for the study area. These quantities' relative and absolute forms are later combined to create 2D surfaces of total bias and uncertainty, respectively. The GKS approach was applied to create 2D surfaces of the biases introduced by the ADCIRC and PBL models covering all nodes considered in this study. In this approach, weights are assigned to each validation data point. From the perspective of each computational node, the weights in Equations (6-3) and (6-4) were assigned to the validation data points based on their distance from the node. These weights are calculated from Equation (3-2) while the optimal kernel size (h_d) for estimating normal densities (Bowman and Azzalini 1997) is determined as a function of the number of validation points and distance to the nodes.

The GKS method for bias leads to the generation of four 2D bias surfaces: (1) ADCIRC absolute bias; (2) ADCIRC relative bias; (3) PBL absolute bias, and (4) PBL relative bias. The next step in this process is to aggregate the

absolute forms of the ADCIRC and PBL biases and, separately, aggregate the relative forms of these model biases, resulting in two new quantities: total absolute model bias and total relative model bias. The same workflow is also later implemented for estimating geospatial uncertainty. The total absolute model bias and total relative model bias are computed for each node as the summation of individual model biases (e.g., ADCIRC, PBL):

$$\mu_{a_{Total}} = \mu_{a_1} + \mu_{a_2} + \cdots + \mu_{a_n} \tag{6-5a}$$

$$\mu_{r_{Total}} = \mu_{r_1} + \mu_{r_2} + \cdots + \mu_{r_n} \tag{6-5b}$$

where $\mu_{a_{Total}}$ = total absolute model bias (m); $\mu_{r_{Total}}$ = total relative model bias (m/m). Following the computation of the $\mu_{a_{Total}}$ and $\mu_{r_{Total}}$ forms of the bias, these values are input using Equation 6-2 to estimate a combined bias μ_c at each node. The average values of the absolute and relative forms of bias estimated in this study are provided in Table 6-4. Plots (2D) of the ADCIRC and PBL geospatial biases are shown in Appendix C.

Table 6-3. Average values of absolute and relative bias estimated in CHS-LA.

Numerical model	Average bias	
	Absolute (m)	Relative
ADCIRC	0.02	−0.02
PBL	−0.23	−0.13
Total (ADCIRC and PBL)	−0.19	−0.15

As previously discussed, uncertainty is estimated from unbiased error quantities. In cases where model bias is non-negligible, bias correction is necessary before uncertainty quantification. Bias is removed from the storm responses (i.e., model output) by subtracting the total combined model bias (μ_c) from each simulated storm response (τ_{sim}). The corrected storm response (τ_{cor}) is given by:

$$t_{cor} = \tau_{sim} - \mu_c \tag{6-6}$$

Bias correction was only conducted for storm surge estimates based on ADCIRC and PBL model validations. Bias correction of wave results was not performed due to sparse data availability.

6.2.5 Estimation of geospatial uncertainty

Numerical model uncertainty is estimated based on three assumptions routinely made in JPM-based studies: (1) the uncertainty terms are independent; (2) their effects can be combined by addition, and (3) the aggregated uncertainties can be represented as a Gaussian distribution with a mean zero. After quantifying and correcting any bias, two forms of model uncertainty are evaluated: (1) absolute, which retains the dimensions of the hydrodynamic responses (2) and relative, which is a nondimensional quantity.

The weighted absolute form of the uncertainty (σ_a) and the relative form (σ_r) are estimated through the following equations:

$$\sigma_a = \sqrt{\frac{\sum_{i=1}^{n} w_i(\varepsilon_a)_i^2}{\frac{(n-1)\sum_{i=1}^{n} w_i}{n}}} = \sqrt{\frac{\sum_{i=1}^{n} w_i(\tau_{sim}-\tau_{obs})_i^2}{\frac{(n-1)\sum_{i=1}^{n} w_i}{n}}} \tag{6-7}$$

$$\sigma_r = \sqrt{\frac{\sum_{i=1}^{N} w_i(\varepsilon_a/\tau_{sim})_i^2}{\frac{(N-1)}{N}\sum_{i=1}^{n} w_i}} = \sqrt{\frac{\sum_{i=1}^{n} w_i[(\tau_{sim}-\tau_{obs})/\tau_{sim}]_i^2}{\frac{(N-1)}{N}\sum_{i=1}^{n} w_i}} \tag{6-8}$$

The application of the GKS method also results in the generation of four 2D uncertainty surfaces for storm surge: (1) ADCIRC absolute uncertainty; (2) ADCIRC relative uncertainty; (3) PBL absolute uncertainty, and (4) PBL relative uncertainty. The next step in this process is to aggregate the absolute forms of the ADCIRC and PBL uncertainties and, separately, aggregate the relative forms of these model uncertainties. Similar to the case of bias, this approach results in two new quantities: total absolute model uncertainty and total relative model uncertainty. The total absolute and relative uncertainties for each node are estimated as the summation of individual numerical model uncertainties:

$$\sigma_{a_{Total}} = \sqrt{\left(\sigma_{a_1}\right)^2 + \left(\sigma_{a_2}\right)^2 + \cdots + \left(\sigma_{a_n}\right)^2} \tag{6-9a}$$

$$\sigma_{r_{Total}} = \sqrt{\left(\sigma_{r_1}\right)^2 + \left(\sigma_{r_2}\right)^2 + \cdots + \left(\sigma_{r_n}\right)^2} \tag{6-9b}$$

where $\sigma_{a_{Total}}$ = total absolute model uncertainty (m); $\sigma_{r_{Total}}$ = total relative model uncertainty (m/m). The $\sigma_{a_{Total}}$ and $\sigma_{a_{Total}}$ are then input into

Equation 6-1 to estimate a total combined uncertainty (σ_c) for each node in the CHS-LA study area. The average values of the total relative and absolute uncertainties estimated in this study are provided in Table 6-4. Additional 2D plots of the ADCIRC and PBL geospatial uncertainties are shown in Appendix C.

In the case of H_{mo}, only a global uncertainty value is estimated. The absolute (σ_a) and relative (σ_r) forms of the SWAN uncertainty are determined as follows:

$$\sigma_a = \sqrt{\frac{\sum_{i=1}^{N}(\varepsilon_a)_i^2}{N-1}} = \sqrt{\frac{\sum_{i=1}^{N}(\tau_{sim}-\tau_{obs})_i^2}{N-1}} \quad (6\text{-}10)$$

$$\sigma_r = \sqrt{\frac{\sum_{i=1}^{N}(\varepsilon_a/\tau_{sim})_i^2}{N-1}} = \sqrt{\frac{\sum_{i=1}^{N}[(\tau_{sim}-\tau_{obs})/\tau_{sim}]_i^2}{N-1}} \quad (6\text{-}11)$$

By taking the average σ_a and σ_r across all validation points i, the uncertainties are input into Equation 6-1 to estimate the global SWAN uncertainty used to compute the CLs for the H_{mo} hazard curves.

Table 6-4. Average values of absolute and relative uncertainty estimated in CHS-LA.

Numerical Model	Average Uncertainty	
	Absolute (m)	Relative (m/m)
ADCIRC	0.33	0.20
PBL	0.26	0.14
Total (ADCIRC & PBL)	0.44	0.22
Numerical Model	Absolute (m)	Relative (m/m)
SWAN (H_{mo})	0.71	0.25

6.3 Astronomical tides

The astronomical tides within the CHS-LA domain have a mean range on the order of .33 m (1 ft), which minimally contributes to the variability in the SWL produced by TCs affecting the region. Similar to FEMA (2008), the hydrodynamic modeling was completed without the influence of

astronomical tides due to the minimal tidal range. Instead, the tide was computed as a stochastic quantity to capture the stochastic variability of a TC occurring at any given tidal phase. The standard deviation of the astronomical tide was calculated and linearly added to the storm surge as a random component, thus considering the effect of the random phasing of the astronomical tide and maximum storm surge.

To estimate the influence of the tide at each node, an analysis of 104 NOAA tide gauges within the study area (Appendix D) was completed using the entire record length available for each gauge. The first step in the analysis was to compute a standard deviation of the predicted tides recorded at the NOAA gauges. A nearest-neighbor interpolation of these values was then implemented to assign a standard deviation of the tide to all nodes considered for surge. The standard deviation computed at each node was applied in the error term to account for the uncertainty within the hazard curves.

6.4 Quantification of the still water level (SWL) hazards

In this study, hazard curves representing the magnitude of SWL (storm surge + astronomical tide + Q), H_{mo}, and T_p as a function of AEF were developed at over 1 million point locations across coastal Louisiana and the vicinity of the HSDRRS. These hazard curves were developed for both deterministic (Q_d) and probabilistic (Q_p) scenarios. For the Q_d scenario, all 645 hydrodynamic simulations incorporated constant Q of 11,327 m^3/s and 4,854 m^3/s for the Mississippi River and Atchafalaya River (Table 6-1). These Q values represent a 70% and 30% split discharge between the Mississippi and Atchafalaya Rivers and were identified as suitable for coastal studies in Louisiana (Cobell and Roberts 2021).

To develop the hazard curves, the peak storm responses resulting from the hydrodynamic simulation of each synthetic TC at any given point-location are assigned the discrete weight of the corresponding TC, as discussed in Section 4.4. For example, estimating the AEF of SWL requires establishing a range of water elevation bins encompassing the entire hazard range. The response's complementary cumulative distribution function is then developed by aggregating the probabilities of all water levels that exceed each of the established bins applying Equation 2-1b. This form of the JPM integral was used since unbiased uncertainty was instead conveyed through non-exceedance CLs. It is standard practice to represent

uncertainty as a Gaussian distribution process with mean zero (Resio et al. 2007; Toro 2008; FEMA 2012). The CL curves are computed from Equation 6-12 as follows:

$$CL = \bar{\tau} + z\sigma_c \quad (6\text{-}12)$$

where CL = confidence limit; $\bar{\tau}$ = mean value of a given TC response τ; z = Z-score or number of standard deviations the CL is above $\bar{\tau}$; and σ_c = total combined model uncertainty associated with τ. This study considered CLs of 10%, 16%, 84%, and 90%; however, only the 10% and 90% CLs are illustrated in the hazard curve plots.

As mentioned in Section 6.1, the GPMs were trained considering the effects of the Q_d scenario. The AEFs were then computed for this scenario and covered the probability space of TC responses from 10 yr^{-1} to 10^{-4} yr^{-1}. Examples of the developed Q_d SWL hazard curves are provided in Figures 6-6 through 6-8, showing the best-estimate (BE) and the CLs as discussed in this section at example locations within the CHS-LA study area. These nodes were selected as examples due to their proximity to NOAA tides and currents gauges. Additional details describing the methods employed to characterize the wave parameters and incorporate the effects of varying riverine discharge are discussed in Sections 6.5 and 6.6, respectively.

Figure 6-6. Example SWL hazard curve near NOAA gauge 8761305 at Shell Beach.

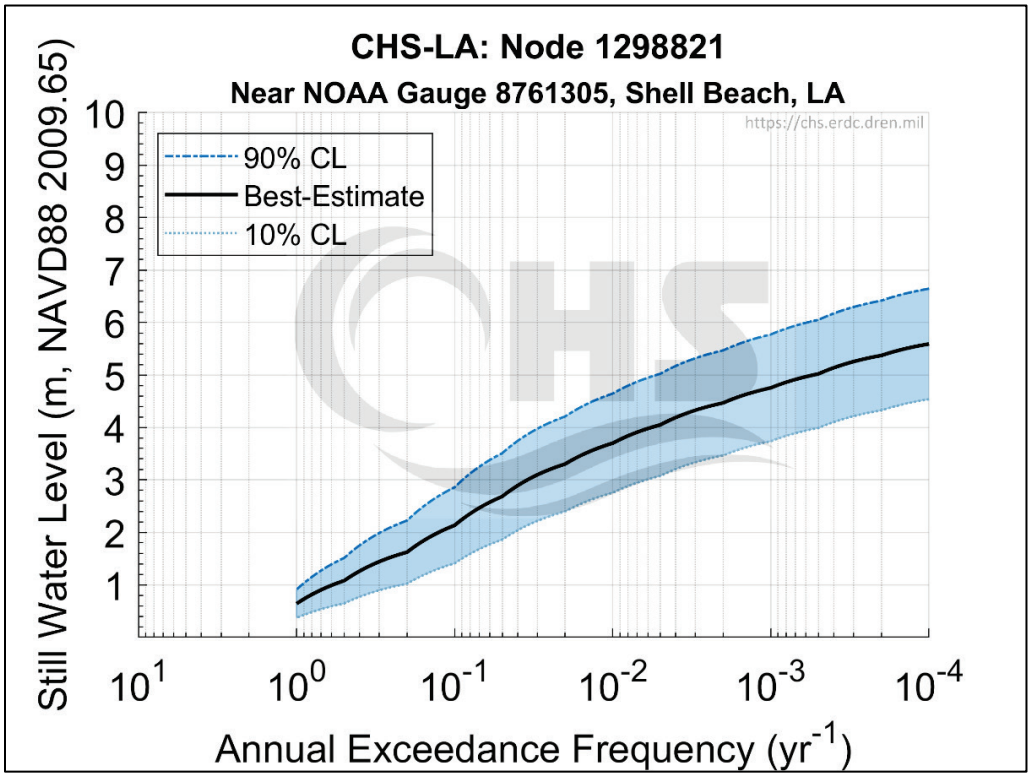


Figure 6-7. Example SWL hazard curve near NOAA gauge 8761724 at Grand Isle.

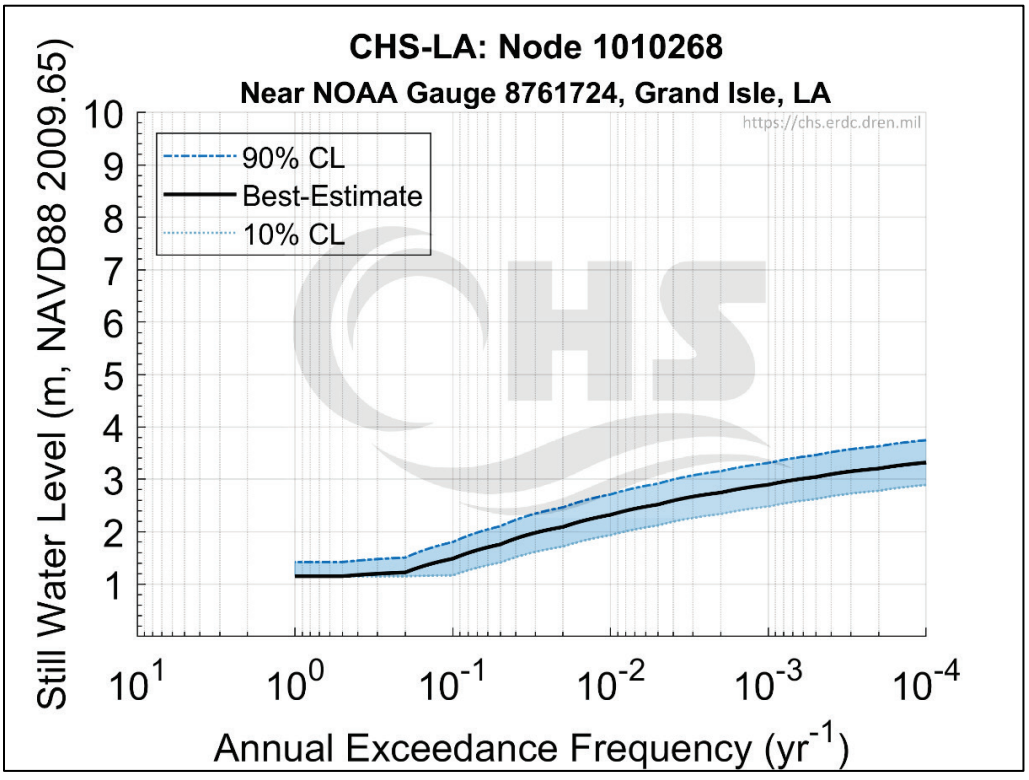
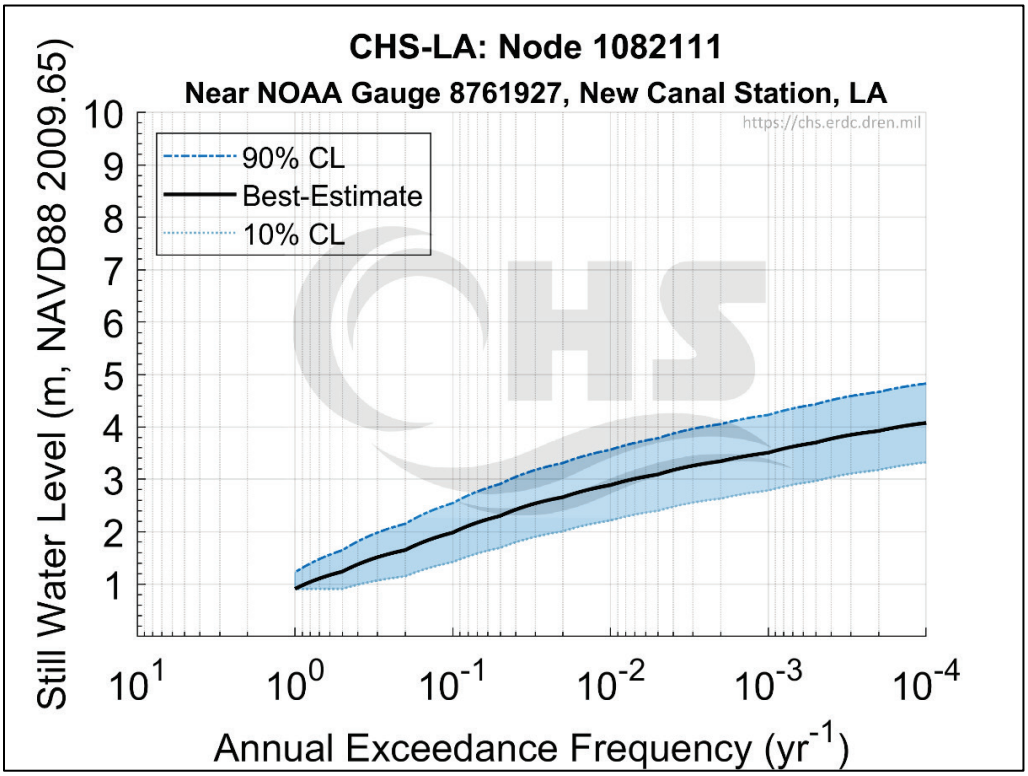


Figure 6-8. Example SWL hazard curve near NOAA gauge 8761927 at New Canal Station.



6.5 Quantification of wave hazards

Quantifying TC wave hazards in the study area included a multistep analysis of the H_{mo} and T_p output of the SWAN model, including geospatially correlating H_{mo} to the SWL simulated by ADCIRC on a node-by-node basis. The following section discusses the methodology employed within the PCHA to develop H_{mo} and T_p hazard curves.

6.5.1 Significant wave height

The first step completed for the probabilistic analysis of waves was the development of marginal hazard curves for the CHS-LA nodes considered for H_{mo} (Table 6-3). The development of the marginal H_{mo} hazard curves followed the same PCHA methodology as described in Section 6.4, including accounting for uncertainty within the SWAN simulations (Section 6.2.1.2). The resulting H_{mo} hazard curves from this initial step are considered marginal probability distributions, which in the context of the joint probability of SWL and H_{mo} strictly apply when the correlation between SWL and H_{mo} is close to 1.0. In other words, from a stochastic

standpoint, the 1×10^{-2} AEF, or 1%, SWL coincides with the 1% H_{mo} when the correlation between both storm responses is 1.0. On the other hand, at locations where H_{mo} is independent of SWL (i.e., correlation of zero), the likelihood of the 1% SWL coinciding with the 1% H_{mo} would be close to 0.01%; in this case, pairing the 1% SWL and 1% H_{mo} would significantly overstate the wave hazard.

Therefore, to properly account for the SWL-H_{mo} joint probability, the process of estimating the wave hazard included quantifying the correlation which exists between SWL and H_{mo}. The H_{mo} hazard curves derived from this second step are conditional probability distributions, that is, P(H_{mo}|SWL). The correlation coefficients for SWL and H_{mo} were determined based on pairwise ADCIRC and SWAN simulation results at every node within the study area. The SWL-H_{mo} correlation was then employed to compute conditional H_{mo} AEFs using a bivariate Gaussian (or Normal) probability distribution model. The bivariate normal distribution (BND) provided a fitted surface to the joint probability analysis relations between the parameters. The BND probability density function is given as

$$f(x,y) = \frac{1}{2\pi\sigma_x\sigma_y\sqrt{1-\rho^2}} \exp\left[-\frac{1}{2(1-\rho^2)}\left(\frac{(x-\mu_x)^2}{\sigma_x^2} - \frac{2\rho(x-\mu_x)(y-\mu_y)}{\sigma_x\sigma_y} - \frac{(y-\mu_y)^2}{\sigma_y^2}\right)\right] \quad (6\text{-}13)$$

where μ_x and μ_y = marginal means, σ_x and σ_y = marginal standard distributions, and ρ = correlation between x and y.

In the case of the BND, the conditional probability distribution for either x (SWL) or y (H_{mo}) is also normally distributed. For example, the conditional probability of x, given a known value of y, can be computed using Equation 6-13. The conditional mean and variance of x are given by

$$\mu_{x/y} = \mu_x + \rho\mu_x\frac{(y-\mu_y)}{\sigma_y} \quad (6\text{-}14)$$

$$\sigma_{x/y} = \sigma_x\sqrt{1-\rho^2} \quad (6\text{-}15)$$

The conditional H_{mo} results, P(H_{mo}|SWL), derived from this model correspond to the expected (mean) H_{mo} associated with each SWL AEF.

Other methodologies only assess the 1% SWL AEF and associated 1% H_{mo} AEF to estimate the wave hazard. However, as previously stated, this approach may produce inaccurate estimations of the hazard by not considering the correlation between H_{mo} and SWL. Calculating the correlation between H_{mo} and SWL is a significant step in developing conditional H_{mo} AEFs. At nodes where the correlation between H_{mo} and SWL is 1, the marginal and conditional H_{mo} are the same. As the SWL-H_{mo} correlation decreases, the magnitude of the conditional H_{mo} also decreases. The BE of the marginal H_{mo} hazard curve for the Q_d scenario is illustrated in Figures 6-9 through 6-11, for example nodes.

Figure 6-9. Example H_{mo} hazard curve near NOAA gauge 8761305 at Shell Beach.

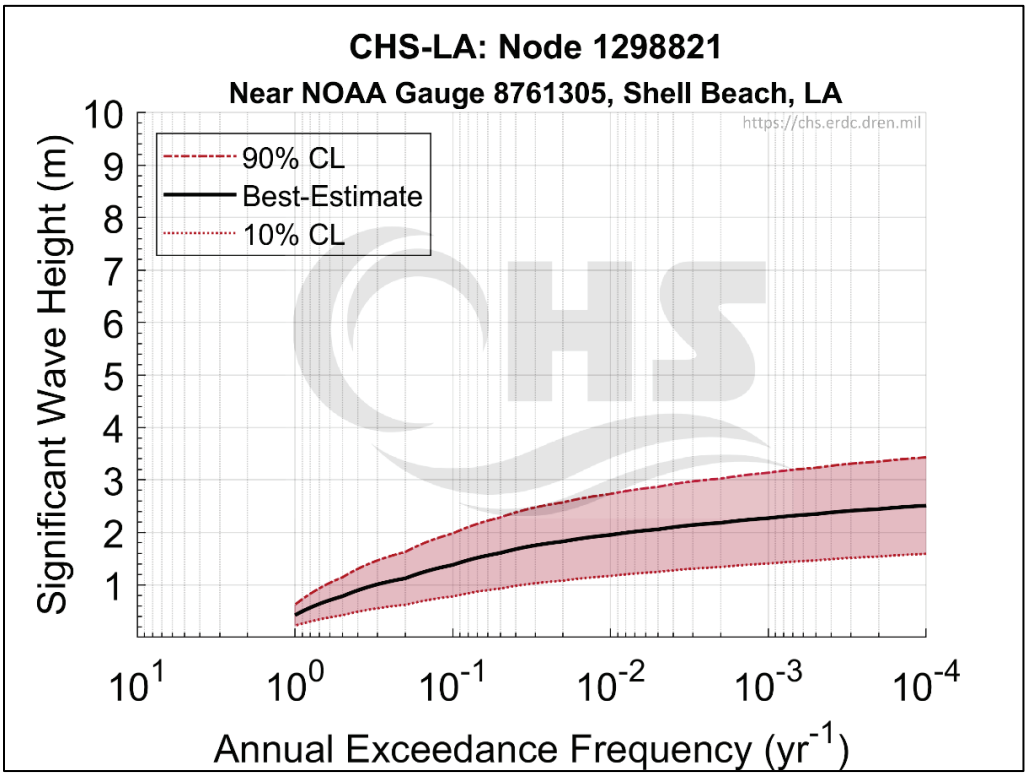


Figure 6-10. Example H_{m0} hazard curve near NOAA gauge 8761724 at Grand Isle.

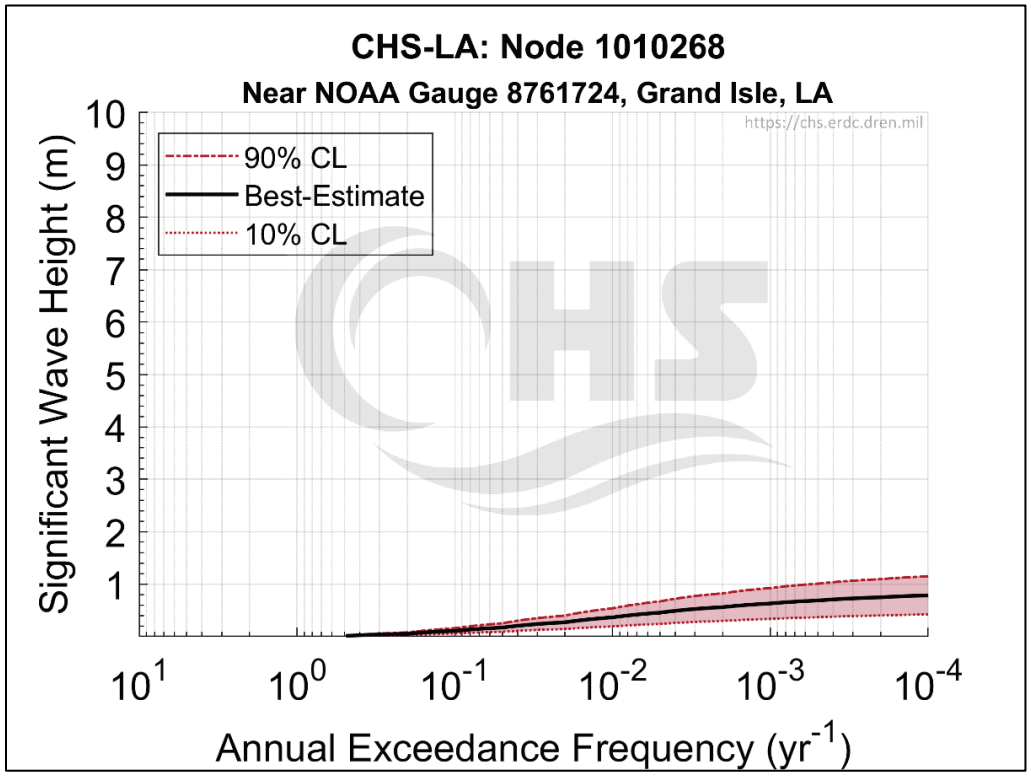
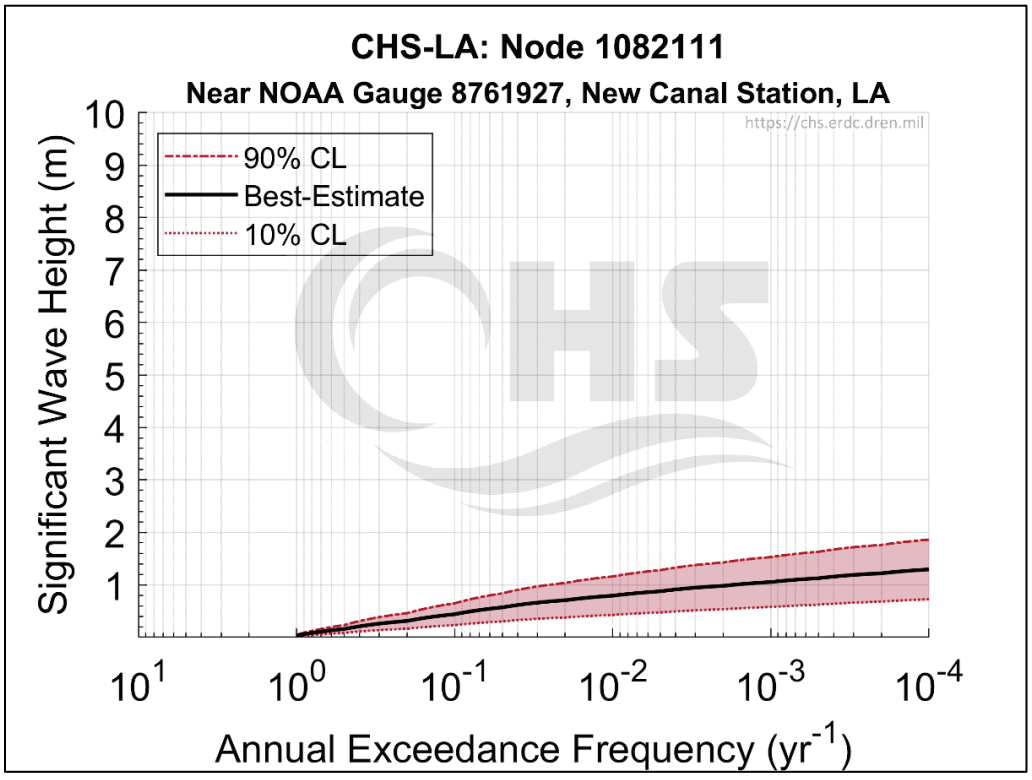


Figure 6-11. Example H_{m0} hazard curve near NOAA gauge 8761927 at New Canal Station.



6.5.2 Peak wave period

Assessment of the wave climate within the CHS-LA study area also required characterizing the hazard related to T_p. Similar to the analysis completed for H_{mo}, marginal T_p hazard curves were initially developed at the nodes by applying the ATCS response data. Figures 6-12 through 6-14 illustrate the marginal T_p BE hazard curves for the Q_d scenario produced locations within the CHS-LA study area.

However, conditional T_p values must also be calculated to account for the relationship between T_p and H_{mo}. This relationship was modeled through a power equation (Chun and Suh 2018), as shown in Equation 6-16, to maintain the physical relationship existing between these wave parameters:

$$T_p = \alpha\left(H_{m0}{}^{\beta}\right) \tag{6-16}$$

where coefficients α and β were estimated with the least-square method. The approach in Equation 6-16 was applied to estimate the expected value of T_p conditional to a given conditional H_{mo} value, as discussed in the previous section, at 1,050,245 locations of interest within the CHS-LA study area.

Figure 6-12. Example T_p hazard curve near NOAA gauge 8761305 at Shell Beach.

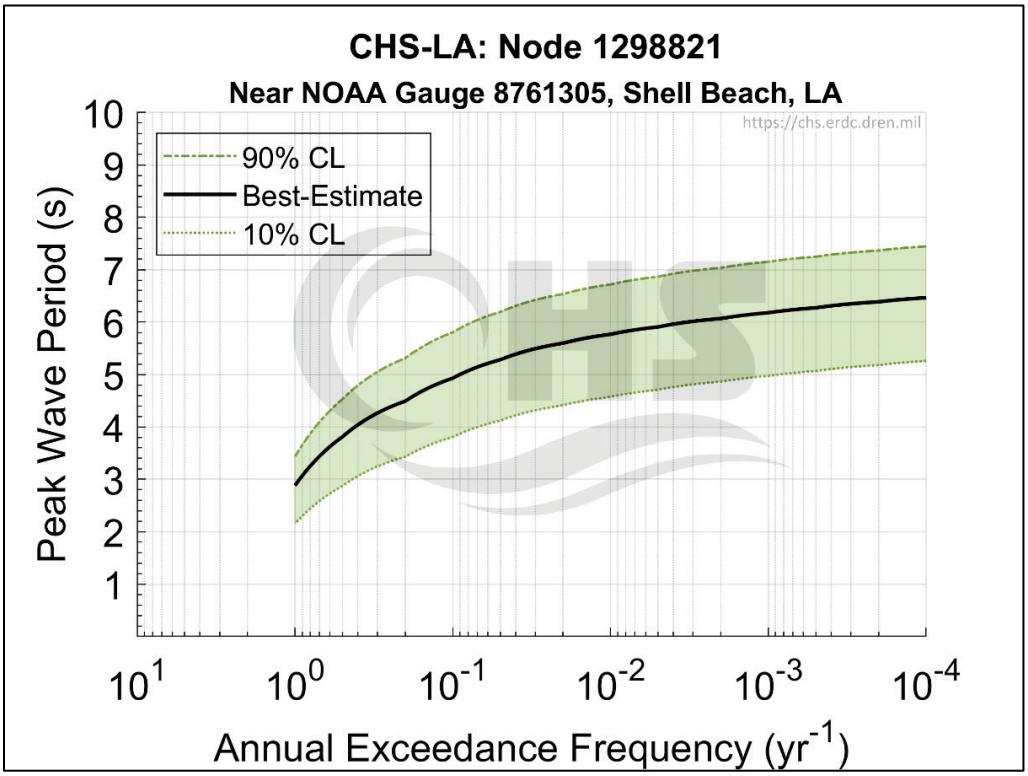


Figure 6-13. Example T_p hazard curve near NOAA gauge 8761724 at Grand Isle.

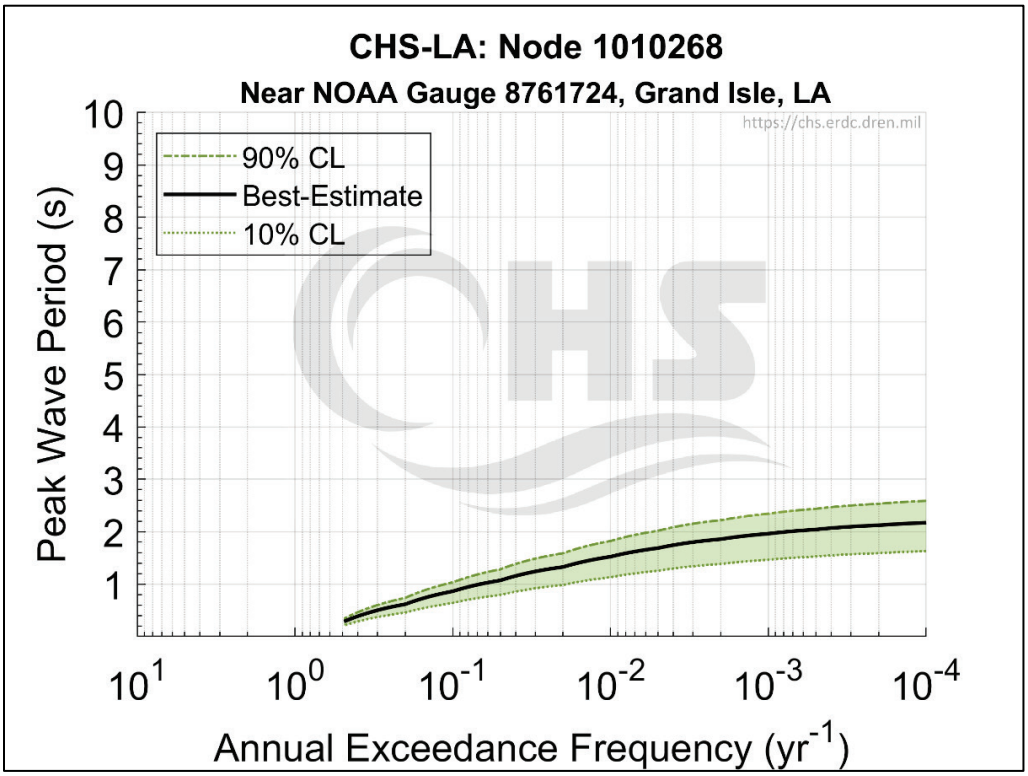
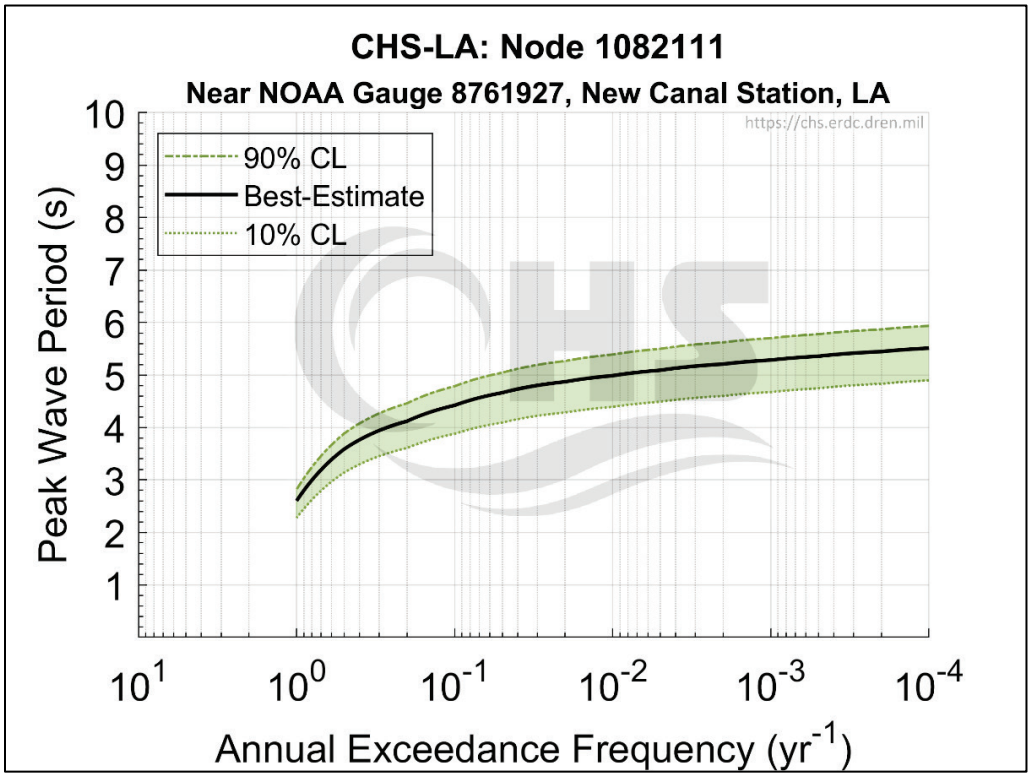


Figure 6-14. Example T_p hazard curve near NOAA gauge 8761927 at New Canal Station.



6.6 Joint probability method-Monte Carlo (JPM-MC) approach for quantifying coastal compound hazards

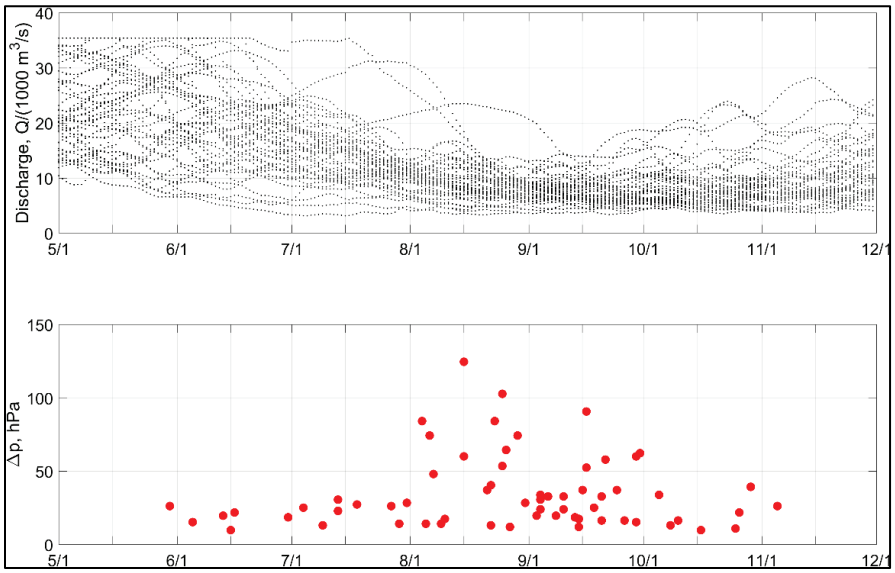
CHS-LA considered two distinct approaches for estimating the AEF of coastal compound hazards resulting from the interaction between storm surge and the discharge from the Mississippi River: (1) a probabilistic-deterministic analysis where a single representative discharge value (Q_d) was used across all TC hydrodynamic simulations (Section 6.4) and (2) a fully probabilistic analysis accounting for the stochastic coincidence between TC hazards and specific Q scenarios. The probabilistic discharge values (Q_p) in the second scenario required the extension of the CHS PCHA framework through a hybrid JPM-MC approach. This approach took advantage of the seasonality of discharge and TC intensity that has been observed, as shown in Figure 6-15, to characterize a relationship between TC simulations and discharge.

6.6.1 Probabilistic Q scenario

To account for the full effect of Q variability in the SWL hazard curves, the AEF of SWL was quantified for the Q_p scenario using JPM-MC. Following this approach, each storm in the ATCS was assigned a month of occurrence, based on the joint probability between TC intensity and seasonality. Subsequently, a Q value was sampled for each storm from the marginal probability distribution of Q given the month of occurrence. Ultimately, each storm in the ATCS was assigned a unique Q value. Application of the JPM-MC relied on historical records of TC occurrences at CRL 128 and Q from the Mississippi River in the vicinity of the HSDRRS (i.e., 70% of the Q recorded at Tarbert Landing).

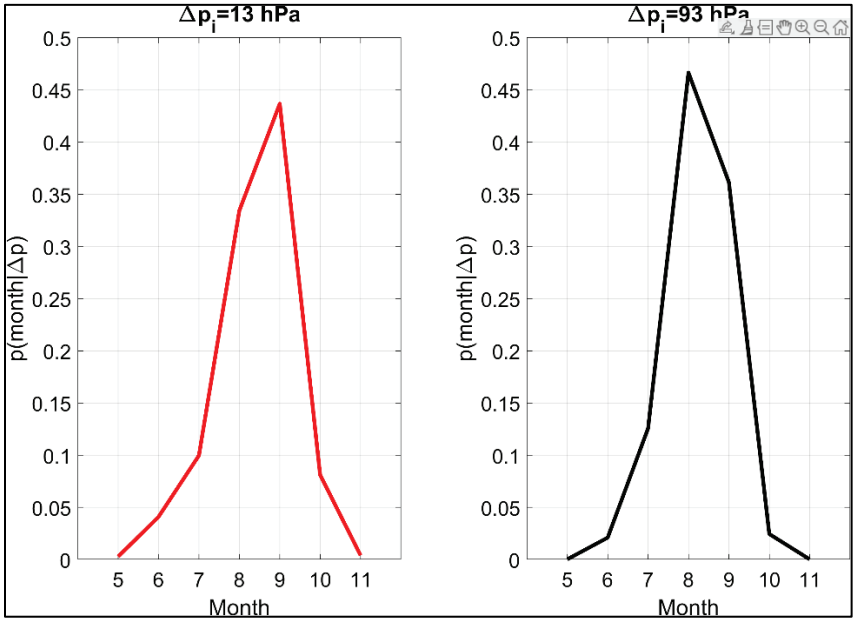
The probability of the SWL including Q was estimated by considering both TC intensity and riverine Q in a particular month (m). Based on past TC events, the conditional probability, $p(m|\Delta p)$, for a TC of a given intensity to have occurred in any month can be estimated from sample pairs of historical TCs. For this analysis, the historical TCs selected at CRL 128, as discussed in Section 3.4, were further refined by reducing the sampling radius to 200 km to capture TCs affecting the vicinity of New Orleans. A total of 64 historical TCs were retained at CRL 128 for application in this analysis. Using Q values corresponding to 70% of the discharge recorded at Tarbert Landing gauge, the conditional probability $p(Q|m)$ between the river Q and the month of the year was also estimated. For Q, gauge readings were used from 1977 to the present due to a shift in the gauge's location. The Q values were separated into months and sorted. Only values below 35,396 m^3/s were retained for the analysis as this is the maximum regulated Q allowed for the Mississippi River discharge (Section 6.1). Figure 6-15 shows the Q values and TC intensity plotted from May to November. The discharge values from 1977 to the present are shown in the top plot; the bottom plot shows the Δp of the 64 historical storms plotted by month.

Figure 6-15. Mississippi River Q (top) and TC intensity (bottom) for May–November.



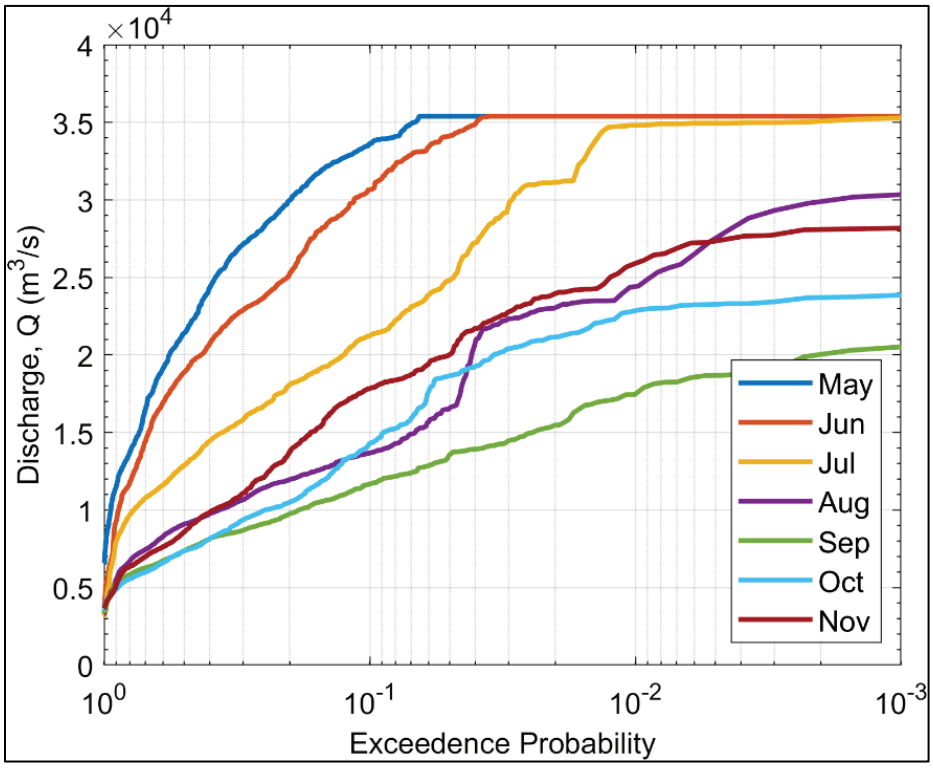
The Δp values for each of the 64 historical storms were binned in 5 hPa bins. The probability for a particular intensity to have occurred in a given month was calculated for each intensity bin. Examples of $p(m|\Delta p)$ for two intensity bins are shown in Figure 6-16. After estimating the probabilities of Δp by month, the augmented TCs were assigned to each Δp bin based on the Δp of the augmented storm. Then, a weighted scheme was used to randomly sample a month within the intensity bin for applying to the augmented storm, with the weight based on the PDFs developed for each intensity bin.

Figure 6-16. Relationship between discrete TC intensity bins and month of the year.



The probability of Q given the month of occurrence is provided by empirical CDF created using Weibull's plotting position, as shown in Figure 6-18, based on data from the Mississippi River.

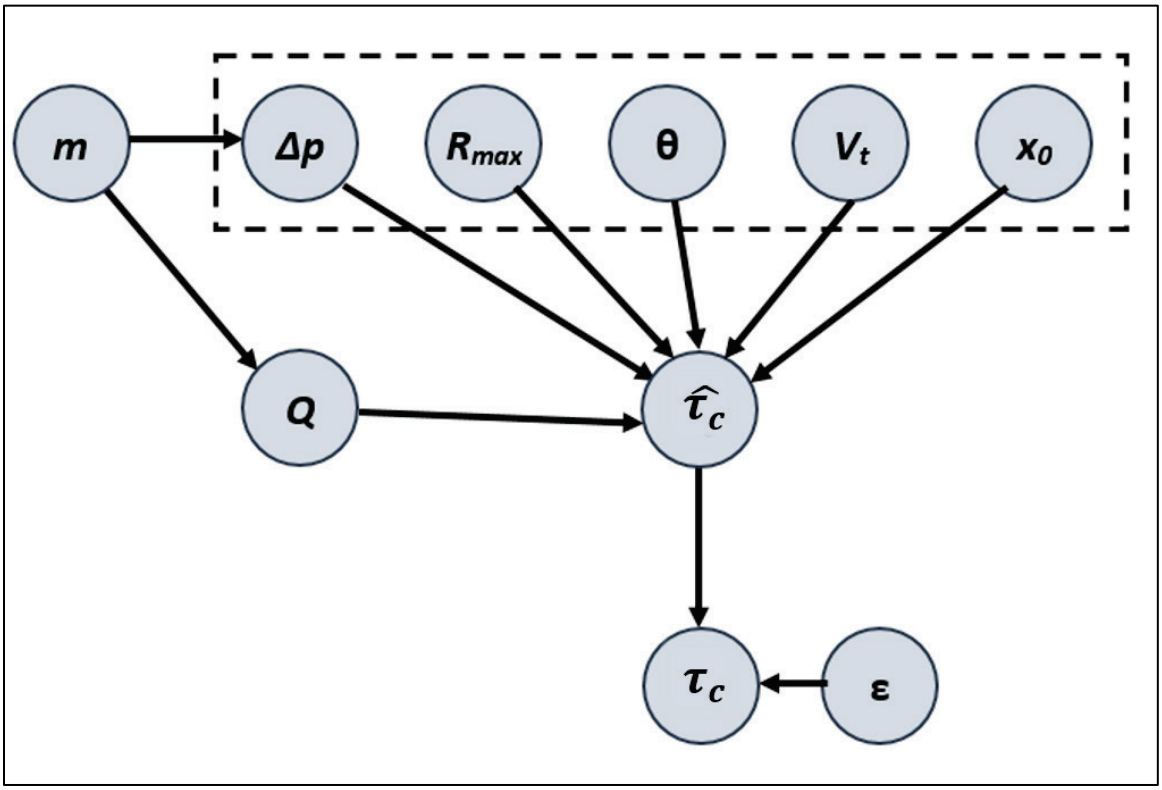
Figure 6-17. Exceedance probability (EP) of Mississippi River Q by month.



Using Monte Carlo sampling, a value of Q was then randomly assigned to each storm in the ATCS according to the probability distributions developed for each Δp bin.

Figure 6-19 shows the relationships between the original TC parameter vector $\hat{x}$ (dashed box), the discharge (Q), and the month (m) to a given storm response (τ), such as storm surge. This graphical model, known as a Bayesian network (Bensi and Der Kiureghian 2011), uses nodes (circles) to represent parameters and arrows to represent probabilistic dependencies, in which the direction of the arrow points from a *parent* node to a *child* node of the parameter. This diagram shows how seasonality (m) is a parent of both discharge (Q) and TC intensity (Δp) and links these parameters, which is key in the approach applied for this study to estimate coastal compound hazards.

Figure 6-18. Graphical representation of parameter dependencies, including Q and m, on the storm response τ.



Simulating sets of storms within the ITCS under the six Q scenarios (Table 6-1) produced 1,145 synthetic TC simulations for this hybrid analysis. A GPM was trained on the hydrodynamic results from these 1,145 simulations, including Q explicitly as an input parameter. At each node, the metamodel efficiently predicted the compound hydrodynamic response of storm surge and Q for all storms in the ATCS. Following the methodology discussed in Section 6.4, the probability of the response, defined as $P[\tau(\hat{x}_c) > \tau|\hat{x}_c]$ where $\hat{x}_c = f(x_o, \theta, \Delta p, R_{max}, V_t, m, Q)$, which now includes the Q, was integrated to obtain the estimated cumulative distribution.

6.6.2 Coastal compound hazard curves

Examples of SWL hazard curves, including Q, developed as part of the PCHA and expanded through the JPM-MC approach are shown in Figures 6-21 through 6-22. The geospatial distribution of example nodes (red circles) along the Mississippi River is shown in Figure 6-20. As illustrated by these hazard curves, the results of this analysis indicate a more substantial impact of compounding Q with the SWL at upstream locations than at nodes in downstream areas.

Figure 6-19. Geospatial distribution of example nodes along the Mississippi River.

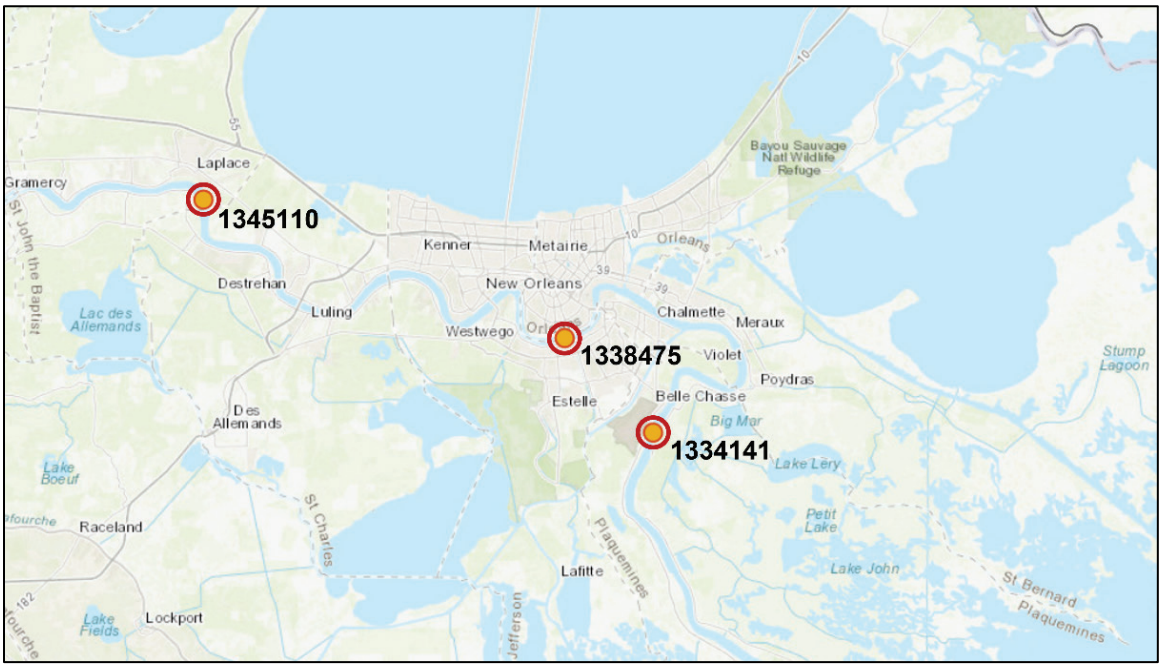


Figure 6-20. SWL hazard curve including Q_p at node 1345110.

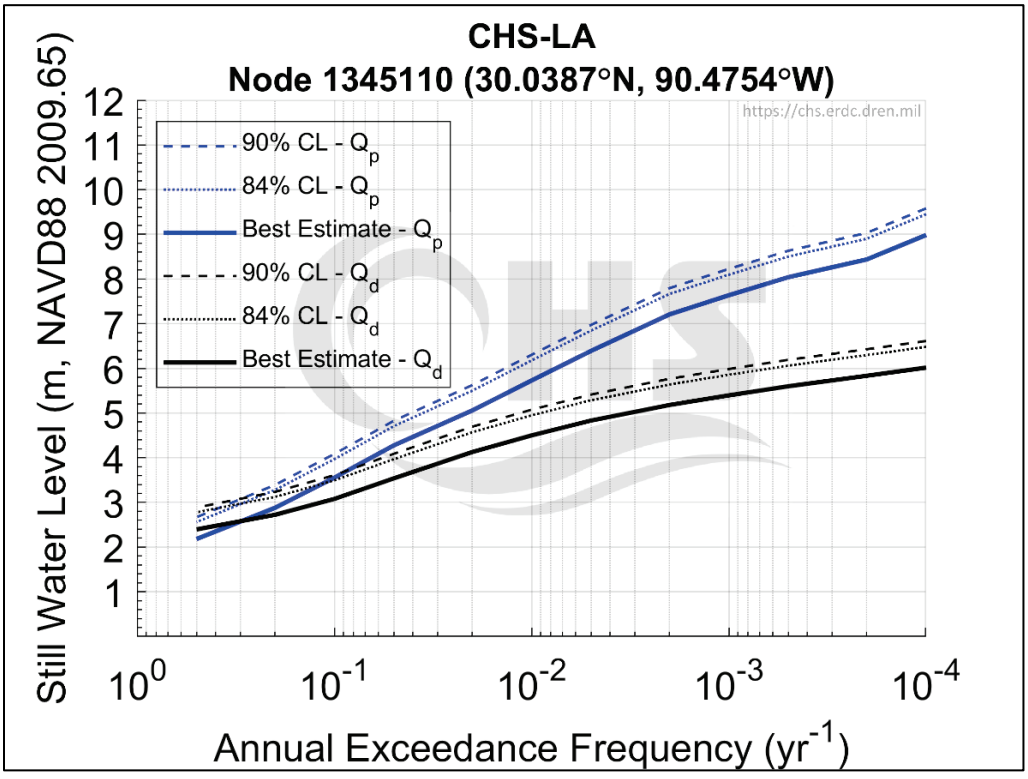


Figure 6-21. SWL hazard curve including Q_p at node 1338475.

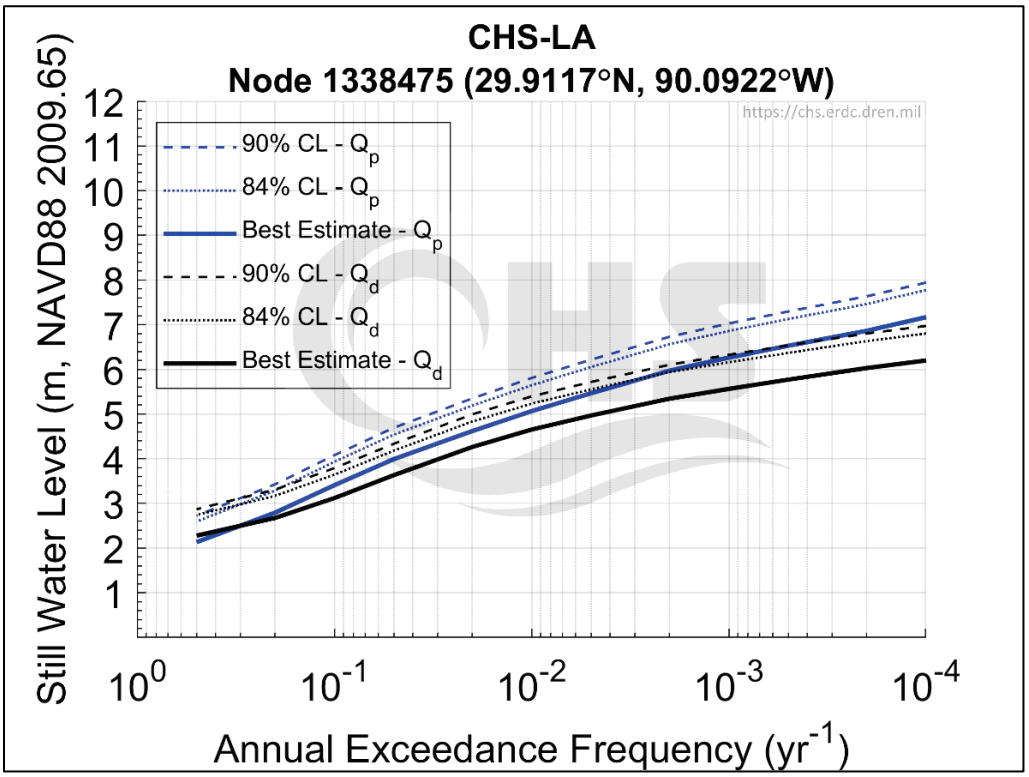
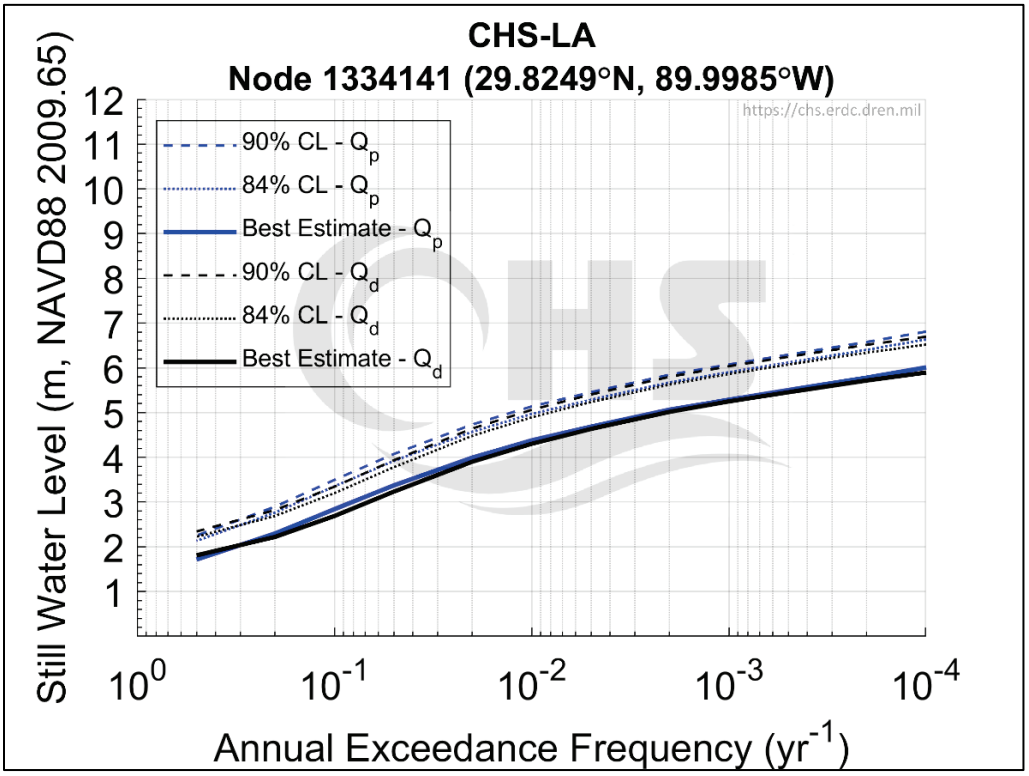


Figure 6-22. SWL hazard curve including Q_p at node 1334141.



7 Conclusions

The Coastal Hazards System–Louisiana (CHS-LA) study was conducted to quantify coastal storm hazards in Louisiana. CHS-LA applied the Probabilistic Coastal Hazard Analysis (PCHA) framework integrating (1) regional storm climatology characterization, (2) marginal distributions of tropical cyclone (TC) atmospheric-forcing parameters, (3) development of synthetic TCs, (4) dependence modeling of TC parameters, (5) joint probability analysis of atmospheric forcing and hydrodynamic responses, (6) high-resolution numerical model simulation, (7) metamodeling prediction of storm responses, and (8) estimation of geospatial bias and uncertainty. Coastal compound hazards were assessed in the vicinity of the Greater New Orleans Hurricane and Storm Damage Risk Reduction System (HSDRRS). Two methods were considered to account for the compound effects of storm surge and the discharge (Q) from the Mississippi River. First, a probabilistic-deterministic analysis where a single deterministic discharge value (Q_d) was used across all hydrodynamic simulations. Second, a fully probabilistic analysis accounting for the stochastic coincidence between TC hazards and multiple probabilistic discharge values (Q_p). The latter required the extension of the CHS PCHA framework through a hybrid joint probability method-Monte Carlo (JPM-MC) approach.

For the Q_d scenario, an initial TC suite (ITCS) of 645 storm events was developed and simulated in high-fidelity, high-resolution hydrodynamic numerical models (i.e., ADCIRC and SWAN), including a Q of 11,327 m^3/s for the Mississippi River in the vicinity of the HSDRRS. The Q_p scenario incorporated a total of 500 additional hydrodynamic simulations conducted for Q values ranging from 0 m^3/s to 35,396 m^3/s. The results from both Q_d and Q_p scenarios were used to train and validate a Gaussian process metamodel (GPM) for efficient and accurate prediction of compound hydrodynamic responses for an augmented TC suite (ATCS) of 748,200 synthetic events, fully covering the TC parameter and probability spaces. Hazards curves of hurricane-induced still water level (SWL), significant wave height (as H_{mo}), and peak wave period (T_p) for annual exceedance frequencies (AEFs) ranging from 10 yr^{-1} to 10^{-4} yr^{-1} were developed at over 1 million nodal locations across coastal Louisiana. The PCHA results from the CHS-LA study will aid in the sustainability of Louisiana's coastal storm risk management and resilience efforts.

References

Bacopoulos, P., W. R. Dally, S. C. Hagen, and A. T. Cox. 2011. "Observations and Simulation of Winds, Surge, and Currents on Florida's East Coast During Hurricane Jeanne (2004)." *Coastal Engineering* 60 (February 2012): 84–94.

Bensi, M., and A. Der Kiureghian. 2011. "A Bayesian Network Approach for Identification of Critical Components of a System." *First Symposium on Uncertainty Modeling and Analysis and Management (ICVRAM 2011); and Fifth International Symposium on Uncertainty Modeling and Analysis (ISUMA) International*, April 11–13, Hyattsville, MD.

Bensi, M., and J. Kanney. 2015. "Development of a Framework for Probabilistic Storm Surge Hazard Assessment for United States Nuclear Power Plants." *Transactions, SMiRT-23*, Manchester, United Kingdom, August 10–14.

Bommer, J. J., and F. Scherbaum. 2008. "The Use and Misuse of Logic Trees in Probabilistic Seismic Hazard Analysis." *Earthquake Spectra* 24 (4): 997–1009.

Bowman, A. W., and A. Azzalini. 1997. *Applied Smoothing Techniques for Data Analysis*. New York: Oxford University Press Inc.

Brun, W., G. B. Keren, G. Kirkebøen, and H. Montogomery. 2011. *Perspectives on Thinking, Judging, and Decisions Making*. Oslo: Universitetsforlaget.

Bunya, S., J. Dietrich, J. Westerink, B. Ebersole, J. Smith, J. Atkinson, R. Jensen, D. Resio, R. Luettich, Jr., C. Dawson, V. Cardone, and A. Cox. 2010. "A High-Resolution Coupled Riverine Flow, Tide, Wind, Wind Wave, and Storm Surge Model for Southern Louisiana and Mississippi. Part I: Model Development and Validation." *Monthly Weather Review* 138:345–377.

Cardone, V. J., A. T. Cox, J. A. Greenwood, and E. F. Thompson. 1994. *Upgrade of Tropical Cyclone Surface Wind Field Model*. Miscellaneous Paper CERC-94-14. Vicksburg, MS: US Army Corps of Engineers Waterways Experiment Station.

Cardone, V. J., and A. T. Cox 2009. "Tropical Cyclone Wind Field Forcing for Surge Models: Critical Issues and Sensitivities." *Natural Hazards* 1:29.

Cardone, V. J., and C. K. Grant. 1994. "Southeast Asia Meteorological and Oceanographic Hindcast Study (SEAMOS)." *OSEA 94132. 10th Offshore Southeast Asia Conference*, 6–9 December, Singapore. https://www.oceanweather.com/about/papers/index.html.

Cardone, V. J., C. V. Greenwood, and J. A. Greenwood. 1992. *Unified Program for the Specification of Tropical Cyclone Boundary Layer Winds over Surfaces of Specified Roughness*. Contract Report CERC 92-1. Vicksburg, MS: US Army Corps of Engineers Waterways Experiment Station.

Cardone, V. J., W. J. Pierson, and E. G. Ward. 1976. "Hindcasting the Directional Spectra of Hurricane Generated Waves." *Journal of Petroleum Technology* 28:385–394.

Cardone, V. J., and D. B. Ross. 1979. "State-of-the-Art Wave Prediction Methods and Data Requirements." In *Ocean Wave Climate*, Vol. 8, edited by M. D. Earle and A. Malahoff. New York, NY: Plenum Publishing Corporation.

Chouinard, L. M., and C. Liu. 1997. "Model for Recurrence Rate of Hurricanes in Gulf of Mexico." *Journal of Waterway, Port, Coastal and Ocean Engineering* 123:113–119.

Chow, S. H. 1971. *A Study of the Wind Field in the Planetary Boundary Layer of a Moving Tropical Cyclone*. Master of Science thesis in meteorology, School of Engineering and Science, New York University.

Chun, H., and Kyung-Duck Suh. 2018. "Estimation of Significant Wave Period from Wave Spectrum." *Ocean Engineering* 163:609–616.

Cialone, M. A., T. C. Massey, M. E. Anderson, A. S. Grzegorzewski, R. E. Jensen, A. Cialone, D. J. Mark, K. C. Peavey, B. L. Gunkel, T. O. McAlpin, N. C. Nadal-Caraballo, J. A. Melby, and J. J. Ratcliff. 2015. *North Atlantic Coast Comprehensive Study (NACCS) Coastal Storm Model Simulations: Waves and Water Levels*. ERDC/CHL TR-15-14. Vicksburg, MS: US Army Engineer Research and Development Center.

Cobell, Z., and H. Roberts. 2021. *2023 Coastal Master Plan: Model Improvement Plan, Storm Surge and Waves (Subtask 8). Version I*. Baton Rouge, LA: Coastal Protection and Restoration Authority.

Cox, A. T., J. A. Greenwood, V. J. Cardone, and V. R. Swail. 1995. "An Interactive Objective Kinematic Analysis System." *4th International Workshop on Wave Hindcasting and Forecasting*. Banff, Alberta, Canada, 16–20 October 1995.

Cox, A. T., and V. J. Cardone. 2007. "Specification of Tropical Cyclone Parameters from Aircraft Reconnaissance." *10th International Wind and Wave Workshop*. Oahu, Hawaii, November 11–16 2007.

Cox, A. T., B. T. Callahan, M. Ferguson, and M. A. Morrone. 2017. "Tropical Cyclone Wind Field Analysis for Ocean Response Modeling: Hurricane Harvey (2017)." *1st International Workshop on Waves, Storm Surges and Coastal Hazards*. Liverpool, UK, 10–15 September 2017.

CPRA (Coastal Protection and Restoration Authority). 2013. *Greater New Orleans Flood Protection System Notice of Construction Completion–Design Assessment by Nonfederal Sponsor*. Bell City, LA: Lonnie G. Harper & Associates.

Demuth, J., M. DeMaria, and J. A. Knaff. 2006. "Improvement of Advanced Microwave Sounder Unit Tropical Cyclone Intensity and Size Estimation Algorithms." *Journal of Applied Meteorology and Climatology* 45:1573–1581.

Der Kiureghian, A., and O. Ditlevsen. 2009. "Aleatory or Epistemic? Does It Matter?" *Structural Safety* 31:105–112.

Dietrich, J. C., J. J. Westerink, A. B. Kennedy, J. M. Smith, R. Jensen, M. Zijlema, L. H. Holthuijsen, C. Dawson, R. A. Luettich, Jr., M. D. Powell, V. J. Cardone, A. T. Cox, G. W. Stone, H. Pourtaheri, M. E. Hope, S. Tanaka, L. G. Westerink, H. J. Westerink, and Z. Cobell. 2011. "Hurricane Gustav (2008) Waves and Storm Surge: Hindcast, Synoptic Analysis and Validation in Southern Louisiana." *Monthly Weather Review* 139:2488–2522.

Fang, H. B., K.-T. Fang, and S. Kotz. 2002. "The Meta-elliptical Distributions with Given Marginals." *Journal of Multivariate Analysis* 82:1–16.

Fang, K. T., S. Kotz, and K. W. Ng. 1990. *Symmetric Multivariate and Related Distributions*. CRC Press: Chapman and Hall.

FEMA (Federal Emergency Management Agency). 1988. *Coastal Flooding Hurricane Storm Surge Model*. Vol. 1 Methodology. Washington, DC: Office of Risk Management, Federal Insurance Administration, FEMA.

FEMA. 2008. *Mississippi Coastal Analysis Project (MCAP)*. Final Report: HMTAP Task Order 18, prepared for the Federal Emergency Management Agency, Department of Homeland Security. Gaithersburg, MD: URS Group, Inc.

FEMA. 2012. *Operating Guidance No. 8-12 for Use by FEMA Staff and Flood Mapping Partners: Joint Probability–Optimal Sampling Method for Tropical Storm Surge*. Washington, DC: Federal Emergency Management Agency, Department of Homeland Security.

Forristall, G. Z. 1980. "A Two-Layer Model for Hurricane Driven Currents on an Irregular Grid." *Journal of Physical Oceanography* 10:1417–1438.

Forristall, G. Z., R. C. Hamilton, and V. J. Cardone. 1977. "Continental Shelf Currents in Tropical Storm Delia: Observations and Theory." *Journal of Physical Oceanography* 7:532–546.

Forristall, G. Z., E. G. Ward, V. J. Cardone, and L. E. Borgman. 1978. "The Directional Spectra and Kinematics of Surface Waves in Tropical Storm Delia." *Journal of Physical Oceanography* 8:888–909.

Gao, F., X. Zhang, N. A. Jacobs, X.-Y. Huang, X. Zhang, and P. P. Childs. 2012. "Estimation of TAMDAR Observational Error and Assimilation Experiments." *Weather and Forecasting* 27:856–877.

Gonzalez, V. M., N. C. Nadal-Caraballo, J. A. Melby, and M. A. Cialone. 2019. *Quantification of Uncertainty in Probabilistic Storm Surge Models: Literature Review*. ERDC/CHL SR-19-1. Vicksburg, MS: US Army Engineer Research and Development Center.

Ho, F. P. 1974. *Storm Tide Frequency Analysis for the Coast of Georgia*. NOAA Technical Memorandum NWS HYDRO-19. Silver Spring, MD: US Department of Commerce.

Ho, F. P., and V. A. Myers. 1975. *Joint Probability Method of Tide Frequency Analysis Applied to Apalachicola Bay and St. George Sound, Florida*. NOAA Technical Report NWS 18. Silver Spring, MD: National Weather Service, National Oceanic and Atmospheric Administration.

Ho, F. P., J. C. Su, K. L. Hanevich, R. J. Smith, and F. P. Richards. 1987. *Hurricane climatology for the Atlantic and Gulf Coasts of the United States*. NOAA Technical Report NWS 38. Silver Spring, MD: National Weather Service, National Oceanic and Atmospheric Administration.

Holland, G. J. 1980. "An Analytic Model of the Wind and Pressure Profiles in Hurricanes." *Monthly Weather Review* 108:1212–1218.

Hope, M. E., J. J. Westerink, A. B. Kennedy, P. C. Kerr, J. C. Dietrich, C. Dawson, C. J. Bender, J. M. Smith, R. E. Jensen, M. Zijlema, L. H. Holthuijsen, R. A. Luettich Jr., M. D. Powell, V. J. Cardone, A. T. Cox, H. Pourtaheri, H. J. Roberts, J. H. Atkinson, S. Tanaka, H. J. Westerink, and L. G. Westerink. 2013. "Hindcast and Validation of Hurricane Ike (2008) Waves, Forerunner, and Storm Surge." *Journal of Geophysical Research* 118:4424–4460.

IPET (Interagency Performance Evaluation Task Force). 2009. *Performance Evaluation of the New Orleans and Southeast Louisiana Hurricane Protection System*. Final Report of the Interagency Performance Evaluation Task Force. Washington, DC: US Army Corps of Engineers, Department of the Army.

Jarvinen, B. R., C. J. Neumann, and M. A. S. Davis. 1984. *A Tropical Cyclone Data Tape for the North Atlantic Basin, 1886–1983: Contents, Limitations, and Uses*. NOAA Tech. Memo 22. Miami, FL: National Hurricane Center, National Weather Service.

Jia, G., A. A. Taflanidis, N. C. Nadal-Caraballo, J. A. Melby, A. B. Kennedy, and J.M. Smith. 2016. "Surrogate Modeling for Peak or Time-Dependent Storm Surge Prediction over an Extended Coastal Region Using an Existing Database of Synthetic Storms." *Natural Hazards* 81:909–938.

Kammerer, A. M. 2013. "Probabilistic Hazard Assessment Approaches: Transferable Methods from Seismic Hazard." In *Proceedings of the Workshop on Probabilistic Flood Hazard Assessment (PFHA) at the US Nuclear Regulatory Commission Headquarters*. NUREG/CP-0302.Rockville, MD: US Nuclear Regulatory Commission.

Kammerer, A. M., and J. P. Ake. 2012. *Practical Implementation Guidelines for SSHAC Level 3 and 4 Hazard Studies*. NUREG-2117 Rev.1 Washington, DC: US Nuclear Regulatory Commission.

Kendall, M. G. 1970. *Rank Correlation Methods*. Griffin: Charles Griffin and Co. Ltd.

Knapp, K. R., H. J. Diamond, J. P. Kossin, M. C. Kruk, and C. J. Schreck. 2018. *International Best Track Archive for Climate Stewardship (IBTrACS) Project, Version 4*. NOAA National Centers for Environmental Information. https://www.ncei.noaa.gov/access/metadata/landing-page/bin/iso?id=gov.noaa.ncdc:C01552.

Knapp, K. R., M. C. Kruk, D. H. Levinson, H. J. Diamond, and C. J. Neumann. 2010. "The International Best Track Archive for Climate Stewardship (IBTrACS): Unifying Tropical Cyclone Best Track Data." *Bulletin of the American Meteorological Society* 91:363–376.

Kyprioti, A. P., A. A. Taflanidis, M. Plumlee, T. G. Asher, E. Spiller, R. A. Luettich, B. Blanton, T. L. Kijewski-Correa, A. Kennedy, and L. Schmied. 2021. "Improvements in Storm Surge Surrogate Modeling for Synthetic Storm Parameterization, Node Condition Classification and Implementation to Small Size Databases." *Natural Hazards* 109:1349–1386.

Landsea, C. W., and J. L. Franklin. 2013. "Atlantic Hurricane Database Uncertainty and Presentation of a New Database Format." *Monthly Weather Review* 141:3576–3592.

Landsea, C. W., G. A. Vecchi, L. Bengtsson, and T. R. Knutson. 2010. "Impact of Duration Thresholds on Atlantic Tropical Cyclone Counts." *Journal of Climate* 23:2508–19.

Mann, M. E., T. A. Sabbatelli, and U. Neu. 2007. "Evidence for a Modest Undercount Bias in Early Historical Atlantic Tropical Cyclone Counts." *Geophysical Research Letters* 34:L22707.

MathWorks. 2022. *kmeans*. Accessed 15 March 2022. https://www.mathworks.com/help/stats/kmeans.html#References.

Melby, J. A., T. C. Massey, F. Diop, H. Das, N. C. Nadal-Caraballo, V. Gonzalez, M. Bryant, A. Tritinger, L. Provost. M. Owensby, and A. Stehno. 2021. *Coastal Texas Protection and Restoration Feasibility Study–Coastal Texas Flood Risk Assessment: Hydrodynamic Response and Beach Morphology*. ERDC/CHL TR-21-11. Vicksburg, MS: US Army Engineer Research and Development Center.

MORPHOS. 2009. *Report: Oceanweather Tropical Planetary Boundary Layer Model, 2009*. https://www.oceanweather.com/about/papers/index.html.

Myers, V. A. 1954. *Characteristics of United States Hurricanes Pertinent to Levee Design for Lake Okeechobee, Florida*. Hydrometeorological Report No. 32. Washington, DC: Weather Bureau, US Department of Commerce.

Myers, V. A. 1970. *Joint Probability Method of Tide Frequency Analysis Applied to Atlantic City and Long Beach Island, NJ*. ESSA Technical Memorandum WBTM HYDRO 11. Washington, DC: Weather Bureau, US Department of Commerce.

Myers, V. A. 1975. *Storm Tide Frequencies on the South Carolina Coast*. NOAA Technical Report NWS-16. Washington, DC: National Weather Service, National Oceanic and Atmospheric Administration.

Nadal-Caraballo, N. C., M. O. Campbell, V. M. Gonzalez, M. J. Torres, J. A. Melby, and A. A. Taflanidis. 2020. "Coastal Hazards System: A Probabilistic Coastal Hazard Analysis Framework. Global Coastal Issues of 2020." *Journal of Coastal Research Special Issue* 95:1211–1216.

Nadal-Caraballo, N. C., J. A. Melby, V. M. Gonzalez, and A. T. Cox. 2015. *North Atlantic Coast Comprehensive Study–Coastal Storm Hazards from Virginia to Maine*. ERDC/CHL TR-15-5. Vicksburg, MS: US Army Engineer Research and Development Center.

Nadal-Caraballo, N. C., V. M. Gonzalez, and L. Chouinard. 2019. *Storm Recurrence Rate Models for Tropical Cyclones–Report 1 of a series on the Quantification of Uncertainties in Probabilistic Storm Surge Models*. ERDC/CHL TR-19-4. Vicksburg, MS: US Army Engineer Research and Development Center.

NHC (National Hurricane Center). 2022. *Saffir-Simpson Hurricane Wind Scale*. Accessed 21 July 2022. https://www.nhc.noaa.gov/pdf/sshws.pdf .

Neumann, C. J., G. W. Cry, E. L. Caso, and B. R. Jarvinen. 1985. *Tropical Cyclones of the North Atlantic Ocean, 1871–1980*. Asheville, NC: National Climatic Center.

Niedoroda, A. W., D. T. Resio, G. R. Toro, D. Divoky, H. S. Has, and C. W. Reed. 2010. "Analysis of the Coastal Mississippi Storm Surge Hazard." *Ocean Engineering* 37:82–90.

Powell, M. D. 2007. *Drag Coefficient Distribution and Wind Speed Dependence in Tropical Cyclones*. Final report to the Joint Hurricane Testbed, April 2007. https://www.nhc.noaa.gov/jht/05-07reports/final_Powell_JHT07.pdf.

Resio, D. T., S. J. Boc, L. Borgman, V. Cardone, A. T. Cox, W. R. Dally, R. G. Dean, D. Divoky, E. Hirsh, J. L. Irish, D. Levinson, A. Niedoroda, M. D. Powell, J. J. Ratcliff, V. Stutts, J. Suhada, G. R. Toro, and P. J. Vickery. 2007. White Paper on estimating hurricane inundation probabilities. Consulting Report prepared by USACE for FEMA. Vicksburg, MS: US Army Engineer Research and Development Center. http://hdl.handle.net/11681/22643.

Ross, D. B., and V. J. Cardone. 1978. "A Comparison of Parametric and Spectral Hurricane Wave Prediction Products." In *Turbulent Fluxes through the Sea Surface, Wave Dynamics, and Prediction*, edited by A. Favre and K. Hasselmann. New York, NY: Plenum Press.

Russell, L. R. 1968a. *Stochastic Models for Hurricane Prediction for the Texas Gulf Coast*. Master's thesis, Stanford University, Stanford, CA.

Russell, L. R. 1968b. *Probability Distributions for Texas Gulf Coast Hurricane Effects of Engineering Interest*. PhD dissertation, Stanford University, Stanford, CA.

Shapiro, L. J. 1983. "The Asymmetric Boundary Layer Flow under a Translating Hurricane." *Journal of the Atmospheric Sciences* 40:1984–1998.

Sklar, A. 1959. "Fonctions de Répartition À N Dimensions Et Leurs Marges." *Publications de Institut Statatistique de I'Universite de Paris* 8:299–331.

Thompson, E. F., and V. J. Cardone. 1996. "Practical Modeling of Hurricane Surface Wind Fields." *ASCE Journal of Waterway, Port, Coastal and Ocean Engineering* 122:195–205.

Toro, G. R. 2008. *Joint Probability Analysis of Hurricane Flood Hazards for Mississippi–Final URS Group Report in Support of the FEMA-HMTAP Flood Study of the State of Mississippi*. Boulder CO: Risk Engineering.

Toro, G. R., A. W. Niedoroda, C. W. Reed, and D. Divoky. 2010a. "Quadrature-Based Approach for Efficient Evaluation of Surge Hazard." *Ocean Engineering* 37:114–124.

Toro, G. R., D. T. Resio, D. Divoky, A.W. Niedoroda, and C. Reed. 2010b. "Efficient Joint-Probability Methods for Hurricane Surge Frequency Analysis." *Ocean Engineering* 37:125–134.

USACE (US Army Corps of Engineers). 2009a. *Flood Insurance Study: Southeastern Parishes, Louisiana. Intermediate Submission 2: Offshore Water Levels and Waves*. Vicksburg, MS: USACE.

USACE. 2009b. *Flood Insurance Study: Southwestern Parishes, Louisiana. Intermediate Submission 2*. Vicksburg, MS: USACE.

USACE. 2009c. *Louisiana Coastal Protection and Restoration (LACPR). Final Technical Report*. New Orleans, LA: New Orleans District, Mississippi Valley Division, USACE.

USACE. 2009d. *Mississippi Coastal Improvements Program (MsCIP), Hancock, Harrison, and Jackson Counties, Mississippi*. Mobile, AL: Mobile District, South Atlantic Division, USACE.

USACE. 2011. *Flood Insurance Study: Coastal Counties, Texas: Scoping and Data Review*. Denton, TX: Federal Emergency Management Agency, Region 6.

USNRC (US Nuclear Regulatory Commission). 1997. *Panel on Seismic Hazard Evaluation. Review of Recommendations for Probabilistic Seismic Hazard Analysis: Guidance on Uncertainty and Use of Experts*. (n.d.). Washington, DC: Panel on Seismic Hazard Evaluation, National Research Council.

Vecchi, G. A., and T. R. Knutson. 2011. "Estimating Annual Numbers of Atlantic Hurricanes Missing from the HURDAT Database (1878–1965) Using Ship Track Density." *Journal of Climate* 24:1736–1746.

Vickery, P. J. 2005. "Simple Empirical Models for Estimating the Increase in Central Pressure of Tropical Cyclones after Landfall along the Coastline of the United States." *Journal of Applied Meteorology* 44:1807–1826.

Vickery, P. J., and B. O. Blanton. 2008. *North Carolina Coastal Flood Analysis System Hurricane Parameter Development*. Technical Report TR-08-06. Chapel Hill, NC: RENCI Renaissance Computing Institute.

Vickery, P. J., and D. Wadhera. 2008. "Statistical Models of Holland Pressure Profile Parameter and Radius to Maximum Winds of Hurricanes from Flight-Level Pressure and H*Wind Data." *Journal of Applied Meteorology and Climatology* 47:2497–2517.

Vrouwenvelder, A.C.W.M. 2003. Uncertainty analysis for flood defense systems in the Netherland. In: Proceedings of European Safety and Reliability (ESREL) Conference 2003, Maastricht, the Netherlands, 15–18 June.

Worley, S. J., S. D. Woodruff, R. W. Reynolds, S. J. Lubker, and N. Lott. 2005. "ICOADS Release 2.1 Data and Products." *Journal of Climatology* 25:823–842.

Zhang, J., A. A. Taflanidis, N. C. Nadal-Caraballo, J. A. Melby, and F. Diop. 2018. "Advances in Surrogate Modeling for Storm Surge Prediction: Storm Selection and Addressing Characteristics Related to Climate Change." *Natural Hazards* 94:1225–1253.

Zhang, L., and V. P. Singh. 2019. *Copulas and Their Applications in Water Resources Engineering*. Cambridge: Cambridge University Press.

Appendix A: Historical TC Selection (CRL 128)

The TC parameters implemented for the development of marginal distributions (Section 4.1) at CRL 128 are reported here. The NHC ID indicates the chronological order the storm occurred in a given year. In Table A-1, the latitude, longitude, and Δp were selected based on the greatest intensity index computed for each storm (Section 3.4). The distance parameter reported indicates the distance from CRL 128 at which the intensity index was recorded. The adjusted Δp and z-score were computed as described in Section 3.6. Tables A-2 and A-3 provide the unadjusted and distance-adjusted TC atmospheric forcing parameters for the historical TCs selected at CRL 128, respectively.

Table A-1. Historical TCs. coordinates, distance from CRL 128, and Δp.

Name	Year	NHC ID	Latitude (deg)	Longitude (deg)	d (km)	Δp (hPa)	z–score	Adj. Δp (hPa)
UNNAMED	1938	3	28	−93	314	30	0	34
UNNAMED	1938	7	28	−92	276	9	−1	11
UNNAMED	1939	1	28.3	−88.4	185	19	−0.41	22
UNNAMED	1939	2	30.4	−86.4	362	28	0.06	32
UNNAMED	1939	4	29.1	−90.2	33	14	−0.67	16
UNNAMED	1940	2	28.6	−90.4	89	43	0.84	48
UNNAMED	1940	6	29.8	−93.4	340	19	−0.41	22
UNNAMED	1941	1	28	−89.3	156	16	−0.57	19
UNNAMED	1941	2	25.9	−91.9	423	47	1.05	52
UNNAMED	1941	5	29.2	−84.6	517	31	0.21	35
UNNAMED	1941	6	27.7	−84.3	578	16	−0.57	19
UNNAMED	1942	2	27.9	−90.1	155	33	0.32	37
UNNAMED	1942	3	26.3	−93.9	512	61	1.78	68
UNNAMED	1943	1	28.2	−91.1	166	23	−0.20	26
UNNAMED	1943	6	29.1	−92.1	212	24	−0.15	27
UNNAMED	1944	6	29.1	−89.6	38	21	−0.31	24
UNNAMED	1945	1	27.6	−86	428	35	0.42	39
UNNAMED	1945	2	26.6	−92.2	373	8	−0.99	10
UNNAMED	1945	5	29.4	−96	588	33	0.32	37
UNNAMED	1946	1	28.8	−90.3	65	8	−0.99	10
UNNAMED	1947	3	29.1	−90.3	41	11	−0.83	13
UNNAMED	1947	4	29.6	−89.5	55	47	1.05	52

Name	Year	NHC ID	Latitude (deg)	Longitude (deg)	d (km)	Δp (hPa)	z–score	Adj. Δp (hPa)
UNNAMED	1947	5	29.5	−87.7	217	17	−0.52	20
UNNAMED	1947	9	32.5	−86.3	498	11	−0.83	13
UNNAMED	1948	2	29.2	−88.2	168	11	−0.83	13
UNNAMED	1948	5	29.1	−90.5	59	30	0.16	34
UNNAMED	1949	5	29.3	−90.6	65	21	−0.31	24
UNNAMED	1949	9	26.4	−92.3	396	8	−0.99	10
UNNAMED	1949	11	30.1	−95.2	517	31	0.21	35
BAKER	1950	2	28.2	−88.7	170	36	0.47	40
EASY	1950	5	28.1	−83.7	622	47	1.05	52
HOW	1950	8	26.4	−90.3	323	10	−0.88	12
KING	1950	11	32.5	−86	518	13	−0.73	15
LOVE	1950	13	26.7	−91	306	19	−0.41	22
HOW	1951	9	25.8	−87.6	450	10	−0.88	12
ALICE	1953	1	29.8	−85.9	394	20	−0.36	23
UNNAMED	1953	8	28.1	−86.3	378	11	−0.83	13
FLORENCE	1953	9	28.9	−86.8	307	44	0.89	49
BARBARA	1954	5	28.5	−91.5	176	12	−0.78	14
UNNAMED	1954	11	25.8	−90.9	399	9	−0.94	11
BRENDA	1955	1	29.3	−89	90	25	−0.10	28
UNNAMED	1955	5	30.1	−89.7	93	10	−0.88	12
UNNAMED	1956	1	29.1	−90.7	77	17	−0.52	20
FLOSSY	1956	7	29.1	−89.4	56	33	0.32	37
UNNAMED	1957	1	28.2	−86.2	383	13	−0.73	15
AUDREY	1957	2	29.8	−93.7	369	67	2.09	74
BERTHA	1957	3	28.3	−91.3	173	15	−0.62	17
DEBBIE	1957	5	28.9	−87.9	202	10	−0.88	12
ESTHER	1957	6	29.2	−90.9	94	22	−0.26	25
ELLA	1958	5	25.6	−91.5	438	16	−0.57	19
ARLENE	1959	1	29.6	−91.6	165	23	−0.20	26
UNNAMED	1959	3	26.3	−86.3	488	11	−0.83	13
DEBRA	1959	5	29.2	−95.2	511	33	0.32	37
IRENE	1959	10	28.4	−88.2	195	11	−0.83	13
BRENDA	1960	3	28.5	−85	488	10	−0.88	12
ETHEL	1960	6	30.4	−89	153	33	0.32	37
CARLA	1961	3	26	−93.2	487	79	2.72	87

Name	Year	NHC ID	Latitude (deg)	Longitude (deg)	d (km)	Δp (hPa)	z–score	Adj. Δp (hPa)
CINDY	1963	4	28	−93.9	413	17	−0.52	20
ABBY	1964	3	28.6	−94.4	441	9	−0.94	11
DORA	1964	6	30.7	−84.7	528	18	−0.47	21
HILDA	1964	10	29.5	−91.5	154	54	1.41	60
UNNAMED	1965	1	28	−89.5	149	8	−0.99	10
BETSY	1965	3	29.2	−90.1	19	67	2.09	74
DEBBIE	1965	5	28.8	−89.8	55	13	−0.73	15
ALMA	1966	1	29.7	−84.6	518	32	0.26	36
UNNAMED	1968	4	29.5	−85	478	8	−0.99	10
CAMILLE	1969	9	30.3	−89.4	124	113	4.49	125
UNNAMED	1969	19	29.2	−86.5	333	8	−0.99	10
UNNAMED	1969	23	29.5	−86.5	333	17	−0.52	20
LAURIE	1969	26	26.3	−89.6	333	40	0.68	45
BECKY	1970	2	28.3	−86	398	16	−0.57	19
CELIA	1970	4	26.2	−92	399	31	0.21	35
FELICE	1970	13	28.8	−92.2	227	15	−0.62	17
UNNAMED	1971	7	29.6	−83.8	595	9	−0.94	11
FERN	1971	11	27.7	−92	268	9	−0.94	11
EDITH	1971	13	30.5	−91.6	210	28	0.06	32
UNNAMED	1971	20	29.3	−84.8	498	8	−0.99	10
AGNES	1972	2	28.5	−85.7	421	35	0.42	39
DELIA	1973	10	26.5	−91	327	19	−0.41	22
UNNAMED	1973	11	26.5	−90.5	315	9	−0.94	11
UNNAMED	1974	2	25.4	−86.2	568	17	−0.52	20
UNNAMED	1974	4	26.5	−91	327	8	−0.99	10
UNNAMED	1974	8	27.8	−93.2	359	8	−0.99	10
CARMEN	1974	10	28.7	−90.8	107	76	2.56	84
UNNAMED	1974	16	25.7	−88	442	8	−0.99	10
ELOISE	1975	13	28.4	−87.3	275	55	1.47	61
UNNAMED	1975	18	29.2	−90.7	75	8	−0.99	10
UNNAMED	1976	1	27	−88	317	14	−0.67	16
UNNAMED	1977	2	29.5	−87.5	237	12	−0.78	14
ANITA	1977	5	26.4	−91	338	22	−0.26	25
BABE	1977	6	29.5	−91.2	125	29	0.11	33
UNNAMED	1977	15	28.5	−91.4	168	9	−0.94	11

Name	Year	NHC ID	Latitude (deg)	Longitude (deg)	d (km)	Δp (hPa)	z–score	Adj. Δp (hPa)
DEBRA	1978	9	29.6	−93.6	357	13	−0.73	15
BOB	1979	4	29.1	−90.6	68	27	0.00	31
CLAUDETTE	1979	6	30.3	−93.9	399	16	−0.57	19
FREDERIC	1979	11	29.7	−88	193	67	2.09	74
ELENA	1979	12	26.5	−93	432	9	−0.94	11
DANIELLE	1980	11	29.4	−93.4	336	9	−0.94	11
JEANNE	1980	16	25.6	−92.8	498	20	−0.36	23
UNNAMED	1981	4	29	−96	590	8	−0.99	10
UNNAMED	1982	2	25.8	−86.4	521	9	−0.94	11
CHRIS	1982	5	29.8	−93.8	379	19	−0.41	22
ALICIA	1983	3	27.4	−93.3	391	22	−0.26	25
BARRY	1983	4	25.8	−93	492	11	−0.83	13
UNNAMED	1984	17	29.5	−87.8	208	8	−0.99	10
DANNY	1985	4	28.9	−92.6	263	25	−0.10	28
ELENA	1985	5	30.4	−89.2	143	54	1.41	60
JUAN	1985	12	29.3	−89.1	81	35	0.42	39
KATE	1985	13	28.3	−86.5	352	48	1.10	54
BONNIE	1986	2	27.2	−91.7	289	16	−0.57	19
BERYL	1988	2	29.6	−89.5	55	12	−0.78	14
FLORENCE	1988	7	29.1	−89.3	65	29	0.11	33
UNNAMED	1988	17	28	−93.5	376	9	−0.94	11
ALLISON	1989	2	31.1	−93.9	432	8	−0.99	10
CHANTAL	1989	4	27.9	−92.8	320	22	−0.26	25
JERRY	1989	14	28.6	−94.8	480	31	0.21	35
ANDREW	1992	4	28.5	−90.5	103	76	2.56	84
ALBERTO	1994	1	29.9	−86.7	320	20	−0.36	23
BERYL	1994	3	30	−85.6	426	13	−0.73	15
ALLISON	1995	1	27.6	−86.1	419	25	−0.10	28
DEAN	1995	4	28.1	−93	327	8	−0.99	10
ERIN	1995	5	30.3	−87.2	287	40	0.68	45
OPAL	1995	17	29	−87.7	219	75	2.51	83
JOSEPHINE	1996	10	26.9	−87.3	370	32	0.26	36
DANNY	1997	5	29.3	−89.7	22	24	−0.15	27
EARL	1998	5	28.7	−87.9	208	25	−0.10	28
FRANCES	1998	6	26.6	−95.2	597	17	−0.52	20

Name	Year	NHC ID	Latitude (deg)	Longitude (deg)	d (km)	Δp (hPa)	z–score	Adj. Δp (hPa)
GEORGES	1998	7	29.3	−88.5	139	52	1.31	58
HERMINE	1998	8	29	−90.9	99	14	−0.67	16
HARVEY	1999	10	27	−86.3	437	15	−0.62	17
HELENE	2000	12	28.4	−87.2	284	17	−0.52	20
ALLISON	2001	1	30.7	−89.4	165	13	−0.73	15
BARRY	2001	3	28.6	−86.4	352	22	−0.26	25
FAY	2002	6	27.7	−94.5	480	12	−0.78	14
HANNA	2002	9	29.1	−89.1	83	10	−0.88	12
ISIDORE	2002	10	29.1	−90.3	41	29	0.11	33
LILI	2002	13	28.1	−91.4	195	56	1.52	62
BILL	2003	3	29.3	−91	104	16	−0.57	19
CLAUDETTE	2003	4	27.3	−93	373	24	−0.15	27
ERIKA	2003	8	26	−92.5	444	12	−0.78	14
HENRI	2003	12	27.8	−86.3	391	11	−0.83	13
BONNIE	2004	2	26.4	−89.6	322	12	−0.78	14
FRANCES	2004	6	31.5	−85	533	25	−0.10	28
IVAN	2004	9	28.9	−88.2	174	82	2.87	91
MATTHEW	2004	14	29.2	−91	104	14	−0.67	16
ARLENE	2005	1	30.1	−87.5	252	22	−0.26	25
CINDY	2005	3	29.2	−90.1	19	22	−0.26	25
DENNIS	2005	4	29.9	−86.9	301	71	2.30	79
KATRINA	2005	12	29.3	−89.6	32	93	3.45	103
RITA	2005	18	27.1	−91.5	287	86	3.08	95
TAMMY	2005	22	30.3	−85.6	433	8	−0.99	10
ALBERTO	2006	1	26.8	−86.3	451	13	−0.73	15
ERIN	2007	5	25.2	−92.9	541	8	−0.99	10
HUMBERTO	2007	9	30.3	−93.6	372	24	−0.15	27
TEN	2007	10	29.7	−86.1	374	8	−0.99	10
OLGA	2007	17	25	−87.2	548	8	−0.99	10
EDOUARD	2008	5	28.3	−91	151	12	−0.78	14
FAY	2008	6	31.3	−90	224	12	−0.78	14
GUSTAV	2008	7	28.8	−90.3	65	58	1.62	64
IKE	2008	9	26.4	−91.1	341	59	1.67	66
CLAUDETTE	2009	4	30.5	−86.6	348	8	−0.99	10
IDA	2009	11	28.5	−88.7	148	23	−0.20	26

Name	Year	NHC ID	Latitude (deg)	Longitude (deg)	d (km)	Δp (hPa)	z–score	Adj. Δp (hPa)
DON	2011	4	24.6	−91.9	556	16	−0.57	19
LEE	2011	13	29.7	−92	205	27	0.00	31
DEBBY	2012	4	27.6	−86.8	359	19	−0.41	22
ISAAC	2012	9	29	−89.7	39	48	1.10	54
ANDREA	2013	1	26.7	−86.1	473	14	−0.67	16
KAREN	2013	12	26.1	−90.5	359	9	−0.94	11
BILL	2015	2	27	−94.3	498	8	−0.99	10
COLIN	2016	3	28.1	−86.1	396	10	−0.88	12
HERMINE	2016	9	27.9	−85.5	459	25	−0.10	28
CINDY	2017	3	27.3	−92.3	320	20	−0.36	23
HARVEY	2017	9	29.8	−93.5	350	22	−0.26	25
IRMA	2017	11	31.9	−84.4	604	27	0.00	31
NATE	2017	16	29.1	−89.2	74	30	0.16	34
ALBERTO	2018	1	28.6	−86	390	23	−0.20	26
GORDON	2018	7	30.4	−88.5	186	17	−0.52	20
MICHAEL	2018	14	29	−86.3	354	79	2.72	87
BARRY	2019	2	28.4	−90.7	124	20	−0.36	23
IMELDA	2019	11	29	−95.4	532	10	−0.88	12
NESTOR	2019	16	27.8	−87.8	266	17	−0.52	20
OLGA	2019	17	28.8	−91.2	135	19	−0.41	22
CRISTOBAL	2020	3	29	−89.8	34	20	−0.37	23
LAURA	2020	13	28.5	−93	311	75	2.49	83
MARCO	2020	14	27.2	−87.9	305	10	−0.89	12
SALLY	2020	19	29.9	−87.8	217	45	0.93	50
BETA	2020	22	26.8	−92.2	355	16	−0.58	19
DELTA	2020	26	30	−92.9	298	42	0.78	47
ZETA	2020	28	30.2	−89.9	102	40	0.67	45

Table A-2. Historical TCs with unadjusted atmospheric parameters at CRL 128.

Name	Year	NHC ID	Δp (hPa)	R_{max} (km)	V_t (km/h)	θ (deg)
UNNAMED	1938	3	30	47	26	−22
UNNAMED	1938	7	9	45	26	−60
UNNAMED	1939	1	19	58	6	180
UNNAMED	1939	2	28	39	17	−49
UNNAMED	1939	4	14	35	17	16
UNNAMED	1940	2	43	118	12	−72
UNNAMED	1940	6	19	98	13	74
UNNAMED	1941	1	16	68	4	−119
UNNAMED	1941	2	47	58	19	−61
UNNAMED	1941	5	31	51	27	−33
UNNAMED	1941	6	16	122	9	10
UNNAMED	1942	2	33	54	16	−55
UNNAMED	1942	3	61	64	24	−51
UNNAMED	1943	1	23	62	16	−83
UNNAMED	1943	6	24	83	10	41
UNNAMED	1944	6	21	75	33	67
UNNAMED	1945	1	35	50	11	48
UNNAMED	1945	2	8	99	13	−64
UNNAMED	1945	5	33	46	9	10
UNNAMED	1946	1	8	58	13	−82
UNNAMED	1947	3	11	56	12	−24
UNNAMED	1947	4	47	74	27	−65
UNNAMED	1947	5	17	66	9	−10
UNNAMED	1947	9	11	81	22	−53
UNNAMED	1948	2	11	46	16	37
UNNAMED	1948	5	30	62	24	24
UNNAMED	1949	5	21	64	29	−13
UNNAMED	1949	9	8	97	11	−48
UNNAMED	1949	11	31	75	20	19
BAKER	1950	2	36	51	23	12
EASY	1950	5	47	54	2	41
HOW	1950	8	10	106	13	−82
KING	1950	11	13	78	13	−56
LOVE	1950	13	19	92	11	−48
HOW	1951	9	10	117	6	17

Name	Year	NHC ID	Δp (hPa)	R_{max} (km)	V_t (km/h)	θ (deg)
ALICE	1953	1	20	88	9	0
UNNAMED	1953	8	11	74	8	24
FLORENCE	1953	9	44	57	29	13
BARBARA	1954	5	12	57	8	−60
UNNAMED	1954	11	9	105	15	−83
BRENDA	1955	1	25	58	15	−26
UNNAMED	1955	5	10	54	25	−77
UNNAMED	1956	1	17	59	36	6
FLOSSY	1956	7	33	55	20	57
UNNAMED	1957	1	13	45	41	40
AUDREY	1957	2	67	57	43	10
BERTHA	1957	3	15	81	15	−51
DEBBIE	1957	5	10	54	24	24
ESTHER	1957	6	22	68	27	25
ELLA	1958	5	16	48	29	−54
ARLENE	1959	1	23	56	12	23
UNNAMED	1959	3	11	83	50	58
DEBRA	1959	5	33	43	11	0
IRENE	1959	10	11	48	24	33
BRENDA	1960	3	10	89	14	21
ETHEL	1960	6	33	54	13	−30
CARLA	1961	3	79	49	15	−51
CINDY	1963	4	17	70	13	−7
ABBY	1964	3	9	74	15	−90
DORA	1964	6	18	80	7	−41
HILDA	1964	10	54	65	16	7
UNNAMED	1965	1	8	29	20	34
BETSY	1965	3	67	47	31	−44
DEBBIE	1965	5	13	62	9	−33
ALMA	1966	1	32	49	17	−11
UNNAMED	1968	4	8	76	17	71
CAMILLE	1969	9	113	59	27	−21
UNNAMED	1969	19	8	84	17	0
UNNAMED	1969	23	17	75	19	5
LAURIE	1969	26	40	45	13	82
BECKY	1970	2	16	84	16	18

Name	Year	NHC ID	Δp (hPa)	R_{max} (km)	V_t (km/h)	θ (deg)
CELIA	1970	4	31	44	21	−69
FELICE	1970	13	15	54	36	−65
UNNAMED	1971	7	9	149	9	−33
FERN	1971	11	9	91	10	−138
EDITH	1971	13	28	74	30	52
UNNAMED	1971	20	8	114	11	−8
AGNES	1972	2	35	55	24	0
DELIA	1973	10	19	77	21	−58
UNNAMED	1973	11	9	72	15	0
UNNAMED	1974	2	17	154	40	49
UNNAMED	1974	4	8	99	11	−119
UNNAMED	1974	8	8	93	25	−47
CARMEN	1974	10	76	39	18	−21
UNNAMED	1974	16	8	106	15	33
ELOISE	1975	13	55	51	28	44
UNNAMED	1975	18	8	70	18	45
UNNAMED	1976	1	14	75	21	52
UNNAMED	1977	2	12	76	23	−12
ANITA	1977	5	22	64	7	−106
BABE	1977	6	29	65	15	12
UNNAMED	1977	15	9	69	29	51
DEBRA	1978	9	13	63	19	26
BOB	1979	4	27	66	25	19
CLAUDETTE	1979	6	16	92	13	0
FREDERIC	1979	11	67	49	25	−11
ELENA	1979	12	9	84	21	−105
DANIELLE	1980	11	9	61	20	−55
JEANNE	1980	16	20	57	24	−57
UNNAMED	1981	4	8	91	24	4
UNNAMED	1982	2	9	95	38	51
CHRIS	1982	5	19	64	15	12
ALICIA	1983	3	22	52	8	−77
BARRY	1983	4	11	43	23	−90
UNNAMED	1984	17	8	85	28	−48
DANNY	1985	4	25	43	21	−18
ELENA	1985	5	54	68	44	−60

Name	Year	NHC ID	Δp (hPa)	R_{max} (km)	V_t (km/h)	θ (deg)
JUAN	1985	12	35	81	21	69
KATE	1985	13	48	53	15	6
BONNIE	1986	2	16	98	14	−57
BERYL	1988	2	12	53	9	−49
FLORENCE	1988	7	29	53	22	0
UNNAMED	1988	17	9	74	16	90
ALLISON	1989	2	8	71	5	90
CHANTAL	1989	4	22	44	18	−33
JERRY	1989	14	31	39	20	−19
ANDREW	1992	4	76	28	20	−48
ALBERTO	1994	1	20	46	20	5
BERYL	1994	3	13	93	2	41
ALLISON	1995	1	25	56	26	4
DEAN	1995	4	8	93	23	−66
ERIN	1995	5	40	50	19	−49
OPAL	1995	17	75	55	34	22
JOSEPHINE	1996	10	32	167	32	55
DANNY	1997	5	24	38	7	60
EARL	1998	5	25	35	20	62
FRANCES	1998	6	17	111	24	0
GEORGES	1998	7	52	56	10	−19
HERMINE	1998	8	14	44	13	14
HARVEY	1999	10	15	100	12	53
HELENE	2000	12	17	111	24	−4
ALLISON	2001	1	13	36	22	53
BARRY	2001	3	22	28	9	0
FAY	2002	6	12	84	7	−74
HANNA	2002	9	10	74	22	0
ISIDORE	2002	10	29	74	30	0
LILI	2002	13	56	71	32	−35
BILL	2003	3	16	47	22	0
CLAUDETTE	2003	4	24	37	13	−31
ERIKA	2003	8	12	46	33	−93
HENRI	2003	12	11	70	15	90
BONNIE	2004	2	12	37	19	46
FRANCES	2004	6	25	28	11	−34

Name	Year	NHC ID	Δp (hPa)	R_{max} (km)	V_t (km/h)	θ (deg)
IVAN	2004	9	82	37	19	0
MATTHEW	2004	14	14	51	25	9
ARLENE	2005	1	22	46	23	−12
CINDY	2005	3	22	46	27	14
DENNIS	2005	4	71	52	28	−20
KATRINA	2005	12	93	72	24	0
RITA	2005	18	86	52	17	−50
TAMMY	2005	22	8	96	17	169
ALBERTO	2006	1	13	167	26	44
ERIN	2007	5	8	92	23	−55
HUMBERTO	2007	9	24	60	21	41
TEN	2007	10	8	115	16	−45
OLGA	2007	17	8	99	36	28
EDOUARD	2008	5	12	37	12	−72
FAY	2008	6	12	75	6	−128
GUSTAV	2008	7	58	101	27	−52
IKE	2008	9	59	93	19	−73
CLAUDETTE	2009	4	8	101	21	−41
IDA	2009	11	23	40	22	−8
DON	2011	4	16	37	22	−70
LEE	2011	13	27	78	9	41
DEBBY	2012	4	19	89	13	31
ISAAC	2012	9	48	178	10	−69
ANDREA	2013	1	14	167	21	18
KAREN	2013	12	9	90	7	−42
BILL	2015	2	8	75	19	−53
COLIN	2016	3	10	49	37	32
HERMINE	2016	9	25	64	22	32
CINDY	2017	3	20	139	16	−55
HARVEY	2017	9	22	106	23	12
IRMA	2017	11	27	19	23	−37
NATE	2017	16	30	48	28	−10
ALBERTO	2018	1	23	74	8	−24
GORDON	2018	7	17	55	26	−36
MICHAEL	2018	14	79	47	25	11
BARRY	2019	2	20	89	10	−56

Name	Year	NHC ID	Δp (hPa)	R_{max} (km)	V_t (km/h)	θ (deg)
IMELDA	2019	11	10	83	20	0
NESTOR	2019	16	17	87	37	45
OLGA	2019	17	19	71	40	32
CRISTOBAL	2020	3	20	68	15	6
LAURA	2020	13	75	43	24	−20
MARCO	2020	14	10	106	16	−18
SALLY	2020	19	45	57	6	30
BETA	2020	22	16	47	4	24
DELTA	2020	26	42	61	27	25
ZETA	2020	28	40	58	45	25

Table A-3. Historical TCs with distance-adjusted atmospheric parameters at CRL 128.

Name	Year	NHC ID	Δp (hPa)	R_{max} (km)	V_t (km/h)	θ (deg)
UNNAMED	1938	3	34	46	27	−16
UNNAMED	1938	7	11	44	27	−54
UNNAMED	1939	1	22	55	6	−174
UNNAMED	1939	2	32	39	17	−43
UNNAMED	1939	4	16	36	17	22
UNNAMED	1940	2	48	103	12	−66
UNNAMED	1940	6	22	87	13	80
UNNAMED	1941	1	19	63	4	−113
UNNAMED	1941	2	52	55	19	−55
UNNAMED	1941	5	35	49	28	−27
UNNAMED	1941	6	19	106	9	16
UNNAMED	1942	2	37	51	16	−49
UNNAMED	1942	3	68	59	25	−45
UNNAMED	1943	1	26	58	16	−77
UNNAMED	1943	6	27	75	10	47
UNNAMED	1944	6	24	68	34	73
UNNAMED	1945	1	39	48	11	54
UNNAMED	1945	2	10	88	13	−58
UNNAMED	1945	5	37	45	9	16
UNNAMED	1946	1	10	55	13	−76
UNNAMED	1947	3	13	53	12	−18
UNNAMED	1947	4	52	68	28	−59
UNNAMED	1947	5	20	61	9	−4
UNNAMED	1947	9	13	73	23	−47
UNNAMED	1948	2	13	45	16	43
UNNAMED	1948	5	34	58	25	30
UNNAMED	1949	5	24	59	30	−7
UNNAMED	1949	9	10	86	11	−42
UNNAMED	1949	11	35	68	21	25
BAKER	1950	2	40	49	24	18
EASY	1950	5	52	51	2	47
HOW	1950	8	12	93	13	−76
KING	1950	11	15	71	13	−50
LOVE	1950	13	22	82	11	−42
HOW	1951	9	12	102	6	23

Name	Year	NHC ID	Δp (hPa)	R_{max} (km)	V_t (km/h)	θ (deg)
ALICE	1953	1	23	79	9	6
UNNAMED	1953	8	13	68	8	30
FLORENCE	1953	9	49	54	30	19
BARBARA	1954	5	14	54	8	−54
UNNAMED	1954	11	11	93	15	−77
BRENDA	1955	1	28	55	15	−20
UNNAMED	1955	5	12	51	26	−71
UNNAMED	1956	1	20	55	37	12
FLOSSY	1956	7	37	52	21	63
UNNAMED	1957	1	15	44	42	46
AUDREY	1957	2	74	54	45	16
BERTHA	1957	3	17	73	15	−45
DEBBIE	1957	5	12	51	25	30
ESTHER	1957	6	25	63	28	31
ELLA	1958	5	19	47	30	−48
ARLENE	1959	1	26	53	12	29
UNNAMED	1959	3	13	75	52	64
DEBRA	1959	5	37	43	11	6
IRENE	1959	10	13	47	25	39
BRENDA	1960	3	12	80	14	27
ETHEL	1960	6	37	51	13	−24
CARLA	1961	3	87	47	15	−45
CINDY	1963	4	20	64	13	−1
ABBY	1964	3	11	68	15	−84
DORA	1964	6	21	72	7	−35
HILDA	1964	10	60	60	16	13
UNNAMED	1965	1	10	31	21	40
BETSY	1965	3	74	46	32	−38
DEBBIE	1965	5	15	58	9	−27
ALMA	1966	1	36	47	17	−5
UNNAMED	1968	4	10	69	17	77
CAMILLE	1969	9	125	55	28	−15
UNNAMED	1969	19	10	76	17	6
UNNAMED	1969	23	20	68	19	11
LAURIE	1969	26	45	44	13	88
BECKY	1970	2	19	76	16	24

Name	Year	NHC ID	Δp (hPa)	R_{max} (km)	V_t (km/h)	θ (deg)
CELIA	1970	4	35	43	22	−63
FELICE	1970	13	17	51	37	−59
UNNAMED	1971	7	11	128	9	−27
FERN	1971	11	11	81	10	−132
EDITH	1971	13	32	68	31	58
UNNAMED	1971	20	10	100	11	−2
AGNES	1972	2	39	52	25	6
DELIA	1973	10	22	70	22	−52
UNNAMED	1973	11	11	66	15	6
UNNAMED	1974	2	20	132	41	55
UNNAMED	1974	4	10	88	11	−113
UNNAMED	1974	8	10	83	26	−41
CARMEN	1974	10	84	39	18	−15
UNNAMED	1974	16	10	93	15	39
ELOISE	1975	13	61	49	29	50
UNNAMED	1975	18	10	64	18	51
UNNAMED	1976	1	16	68	22	58
UNNAMED	1977	2	14	69	24	−6
ANITA	1977	5	25	59	7	−100
BABE	1977	6	33	60	15	18
UNNAMED	1977	15	11	64	30	57
DEBRA	1978	9	15	59	19	32
BOB	1979	4	31	61	26	25
CLAUDETTE	1979	6	19	82	13	6
FREDERIC	1979	11	74	47	26	−5
ELENA	1979	12	11	76	22	−99
DANIELLE	1980	11	11	57	21	−49
JEANNE	1980	16	23	54	25	−51
UNNAMED	1981	4	10	81	25	10
UNNAMED	1982	2	11	84	39	57
CHRIS	1982	5	22	59	15	18
ALICIA	1983	3	25	50	8	−71
BARRY	1983	4	13	43	24	−84
UNNAMED	1984	17	10	76	29	−42
DANNY	1985	4	28	43	22	−12
ELENA	1985	5	60	63	46	−54

Name	Year	NHC ID	Δp (hPa)	R_{max} (km)	V_t (km/h)	θ (deg)
JUAN	1985	12	39	73	22	75
KATE	1985	13	54	51	15	12
BONNIE	1986	2	19	87	14	−51
BERYL	1988	2	14	51	9	−43
FLORENCE	1988	7	33	51	23	6
UNNAMED	1988	17	11	68	16	96
ALLISON	1989	2	10	65	5	96
CHANTAL	1989	4	25	43	18	−27
JERRY	1989	14	35	39	21	−13
ANDREW	1992	4	84	30	21	−42
ALBERTO	1994	1	23	45	21	11
BERYL	1994	3	15	83	2	47
ALLISON	1995	1	28	53	27	10
DEAN	1995	4	10	83	24	−60
ERIN	1995	5	45	48	19	−43
OPAL	1995	17	83	52	35	28
JOSEPHINE	1996	10	36	143	33	61
DANNY	1997	5	27	39	7	66
EARL	1998	5	28	36	21	68
FRANCES	1998	6	20	97	25	6
GEORGES	1998	7	58	53	10	−13
HERMINE	1998	8	16	43	13	20
HARVEY	1999	10	17	89	12	59
HELENE	2000	12	20	97	25	2
ALLISON	2001	1	15	37	23	59
BARRY	2001	3	25	30	9	6
FAY	2002	6	14	76	7	−68
HANNA	2002	9	12	68	23	6
ISIDORE	2002	10	33	68	31	6
LILI	2002	13	62	65	33	−29
BILL	2003	3	19	46	23	6
CLAUDETTE	2003	4	27	38	13	−25
ERIKA	2003	8	14	45	34	−87
HENRI	2003	12	13	64	15	96
BONNIE	2004	2	14	38	19	52
FRANCES	2004	6	28	30	11	−28

Name	Year	NHC ID	Δp (hPa)	R_{max} (km)	V_t (km/h)	θ (deg)
IVAN	2004	9	91	38	19	6
MATTHEW	2004	14	16	49	26	15
ARLENE	2005	1	25	45	24	−6
CINDY	2005	3	25	45	28	20
DENNIS	2005	4	79	50	29	−14
KATRINA	2005	12	103	66	25	6
RITA	2005	18	95	50	17	−44
TAMMY	2005	22	10	85	17	175
ALBERTO	2006	1	15	143	27	50
ERIN	2007	5	10	82	24	−49
HUMBERTO	2007	9	27	56	22	47
TEN	2007	10	10	101	16	−39
OLGA	2007	17	10	88	37	34
EDOUARD	2008	5	14	38	12	−66
FAY	2008	6	14	68	6	−122
GUSTAV	2008	7	64	89	28	−46
IKE	2008	9	66	83	19	−67
CLAUDETTE	2009	4	10	89	22	−35
IDA	2009	11	26	40	23	−2
DON	2011	4	19	38	23	−64
LEE	2011	13	31	71	9	47
DEBBY	2012	4	22	80	13	37
ISAAC	2012	9	54	151	10	−63
ANDREA	2013	1	16	143	22	24
KAREN	2013	12	11	80	7	−36
BILL	2015	2	10	68	19	−47
COLIN	2016	3	12	47	38	38
HERMINE	2016	9	28	59	23	38
CINDY	2017	3	23	120	16	−49
HARVEY	2017	9	25	93	24	18
IRMA	2017	11	31	23	24	−31
NATE	2017	16	34	47	29	−4
ALBERTO	2018	1	26	68	8	−18
GORDON	2018	7	20	52	27	−30
MICHAEL	2018	14	87	46	26	17
BARRY	2019	2	23	80	10	−50

Name	Year	NHC ID	Δp (hPa)	R_{max} (km)	V_t (km/h)	θ (deg)
IMELDA	2019	11	12	75	21	6
NESTOR	2019	16	20	78	38	51
OLGA	2019	17	22	65	41	38
CRISTOBAL	2020	3	23	63	15	12
LAURA	2020	13	83	43	25	−14
MARCO	2020	14	12	93	16	−12
SALLY	2020	19	50	54	6	36
BETA	2020	22	19	46	4	30
DELTA	2020	26	47	57	28	31
ZETA	2020	28	45	55	47	31

Appendix B: Synthetic Tropical Cyclone Suite

Table B-1. Master tracks defined for the CHS-LA ITCS.

CHS-LA Master Track ID	θ (deg)	Reference Latitude (deg N)	Reference Longitude (deg W)
1	−80	28.12	−93.61
2	−80	28.52	−92.76
3	−80	28.98	−92.18
4	−80	28.65	−86.54
5	−80	29.28	−87.06
6	−80	29.8	−86.88
7	−60	27.87	−92.98
8	−60	28.24	−92.51
9	−60	28.52	−91.85
10	−60	28.5	−90.63
11	−60	28.01	−88.45
12	−60	27.87	−86.96
13	−60	28.61	−87.2
14	−60	29.15	−87.05
15	−60	29.08	−85.67
16	−60	29.25	−84.77
17	−40	27.31	−93.52
18	−40	27.66	−93.07
19	−40	27.9	−92.52
20	−40	28.03	−91.87
21	−40	27.82	−90.9
22	−40	28.08	−90.36
23	−40	27.47	−88.99
24	−40	27.68	−88.41
25	−40	27.44	−87.39
26	−40	28.6	−87.7
27	−40	28.6	−86.9
28	−40	28.51	−86.02

CHS-LA Master Track ID	θ (deg)	Reference Latitude (deg N)	Reference Longitude (deg W)
29	−40	28.66	−85.36
30	−20	26.76	−94.5
31	−20	27.18	−94.04
32	−20	27.43	−93.51
33	−20	27.59	−92.93
34	−20	27.65	−92.32
35	−20	27.43	−91.6
36	−20	27.7	−91.06
37	−20	27.09	−90.17
38	−20	27.2	−89.58
39	−20	27.19	−88.93
40	−20	26.98	−88.2
41	−20	28.27	−88.07
42	−20	28.27	−87.43
43	−20	28.15	−86.73
44	−20	28.28	−86.13
45	0	26.55	−95.54
46	0	27.05	−94.93
47	0	27.31	−94.32
48	0	27.48	−93.71
49	0	27.5	−93.1
50	0	27.3	−92.49
51	0	27.49	−91.88
52	0	27.25	−91.27
53	0	26.9	−90.66
54	0	26.95	−90.05
55	0	26.9	−89.44
56	0	28.14	−88.83
57	0	28.1	−88.22
58	0	28	−87.61
59	0	28.14	−87

CHS-LA Master Track ID	θ (deg)	Reference Latitude (deg N)	Reference Longitude (deg W)
60	20	26.47	−96.84
61	20	26.92	−96.01
62	20	27.46	−95.15
63	20	27.64	−94.45
64	20	27.59	−93.84
65	20	27.42	−93.26
66	20	27.62	−92.56
67	20	27.26	−92.06
68	20	27.04	−91.52
69	20	27.36	−90.76
70	20	27.02	−90.27
71	20	28.26	−89.13
72	20	28.13	−88.56
73	20	28.27	−87.87
74	40	27.94	−95.6
75	40	28.02	−94.73
76	40	27.82	−94.13
77	40	27.89	−93.27
78	40	27.6	−92.76
79	40	27.54	−92.03
80	40	27.55	−91.25
81	40	28.48	−89.57
82	40	28.65	−88.64
83	60	28.39	−94.55
84	60	28.31	−93.47
85	60	27.97	−92.92
86	60	28.01	−91.64

Table B-2. Atmospheric-forcing parameters of the CHS-LA ITCS.

CHS–LA TC ID	Master Track ID	θ (deg)	Δp (hPa)	R_{max} (km)	V_t (km/h)
1	1	−80	148	20.2	17.6
2	1	−80	128	27.2	28.4
3	1	−80	108	10.9	21.8
4	1	−80	88	17	9.1
5	1	−80	68	28.7	31
6	1	−80	48	58	15.4
7	1	−80	28	109.3	18.9
8	1	−80	8	43.3	9.9
9	2	−80	148	16.7	38.2
10	2	−80	128	9.4	13.5
11	2	−80	108	50.6	16
12	2	−80	88	46.8	18.9
13	2	−80	68	50.9	8.9
14	2	−80	48	41.4	17.2
15	2	−80	28	21.6	17.9
16	2	−80	8	82.5	20.1
17	3	−80	148	9.3	18.2
18	3	−80	128	22.1	26.7
19	3	−80	108	30.3	9.4
20	3	−80	88	18.9	31.9
21	3	−80	68	68.1	14.5
22	3	−80	48	46.5	18.2
23	3	−80	28	16.6	8.6
24	3	−80	8	104.9	22.7
25	4	−80	148	11.2	20.1
26	4	−80	128	14.8	9.7
27	4	−80	108	36.6	19.4
28	4	−80	88	78.3	12.4
29	4	−80	68	49.1	32.4
30	4	−80	48	21.1	15.9
31	4	−80	28	94.8	21.8
32	4	−80	8	66.5	9.6
33	5	−80	148	14.2	20.7
34	5	−80	128	29	33.5
35	5	−80	108	33.2	21.2

CHS–LA TC ID	Master Track ID	θ (deg)	Δp (hPa)	R_{max} (km)	V_t (km/h)
36	5	−80	88	21.8	15.8
37	5	−80	68	91.9	17.3
38	5	−80	48	50.2	9.3
39	5	−80	28	35.2	8.3
40	5	−80	8	61.8	24.4
41	6	−80	148	16.3	11.7
42	6	−80	128	11.6	21
43	6	−80	108	53.7	24.5
44	6	−80	88	64.5	14.8
45	6	−80	68	32.6	11.4
46	6	−80	48	43.1	31.5
47	6	−80	28	40.6	15.7
48	6	−80	8	115.6	14.3
49	7	−60	138	32.8	17.8
50	7	−60	118	30.3	29.4
51	7	−60	98	16.4	16.2
52	7	−60	78	17.3	17.8
53	7	−60	58	24	31.2
54	7	−60	38	94.2	21.3
55	7	−60	18	60.4	8.8
56	8	−60	138	25.7	40.5
57	8	−60	118	17.4	27.6
58	8	−60	98	14	17.2
59	8	−60	78	41.4	19.5
60	8	−60	58	29.6	9.9
61	8	−60	38	90.1	22
62	8	−60	18	27.7	22.2
63	9	−60	138	14	45.1
64	9	−60	118	18	24.5
65	9	−60	98	35.9	10.2
66	9	−60	78	82.2	14.9
67	9	−60	58	17.1	15.4
68	9	−60	38	66.4	23.3
69	9	−60	18	51.9	15.6
70	10	−60	138	24.8	9.9
71	10	−60	118	21.8	32.5

CHS–LA TC ID	Master Track ID	θ (deg)	Δp (hPa)	R_{max} (km)	V_t (km/h)
72	10	−60	98	18	17.8
73	10	−60	78	28.6	9
74	10	−60	58	50	10.7
75	10	−60	38	83	18.1
76	10	−60	18	20.7	11.2
77	11	−60	138	20.7	25.1
78	11	−60	118	24.5	17
79	11	−60	98	38.4	26.8
80	11	−60	78	88.9	17.3
81	11	−60	58	22.6	17.8
82	11	−60	38	53.4	11.4
83	11	−60	18	87.1	27.8
84	12	−60	138	24	12.6
85	12	−60	118	23.8	28.5
86	12	−60	98	26.7	23.1
87	12	−60	78	77.2	16.8
88	12	−60	58	41.6	25.1
89	12	−60	38	37	10.3
90	12	−60	18	102.7	20.3
91	13	−60	138	14.4	15.4
92	13	−60	118	13.4	17.5
93	13	−60	98	51.2	15.1
94	13	−60	78	27.4	24.5
95	13	−60	58	94.9	18.3
96	13	−60	38	27	20.2
97	13	−60	18	69.8	9.5
98	14	−60	138	17.7	18.4
99	14	−60	118	34.6	10.6
100	14	−60	98	24.9	12.7
101	14	−60	78	19.5	27.7
102	14	−60	58	109.6	23.6
103	14	−60	38	61.8	22.6
104	14	−60	18	62.6	16.4
105	15	−60	138	27.8	23.6
106	15	−60	118	12.3	21.1
107	15	−60	98	33.7	10.7

CHS–LA TC ID	Master Track ID	θ (deg)	Δp (hPa)	R_{max} (km)	V_t (km/h)
108	15	−60	78	21.7	26.8
109	15	−60	58	101.2	19.9
110	15	−60	38	43.9	24.8
111	15	−60	18	127.9	17.3
112	16	−60	138	11.8	16
113	16	−60	118	37.2	19.9
114	16	−60	98	19.7	16.7
115	16	−60	78	25.1	29.7
116	16	−60	58	35.4	10.3
117	16	−60	38	127.1	17.1
118	16	−60	18	42.2	13.6
119	17	−40	148	17.1	14.6
120	17	−40	128	18.2	39.3
121	17	−40	108	14.9	25.3
122	17	−40	88	61.4	18.4
123	17	−40	68	34	12.7
124	17	−40	48	16.6	28.8
125	17	−40	28	67.3	17
126	17	−40	8	28.6	8.6
127	18	−40	148	10.4	15.8
128	18	−40	128	31.1	43.8
129	18	−40	108	19.8	15
130	18	−40	88	12.3	21.8
131	18	−40	68	60.8	35.9
132	18	−40	48	74.9	10.1
133	18	−40	28	48.1	20
134	18	−40	8	23.3	8
135	19	−40	148	11.5	30
136	19	−40	128	10.3	30.2
137	19	−40	108	21.2	28.5
138	19	−40	88	54.1	15.3
139	19	−40	68	65.5	10.6
140	19	−40	48	24.1	9
141	19	−40	28	58.2	29
142	19	−40	8	26.8	16.6
143	20	−40	148	8.5	43.8

CHS–LA TC ID	Master Track ID	θ (deg)	Δp (hPa)	R_{max} (km)	V_t (km/h)
144	20	−40	128	18.7	34.7
145	20	−40	108	18.3	12.4
146	20	−40	88	48.5	26.8
147	20	−40	68	17.4	20
148	20	−40	48	88.2	12.5
149	20	−40	28	56.1	9.3
150	20	−40	8	37.7	17.1
151	21	−40	148	23.5	50
152	21	−40	128	13.9	23
153	21	−40	108	35.5	11.4
154	21	−40	88	22.8	16.3
155	21	−40	68	14.9	34
156	21	−40	48	72.1	24.2
157	21	−40	28	38.8	21.1
158	21	−40	8	74	14.6
159	22	−40	148	10.9	36.7
160	22	−40	128	37.5	31.2
161	22	−40	108	17	38.9
162	22	−40	88	25.8	13.3
163	22	−40	68	13.7	26.8
164	22	−40	48	69.5	10.9
165	22	−40	28	64.9	24.7
166	22	−40	8	19.8	13.6
167	23	−40	148	24.7	25.7
168	23	−40	128	9.9	16.8
169	23	−40	108	26.7	10.4
170	23	−40	88	43.7	28.6
171	23	−40	68	54.6	11.8
172	23	−40	48	60.1	16.8
173	23	−40	28	133.7	20.5
174	23	−40	8	30.4	15.8
175	24	−40	148	12.6	17
176	24	−40	128	25.5	17.4
177	24	−40	108	25.9	26.8
178	24	−40	88	72.4	14.3
179	24	−40	68	27.4	27.7

CHS–LA TC ID	Master Track ID	θ (deg)	Δp (hPa)	R_{max} (km)	V_t (km/h)
180	24	−40	48	54	35.7
181	24	−40	28	50	17.5
182	24	−40	8	109.9	18
183	25	−40	148	17.6	22.1
184	25	−40	128	28	24.4
185	25	−40	108	14.2	13.9
186	25	−40	88	50.2	11
187	25	−40	68	41.1	28.7
188	25	−40	48	119	19.2
189	25	−40	28	23.3	32.8
190	25	−40	8	100.4	11.8
191	26	−40	148	21.6	22.8
192	26	−40	128	32.4	14
193	26	−40	108	25.1	30.5
194	26	−40	88	14.2	24.5
195	26	−40	68	35.4	14
196	26	−40	48	109.8	15
197	26	−40	28	46.2	27.7
198	26	−40	8	89	21.3
199	27	−40	148	12.3	15.2
200	27	−40	128	13.4	32.3
201	27	−40	108	31.2	22.5
202	27	−40	88	15.1	17.3
203	27	−40	68	63.1	22.4
204	27	−40	48	30.1	9.7
205	27	−40	28	123.4	18.4
206	27	−40	8	59.6	19
207	28	−40	148	10.1	12.3
208	28	−40	128	21.5	21.7
209	28	−40	108	13.5	26
210	28	−40	88	58.7	10.5
211	28	−40	68	56.5	18.4
212	28	−40	48	67	21.5
213	28	−40	28	28.3	11.8
214	28	−40	8	34	28.1
215	29	−40	148	15.2	25

CHS–LA TC ID	Master Track ID	θ (deg)	Δp (hPa)	R_{max} (km)	V_t (km/h)
216	29	−40	128	16.7	10.2
217	29	−40	108	12.9	20
218	29	−40	88	39.5	23.1
219	29	−40	68	81.6	14.9
220	29	−40	48	33.3	25
221	29	−40	28	77.9	13.3
222	29	−40	8	25	11.2
223	30	−20	138	14.8	34.4
224	30	−20	118	19.2	18.1
225	30	−20	98	37.1	31.7
226	30	−20	78	66.5	9.9
227	30	−20	58	14.4	28.7
228	30	−20	38	31.9	9.5
229	30	−20	18	107.6	19.8
230	31	−20	138	12.2	28.3
231	31	−20	118	35.8	9.6
232	31	−20	98	11.6	20.6
233	31	−20	78	18.4	37.3
234	31	−20	58	57.7	22.2
235	31	−20	38	51.4	13.7
236	31	−20	18	34.8	12.9
237	32	−20	138	29.1	29.2
238	32	−20	118	19.9	12.7
239	32	−20	98	31.6	34.3
240	32	−20	78	15.2	23.8
241	32	−20	58	38.5	34.6
242	32	−20	38	103.9	11.8
243	32	−20	18	49.9	11.5
244	33	−20	138	19.6	32.1
245	33	−20	118	10.1	26
246	33	−20	98	29.5	11.2
247	33	−20	78	22.8	33.5
248	33	−20	58	51.9	18.8
249	33	−20	38	33.6	15
250	33	−20	18	94.2	14
251	34	−20	138	12.9	42.6

CHS–LA TC ID	Master Track ID	θ (deg)	Δp (hPa)	R_{max} (km)	V_t (km/h)
252	34	−20	118	22.4	21.8
253	34	−20	98	62.9	27.7
254	34	−20	78	14.1	11.7
255	34	−20	58	40	9.5
256	34	−20	38	38.7	19.6
257	34	−20	18	65	20.9
258	35	−20	138	15.6	13.7
259	35	−20	118	15.1	35
260	35	−20	98	53.5	39.9
261	35	−20	78	32.2	20
262	35	−20	58	34	8.7
263	35	−20	38	71.4	20.7
264	35	−20	18	17.3	9.8
265	36	−20	138	21.3	20.3
266	36	−20	118	14	11.1
267	36	−20	98	49.1	9.3
268	36	−20	78	54.6	18.9
269	36	−20	58	18.5	14.5
270	36	−20	38	42.2	15.8
271	36	−20	18	77.8	9.1
272	37	−20	138	21.9	27.4
273	37	−20	118	27.6	25.2
274	37	−20	98	27.6	14.6
275	37	−20	78	52.7	10.3
276	37	−20	58	85.3	19.3
277	37	−20	38	49.5	14.1
278	37	−20	18	58.2	31.4
279	38	−20	138	9.1	19
280	36	−20	118	32.3	14.8
281	36	−20	98	67.8	29.5
282	36	−20	78	40	12.1
283	36	−20	58	31	32.7
284	36	−20	38	40.4	26.6
285	36	−20	18	80.7	18.2
286	39	−20	138	13.6	30.1
287	39	−20	118	15.7	15.9

CHS–LA TC ID	Master Track ID	θ (deg)	Δp (hPa)	R_{max} (km)	V_t (km/h)
288	39	−20	98	47.3	9.8
289	39	−20	78	44.3	16.3
290	39	−20	58	81.5	21
291	39	−20	38	30.3	15.4
292	39	−20	18	98.3	24.5
293	40	−20	138	16.8	19.6
294	40	−20	118	14.6	23.8
295	40	−20	98	30.5	32.9
296	40	−20	78	36	10.8
297	40	−20	58	74.8	12.4
298	40	−20	38	68.8	27.7
299	40	−20	18	29.5	12.6
300	41	−20	138	30.7	11
301	41	−20	118	23.1	30.4
302	41	−20	98	15.6	18.9
303	41	−20	78	24	18.4
304	41	−20	58	43.2	12
305	41	−20	38	109.9	24
306	41	−20	18	33	18.7
307	42	−20	138	9.7	26.6
308	42	−20	118	40.6	15.3
309	42	−20	98	28.6	28.6
310	42	−20	78	61.2	35.2
311	42	−20	58	19.9	13.7
312	42	−20	38	57.5	13.3
313	42	−20	18	46	29.4
314	43	−20	138	10.4	13.2
315	43	−20	118	28.5	31.4
316	43	−20	98	42.4	14.1
317	43	−20	78	47.5	32.1
318	43	−20	58	26.8	16.4
319	43	−20	38	117.3	18.6
320	43	−20	18	56.1	19.2
321	44	−20	138	15.2	25.8
322	44	−20	118	26.8	14.3
323	44	−20	98	21.4	18.3

CHS–LA TC ID	Master Track ID	θ (deg)	Δp (hPa)	R_{max} (km)	V_t (km/h)
324	44	−20	78	73.1	22.4
325	44	−20	58	53.7	14.1
326	44	−20	38	76.9	10.6
327	44	−20	18	26	22.9
328	45	0	148	12.9	10
329	45	0	128	15.7	36.1
330	45	0	108	11.5	17.1
331	45	0	88	56.3	17.8
332	45	0	68	42.7	23.7
333	45	0	48	28.6	16.3
334	45	0	28	69.8	14.5
335	45	0	8	39.5	9.3
336	46	0	148	20.9	19.5
337	46	0	128	11.2	41.3
338	46	0	108	29.3	44.3
339	46	0	88	40.9	25.3
340	46	0	68	23.6	13.6
341	46	0	48	81	10.5
342	46	0	28	42.4	15.3
343	46	0	8	51.2	11.5
344	47	0	148	13.2	29
345	47	0	128	20.4	37.6
346	47	0	108	15.6	35.4
347	47	0	88	68	20.6
348	47	0	68	21.1	16.8
349	47	0	48	62.3	26.7
350	47	0	28	60.4	9
351	47	0	8	47.2	17.5
352	48	0	148	8	39.8
353	48	0	128	19.3	12.4
354	48	0	108	19.1	23.8
355	48	0	88	28.9	36.4
356	48	0	68	24.8	17.8
357	48	0	48	97.3	13.3
358	48	0	28	75.1	16.1
359	48	0	8	32.2	12.2

CHS–LA TC ID	Master Track ID	θ (deg)	Δp (hPa)	R_{max} (km)	V_t (km/h)
360	49	0	148	18	35.4
361	49	0	128	13	47.1
362	49	0	108	32.2	37
363	49	0	88	20.8	10.1
364	49	0	68	74.1	15.4
365	49	0	48	56	11.7
366	49	0	28	18.2	12.2
367	49	0	8	57.4	20.7
368	50	0	148	13.5	12.9
369	50	0	128	12.5	27.5
370	50	0	108	40.7	32.7
371	50	0	88	26.8	38.6
372	50	0	68	58.6	20.5
373	50	0	48	36.4	14.1
374	50	0	28	90.9	9.7
375	50	0	8	18	10.2
376	51	0	148	22.5	33
377	51	0	128	15.3	23.7
378	51	0	108	42.2	9.9
379	51	0	88	13.2	33.2
380	51	0	68	39.7	21.1
381	51	0	48	19.6	8.6
382	51	0	28	80.8	10.8
383	51	0	8	64.1	16.2
384	52	0	148	19.6	31.9
385	52	0	128	24.8	16.2
386	52	0	108	20.5	13.4
387	52	0	88	23.8	23.8
388	52	0	68	86.2	18.9
389	52	0	48	48.3	25.8
390	52	0	28	33.5	14.1
391	52	0	8	76.8	15
392	53	0	148	8.3	16.4
393	53	0	128	40.2	19.8
394	53	0	108	48	10.9
395	53	0	88	34.5	21.2

CHS–LA TC ID	Master Track ID	θ (deg)	Δp (hPa)	R_{max} (km)	V_t (km/h)
396	53	0	68	45.8	11
397	53	0	48	34.8	20.9
398	53	0	28	19.9	12.9
399	53	0	8	130.5	15.4
400	54	0	148	13.9	24.2
401	54	0	128	19.8	25.9
402	54	0	108	44	34
403	54	0	88	19.9	20
404	54	0	68	31.3	9.7
405	54	0	48	52	13.7
406	54	0	28	115.6	16.6
407	54	0	8	49.1	25.4
408	55	0	148	9	23.5
409	55	0	128	33.8	15.1
410	55	0	108	17.6	11.9
411	55	0	88	31.1	27.7
412	55	0	68	16.2	23
413	55	0	48	92.5	22.1
414	55	0	28	31.8	25.6
415	55	0	8	85.7	10.5
416	56	0	148	8.8	10.6
417	56	0	128	17.7	18.6
418	56	0	108	57.9	18.8
419	56	0	88	45.2	26
420	56	0	68	47.4	10.1
421	56	0	48	18.1	14.6
422	56	0	28	72.4	11.1
423	56	0	8	92.5	23.5
424	57	0	148	14.8	27.3
425	57	0	128	22.8	10.8
426	57	0	108	24.3	23.1
427	57	0	88	27.9	16.8
428	57	0	68	30	19.4
429	57	0	48	64.6	27.7
430	57	0	28	99.1	14.9
431	57	0	8	41.4	12.9

CHS–LA TC ID	Master Track ID	θ (deg)	Δp (hPa)	R_{max} (km)	V_t (km/h)
432	58	0	148	10.6	14
433	58	0	128	14.3	29.3
434	58	0	108	37.9	16.6
435	58	0	88	30	29.6
436	58	0	68	22.3	24.4
437	58	0	48	102.9	30
438	58	0	28	52	19.4
439	58	0	8	71.4	12.5
440	59	0	148	26.3	18.8
441	59	0	128	10.7	15.7
442	59	0	108	22.7	27.7
443	59	0	88	35.7	34.7
444	59	0	68	36.8	15.9
445	59	0	48	39.7	12.1
446	59	0	28	103.8	22.4
447	59	0	8	35.8	19.5
448	60	20	138	12.5	31.1
449	60	20	118	38.8	10.1
450	60	20	98	12.4	19.4
451	60	20	78	20.6	40
452	60	20	58	62	22.9
453	60	20	38	55.4	14.5
454	60	20	18	36.6	13.3
455	61	20	138	10.1	22.2
456	61	20	118	10.7	19.3
457	61	20	98	43.9	21.2
458	61	20	78	29.8	28.7
459	61	20	58	44.9	15.9
460	61	20	38	15.9	12.5
461	61	20	18	40.3	8.1
462	62	20	138	10.8	22.9
463	62	20	118	11.2	22.4
464	62	20	98	45.5	21.8
465	62	20	78	31	30.8
466	62	20	58	48.3	16.8
467	62	20	38	17.4	12.9

CHS–LA TC ID	Master Track ID	θ (deg)	Δp (hPa)	R_{max} (km)	V_t (km/h)
468	62	20	18	44	8.5
469	63	20	138	16.4	14.9
470	63	20	118	16.3	38.2
471	63	20	98	56.1	35.8
472	63	20	78	34.7	21.2
473	63	20	58	36.9	9.1
474	63	20	38	74.1	16.7
475	63	20	18	19	10.1
476	64	20	138	18.2	11.5
477	64	20	118	25.3	45.7
478	64	20	98	13.2	25.3
479	64	20	78	56.7	15.8
480	64	20	58	28.2	24.3
481	64	20	38	25.4	8.4
482	64	20	18	83.8	14.8
483	65	20	138	8.7	16.6
484	65	20	118	48.6	13.7
485	65	20	98	32.6	42.8
486	65	20	78	50.9	13
487	65	20	58	21.2	11.2
488	65	20	38	22.2	28.9
489	65	20	18	138.6	16
490	66	20	138	18.7	21.6
491	66	20	118	21.1	36.5
492	66	20	98	14.8	13.1
493	66	20	78	33.4	11.2
494	66	20	58	66.7	21.6
495	66	20	38	23.8	30.3
496	66	20	18	113.2	14.4
497	67	20	138	23.2	12.1
498	67	20	118	16.9	33.7
499	67	20	98	59.1	37.7
500	67	20	78	49.2	15.4
501	67	20	58	15.8	15
502	67	20	38	64.1	9.2
503	67	20	18	72.4	21.5

CHS–LA TC ID	Master Track ID	θ (deg)	Δp (hPa)	R_{max} (km)	V_t (km/h)
504	68	20	138	17.3	33.2
505	68	20	118	29.4	11.6
506	68	20	98	34.8	22.5
507	68	20	78	16.2	14.4
508	68	20	58	71.9	17.3
509	68	20	38	45.8	8.8
510	68	20	18	67.4	25.5
511	69	20	138	13.3	10.4
512	69	20	118	31.3	20.5
513	69	20	98	20.5	20
514	69	20	78	38.6	25.2
515	69	20	58	32.5	25.9
516	69	20	38	98.7	16.2
517	69	20	18	47.9	10.5
518	70	20	138	16	17.2
519	70	20	118	45.2	12.2
520	70	20	98	23.1	12.2
521	70	20	78	58.8	23.1
522	70	20	58	25.4	29.9
523	70	20	38	47.6	19.1
524	70	20	18	75	11.9
525	71	20	138	11.1	14.3
526	71	20	118	18.6	18.7
527	71	20	98	41	15.6
528	71	20	78	69.5	13.5
529	71	20	58	46.5	27.7
530	71	20	38	20.6	17.6
531	71	20	18	90.5	10.8
532	72	20	138	20.2	20.9
533	72	20	118	20.5	23.1
534	72	20	98	17.2	26
535	72	20	78	63.7	12.6
536	72	20	58	55.7	37.1
537	72	20	38	35.3	9.9
538	72	20	18	54	23.7
539	73	20	138	19.1	35.7

CHS–LA TC ID	Master Track ID	θ (deg)	Δp (hPa)	R_{max} (km)	V_t (km/h)
540	73	20	118	26	13.2
541	73	20	98	22.2	24.5
542	73	20	78	42.8	20.6
543	73	20	58	59.8	13.2
544	73	20	38	79.9	34.3
545	73	20	18	24.2	15.2
546	74	40	148	9.6	41.6
547	74	40	128	24.1	14.6
548	74	40	108	23.5	18.2
549	74	40	88	37	41.4
550	74	40	68	99.5	16.4
551	74	40	48	15.1	18.7
552	74	40	28	30	10
553	74	40	8	68.9	18.5
554	75	40	148	14.5	11.1
555	75	40	128	23.4	20.4
556	75	40	108	34.3	41.2
557	75	40	88	33.4	11.9
558	75	40	68	19.8	25.1
559	75	40	48	22.6	33.3
560	75	40	28	54	12.6
561	75	40	8	141.4	13.9
562	76	40	148	15.6	26.5
563	76	40	128	12.1	25.2
564	76	40	108	45.9	31.5
565	76	40	88	38.2	11.4
566	76	40	68	44.2	38.6
567	76	40	48	27.1	19.8
568	76	40	28	26.6	11.5
569	76	40	8	96.3	8.3
570	77	40	148	18.5	46.5
571	77	40	128	21	18
572	77	40	108	12.2	20.6
573	77	40	88	52.1	9.6
574	77	40	68	26.1	9.3
575	77	40	48	31.7	23.5

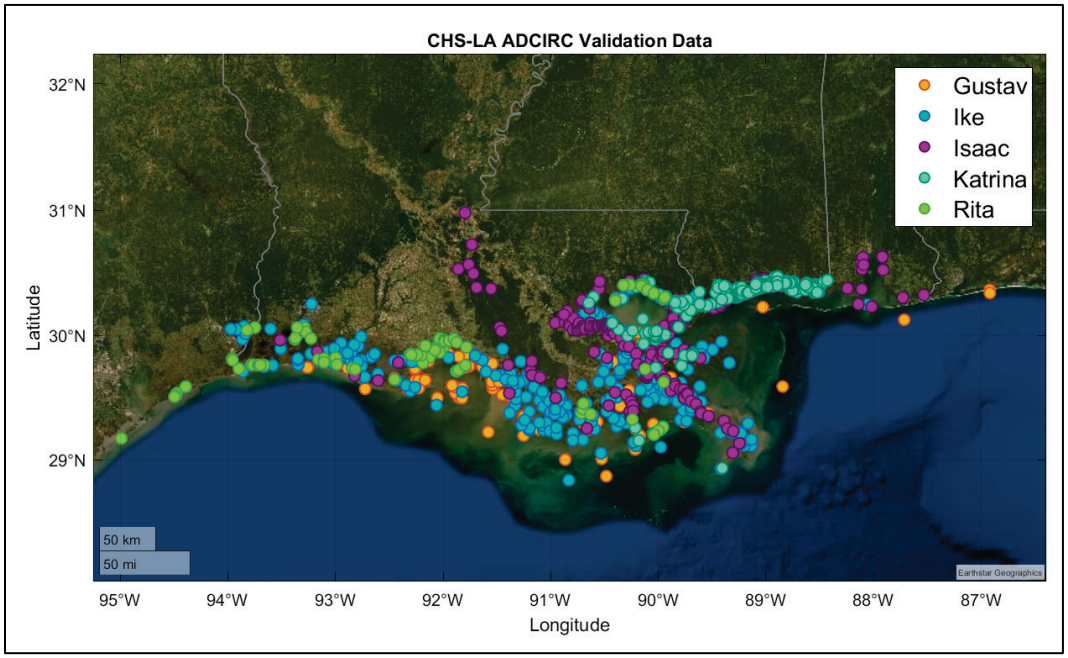
CHS–LA TC ID	Master Track ID	θ (deg)	Δp (hPa)	R_{max} (km)	V_t (km/h)
576	77	40	28	84	26.6
577	77	40	8	53.2	10.9
578	78	40	148	12	13.4
579	78	40	128	30	11.3
580	78	40	108	22	17.7
581	78	40	88	42.3	30.7
582	78	40	68	18.6	21.7
583	78	40	48	84.5	17.7
584	78	40	28	44.3	13.7
585	78	40	8	45.2	22
586	79	40	148	9.8	30.9
587	79	40	128	35.5	11.9
588	79	40	108	16.3	15.5
589	79	40	88	32.2	19.5
590	79	40	68	52.7	29.8
591	79	40	48	44.8	12.9
592	79	40	28	87.3	30.7
593	79	40	8	21.5	26.6
594	80	40	148	15.9	28.2
595	80	40	128	16.2	22.3
596	80	40	108	39.2	12.9
597	80	40	88	16.1	12.9
598	80	40	68	38.2	12.3
599	80	40	48	77.8	20.3
600	80	40	28	37	23.1
601	80	40	8	55.3	13.2
602	81	40	148	19.1	34.1
603	81	40	128	17.2	12.9
604	81	40	108	28.4	14.5
605	81	40	88	24.8	13.8
606	81	40	68	77.6	25.9
607	81	40	48	25.6	22.8
608	81	40	28	62.6	23.9
609	81	40	8	79.6	8.9
610	82	40	148	11.8	21.4
611	82	40	128	26.3	19.2

CHS–LA TC ID	Master Track ID	θ (deg)	Δp (hPa)	R_{max} (km)	V_t (km/h)
612	82	40	108	27.6	29.5
613	82	40	88	18	22.5
614	82	40	68	71	13.1
615	82	40	48	38.1	11.3
616	82	40	28	24.9	10.4
617	82	40	8	122.3	30
618	83	60	138	22.6	37.1
619	83	60	118	11.8	26.8
620	83	60	98	39.6	11.7
621	83	60	78	37.3	21.8
622	83	60	58	89.7	20.4
623	83	60	38	19	11
624	83	60	18	38.4	26.6
625	84	60	138	11.5	24.3
626	84	60	118	33.4	40.1
627	84	60	98	18.9	30.6
628	84	60	78	45.9	9.4
629	84	60	58	78	12.8
630	84	60	38	59.6	25.7
631	84	60	18	22.5	12.2
632	85	60	138	9.4	48.6
633	85	60	118	42.7	16.4
634	85	60	98	24	23.8
635	85	60	78	13	26
636	85	60	58	64.2	26.7
637	85	60	38	28.6	12.2
638	85	60	18	119.8	16.8
639	86	60	138	26.6	38.7
640	86	60	118	12.9	42.5
641	86	60	98	25.8	13.6
642	86	60	78	26.2	13.9
643	86	60	58	69.2	11.6
644	86	60	38	86.4	32
645	86	60	18	31.2	17.8

Appendix C: Geospatial Bias and Uncertainty

The bias and uncertainty for CHS-LA were estimated using validation data from Hurricanes Gustav (2008), Ike (2008), Isaac (2012), Katrina (2005), and Rita (2005), and the distribution of this data are shown in Figure C-1. As described in Section 6.2, the following figures illustrate the geospatial bias and uncertainty computed for the study area. The absolute and relative forms of both bias and uncertainty were computed on a nodal basis as shown below. Additionally, the WBV and LPV structures are illustrated in these plots for reference of their location.

Figure C-1. Distribution of validation data points within the CHS-LA study area.



C.1 Bias and uncertainty of ADCIRC simulations

Figure C-2. Absolute form of ADCIRC bias for the CHS-LA study area.

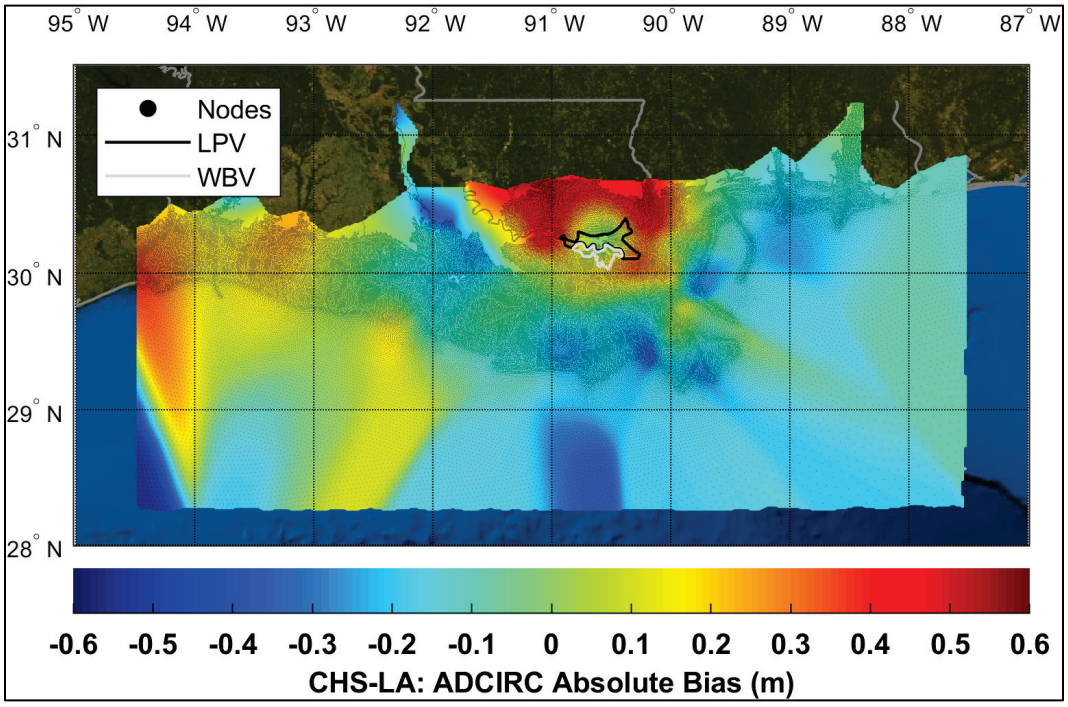


Figure C-3. Relative form of ADCIRC bias for the CHS-LA study area.

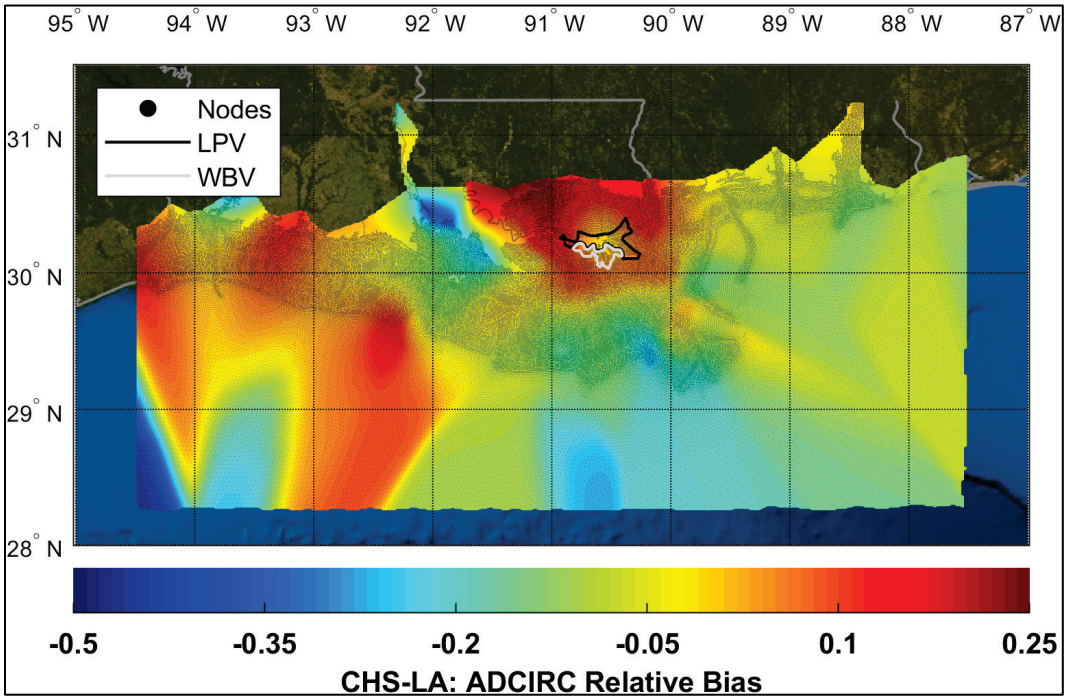


Figure C-4. Absolute form of ADCIRC uncertainty for the CHS-LA study area.

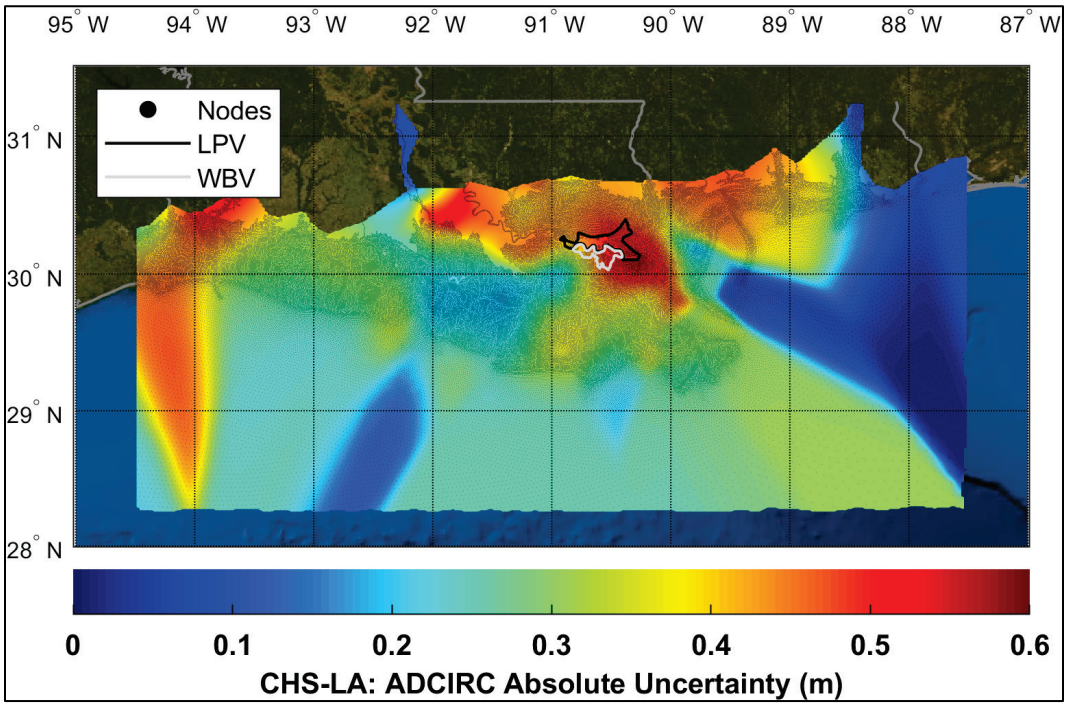
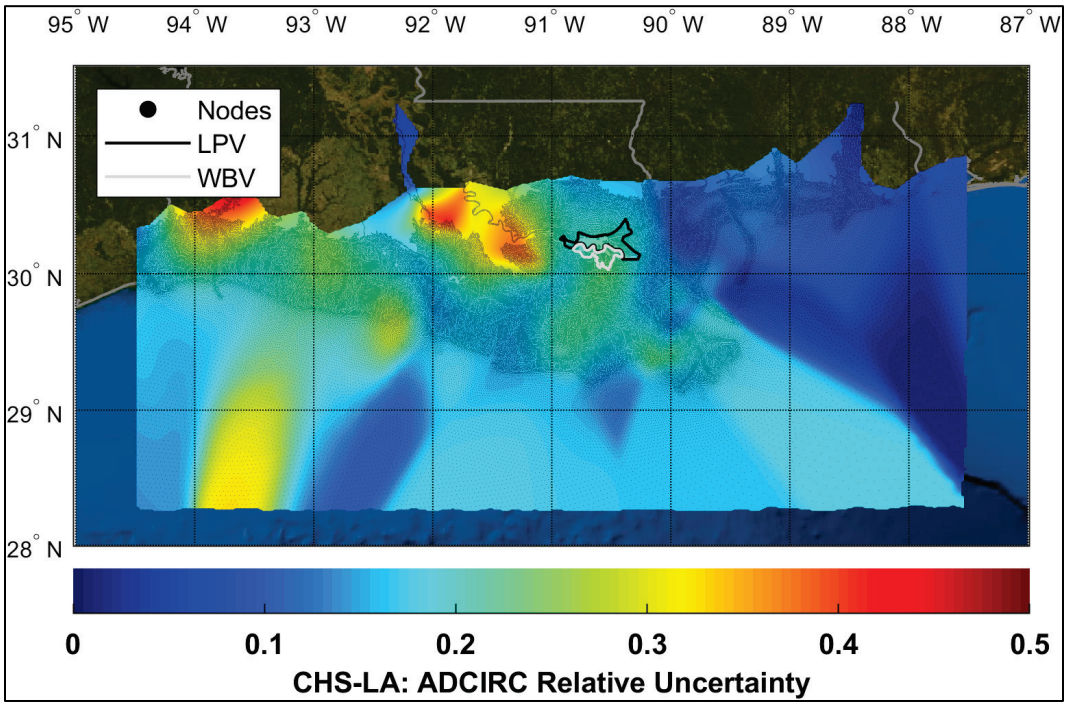


Figure C-5. Relative form of ADCIRC uncertainty for the CHS-LA study area.



C.2 Bias and uncertainty of PBL simulations

Figure C-6. Absolute form of PBL bias for the CHS-LA study area.

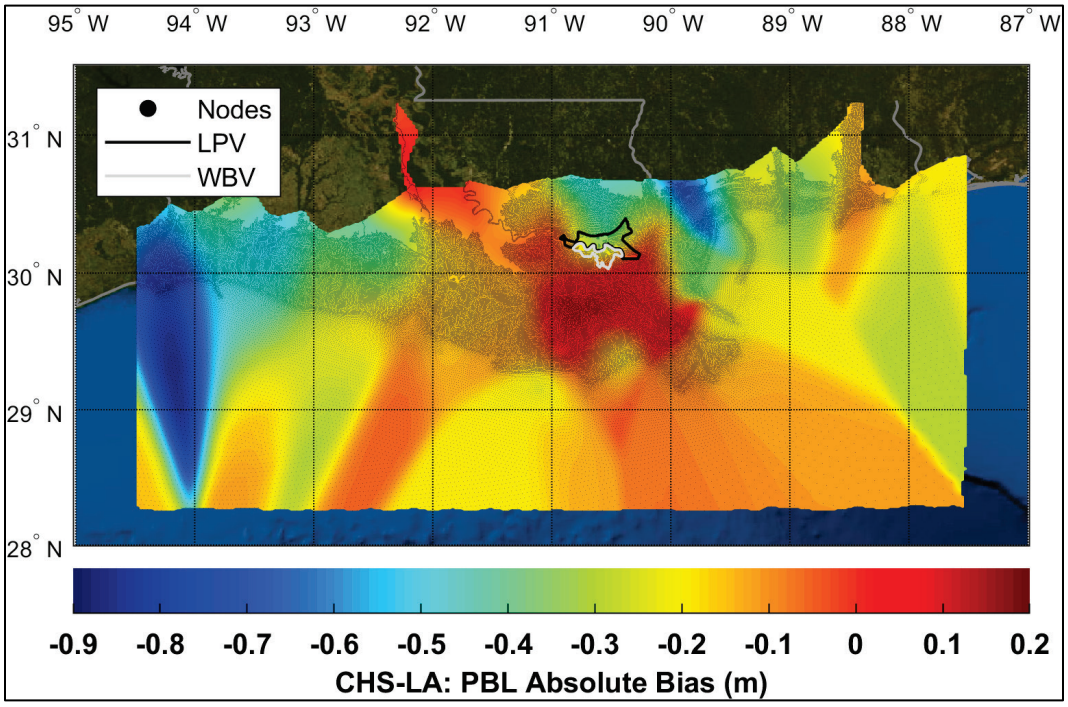


Figure C-7. Relative form of PBL bias for the CHS-LA study area.

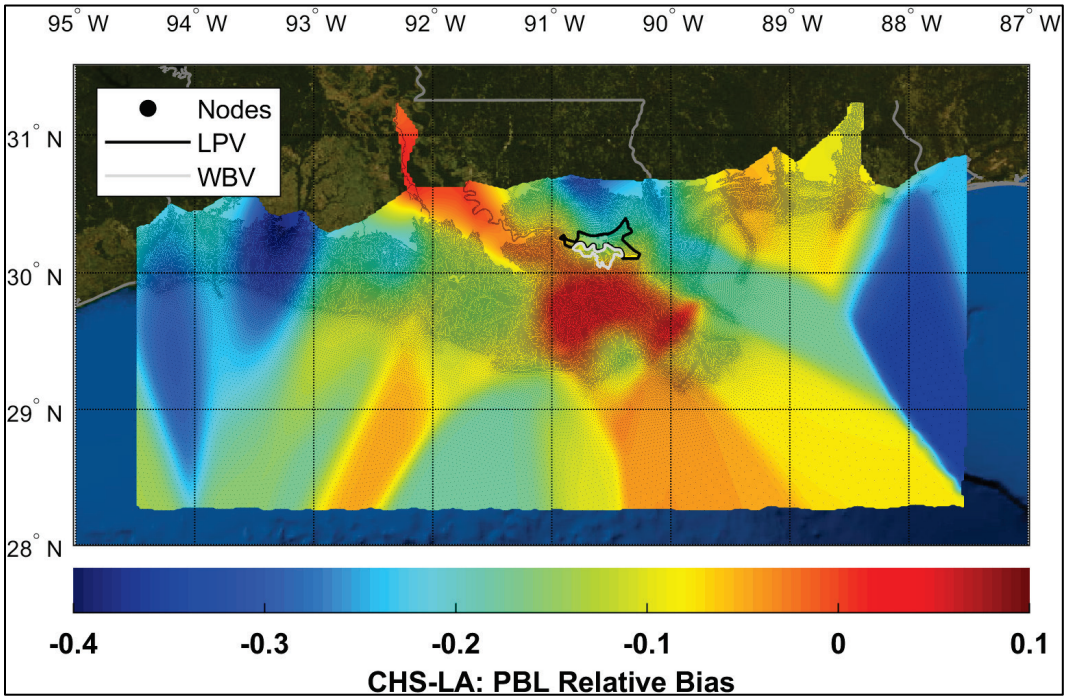


Figure C-8. Absolute form of PBL uncertainty for the CHS-LA study area.

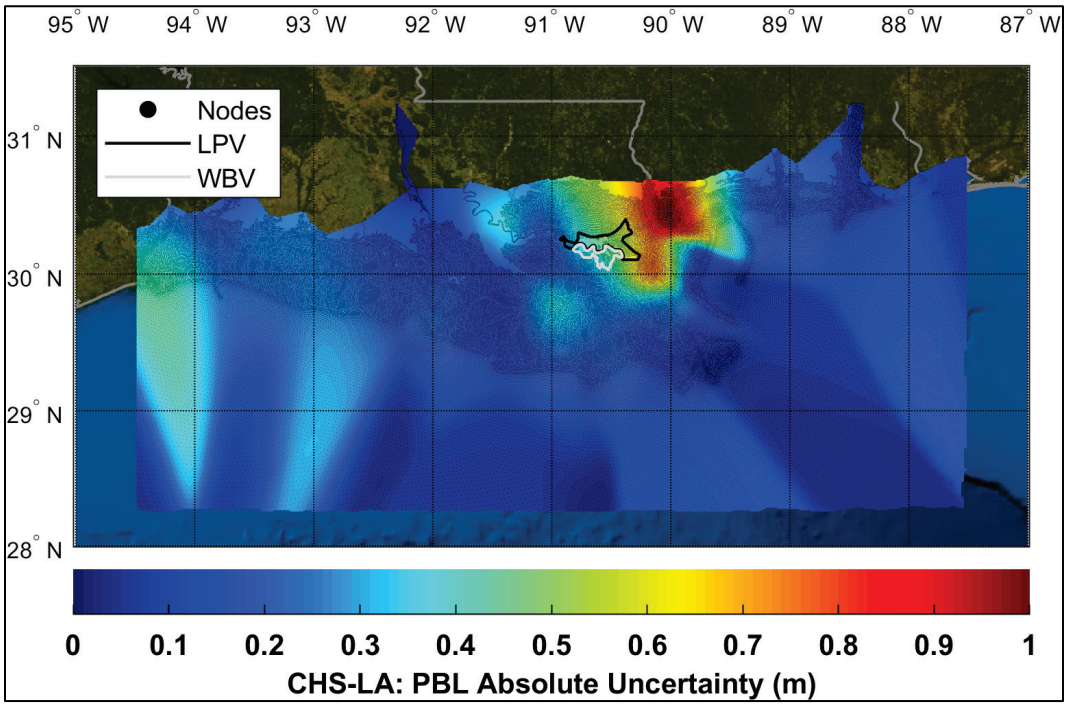
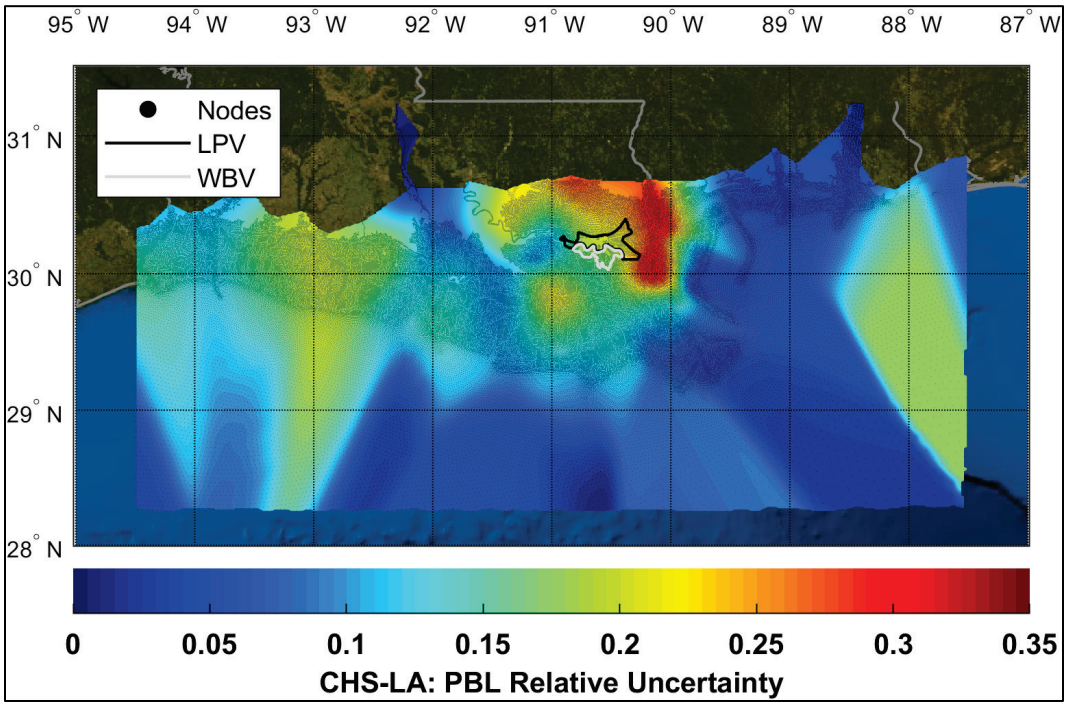


Figure C-9. Relative form of PBL uncertainty for the CHS-LA study area.



Appendix D: Astronomical Tide Uncertainty

Table D-1. Tidal uncertainty computed at NOAA gauges surrounding the CHS-LA study area.

Gauge Count	Station ID	Name	State	Latitude	Longitude	Standard Deviation (m)
1	8729747	Shield Point, Blackwater River	AL	30.6	−87.0	0.18
2	8729753	Blackwater River	AL	30.6	−87.0	0.18
3	8729791	Hernandez Point North	FL	30.5	−87.1	0.13
4	8729806	Fishing Bend, Santa Rosa Sound	FL	30.3	−87.1	0.15
5	8729816	Lora Point, Escambia Bay	FL	30.5	−87.2	0.17
6	8729824	Floridatown, Escambia Bay	FL	30.6	−87.2	0.15
7	8729840	Pensacola	FL	30.4	−87.2	0.18
8	8729905	Millview, Perdido Bay	FL	30.4	−87.4	0.09
9	8729909	Big Lagoon	FL	30.3	−87.4	0.14
10	8729941	Blue Angels Park	FL	30.4	−87.4	0.08
11	8731439	Gulf Shores, Icww	AL	30.3	−87.7	0.14
12	8732828	Weeks Bay, Mobile Bay	AL	30.4	−87.8	0.16
13	8733821	Point Clear, Mobile Bay	AL	30.5	−87.9	0.19
14	8733839	Meaher State Park, Mobile Bay	AL	30.7	−87.9	0.19
15	8735180	Dauphin Island	AL	30.3	−88.1	0.16
16	8735181	Dauphin Island Hydro	AL	30.3	−88.1	0.18
17	8735391	Dog River Bridge	AL	30.6	−88.1	0.16
18	8735523	East Fowl River Bridge	AL	30.4	−88.1	0.16
19	8736897	Coast Guard Sector Mobile	AL	30.6	−88.1	0.15
20	8737048	Mobile State Docks	AL	30.7	−88.0	0.18
21	8737138	Chickasaw Creek	AL	30.8	−88.1	0.15
22	8737373	Lower Bryant Landing	AL	31.0	−87.9	0.21
23	8738043	West Fowl River Bridge	AL	30.4	−88.2	0.16
24	8739803	Bayou La Batre Bridge	AL	30.4	−88.2	0.17
25	8740166	Grand Bay Nerr, Mississippi Sound	MS	30.4	−88.4	0.15
26	8740405	Petit Bois Island, Miss. Sound	MS	30.2	−88.4	0.14
27	8741041	Dock E, Port Of Pascagoula	MS	30.3	−88.5	0.18
28	8741196	Pascagoula Point	MS	30.3	−88.5	0.16

Gauge Count	Station ID	Name	State	Latitude	Longitude	Standard Deviation (m)
29	8741533	Pascagoula Noaa Lab	MS	30.4	−88.6	0.18
30	8741798	Gautier	MS	30.4	−88.6	0.18
31	8742205	Graveline Bayou Entrance	MS	30.4	−88.7	0.17
32	8742221	Horn Island	MS	30.2	−88.7	0.19
33	8742523	North Shore	MS	30.4	−88.7	0.19
34	8743081	Hollingsworth Point, Davis Bayou	MS	30.4	−88.8	0.19
35	8743181	Old Fort Bayou, Ocean Springs Marina	MS	30.4	−88.8	0.19
36	8743281	Ocean Springs	MS	30.4	−88.8	0.20
37	8743301	Bayou Talla, Back Bay Of Biloxi	MS	30.4	−88.8	0.20
38	8743495	Ocean Springs, Old Fort Bayou	MS	30.4	−88.8	0.20
39	8743639	Bayou Poito, Back Bay Of Biloxi	MS	30.4	−88.8	0.20
40	8743735	Biloxi (Cadet Point)	MS	30.4	−88.9	0.20
41	8743812	Deer Island	MS	30.4	−88.9	0.20
42	8743838	Langley Point	MS	30.4	−88.9	0.20
43	8744117	Biloxi	MS	30.4	−88.9	0.20
44	8744284	Keesler Afb, Back Bay Of Biloxi	MS	30.4	−88.9	0.20
45	8744663	Tchoutacabouffa River Entrance	MS	30.4	−89.0	0.20
46	8744671	Popps Ferry, Back Bay Of Biloxi	MS	30.4	−89.0	0.20
47	8744756	Ship Island, Mississippi Sound	MS	30.2	−89.0	0.16
48	8744934	Biloxi River, Lower End	MS	30.4	−89.0	0.16
49	8745101	Handsboro Bridge, Bernard Bayou	MS	30.4	−89.0	0.14
50	8745555	Landon	MS	30.4	−89.1	0.14
51	8745557	Gulfport Harbor	MS	30.4	−89.1	0.21
52	8746819	Pass Christian Yacht Club, Miss. Sound	MS	30.3	−89.2	0.21
53	8747437	Bay Waveland Yacht Club	MS	30.3	−89.3	0.20
54	8747766	Waveland	MS	30.3	−89.4	0.21
55	8760417	Devon Energy Facility	LA	29.2	−89.0	0.19

Gauge Count	Station ID	Name	State	Latitude	Longitude	Standard Deviation (m)
56	8760551	South Pass	LA	29.0	−89.1	0.17
57	8760668	Grand Pass	LA	30.1	−89.2	0.13
58	8760721	Pilottown	LA	29.2	−89.3	0.12
59	8760849	Venice, Grand Pass	LA	29.3	−89.4	0.12
60	8760889	Olga Compressor Station, Grand Bay	LA	29.4	−89.4	0.16
61	8760922	Pilots Station East, S.W. Pass	LA	28.9	−89.4	0.15
62	8760943	Sw Pass	LA	28.9	−89.4	0.15
63	8761193	Empire, Mississippi River	LA	29.4	−89.6	0.15
64	8761305	Shell Beach	LA	29.9	−89.7	0.17
65	8761385	Vicinity Of Uno Chef Menteur	LA	30.1	−89.8	0.17
66	8761402	The Rigolets	LA	30.2	−89.7	0.07
67	8761494	West Point A La Hache, Miss. River	LA	29.6	−89.8	0.07
68	8761529	Martello Castle, Lake Borgne	LA	29.9	−89.8	0.14
69	8761724	Grand Isle	LA	29.3	−90.0	0.14
70	8761727	Alliance, Mississippi River	LA	29.7	−90.0	0.14
71	8761742	Mendicant Island, Barataria Bay	LA	29.3	−90.0	0.14
72	8761819	Texaco Dock, Hackberry Bay	LA	29.4	−90.0	0.13
73	8761826	Cheniere Caminada, Caminada Pass	LA	29.2	−90.0	0.15
74	8761899	Lafitte, Barataria Waterway	LA	29.7	−90.1	0.08
75	8761927	New Canal Station	LA	30.0	−90.1	0.10
76	8761955	Carrollton	LA	29.9	−90.1	0.10
77	8762075	Port Fourchon, Belle Pass	LA	29.1	−90.2	0.16
78	8762084	Leeville, Bayou Lafourche	LA	29.2	−90.2	0.12
79	8762184	Golden Meadow, Plaisance Canal	LA	29.4	−90.3	0.06
80	8762223	East Timbalier Island, Timbalier Bay	LA	29.1	−90.3	0.17
81	8762372	East Bank 1, Norco, B. LaBranche	LA	30.1	−90.4	0.10
82	8762482	West Bank 1, Bayou Gauche	LA	29.8	−90.4	0.10
83	8762483	I−10 Bonnet Carre Floodway	LA	30.1	−90.4	0.10
84	8762888	E. Isle Dernieres, Lake Pelto	LA	29.1	−90.6	0.15

Gauge Count	Station ID	Name	State	Latitude	Longitude	Standard Deviation (m)
85	8762928	Cocodrie	LA	29.2	−90.7	0.13
86	8763535	Texas Gas Platform, Caillou Bay	LA	29.2	−91.0	0.16
87	8764025	Stouts Pass at Six Mile Lake	LA	29.7	−91.2	0.07
88	8764044	Berwick, Atchafalaya River	LA	29.7	−91.2	0.23
89	8764227	LAWMA, Amerada Pass	LA	29.4	−91.3	0.17
90	8764311	Eugene Island	LA	29.4	−91.4	0.17
91	8764314	Eugene Island, North of , Gulf of Mexico	LA	29.4	−91.4	0.18
92	8765148	Weeks Bay	LA	29.8	−91.8	0.15
93	8765171	New Iberia	LA	29.9	−91.8	0.15
94	8765251	Cypremort Point	LA	29.7	−91.9	0.16
95	8766072	Freshwater Canal Locks	LA	29.6	−92.3	0.21
96	8767816	Lake Charles	LA	30.2	−93.2	0.15
97	8767961	Bulk Terminal	LA	30.2	−93.3	0.12
98	8768094	Calcasieu Pass	LA	29.8	−93.3	0.20
99	8770475	Port Arthur	TX	29.9	−93.9	0.12
100	8770520	Rainbow Bridge	TX	30.0	−93.9	0.12
101	8770570	Sabine Pass North	TX	29.7	−93.9	0.18
102	8770597	Orange	TX	30.1	−93.7	0.18
103	8770822	Texas Point, Sabine Pass	TX	29.7	−93.8	0.18
104	8771081	Sabine Offshore	TX	29.5	−93.6	0.18

Symbols

Δp	Central pressure deficit of tropical cyclone, computed as the difference between a far-field atmospheric pressure of 1,013 hPa and central pressure (hPa)
θ	Track direction of tropical cyclone (deg)
ε	Epsilon term
μ	Mean
σ	Standard deviation
σ_ε	Standard deviation of the error
λ	Storm recurrence rate (storms/yr/km)
ρ	Correlation coefficient
B	Holland B
C	Copula
c_p	Central pressure (hPa)
H_{mo}	Significant wave height (m)
m	Month
Q	Discharge
Q_d	Deterministic discharge value
Q_p	Probabilistic discharge value
R_{max}	Radius of maximum winds of tropical cyclone (km)
R_p	Scale pressure radius
T_p	Peak wave period (s)
V_t	Forward translation speed of tropical cyclone (km/h)
x_0	Tropical cyclone reference location

Abbreviations

2D	Two-dimensional
ADCIRC	ADvanced CIRCulation numerical model
AEF	Annual exceedance frequency (yr^{-1})
AEP	Annual exceedance probability (yr^{-1})
ARI	Average recurrence interval (yr)
ATCF	Automated Tropical Cyclone Forecast
ATCS	Augmented TC suite
BE	Best-estimate
BND	Bivariate normal distribution
BQ	Bayesian Quadrature
CHS	Coastal Hazards System
CHS-LA	Coastal Hazards System-Louisiana
CL	Confidence limit
CPRA	Coastal Protection and Restoration Authority
CRL	Coastal reference location
CSR	Coastal structure reliability
DNC	Dry-node correction
DSRR	Directional storm recurrence rate
DSW	Discrete storm weight
DTWB	Doubly truncated Weibull distribution
EBTRK	Extended best track

EKF	Epanechnikov kernel function
FEMA	Federal Emergency Management Agency
FIS	Flood Insurance Studies
GKF	Gaussian kernel function
GKS	Gaussian kernel surface
GOM	Gulf of Mexico
GPM	Gaussian process metamodeling
HI	High intensity
HSDRRS	Hurricane and Storm Damage Risk Reduction System
HURDAT2	HURricane DATa 2nd generation
HWM	High-water marks
IBTracs	International Best Track Archive for Climate Stewardship
ID	Identifier
IOKA	Interactive Objective Kinematic Analysis
IPET	Interagency Performance Evaluation Task Force
ITCS	Initial TC suite
JPM	Joint probability method
JPM-MC	Joint probability method-Monte Carlo
JPM-OS	JPM with optimal sampling
JPM-OS-BQ	JPM by Bayesian Quadrature
JPM-OS-RS	JPM with augmented sampling using a Response Surface
*k*NN	*k*-nearest neighbor

LCPRA	Louisiana Coastal Protection and Restoration Authority
LI	Low intensity
LPV	Lake Pontchartrain & Vicinity
MCAP	Mississippi Coastal Analysis Project
MCS	Monte Carlo simulations
MGC	Meta-Gaussian copula
MI	Medium intensity
MSL	Mean-sea-level
NACCS	North Atlantic Coast Comprehensive Study
NHC	National Hurricane Center
NOAA	National Oceanic and Atmospheric Administration
ODGP	Ocean Data Gathering Program
ORP	Offshore reference point
OS	Optimal sampling
OWI	Oceanweather, Inc.
PBL	Planetary boundary layer
PCHA	Probabilistic Coastal Hazard Analysis
PDF	Probability distribution functions
PROS	Peaks, Runup, Overtopping, and Stone
RS	Response surface
SACS	South Atlantic Coastal Study; also referenced as South Atlantic Coast Comprehensive Study (SACCS)
SLR	Sea level rise

SRR	Storm recurrence rate
SSHWS	Saffir-Simpson Hurricane Wind Scale
SST	Stochastic Simulation Technique
SWAN	Simulating WAves Nearshore
SWL	Still water level (storm surge + astronomical tide)
TC	Tropical cyclone
UKF	Uniform kernel function
USACE	US Army Corps of Engineers
WBV	West Bank & Vicinity
XC	Extratropical cyclone
Z	Basic *z*-score

REPORT DOCUMENTATION PAGE

Form Approved

OMB No. 0704-0188

Public reporting burden for this collection of information is estimated to average 1 hour per response, including the time for reviewing instructions, searching existing data sources, gathering and maintaining the data needed, and completing and reviewing this collection of information. Send comments regarding this burden estimate or any other aspect of this collection of information, including suggestions for reducing this burden to Department of Defense, Washington Headquarters Services, Directorate for Information Operations and Reports (0704-0188), 1215 Jefferson Davis Highway, Suite 1204, Arlington, VA 22202-4302. Respondents should be aware that notwithstanding any other provision of law, no person shall be subject to any penalty for failing to comply with a collection of information if it does not display a currently valid OMB control number. PLEASE DO NOT RETURN YOUR FORM TO THE ABOVE ADDRESS.

1. REPORT DATE	2. REPORT TYPE	3. DATES COVERED (From–To)
August 2022	Final	FY20–FY22

4. TITLE AND SUBTITLE
Coastal Hazards System–Louisiana (CHS-LA)

5a. CONTRACT NUMBER

5b. GRANT NUMBER

5c. PROGRAM ELEMENT

6. AUTHOR(S)
Norberto C. Nadal-Caraballo, Madison C. Yawn, Luke A. Aucoin, Meredith L. Carr, Alexandros A. Taflanidis, Aikaterini P. Kyprioti, Jeffrey A. Melby, Efrain Ramos-Santiago, Victor M. Gonzalez, Thomas C. Massey, Zach Cobell, and Andrew T. Cox

5d. PROJECT NUMBER

5e. TASK NUMBER

5f. WORK UNIT NUMBER

7. PERFORMING ORGANIZATION NAME(S) AND ADDRESS(ES)
US Army Engineer Research and Development Center (ERDC)
Coastal and Hydraulics Laboratory (CHL)
3909 Halls Ferry Road
Vicksburg, MS 39180-6199

8. PERFORMING ORGANIZATION REPORT NUMBER
ERDC/CHL TR-22-16

9. SPONSORING / MONITORING AGENCY NAME(S) AND ADDRESS(ES)
Coastal Protection and Restoration Authority (CPRA) of Louisiana
P.O. Box 44027
Baton Rouge, LA 70804-4027

10. SPONSOR/MONITOR'S ACRONYM(S)
CPRA

11. SPONSOR/MONITOR'S REPORT NUMBER(S)

12. DISTRIBUTION / AVAILABILITY STATEMENT
Approved for public release; distribution is unlimited.

13. SUPPLEMENTARY NOTES
Funds were provided by the Coastal Protection and Restoration Agency (CPRA) of Louisiana through Cooperative Research and Development Agreement (CRADA) 65K08-B54G0B.

14. ABSTRACT
The US Army Engineer Research and Development Center (ERDC), Coastal and Hydraulics Laboratory (CHL) expanded the Coastal Hazards System (CHS) to quantify storm surge and wave hazards for coastal Louisiana. The CHS Louisiana (CHS-LA) coastal study was sponsored by the Louisiana Coastal Protection and Restoration Authority (CPRA) and the New Orleans District (MVN), US Army Corps of Engineers (USACE) to support Louisiana's critical coastal infrastructure and to ensure the effectiveness of coastal storm risk management projects. The CHS-LA applied the CHS Probabilistic Coastal Hazard Analysis (PCHA) framework to quantify tropical cyclone (TC) responses, leveraging new atmospheric and hydrodynamic numerical model simulations of synthetic TCs developed explicitly for the Louisiana region. This report focuses on documenting the PCHA conducted for the CHS-LA, including details related to the characterization of storm climate, storm sampling, storm recurrence rate estimation, marginal distributions, correlation and dependence structure of TC atmospheric-forcing parameters, development of augmented storm suites, and assignment of discrete storm weights to the synthetic TCs. As part of CHS-LA, coastal hazards were estimated within the study area for annual exceedance frequencies (AEFs) over the range of 10 yr-1 to 1×10-4 yr-1.

15. SUBJECT TERMS
Floods, Louisiana—Coasts, Risk assessment, Risk management, Storm surges, Tides

16. SECURITY CLASSIFICATION OF:			17. LIMITATION OF ABSTRACT	18. NUMBER OF PAGES	19a. NAME OF RESPONSIBLE PERSON
a. REPORT	b. ABSTRACT	c. THIS PAGE			Norberto C. Nadal-Caraballo
Unclassified	Unclassified	Unclassified	SAR	189	19b. TELEPHONE NUMBER (include area code) (601) 634-2008